Experimental and CFD simulation investigations into fouling reduction by gas-liquid two-phase flow for submerged flat sheet membranes

Author:
Ndinisa, Nkosinathi Vincent

Publication Date:
2006

DOI:
https://doi.org/10.26190/unsworks/17742

Experimental and CFD Simulation Investigations into Fouling Reduction by Gas-Liquid Two-Phase Flow for Submerged Flat Sheet Membranes

A thesis submitted in partial fulfilment
of the requirements for the degree of
Doctor of Philosophy

By

Nkosinathi Vincent Ndinisa

The School of Chemical Sciences and Engineering
UNESCO Centre for Membrane Science and Technology
The University of New South Wales
Sydney Australia

2006

CERTIFICATE OF ORIGINALITY

I hereby declare that this submission is my own work and to the best of my knowledge it contains no material previously published or written by another person, nor material which to a substantial extent has been accepted for the award of any other degree or diploma at UNSW or any other educational institution, except where due acknowledgement is made in the thesis. Any contribution made to the research by others, with whom I have worked at UNSW and DIT is explicitly acknowledged in the thesis.

I also declare that the intellectual content of this thesis is the product of my own work, except to the extent that assistance from others in the project's design and conception or in style, presentation and linguistic expression is acknowledged.

Nkosinathi Vincent Ndinisa

ACKNOWLEDGEMENTS

Firstly I would like to express my appreciation and sincere gratitude to my supervisors Associate Professor Dianne Wiley, Professor Tony Fane and Associate Professor David Fletcher for their encouragement, guidance, enthusiasm and support for the duration of this project.

I would like to acknowledge Professor Lingam Pillay for his support, guidance and for partly supervising the work that was completed at the Durban Institute of Technology.

I would like to acknowledge Dr. Jörn Schwinge for teaching me the basics of the CFD software called CFX from Ansys.

I would also like to thank the professional officer Dr. Deyan Guang for his support and organisational skills in the laboratory.

My sincere gratitude also goes to Associate Professor Russell Standish at the Center for Advanced Computational and Communications for help with access to the high performance computers used in this work. I would like to thank Ms Ee Meen Iliffe and Mr Craig Howie as well for helping with the connection to the high performance computers.

I would like to thank Mr Paul Brockbank and Mr Phil Thompson at the school's workshop for their help with construction of the experimental rig.

It has been a great privilege for me to study in the UNESCO Centre for Membrane Science and Technology, support and help from colleagues and staff is greatly appreciated.

I would also like thank the Australian Agency for International Development (AusAID) for providing bulk of the financial support for this project.

I would like to thank the National Research Foundation (NRF) in South Africa for providing financial resources for the work that was conducted there.

I would like to thank all my colleagues at the Chemical Engineering Department at the Durban Institute of Technology for all their support and encouragement during the time when I was on study leave.

Finally, I would like to thank my parents, my brothers and my sister in-law for their moral support and inspiring me to achieve my goals.

PAPERS EMANATING FROM THIS THESIS

Ndinisa, N. V., Wiley, D. E. & Fletcher, D. F.; Computational Fluid Dynamics Simulations of Taylor Bubbles in Tubular Membranes – Model Validation and Application to Laminar Flow Sytems; *Chem. Eng. Res & Design*, 2005, **83**(A1): 40 – 49.

Ndinisa, N. V., Wiley, D. E. & Fletcher, D. F.; CFD Simulations of Single Gas Bubbles Rising Through Stagnant Liquids – Validation of Numerical Methods; *Poster Presentation at IMSTEC03*, 14 November 2003, Sydney Australia.

Ndinisa, N. V., Fane, A. G. & Wiley, D. E.; Fouling Control in a Submerged Flat Sheet Membrane System: Part I – Bubbling and Hydrodynamic Effects; *Separation Science & Technology Journal;* 2006, **41**: 1383 – 1409.

Ndinisa, N. V., Fane, A. G., Wiley, D. E. & Fletcher, D. F.; Fouling Control in a Submerged Flat Sheet Membrane System: Part II –Two-Phase Flow Characterization and CFD SimulationS; *Separation Science & Technology Journal;* 2006, **41**: 1411 – 1445.

ABSTRACT

Submerged flat sheet membranes are mostly used in membrane bioreactors for wastewater treatment. The major problems for these modules are concentration polarization and subsequent fouling. By using gas-liquid two-phase flow, these problems can be ameliorated. This thesis aimed to optimize the use of gas-liquid two-phase flow as a cleaning mechanism for submerged flat sheet membrane. The effect of various hydrodynamic factors such as airflow rate, nozzle size, nozzle geometry, intermittent bubbling, intermittent filtration, channel gap width, feed concentration and membrane baffles were investigated for model feed materials (yeast suspensions and mixed liquor from activated sludge plants). Insights into mechanisms by which two-phase flow reduces fouling for submerged flat sheet membranes were obtained by using Computational Fluid Dynamics.

Experiments conducted showed that an optimal airflow rate exists beyond which no further flux enhancement was achieved. Fouling reduction increased with nozzle size at constant airflow. Nozzles of equal surface area but different geometries performed differently in terms of fouling reduction. Bubble size distribution analyses revealed that the percentage of larger bubbles and bubble rise velocities increased with the airflow rate and nozzle size. Thus the results of this study suggest that the effectiveness of two-phase flow depends on the bubble size. CFD simulations revealed that average shear stress on the membrane increased with airflow rate and bubble size and further indicated that an optimal bubble size possible exists. Using intermittent filtration as an operating strategy was found to be more beneficial than continuous filtration. This study also showed the importance of the size of the gap between the submerged flat sheet membranes. Increasing the gap from 7 mm to 14 mm resulted in an increase in fouling by about 40% based on the rate of increase in suction pressure (dTMP/dt).

Finally, this is the first study which investigated the effect of baffles in improving air distribution across a submerged flat sheet membrane. It was found that baffles decreased the rate of fouling at least by a factor of 3.0 based on the dTMP/dt data.

TABLE OF CONTENTS

NOMENCLATURE

a	constant in Equation 4.10
A	cross section area (m^2)
b	constant in Equation 4.10
C_b	bulk concentration (kg/m^3)
C_d	drag coefficient
d,D	diameter (m)
f	fraction of space occupied by the liquid phase
F_{SF}	surface tension force
g	gravitational acceleration (m/s^2)
G	mass flowrate (kg/s)
J	permeate flux ($l/m^2.hr$)
K	permeability of the system ($l/m^2.hr.Pa$) (Eqn 4.9)
K'	constant that depends on membrane properties (Eqn. 4.10)
Ko	orifice constant determined experimentally
l	length of pipe (m)
L_i	instantaneous permeability ($l/m^2.hr.Pa$)
m	mass of deposited cake (kg)
$\boldsymbol{M_{kl}}$	inter-phase momentum exchange term between phase *k* and phase *l*
MLSS	mixed liquor suspended solids concentration (g/l)
N_f	fouling or resistance number
N_s	shear stress number
p	absolute pressure (atm)
P	pressure (Pa)
ΔP	pressure drop (Pa)
Q	volumetric flowrate (m^3/s)
R_f	fouling resistance (m^{-1})
R_h	hydraulic resistance (m^{-1})
R_m	membrane resistance (m^{-1})
R_{tot}	total resistance across the membrane (m^{-1})
t	time (s)
TMP	trans-membrane pressure (kPa)

u fluid velocity (m/s)

u^* two-phase flow velocity (m/s)

U superficial fluid velocities calculated (m/s)

v_m specific volume of air (m^3/kg)

V volume of the spherical bubble (m^3)

V_L lift velocity (m/s)

Greek letters

α specific cake resistance (m/kg) (Eqn 3.1)

volume fraction (chapter 6)

ϕ TMP reduction factor (Equation 3.2)

geometric hindrance factor of the membrane (Eqn. 4.10)

friction factor (Eqn. 5.1)

μ fluid viscosity (Pa.s)

ρ density of the fluid (kg/m^3)

σ surface tension (dyne/cm)

τ viscous stress tensor

Superscripts and subscripts

bl bubble

c filter cake

crit critical flux

g gas phase (air)

l liquid phase (water)

or orifice

ss steady state condition

Dimensionless numbers

Eötvös $\rho g D^2/\sigma$

Froude U_t^2/gD

Morton $g\mu^4/\rho\sigma^3$

Reynolds $\rho U_t d_{bl}/\mu$

Weber $\rho U_t^2 d_{bl}/\sigma$

Chapter 1

INTRODUCTION

1.1 THE GLOBAL WATER CRISIS

Among the natural resources that are indispensable for human welfare and socio-economic development, water is ranked number one. However, scarcity and misuse of this life-supporting resource poses a serious and growing threat to food security, human health and the environment. The United Nations International Drinking Water and Sanitation Decade (1981-1990) set its goal to provide safe drinking water and sanitation for the entire world's people. However, a decade later more than one billion people in the world still do not have access to clean drinking water and more than 1.7 billion lack access to sanitation (Vigneswaran and Visvanathan, 1995). Problems arise because the fresh water resources are distributed unevenly over the earth's surface. There are four major global problems concerning fresh water: 1) shortage of renewable supplies, 2) unequal distribution of supplies, 3) problems of water quality and health, and 4) disastrous effects of unrestrained construction of dams (Gleick, 2004).

The World Bank at some time stated that the way the human race is dealing with its fresh water supplies needs to change drastically, and that people will have to acknowledge that fresh water is a scarce natural resource that needs to be treated with great care (Brans, 1997). Consequently, governments around the world are now laying very stringent standards for treated wastewater effluent in order to enable water recycling. Whilst recycled water is primarily being used for secondary purposes, such as agriculture and industrial use, in some countries like Namibia and Singapore, it is used for human consumption.

1.2 BACKGROUND TO THE PROPOSED RESEARCH

Conventional wastewater treatment processes are no longer able to meet the newly laid standards for treated wastewater effluent. Amongst various technologies that have been developed or are in the process of development in order to overcome the inadequacies of traditional wastewater treatment processes, are membrane bioreactors (MBRs). Membrane bioreactors involve the combination of membranes, mainly micro- and ultrafiltration, with biological reactors. There are three generic ways in which membranes can be coupled to biological reactors for: 1) separation of and retention of solids; 2) bubble-less aeration within the bioreactor; and, 3) extraction of key organic pollutants from industrial wastewaters. Utilisation of MBRs for solid-liquid separation is, however, the most widely studied and has found full-scale application in many and mostly developed countries (Visvanathan et al., 2000). The membranes can be placed in an external circuit of the bioreactor or they can be submerged directly into the bioreactor.

Over the past few decades, the submerged MBR has been scaled-up from laboratory-scale to commercial-scale wastewater treatment technology of up to 10, 000 m^3 / day (Churchouse & Wildgoose, 1999). Improvements in membrane properties and dramatic reductions in membrane costs make submerged MBRs increasingly competitive with conventional sewage treatment technologies. This technology has proved to have advantages of a small footprint, high removal of chemical oxygen demand (COD), effective nitrification/denitrification, less production of excess sludge, and to be a reliable and simple technology to operate (Visvanathan et al., 2000). Despite MBRs having superior performance to conventional wastewater treatment processes, they still suffer from the problem of permeate flux decline with time which is inherent to all membrane processes. Decline of flux with time has been linked to concentration polarisation (CP) and fouling (Fane, 2000).

There are several strategies that have been researched in order to improve the flux in membrane processes such as insertion of turbulence promoters in the feed channel (Finnigan & Howell, 1990), rotating membranes (Kroner et al., 1987), use of Dean vortices (Mouline et al., 1996) and unsteady or pulsatile flow (Gupta et al., 1992). These strategies are reviewed briefly in Chapter 2 in order to reveal their limitations. In this study the potential of gas-liquid two-phase flow, as a flux enhancing mechanism for a submerged flat sheet membrane has been researched.

Membranes can be configured mainly in four different types of modules. These are: tubular, hollow fibre, flat sheet / plate and frame, and spiral wound. Gas-liquid two-phase flow has been shown to be successful in reducing fouling in all these modules except the spiral wound module. The advantages and disadvantages of the four major types of modules have been summarized in Table 1.1. Modules employed in commercial MBR systems range from flat sheet / plate and frame (Kubota, Japan; Rhodia Pleiade-based MBR system, France) to tubular (Milleniumpore, UK) or hollow fibre (Zenon Environmental Ltd., Canada). The choice of the configuration is influenced by whether the membrane element is placed within the bioreactor or external to it.

Table 1.1 Module concepts and their characteristics (after Fane, 2000)

Characteristics	**Module concepts**			
	Flat plate	**Spiral wound**	**Shell and tube**	**Hollow fibre**
Packing density (m^2/m^3)	Moderate (200 – 400)	Moderate (300 –900)	Low (150 – 300)	High (9000 – 30,000)
Fluid management	Good (with spacers)	Good (with spacers)	High pumping cost	Good
Suspended-solids capacity	Moderate	Poor	good	poor
Cleaning	Sometimes difficult	Sometimes difficult	easy	Bachwashing possible
replacement	Sheets or cartridge	Cartridge	tubes	cartridge

1.3 JUSTIFICATION FOR THE PROPOSED RESEARCH

The concept of using gas bubbles to enhance membrane processes was first introduced by Imasaka and co-workers in 1989. Since then, the introduction of gas-liquid two-phase flow has been shown in many studies to significantly enhance the performance of various membrane processes. The majority of studies on bubbling have been conducted for the membrane applications in which the feed suspension flows inside the membrane module. Despite a fast increasing number of publications regarding the use of two-phase flow for these types of modules, the mechanism of flux enhancement is not yet fully understood and hence the use of two-phase flow in these membrane modules has not been optimised.

The introduction of submerged membrane systems with membranes in a tank rather than a cross-flow vessel, has led to a greater interest in bubbling. The advent of submerged, or immersed, membranes has, on the one hand, eliminated the need for the pressurised module but, on the other hand, provided a challenge for achieving control of concentration polarisation and fouling. To date there has been considerably more attention given to the application of two-phase flow in submerged hollow fibre systems than to submerged flat sheet membranes. Limited data of a fundamental nature have been published for bubble interactions with submerged flat sheet membranes. This limited data has largely come from commercial suppliers of membrane systems and, as a result, much of the know-how is not published. There is therefore a need to study the use of gas-liquid two-phase flow for submerged flat sheet membranes in order to fully understand the mechanisms involved in flux enhancement so that the process could be optimised.

Bubbling, in common with other polarisation control techniques has an energy demand and efforts must be aimed at the minimisation of this energy. The energy involved in providing bubbling to submerged membranes can become a considerable cost factor, particularly for MBRs which must compete with conventional wastewater bioreactors where aeration is only required for the biological processing. Fortunately, membrane costs are showing a declining trend that lowers the capital costs of membrane plants, but if bubbling is not optimised, it is likely to keep the operating costs high.

Moreover, there are also unresolved issues in terms of the required bubble size and frequency for optimal operation. The correct combination is module and feed specific. To identify the best strategies it is necessary to model bubbling systems using techniques such as computational fluid dynamics (CFD). For submerged systems, the bubble-induced depolarisation mechanism needs to be better understood and CFD modelling could play a vital role. The overall aim of this work is therefore to study and optimise the use of gas bubbling for submerged flat sheet membrane and to gain a better insight into the flux enhancement mechanism by conducting experiments as well as CFD modelling.

1.4 OBJECTIVES OF THIS THESIS

The objectives of this thesis are as follows:

- Characterize the effect of hydrodynamic operating parameters (such as, air flow rate, nozzle size and geometry, channel gap width, intermittent suction and intermittent bubbling) on two-phase flow characteristics (such as bubble size distribution, bubble rise velocity) and on membrane performance (in terms of flux, trans-membrane pressure, critical flux and permeate quality) using model feeds.
- Evaluate the viability of using membrane baffles as a possible means of improving the efficiency of two-phase flow for submerged flat sheet membranes.
- Identify optimum two-phase flow operating conditions for a given feed solution.
- Validate two-phase flow numerical models and then use them to model two-phase flow dynamics in submerged flat sheet membranes using a commercially available computational fluid dynamics code.

1.5 ORGANIZATION OF THIS THESIS

This thesis contains eight chapters.

Chapter 1 states the general background to the problem being researched which presents the basis for this study. The justification for and the objectives of the research are given.

Chapter 2 provides a literature review of membrane bioreactors, flux enhancing strategies and use of two-phase flow to enhance flux in membrane processes.

In Chapter 3 the experimental results on the filtration of a yeast suspension are presented. The effects of different air flow rates, different nozzle geometries and different nozzle sizes, as well as other hydrodynamic parameters, have been studied. A comparison between bubbling with and without membrane baffles is also presented.

Chapter 4 will present results of experiments almost similar in nature to those in chapter 3 but conducted on a real waste activated sludge suspension which is a typical feed for commercial membrane bioreactors operate with.

Chapter 5 deals with the characterization of two-phase flow in terms of bubble properties and size distribution. Analyses of digital images and videos recorded for different bubbling conditions have been conducted using particle imaging software. A correlation between bubble properties and degree of flux enhancement as realised in chapters 3 and 4 is developed.

Chapter 6 presents validation of the two-phase flow numerical methods commonly used in literature to model two-phase flow. Published experimental data are used to validate the models. The validated models are then used to simulate laminar two-phase flow inside tubular membranes in order to gain some insights into wall extraction effects.

In Chapter 7, results of the two-phase flow CFD simulations for a submerged flat sheet membrane are presented. Simulations completed on a single bubble rising in a rectangular tank between narrow walls and those of two-phase flow in a flat sheet submerged MBR obtained by using a two-fluid Eulerian model are discussed.

Chapter 8 summarises the main findings, provides general conclusions, and makes recommendations for future work.

Chapter 2

LITERATURE REVIEW

2.1 INTRODUCTION

Studies on the application of gas-liquid two-phase flow as a fouling mitigation strategy in membrane systems are on the increase, particularly because this strategy promises lower energy demands compared to other well studied flux enhancing strategies such as high cross-flow velocities, Dean vortices and rotating membranes. Consequently, the number of publications on the use of gas-liquid two-phase flow in membrane applications has risen sharply in the last decade. Although two-phase flow can be used in a wide range of membrane applications, it is currently being predominantly used in commercial membrane bioreactors (MBRs), most of which use a submerged membrane module, either hollow fibre or flat sheet.

This chapter will start by reviewing the development of MBRs as they are the central focus of this study. The knowledge gained in this research will mostly be applicable to MBRs. Since the main objective of this thesis is optimization of a flux enhancing strategy, a review of traditional flux enhancing strategies will be conducted in section 2.3 in order to pinpoint their inherent deficiencies.

The bulk of this chapter contains a review of the studies on two-phase flow applications in membrane processes (section 2.4). Despite the commercial dominance of the submerged MBR process, there are a limited number of studies which have reported on the air sparging in a submerged MBR configuration, particularly the submerged flat sheet setup. Most two-phase flow studies have concentrated on bubbling inside tubular or hollow fibre modules. At the end of this chapter a summary of important findings from all the studies reviewed will be provided and the knowledge gap which laid the foundations for this study will be clearly identified.

This thesis also covers work on the simulation of two-phase flow using CFD tools. However, literature pertaining to the CFD investigations will not be reviewed in this chapter but instead will be integrated into the respective CFD chapters, namely, chapter 6 and 7. Basic membrane principles have also not been reviewed in this chapter as this is considered now to be fairly common knowledge. Detailed description of the principle of operation of membrane processes can be found in the works of Fane (1986), Mulder (1996) Stephenson et al. (2000) and Roest (2002).

2.2 OVERVIEW OF MEMBRANE BIOREACTORS

The use of biological treatment can be traced back to the late nineteenth century. By the late 1930s, it was a standard method of wastewater treatment (Rittmann, 1987). During the course of anaerobic or aerobic digestion, soluble organic matter is biodegraded into various end-products such as H_2O, CO_2, CH_4 and biological cells. After removal of the soluble biodegradable matter in the biological process, any biomass formed must be separated from the liquid stream to produce the required effluent quality. A secondary settling tank is traditionally used for the separation and this clarification is often the limiting factor in effluent quality (Benefield & Randal, 1980).

The quality of the final effluent from conventional biological treatment systems is highly dependent on the hydrodynamic conditions in the sedimentation tank and the settling characteristics of the sludge. Consequently, large volume sedimentation tanks offering several hours of residence time are required to obtain adequate solid-liquid separation (Fane et al., 1978). At the same time, close control of the biological treatment unit is necessary to avoid conditions that lead to poor settleability and / or bulking of sludge. A correct food to microorganism ratio (F/M) must be maintained in order to deter proliferation of filamentous bacteria that results in sludge with poor settling properties. Very often, however, economic constraints limit such control options. Even with such controls, further treatment, such as filtration or carbon adsorption are needed for most wastewater reuse applications. Therefore, a solid-liquid separation method different from conventional methods is desirable.

Application of membrane separation techniques for bio-solid separation can overcome the disadvantages of the sedimentation tank and biological treatment steps. The membrane offers a complete barrier to suspended solids and yields high quality effluent. Although the concept of an activated sludge process coupled with ultrafiltration was commercialised in the late 1960s by Dorr-Oliver (Smith et al., 1969), the application has only recently started to attract serious attention and there has been considerable development and applications of membranes processes in combination with biological treatment over the last 10 years (Churchouse & Wildgoose, 1999). Full-scale commercial aerobic MBR processes first appeared in North America in the late 1970s and then in Japan in the early 1980. The MBR technology did not enter Europe on a commercial scale until the mid – 1990s. According to Stephenson et al. (2000) there are over 500 commercial units in operation worldwide, 66% of which are in Japan. Around 98 % of these MBR combine membranes with aerobic process rather than anaerobic process. The MBR process in general, offers several advantages over the conventional processes currently available and these are tabulated in table 2.1.

Table 2.1. Advantages and disadvantages of MBR systems

Advantages of MBRs	**Disadvantages of MBRs**
Small footprint	Aeration limitations
Complete suspended solids removal from the effluent	Membrane fouling
Effluents disinfection	Membrane costs
Combined COD, solids and nutrients removal in a single unit	
High loading rate capabilities	
Low/zero sludge production	
Rapid start up	
Sludge bulking is not a problem	

2.2.1 Typical MBR configurations

Two main configurations are used for MBR systems, membranes submerged in the bioreactor or membranes external to the bioreactor (Figure 2.1). Both approaches have advantages and disadvantages (Table 2.2). For both approaches fouling is a major concern. As in any membrane system, membrane fouling by accumulation of various particulate and soluble materials in the mixed liquor needs to be properly controlled. The earliest MBR systems relied on placing the membranes in an external loop and applying a cross-flow, where the feed is introduced parallel to the membrane surface. Such an arrangement sweeps the accumulated solids away from the membrane surface.

Table 2.2. Comparison between external and submerged MBRs (after Cho, 2002)

Characteristic	Submerged	External
Flux	Low	Moderate
Fouling	Difficult	Less Difficult
Energy Use	Moderate	High to Moderate
Retrofit	Less Easy	Easy
Flexibility	Limited	Good

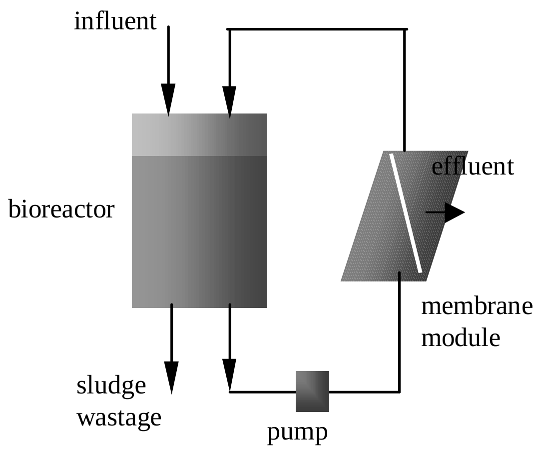

(A)

Figure 2.1 (a). Typical setup of an external side stream MBR system.

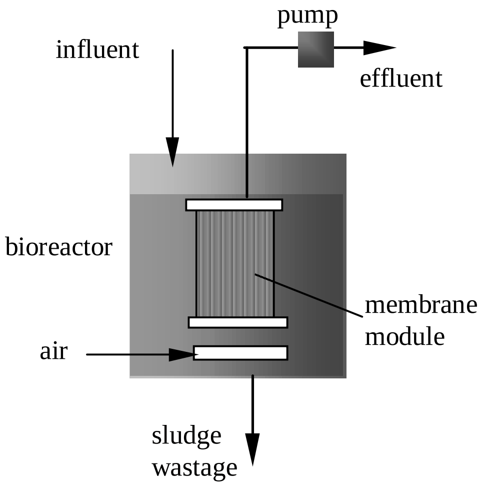

(B)

Figure 2.1 (b). Typical setup of a submerged MBR system.

In a side stream MBR [Figure 2.1 (a)], the cross-flow velocity typically ranges from 0.5 to 6 m s^{-1} (Lubbecke et al., 1995) with trans-membrane pressures up to 500 kPa. The operating conditions used depend on the degree of fouling and the membrane type. The tubular module is one of the most popular configurations among the family of membrane modules. Although the tubular module has disadvantages in terms of low packing density and high-energy demand, excellent control of concentration polarisation is possible through use of a high Reynolds number. Pumping costs in a typical external loop MBR process contribute 60 to 80 % of total operating cost, and energy usage can be in the range 4 ~ 12 kW h m^{-3} (Côté & Thompson, 1999).

In an attempt to reduce the energy demand in membrane operation, Yamamoto et al. (1989) immersed the membrane module inside the aeration tank and the permeate was extracted through the membrane by a suction pump. In this configuration, the need for the circulation pumping for the cross-flow was eliminated and the energy demand for the MBR process was substantially reduced. Côté and Thompson (1999) reported that the energy requirement for the submerged MBR is between 0.3 to 0.6 kW h m^{-3} including pumping and aeration. However, this energy demand is still higher than that for the conventional activated sludge process, which uses gravity and requires very little energy for the solid-liquid separation.

The advantages of the submerged system as opposed to the external membrane are:

- Elimination of the pressure vessel
- Reduction in energy requirements
- Ease of membrane replacement
- Simplified module scale-up

2.3 FLUX ENHANCING STRATEGIES

In almost all membrane processes, decline of permeate flux with time occurs if the driving force, for example, pressure, is kept constant; or the driving force increases with time if the permeate flux is kept constant. This occurs as a result of concentration polarisation and fouling which build up on the membrane surface. Consequently strategies are required to reduce the occurrence of concentration polarisation and fouling. The major factors which cause the flux to decline are attributable to increases of the cake resistance and membrane resistance. Approaches to preventing flux decline are therefore focused on preventing increases in these resistances. Depending on the factors limiting flux in specific applications, the flux enhancing strategies can be classified into three groups, as shown in Table 2.3. The gas-liquid two-phase flow strategy studied in this work is a hydrodynamic strategy, therefore only other strategies which involves manipulation of hydrodynamic conditions will be briefly reviewed.

Table 2.3. Some strategies for control of flux decline

STRATEGY	**TECHNIQUE**
Control of membrane properties	Alteration of hydrophilicity Alteration of surface charge
Pre-treatment of the feed	Removal of suspended solids Adjustment of pH and ionic strength
Hydrodynamic / operational control	Alteration of crossflow velocity Use of rotating membranes Generation of secondary flows Design of inserts Pulsation

2.3.1. Operational / hydrodynamic modifications

The approach of modifying operational or hydrodynamic conditions aims to prevent flux reduction by preventing the deposition of the particle layer. The methods include increasing the shear rate on the membrane by increasing the cross-flow velocity, generation of secondary flows (e.g. in curved flow channels), rotating the membrane, putting inserts inside the membrane channel to promote the shear in local regions, applying pulsatile flow, or combining pulsatile flow with inserts. The following sections give a more detailed review of these methods.

2.3.1.1. Increased cross-flow velocity

Many works (Baker et al., 1985; Riesmeier et al., 1987; Bertram et al., 1991) have studied the influence of cross-flow velocity on the permeate flux. The results consistently show that higher fluxes were obtained at higher cross-flow velocities. This was attributed to increased shear-induced particle back-transport to the bulk flow. The major downfall of increasing the cross-flow velocity is that energy consumption increases with an increase in velocity.

Fisher and Raasch (1985) and Mackley and Sherman (1992) reported that beyond a certain velocity value, the flux decreased with increasing cross-flow for microfiltration of particles with larger mean sizes (20 µm and 150 µm, respectively) and with a relatively broad particle size distribution. Both of these studies showed that, although the cake thickness decreased significantly with increasing cross-flow velocity, the cake resistance did not decrease. This was attributed to the fact that at higher velocities the mean particle size of the cake layer was smaller, despite the fact that the cake layer was thinner at lower velocities. Consequently, the cake resistance was higher at higher velocities with smaller particles than at lower velocities with bigger particles.

2.3.1.2. Curved channel

Brewster et al. (1993) studied the possibility of using Dean vortices in a curved channel to utilise the fluid instability of the flow to reduce the build-up of the solute near the membrane wall. Figure 2.2 (f) presents a schematic diagram of the vortices in curved channels. Brewster et al. (1993) proposed a way of designing a spiral wound module so as to satisfy the neutral stability at every point of the curved channel. A major disadvantage of the curved channels is that they have very high pressure drop across the module.

2.3.1.3 Rotational membrane modules

Rotational membrane modules are also known as dynamic filters or shear filters (Kroner & Nissinen, 1988; Müller & Kroner, 1992). The membrane module is constructed with an inner (or in some cases an outer) annular rotating cylinder [refer to Figure 2.2 (e)]. The rotation enhances shear near the membrane wall. For the inner rotated filter, the actual wall shear is enhanced by means of Taylor vortices. The disadvantages of this type of module include the extra energy requirement for the rotation and the complexity of the module design.

2.3.1.4 Surface shape

Use of the shape of the membrane surface to enhance vortices or radial mixing has also been studied (Jeffree et al., 1981; Ralph, 1986). With this method [Figure 2.2 (b)], it has been demonstrated that high shear produced by bulk flow instabilities can result in substantial increases in membrane permeation rates for “difficult” feeds. However, it is difficult to scale-up these modules to intermediate or larger sizes and their applications are often limited by their inordinately high axial pressure drop (Winzeler & Belfort, 1993).

2.3.1.5 Inserts

Inserts have also been introduced into the membrane channel as static mixing devices and turbulence promoters (Peri & Dunkley, 1971; Mavrov et al., 1992) [refer to Figure 2.2 (a) and (c)]. Experiments showed that compared with empty feed channels, turbulence promoters often enhance the convection of particles from the region of the membrane back to the bulk flow thus producing higher permeate flux for the same feed velocity. However, use of these devices is limited to tubular designs (Illias & Govind, 1990).

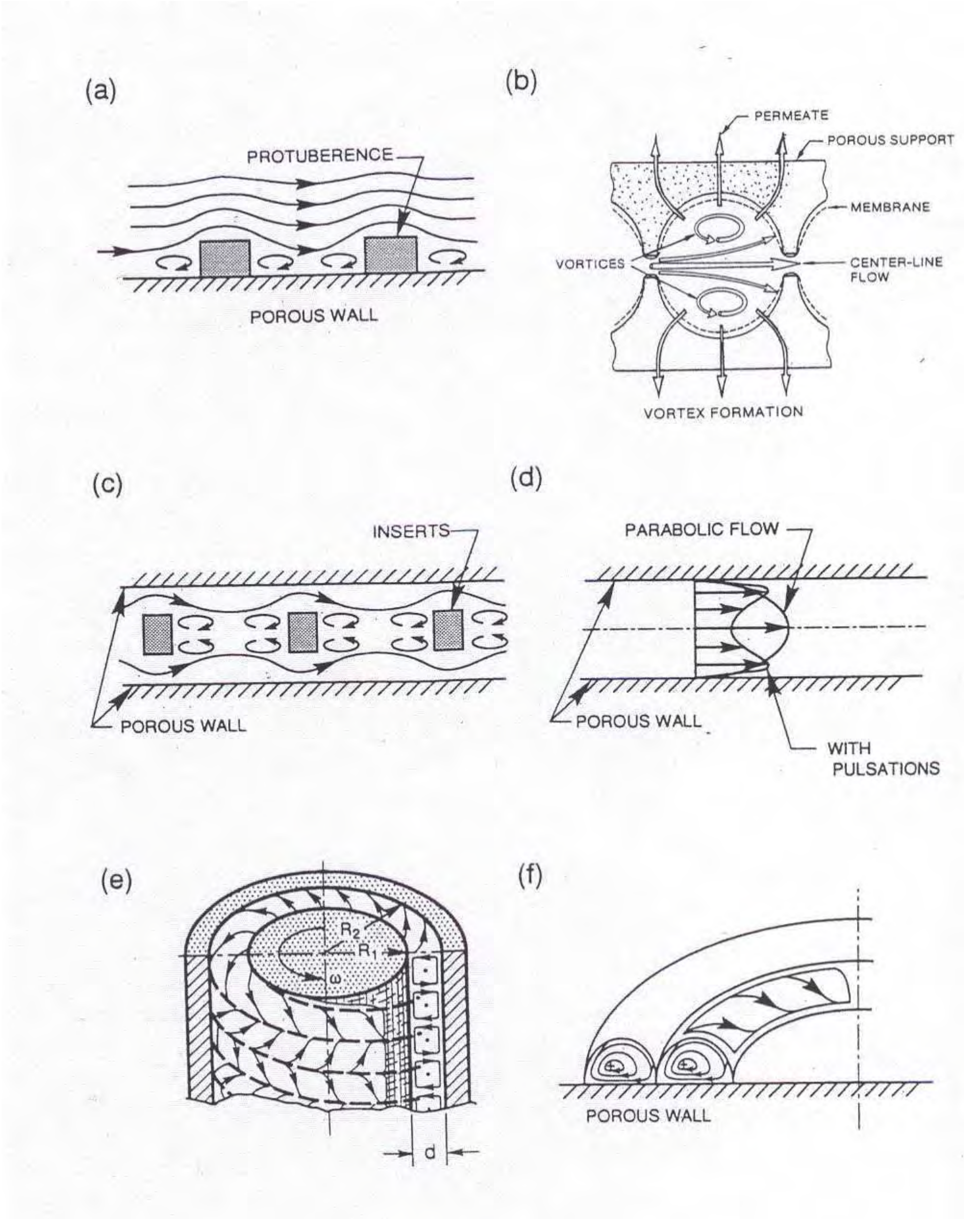

Figure 2.2. Flux enhancing mechanisms: (a) placing turbulence promoters on the membrane, (b) using corrugated membrane surface, (c) placing inserts within the flow channel, (d) inducing flow pulsations, (e) rotating membrane to form Taylor vortices, and (f) flow in a curved channel to produce Dean vortices (after Winzeler and Belfort, 1993).

Krstić et al. (2002) studied the effectiveness of turbulence promoters on cross-flow microfiltration of skimmed milk. A Kenics static mixer was employed as a turbulence promoter for organic membranes with pore sizes of 50, 100 and 200 nm. Flux enhancements of up to 500 % were achieved. They also found that using turbulence promoters was more energy efficient than operation without them. Permeate flux enhancement was correlated with the increase in wall shear stress generated by the static mixer.

Finnigan and Howell (1989; 1990) used baffle inserts together with pulsatile flow to generate a vortex to enhance the mixing of the fluid in the region of membrane surface and / or interrupt the development of the concentration polarisation layer or cake layer, thereby improving the permeate flux. They reported flux increases of a factor of 2.5 by incorporation of periodically spaced baffles of a doughnut or disc shape within the membrane tube. Colman and Mitchell (1990) estimated the mass transfer coefficient and residence time distribution for a baffled pulsatile flow with ultrafiltration. Their results showed that the mass transfer at the membrane surface was significantly enhanced by a baffled channel, and it was further improved with pulsatile crossflow.

Millward et al. (1995) used screw-thread promoters to improve flux for ultrafiltration and microfiltration of Bovine Serum Albumin (BSA) and bovine blood in a half-inch tubular membrane. The convective mixing in each system was augmented through a combination of two vortex patterns: helical flow around a semi-circular section and flow through a sudden expansion. Whilst they found the internal screw-thread to perform poorly when applied to the separation of plasma from whole blood because the centrifugal forces appeared to complement concentration polarisation, the external screw-thread on the other hand was found to be an effective anti-fouling technique and it tripled the microfiltration performance.

A common characteristic of the above approaches is the variation of fluid hydrodynamics in the membrane module in order to increase the shear or to promote flow vortices (Taylor, Dean vortices) in order to reduce the resistance to permeation due to fouling or particle deposition. A major setback of these strategies that use inserts is that they are energy intensive, depend on the module type and application process, and some of them are not easy to scale-up.

2.3.1.6 Pulsatile flow

Kennedy et al. (1974) reported that pulsating the feed flow over the membrane increased the mass transfer coefficient in reverse osmosis of sucrose solution. The permeate flux was increased up to 80 % with a pulsating frequency of 1 Hz. Bauser et al. (1982)

reported a 40 % increase in flux at 0.5 and 1 Hz frequency for whey and whole blood, respectively. These authors suggested that manipulation of the amplitude and frequency of the oscillatory components were required to reduce concentration polarisation and fouling. Jaffrin and his co-workers have also conducted a series of experiments involving pulsatile crossflow filtration (Jaffrin et al., 1989; Jaffrin, 1989; Jaffrin et al., 1992). Their latest studies looked in some detail at the mechanics of pulsatile flow during the filtration process. In a study on the effect of pulsatile flow on plasma separation with a microfiltration membrane, flux enhancement was attributed to the enhanced shear during pulsatile flow.

Gupta et al. (1992) investigated flux enhancement by pressure and flow pulsations in microfiltration with mineral membranes. The pulsations were generated by a piston in a cylinder, and various wave forms were generated by controlling the piston motion. Four types of wave forms were generated with different pressure wave shapes at a frequency of 1 Hz. Higher fluxes were obtained for all four types of pulsatile flows. The largest permeate increase observed from a typical wave form was 45 %. It was observed that the permeate flux increased almost simultaneously with increasing pressure, but decreased more slowly than decreasing pressure. The authors speculated that the drop in pressure destabilised the deposited particles, thereby enhancing the flux more effectively than increasing the pressure.

2.3.1.7 Backflushing

Backflushing involves reversal of the permeate flow which is achieved by applying a higher pressure on the permeate side. One of the most important features of the Memtec Ltd Memcor® continuous microfiltration (CMF) operation is the patented air backwash system (Fane, 2000). In the CMF operation, when the pressure difference across the membrane (TMP) reaches a pre-set level, filtration stops and high pressure air is injected at the permeate sides of the membrane. The air blasts through the membrane pores dislodging the accumulated sediments. This air backwash process is illustrated in Figure 2.3.

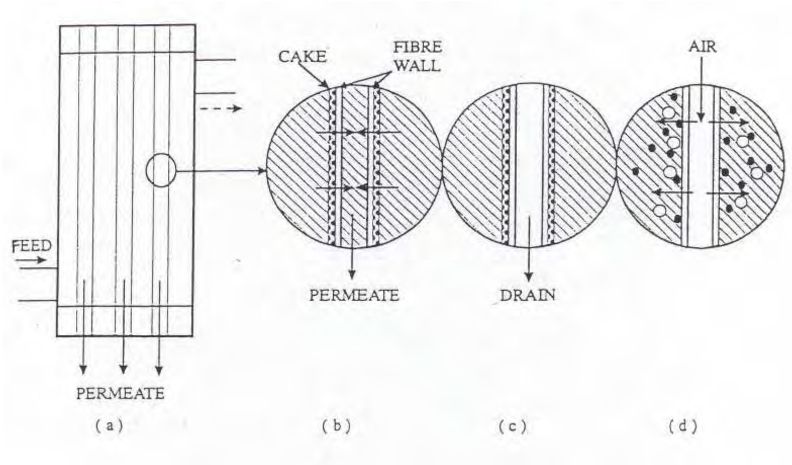

Figure 2.3. Principle operation of the Memtec air backflush system: (a) module schematic, (b) filtration stage – single fibre, (c) lumen drainage, (d) air back-pulse (from Fane, 2000).

Rodgers and Sparks (1991) investigated the influence of back pulsing of trans-membrane pressure (TMP) on ultrafiltration fouling reduction. In their studies, the pulse was produced by periodically pressurising the permeate with nitrogen gas so that an instantaneous negative TMP was produced. With the pulsed process, the permeate flux was dramatically increased for the ultrafiltration of protein compared to the steady-state operation.

Wenten et al. (1994) also experimented with backflushing during microfiltration of yeast and obtained much higher permeate flux compared with the "normal" flux at steady-state. The authors reported that the level of back pressure (that is, reversed TMP) and the intervals between two backflushes were the significant parameters which influenced the flux performance. With this technique, a stable high flux over a long period of time, low trans-membrane pressure and low cross-flow velocity was reported.

Some of the negative aspects of the backflushing process are that sometimes the permeate is used in the backflushing process which is counterproductive and energy is required to create TMP reversal. This technique is also not suitable for some membrane modules, for example, it cannot be used on most flat sheet membranes.

2.4 THE USE OF GAS BUBBLING TO ENHANCE MEMBRANE PROCESSES

The most recent studies on enhancing mass transfer in membrane processes have focused on gas-liquid two-phase flow (Mercier-Bonin et al., 2004; Pospisil et al., 2004; Laborie & Cabassud, 2005; Sur & Cui, 2005). This technique was first proposed by Imasaka and co-workers in 1989 who developed a gas-liquid two-phase cross-flow microfiltration process coupled with an anaerobic digester. The methane generated was injected into ceramic membrane modules and proved to be effective in reducing the rate of membrane fouling and to have low energy usage. Most of the studies on two-phase flow have focused on external types of membrane application systems, where bubbling is on the lumen side of the membrane. The membrane modules that have been extensively studied are the hollow fibres (HF) and tubular membranes because most membrane systems employ these types of modules. For flat sheet modules, very few studies have been reported. Lee et al. (1993) reported that two-phase flow enhanced flux for ultrafiltration (UF) and microfiltration (MF) flat sheet organic membranes and Meircier-Bonin et al. (2000a) also reported enhancement of flux by two-phase flow in filtration of bakers' yeasts suspension using a ceramic flat sheet membrane. Recently, Ducom et al. (2002a) observed benefits of injecting gas during nanofiltration of oil/water suspensions by a flat sheet membrane. Although these studies used flat sheet membranes, they were external type applications where the two-phase flow mixture was pumped across the membrane surface. For submerged flat sheet membranes, the only studies reported are for the membrane bioreactor (MBR) application for wastewater treatment (e.g. Churchouse & Wildgoose, 1998; Howell et al., 2004), in which the gas-liquid two-phase flow serves two purposes: (1) to reduce fouling, (2) to provide oxygen needed for biological degradation.

2.4.1 Characterisation of gas-liquid two-phase flow

2.4.1.1 Two-phase flow in vertical tubes

For gas-liquid mixtures flowing in a tube, different flow patterns can be observed. Depending on the distribution of the two phases in the duct, four basic flow patterns were suggested by Taitel et al. (1980) (see Figure 2.4):

- Bubble flow: The gas phase is approximately uniformly distributed in the form of discrete bubbles in a continuous liquid phase.
- Slug flow: most of the gas is located in large bullet shaped bubbles which have a diameter almost equal to the pipe diameter and are sometimes designated as "Taylor bubbles”. They move uniformly upward and are separated by liquid slugs which may contain small gas bubbles. Around the Taylor bubbles, there is a thin falling liquid film, which generates turbulence in the wake of the Taylor bubble.

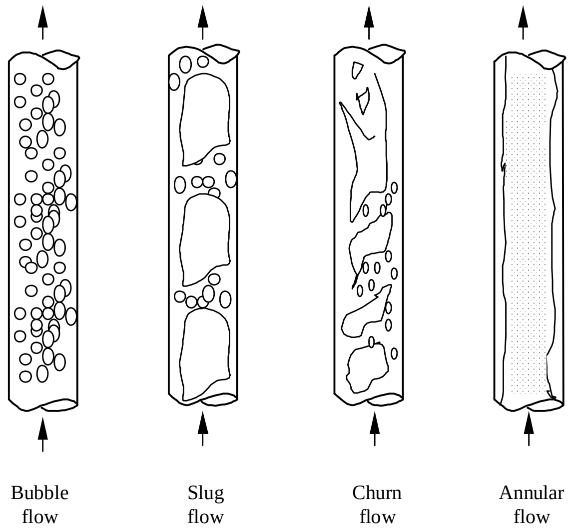

Figure 2.4. Different flow patterns for two-phase flow in a vertical pipe (after Taitel et al., 1980).

- Churn flow: Churn flow is somewhat similar to slug flow. It is, however, much more chaotic, frothy and disordered.
- Annular flow: Annular flow is characterized by the continuity of the gas phase along the core of the pipe. The liquid phase moves upwards, partly as wavy liquid film and partially in the form of drops entrained in the gas flow.

The flow pattern depends on the gas and liquid flow rate, as well as the diameter of the duct (Taitel et al., 1980; Hewitt, 1990). For two-phase flow filtration, the flow path for the gas-liquid mixture is relatively narrow and the liquid velocity is usually set at a low value, so the prevalent flow pattern for two-phase flow filtration is slug flow.

Slug flow is a highly unsteady flow. During the filtration, the falling film zone around the Taylor bubble and the liquid slug zone alternately contact the membrane surface. The hydrodynamic environment in the liquid zone and the shear rate caused by the falling film flow exert important effects on filtration performance. A number of studies have demonstrated that the turbulence caused by air injection is effective for control of concentration polarization and particle deposition on the membrane surface (Cui & Wright, 1994 & 1996; Mercier et al., 1995; Cabassud et al., 1997).

2.4.1.2 Two-phase flow in wide channels

When two-phase flow occurs in wide channels, which are not as restrictive as tubular or hollow fibre geometries, different flow patterns are observed. The commonly observed bubble shapes in these channels are spherical, ellipsoidal or hemispherical depending on the bubble size. Clift and co-workers (1978) conducted a series of investigations and developed a chart which can be used to predict the shape of the bubble. Figure 2.5 correlates the shape of the bubble with the Reynolds number and the Eötvös number. The properties of various bubbles can be summarised as follows (Cui et al., 2003).

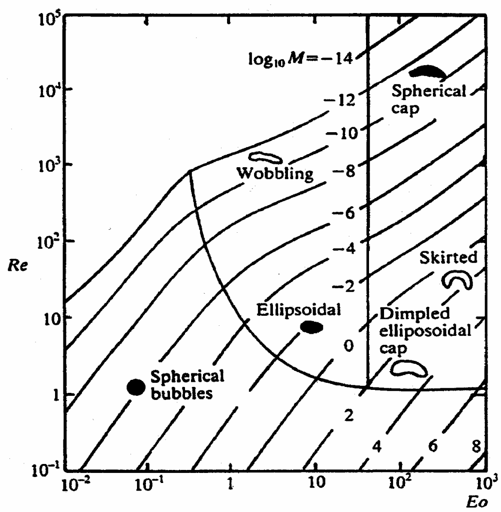

Figure 2.5. Bubble characteristic chart (after Clift et al., 1978).

Spherical Bubbles: The size is typically < 1 mm and the bubble can be treated as a solid particle which is lighter than the surrounding liquid. The terminal rise velocity of isolated bubbles is approximated by Stokes Law (Re < 1),

$$u_{bl} = \frac{d_{bl}{}^2 g(\rho_l - \rho_g)}{18\mu_l} \qquad (2.1)$$

which predicts a rise velocity of about 0.1 m/s for a 0.8 mm bubble. In Equation 2.1, d_{bl} is the equivalent bubble diameter, ρ_l and ρ_g are liquid and gas densities respectively, g is gravitational acceleration and μ_l is the liquid viscosity. There is no boundary layer separation around the bubble, and hence no bubble wake. For bubbles rising in a swarm, as would be typical in a submerged membrane process, the rise velocity is reduced as the drag coefficient increases. Equation (2.1) also predicts that the bubble rise velocity is inversely proportional to the liquid viscosity and this can be significantly greater than for water in biomass suspensions, protein separations etc.

Ellipsoidal Bubbles: Sizes are typically 1.5 to 15 mm. The boundary layer separation occurs at a point on the bubble rim, and this point moves along the rim. The bubble is observed as a rocking disc and leaves a helical vortex starting at the boundary layer separation point at the rim. In the diameter range of 4 ~ 15 mm the bubble rise velocity in water does not change much and is approximately 0.24 m/s. This value would also tend to be lower in a swarm of bubbles and in liquids or suspensions of increased viscosity.

Spherical Cap Bubbles: Big bubbles (> 15 mm) take a spherical cap shape, and the boundary layer separates at the circular rim which shields vortex rings. The primary wake is about 4.5 times the volume of the bubble. These big bubbles can create a strong secondary flow effect and enhance local mixing in the liquid. In water, the rise velocity of these bubbles is approximated by,

$$u_{bl} = 0.71\ (g\ d_{bl})^{0.5} \qquad (2.2)$$

This equation predicts a rise velocity of about 0.3 m/s for a 20 mm bubble.

2.4.2 Flux enhancement by gas-liquid two-phase flow

2.4.2.1 Effect of injecting air and gas velocity

Cabassud and Ducom (2001) studied the effect of injecting air for a flat sheet "in-out" nanofiltration (NF) membrane. Clay suspension was the model fluid. Their results showed that, the higher the air flowrate, the higher the factor by which flux is enhanced. Filtration of a clay suspension was also studied by Laborie et al. (1997), where HF UF membranes were used. Their findings were similar to those of Cabassud and Ducom (2001) but they additionally observed that there was an optimal air velocity beyond which any further increase in air flow had a negative effect on flux. The critical gas velocity was 0.34 m/s, at which the flux was enhanced by 155 %. Optimal bubbling rates were also observed by Mercier et al. (1995) and Laborie et al. (1998), in which the optimal gas velocities were respectively found to be 0.43 m/s and 0.35m/s (see Figure 2.6).

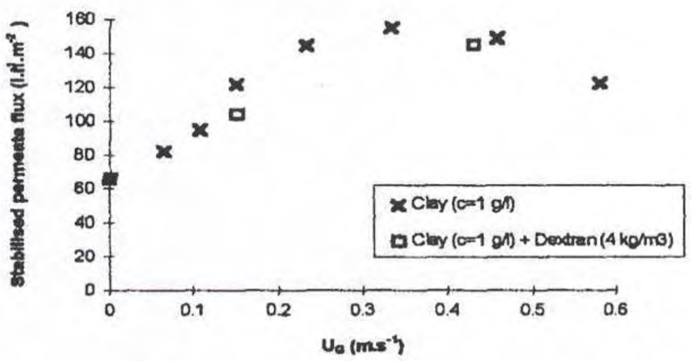

Figure 2.6. Effect of air velocity on the steady-state flux (after Laborie et al., 1998).

In a study by Li et al. (1997b) where macromolecules such as human serum albumin (HSA) and human immunoglobulin (IgG) were filtered, the gas injection was found to be effective but flux enhancement was not sensitive to the increase in airflow. They deduced that flux enhancement by gas-liquid two-phase flow is linked to secondary flow induced by air bubbles. The flux was improved by up to 50% for HSA and IgG ultrafiltration. During crossflow ultrafiltration flux declines with time. Cabassud et al. (1997) demonstrated that the introduction of a gas can curb the decline of flux and that the higher the gas flow rate the higher the steady-state flux achieved (Figure 2.7). Unlike the previously cited studies, they did not observe an optimal gas flow rate beyond which any further increase in the gas flow rate was detrimental to the flux.

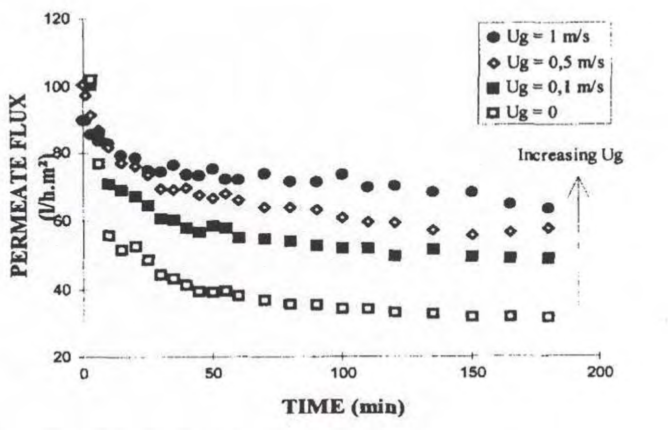

Figure 2.7. Effect of an intermittent injection process (source: Cabassud et al., 1997).

The effect of bubbling on a submerged "out-in" HF module was investigated by Chang and Fane (2001) in a specially designed cell, which caused the two-phase flow between the fibres to be slug flow. A yeast suspension was filtered. From their results, the filtrate collected after 90 minutes was 20 – 30 % higher than that obtained without bubbling. Another type of "out-in" application system was studied by Bouhabila et al. (1998). During the filtration of activated sludge they found that the fluxes obtained were always much less than the pure water fluxes, no matter the aeration rate used. This was explained by the existence of internal fouling. However, they identified a critical flux of about 20-25 $l/hr\cdot m^2$ (LMH) below which it was possible to operate without any internal fouling occurring of the membrane.

In a study by Sur and Cui (2001), bubbling was found to be most effective at low gas flow rates. In their study, a bakers' yeast suspension was cross-flow filtered through a 5 mm tubular MF membrane. It was observed that as the gas velocity increased from 0 to 0.18 m/s, there was a large change in flux but any further increase in gas velocity, up to 5 times more, had a rather minor effect. This implies that only a limited amount of gas, and hence energy, is required for flux enhancement by bubbling.

The recent studies of Mikulasek et al. (2002), Chua et al. (2002), Cui and Taha (2003), and Pospisil et al. (2004) all confirmed the effectiveness of two-phase flow in different membrane modules. These studies linked flux enhancement to bubble-induced secondary flow which promotes local mixing and hence enhance flux. Using CFD simulations, Cui and Taha (2003) observed high shear rates in the falling film between the bubble and the membrane wall in tubular membranes whilst the shear rate dropped to zero in hollow fibres, which explained why the observed flux enhancement was higher in tubular membranes than in hollow fibres.

2.4.2.2 Effect of liquid velocity

Liquid velocity is achieved by pumping the liquid across the membrane surface, but pumping the gas only, as is the case with some submerged membrane systems, also induces a liquid velocity across the membrane surface. This is known as an airlift system. Comparative studies between the pumped system and the airlift have been conducted. Chang and Fane (2001) obtained fluxes for pumped re-circulation which were 33 % higher than for the airlift submerged system using HF membranes (Figure 2.8). These researchers found that this difference in flux diminishes with a decrease in fibre diameter. Cui et al. (1997) also performed a comparison study between a pumped and an air lift system. In contrast, they found that the fluxes for the airlift system were about 30 % higher when compared with those for the single-phase flow pumped system (see Figure 2.9).

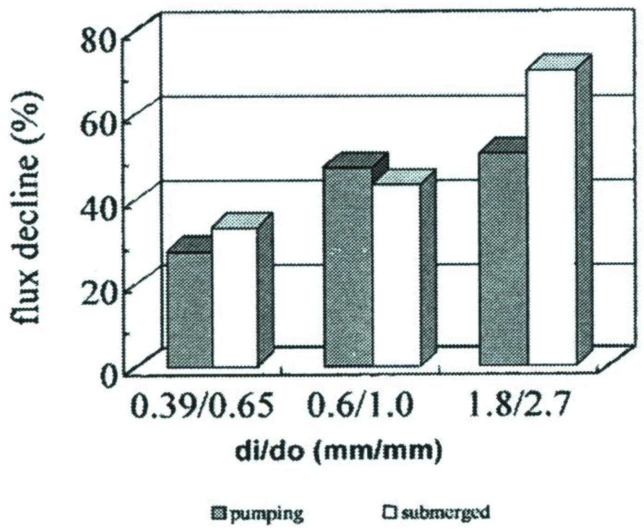

Figure 2.8. Flux decline after 90 min of filtration with pumping and airlift submerged system. Flux decline is higher for the submerged system. (Source: Chang & Fane, 2001). di and do are the hollow fibre internal and external diameters respecivley.

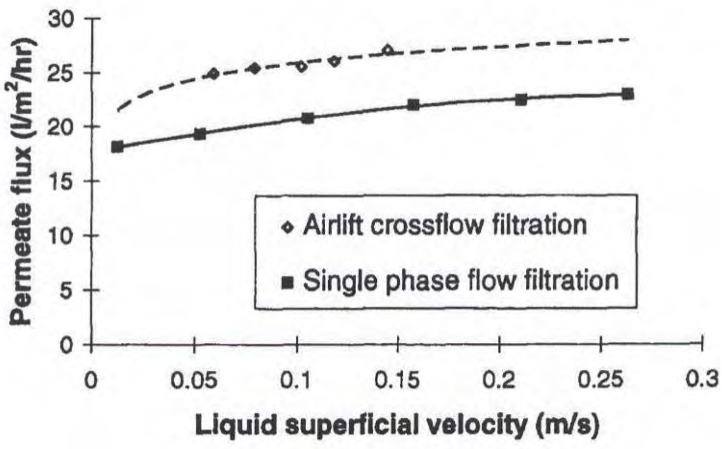

Figure 2.9. Comparison between the airlift and the single-phase flow system (Source: Cui et al., 1997).

Using an external HF membrane, Taha and Cui (2002a) studied the effect of liquid flow rate during the ultrafiltration of dextran. The gas flow rate was kept constant at 0.4 l/min. It was observed that when the liquid flow rate was increased from 2 to 3 l/min, the permeate flux increased but then decreased when the liquid flow rate was increased from 1 to 2 l/min. The same behaviour was observed by Sur et al. (1998). The fall in the flux is caused by shortening of the liquid slugs as the liquid velocity is increased but further increase in the liquid velocity causes the flow to be more turbulent and hence the mass transfer coefficient is increased again. These results are also supported by the findings of Cui and Wright (1996), who found that flux enhancement first increases with the gas-liquid mixture Reynolds number up to a ceiling, then any further increase in the Reynolds number resulted in flux decline (Figure 2.10). Recently, Smith and Cui (2004a) observed an optimal liquid flow rate for both single and two-phase flows for hollow fibre membranes. Beyond an optimal gas flow rate, both the permeability of the membrane and flux enhancement decreased when the liquid flow rate was increased.

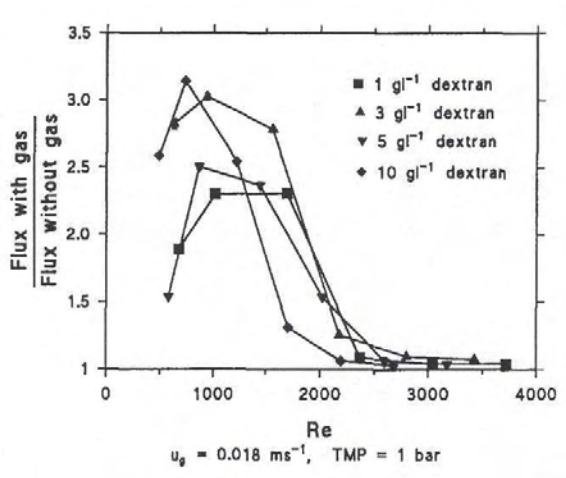

Figure 2.10. Effect of Reynolds number on flux enhancement (Source: Cui & Wright, 1996).

Research conducted by Mercier and co-workers (1995) revealed that the increase in the liquid velocity alone did not result in the same degree of flux enhancement as when the gas phase is present. When the velocity of the liquid in single phase flows is the same as that of superficial liquid velocity in the two-phase flow, much higher fluxes are achieved in the two-phase flow. In a study by Sur and Cui (2001), it was noted that flux enhancement by bubbling is more pronounced at low liquid flow rates and high concentration (Fig 2.11). The degree of flux enhancement (ε) decreased with an increase in liquid flow. This result suggests that flux enhancement by bubbling is due to the destabilization of the concentration boundary layer.

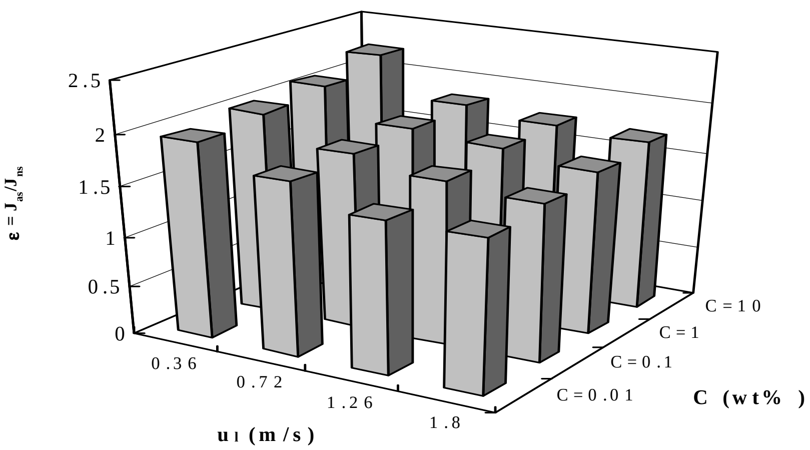

Figure 2.11. Effect of liquid velocity and concentration on flux enhancement (after Sur & Cui, 2001).

2.4.2.3 Effect of particle concentration

The effect of particle concentration was studied by Cabassud and co-workers (1997) using HF UF membranes and clay suspension as a model fluid. They reported that for filtration without bubbling, the permeate flux increased with concentration. This was attributed to the fact that if more particles are present, particles will flocculate and then form a highly porous cake upon depositing on the membrane wall. For gas velocities from 0.1 to 1 m/s, the flux was observed to decrease with concentration and then seemed to increase again (see figure 2.12). The explanation given for this behaviour was that air bubbling does not allow particles to flocculate and hence more particles lead to the formation of a more dense cake. However, if the concentration is continually increased, the air becomes ineffective in preventing particle flocculation and so the flux starts to increase again.

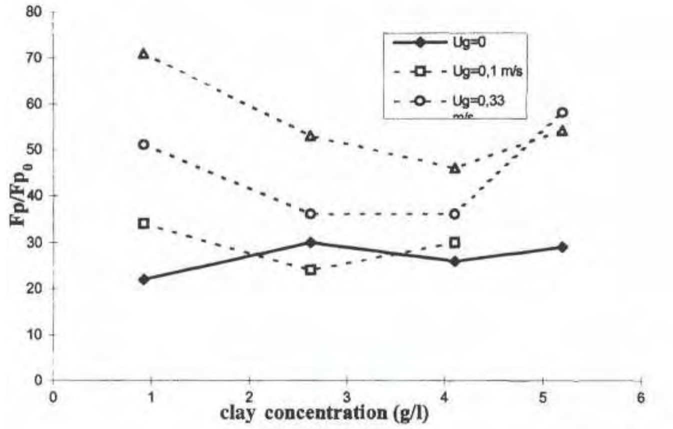

Figure 2.12. Effect of particle concentration on flux enhancement (after Cabassud et al., 1997).

Results contradictory to those reported by Cabassud et al. (1997) were obtained by Bellara et al. (1996) (see Figure 2.13), Mercier-Bonin et al. (2000a), Pospisil et al. (2004), and Sur and Cui (2005). In their work, where a suspension of commercial baker’s yeast was microfiltered in a ceramic flat sheet membrane, Mercier-Bonin et al. (2000a) found that the increase in particle concentration had a detrimental effect on flux in both single and two-phase flow systems. Nevertheless, fluxes with unsteady flow were always higher than those for steady flow. Pospisil et al. (2004) also made a similar observation during filtration of aqueous titanium dioxide dispersions using alumina tubular membranes.

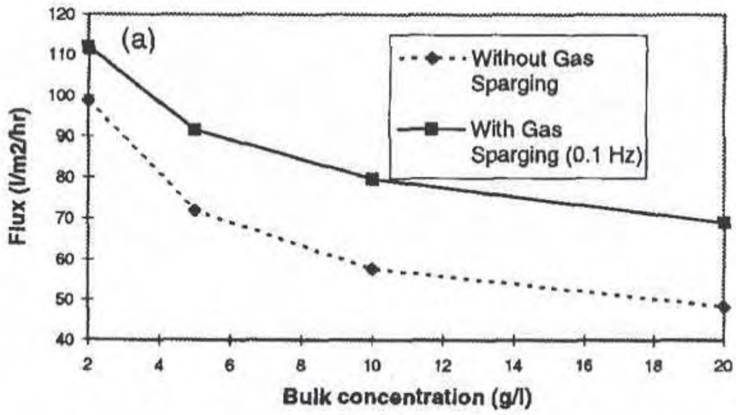

Figure 2.13. Effect of concentration on flux (Source: Bellara et al., 1996).

Bellara et al. (1996) during ultrafiltration of industrial grade dextran with a HF membrane, observed almost similar degrees of flux enhancement at different concentrations when the gas flow was constant and thus came to a conclusion that the effect of air bubbling on flux enhancement was insensitive to the feed concentration, particularly when the bubbling frequency was high. Contrary to this, Cui and Wright (1996) and Sur and Cui (2001) reported that more flux enhancement occurred at higher concentrations. In the work of Cui and Wright (1996), solutions of dextrans with an average molecular mass of 260 kD were used as test media, whilst Sur and Cui (2001) used a yeast suspension. In both these studies, the authors interpreted their observations as a clear indicator that flux enhancement by two-phase flow is due to the suppression of the concentration polarization layer. This conclusion is supported further by the findings of Smith and Cui (2004a) who observed that, whilst permeability and hence flux decreased with concentration, flux enhancement, on the other hand, first increased with concentration up to a ceiling, and then decreased when concentration was increased further (figure 2.14). Smith and Cui (2004a) were filtering dextran solutions through HF UF membranes.

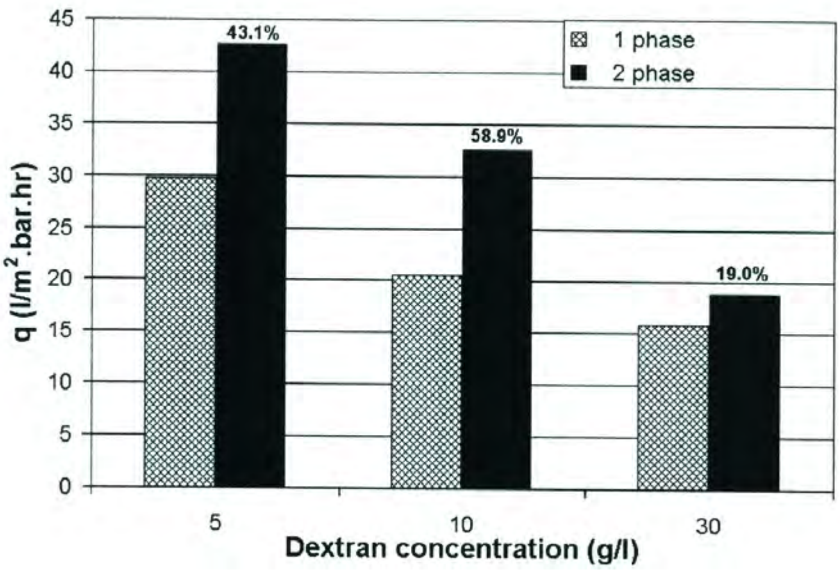

Figure 2.14. The effect of concentration on one- and two-phase permeability. Percentage flux enhancement is listed for each case. (Source: Smith & Cui, 2004a).

2.4.2.4 Effect of two-phase flow on cake characteristics

It is generally agreed in the literature that gas-liquid two-phase flow limits the cake buildup on the membrane wall by disturbing the concentration polarization boundary layer (Cui et al., 2003). In the absence of air sparging, a thick particle deposit was observed on the membrane surface by Ducom and co-workers (2002b) during nanofiltration of a clay suspension. They noticed that lower liquid velocities resulted in a thicker cake. Laborie et al. (1997) conducted a detailed investigation, also with clay (bentonite Clarsol FB2, mean particle diameter = 1 μm) suspension, on the effect of unsteady flow on the cake characteristics. A mathematical model was used to estimate the cake thickness, cake porosity and cake resistance. They reported that air injection seems to expand the particle cake; the cake obtained is thicker but more porous and thus allows higher permeation rates. Cake thickness and porosity increase with the airflow rate up to a ceiling and then seem to decline, whereas the cake resistance decreases with increasing air velocities. Similar observations were made by Cabassud et al. (2001) using a clay suspension (see Figure 2.15) and Mikulasek et al. (2002) using an aqueous titanium dioxide suspension. In this study only the specific cake resistance was considered and these results are presented in chapter 3.

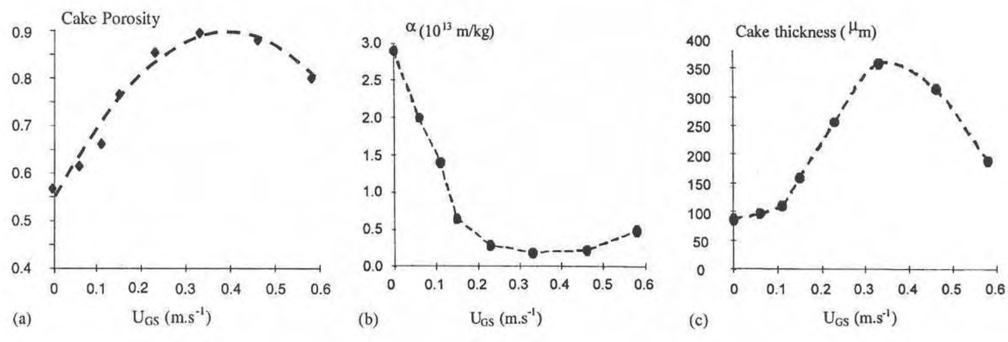

Figure 2.15. Influence of gas velocity on (a) cake porosity, (b) specific cake resistance and (c) cake thickness (Source: Cabassud et al., 2001).

Mercier et al. (1995) monitored the evolution of the hydraulic resistance with time during steady and unsteady filtration of a bentonite suspension. The hydraulic resistance (R_h) was defined as:

$$R_h = \frac{J_o}{J} - 1 \qquad (2.3)$$

where J_o was the initial flux and J was the instantaneous flux at a particular time. The evolution of the hydraulic resistance was much faster during steady filtration as opposed to unsteady (two-phase flow) filtration.

2.4.2.5 Effect of air sparging on energy consumption

Comparative investigations of energy consumption between single-phase flow and two-phase flow were made by Laborie et al. (1998). They studied an external HF membrane system in which most energy was consumed by the air compressor and the re-circulation pump. The energy consumed by the system was calculated at two different liquid velocities: 0.5 m/s and 0.9 m/s with and without air bubbling. It was found that, for both liquid velocities, injecting air reduces the energy consumption significantly. When the gas velocity was varied from 0 to 0.15 m/s, the energy consumed was reduced by 15 % for a liquid velocity of 0.5 m/s and by 31 % for a liquid velocity of 0.9 m/s. They were also able to define an optimal gas velocity of 0.3 m/s, above which increasing the airflow is no longer beneficial (Figure 2.16).

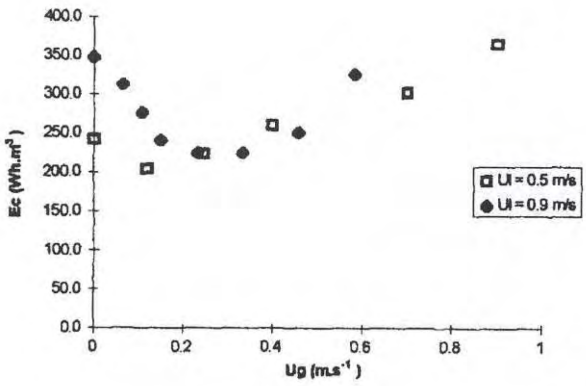

Figure 2.16. Evolution of energy consumption versus air velocity for two liquid velocities. (after Laborie et al., 1998).

In a different comparative study, Mercier-Bonin et al. (2000a) also confirmed that two-phase flow is more energy efficient and further stated that the energy consumption increases with permeate flux in both steady and unsteady processes. During the filtration of yeasts suspensions, Mercier et al. (1997) reported that the energy consumption was 10 kW h m^{-3} of permeate with slug flow and 30 kW h m^{-3} under steady-state conditions with no bubbling. Mercier-Bonin et al. (2003) also observed that energy consumption increases with flux, but for a certain specific energy, fluxes in two-phase flow systems were almost double those in single phase flows (see figure 2.17).

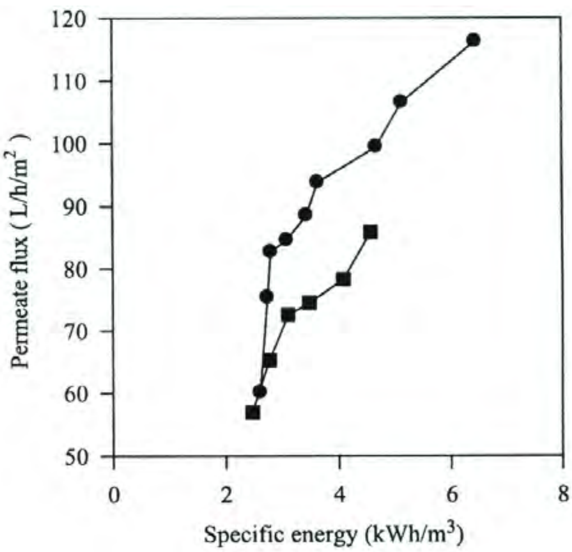

Figure 2.17. Energy consumption under single-phase (■) and two-phase flow (●) conditions. (after Mercier-Bonin et al. 2003).

Almost 80% of the energy in a submerged MBR system is consumed by aeration (Cho, 2002). In order to reduce this energy consumption, Guibert et al. (2002) formulated an aeration technique which they called "air-cycling". This technique was designed specifically for the Zenon Environmental ZeeWeed 500® series immersed hollow fibre MBR. The "air-cycling" technique involves creating aerated and non-aerated zones within the HF module which creates instability and increases mixing between the fibres. This technique was found to reduce energy consumption by more than 30%.

In an airlift system, in which a dextran solution was ultrafiltered, the energy consumption was found to be lower than that of a pumped system (Cui et al., 1997). These authors concluded that the airlift system was therefore more energy efficient than the pumped system, although it may result in slightly lower fluxes.

2.4.2.6 Effect of membrane geometry and membrane pore size

Most experimental work on bubbling in membrane systems has been conducted with tubular and hollow fibre membrane modules, which were either ultrafilters or microfilters. Some comparisons between these types of modules and filters have been made. Mercier-Bonin et al. (2000b) studied two-phase flow in different sized MF tubular membranes: 6 mm and 15 mm. The liquid slugs in the 6 mm tube were found to be always less aerated than in the 15 mm tube and bubble length in the 6 mm tube were 6.25 times longer than in the 15 mm tube. Better flux enhancement was achieved in the larger tube. Higher flux improvement in larger tubes was attributed to the fact that in larger tubes, the velocity of the falling liquid film around the gas slug is much higher. This result implies that bubbling in small-bore tubes, such as hollow fibres, may not be too effective.

Li and co-workers (1998) compared polysulphone and polyethersulphone UF flat sheet membranes with molecular weight cut-off of 100 kD. Using four protein solutions, human serum albumin (HSA), bovine serum albumin (BSA), human immunoglobulin (IgG), and lysozyme, they tested the effect of air injection on permeate flux and protein transmission. Gas sparging increased the permeate flux by 7% to 50%. Protein transmission was considerably reduced. Gas sparging was found to be equally effective for both membranes. Comparing their results with those obtained by other researchers for HF or tubular membranes, they found that flux enhancement with flat sheet modules was less than that for HF and tubular modules. According to them, the reason for this could be that in their system the cross flow channel was very narrow (2 mm high), thus there was high liquid shear in the channel which left very little room for further flux enhancement by air injection. A similar conclusion was made by Bellara et al. (1997) who found that the flux improvement attained with tubular membranes was much higher than with HF membranes. The lower flux enhancement in the HF module was explained by the inherently high shear rate present in HF modules due to their narrower channels. The shear rate in single-phase flow was two orders of magnitude higher in HF modules than in tubular ones.

During filtration of a bacterial suspension, Lee and co-workers (1993) found that air slugs were 50 % more effective in reducing filtration resistance using a UF membrane than in MF membrane. They stated that a possible reason for this is that, in MF membranes, pore plugging may occur due to their significantly larger pores, thus resulting in lower flux enhancement by two-phase flow. They also found that the reduction of the filtration resistance was higher in HF than in flat plate modules. However, the flux recovery in HF modules during intermittent bubbling is lower when compared with other modules. On the other hand, Mercier et al. (1998) did not observe any significant difference in the flux improvement by gas sparging for UF and MF membrane systems provided that external fouling was the main limiting phenomenon.

2.4.2.7 Effect of flow direction and membrane orientation

Using ceramic flat sheet membranes, Mercier-Bonin et al. (2000a) studied the effect of membrane orientation: vertical versus horizontal. The efficiency of two-phase flow was found to be always lower by about 25 % when the membrane was installed vertically. This difference was, however, reduced when the liquid velocity was increased. The superiority of air scouring in horizontal membranes was linked to two factors: firstly, the feed was injected into the module through five slots, which were located slightly higher than the membrane surface. Jets resulted when the feed was injected. These jets generated a certain amount of turbulence upon attaching to the membrane surface. The effects of the jets are much lower when the membranes are inclined vertically. Secondly, bubbles in horizontal membranes moves slower and hence they stay inside the membrane for a longer time. In vertical membranes, the buoyant force increases the speed of the bubbles, thus reducing their residence times inside the membrane. Contrary to these findings, Cui and Wright (1996) found that vertical orientation was much more effective for tubular membranes than the horizontal orientation (Figure 2.18). The main reason for this difference was thought to be the improper distribution of bubbles across the tube diameter in horizontal alignments.

According to the results obtained by Chang and Fane (2001) for a submerged HF system, the denser the fibre bundle, the lower the flux enhancement. When fibres are densely packed, smaller bubbles result, thus lowering the shear stress on the membrane. These researchers also studied the effect of transverse versus axial orientation for HF with bubbling employed on the external side of the fibres. In the same study, horizontal orientation was compared with vertical fibre orientation. The results obtained indicated that fluxes in axial vertical fibres are higher than those with transverse fibres. One of the reasons given for this difference was that, with axial fibres, the bubbles rise along the fibre and slug flow forms between fibres, while in transverse orientation, the bubbles can become trapped between fibres and the bubbles will oscillate from left to right.

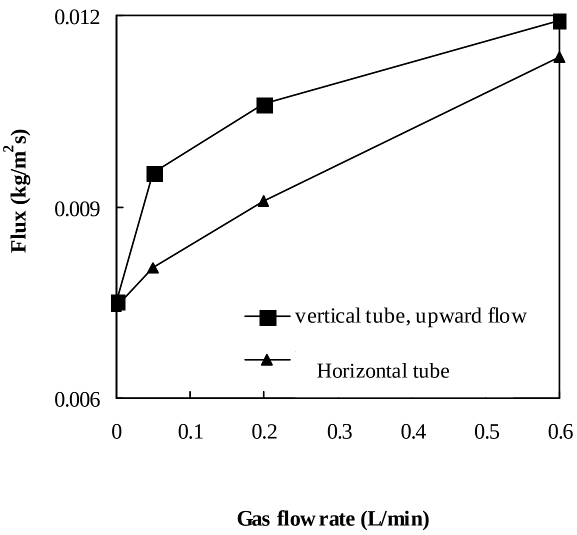

Figure 2.18. Effect of membrane orientation (after Cui & Wright, 1994).

In the case of vertically inclined membranes, the feed can be pumped either upwards or downwards. In order to verify which flow direction yields the best results for tubular membranes, Cui and Wright (1996) studied both flow directions for filtration of dextran solutions. The highest flux enhancement of 320% was obtained for downward co-current two-phase flow. These results were recently reinforced by the study of Cui and Taha (2003) (see Figure 2.19). One of the reasons for downward flow being more effective could be that bubbles spend a longer time in the membrane because the buoyant force acts against their flow direction and slows them down. These authors indicated that the downward flow system can be optimized such that once a sufficient amount of bubbles has been injected, the operating parameters can then be manipulated such that the bubbles are permanently held inside the membrane. Such a system would result in tremendous savings in energy consumption.

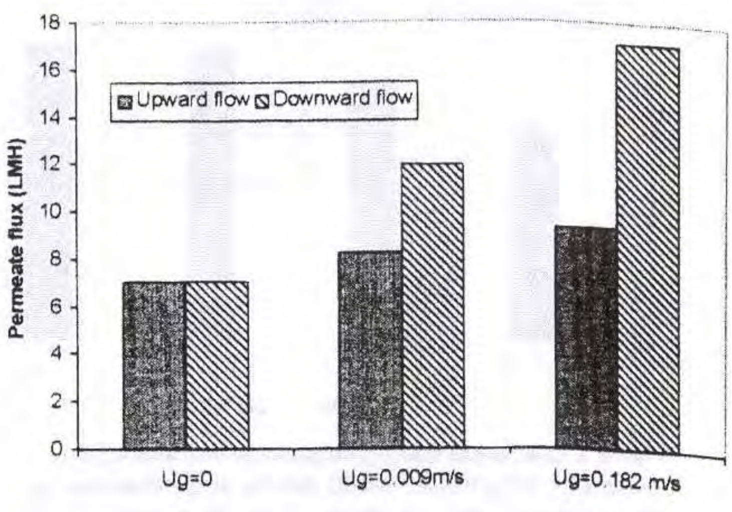

Figure 2.19. Effect of flow orientation on permeate flux in tubular membranes (source: Cui & Taha, 2003).

2.4.2.8 Effect of intermittent bubbling and bubbling frequency

During the filtration of clay suspensions (Cabassud & Ducom, 2001), air was injected at different flow rates after 180 mL of permeate had been collected. The injection of air stabilized the declining flux but did not improve it. Hence it was concluded that air sparging was unable to dislodge and remove already deposited particles. Contrary to the results of that study, Lee et al. (1993) observed that, as soon as the air slugs were introduced, the filtration flux increased rapidly with no significant decline afterwards as long as the gas bubbling was maintained (Figure 2.20).

In order to evaluate the influence of two-phase flow on a previously deposited cake, Mercier-Bonin et al. (2000a) also tried an intermittent bubbling operation, consisting of a succession of single phase and two-phase flows. They found that two-phase flow was unable to remove a previously deposited cake but resulted in quicker stabilisation of the permeate flux. The steady-state flux with intermittent bubbling was found to be 80% of the value obtained with continuous bubbling. The effect of intermittent bubbling will also be investigated in this study.

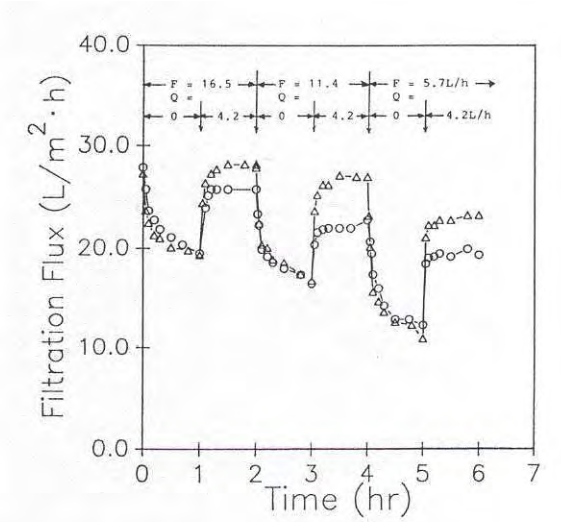

Figure 2.20. Intermittent bubbling at various crossflow rates (F) for a (Δ) UF membrane and a (O) MF membrane (Source: Lee et al., 1993).

The effect of bubbling frequency on permeate flux was studied by Bellara and co-workers (1997). In their study, macromolecules were ultrafiltered. The injection of air slugs into the HF module was controlled via a solenoid valve connected to a timer. A range of bubbling frequencies were used from 0.1 to 0.25 Hz at different TMPs and feed concentrations. It was found that, for the bubbling frequency range of 0.125 to 0.25 Hz, the flux at two different liquid velocities remained identical despite the fact that there was a difference of a factor of two between the cross flow velocities. The permeate flux was found to increase with bubbling frequency up to 0.125 Hz (see Figure 2.21).

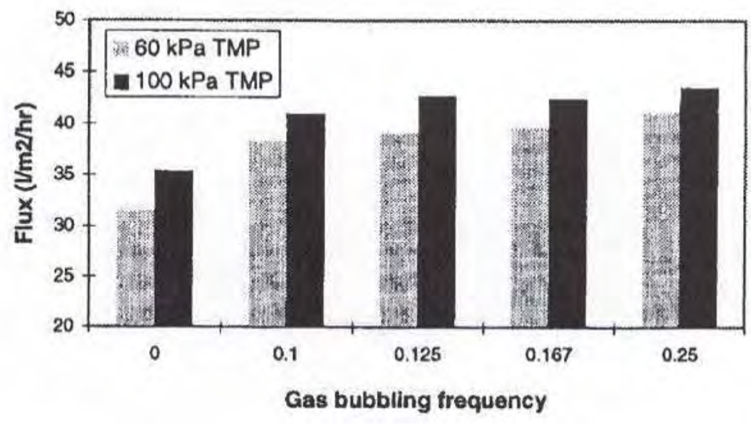

Figure 2.21. Effect of gas bubbling frequency on the permeate flux (Source: Bellara et al., 1997).

Cabassud et al. (1997) studied an intermittent air injection process, during which air was injected into HF membranes for one minute after every 15 minutes. After each interruption, the permeate flux decreased sharply. Intermittent gas flow was found to be less effective than continuous bubbling but it was still better than no bubbling at all (Figure 2.22). These results agree with those of Smith et al. (2002) and Smith and Cui (2004a).

For a tubular membrane, flux was observed to increase with bubbling frequency from 0 to 1 Hz (Li et al, 1997a). If the frequency was increased further, the primary wakes of neighbouring bubbles tended to overlap each other and the wake region of each bubble became indistinguishable. This has a negative effect on the flux. On the other hand, Smith and Cui (2004a) observed a minimum critical bubbling frequency of 1.17 min^{-1} below which no flux enhancement occurred for a UF HF system with "in-out" filtration (see figure 2.23).

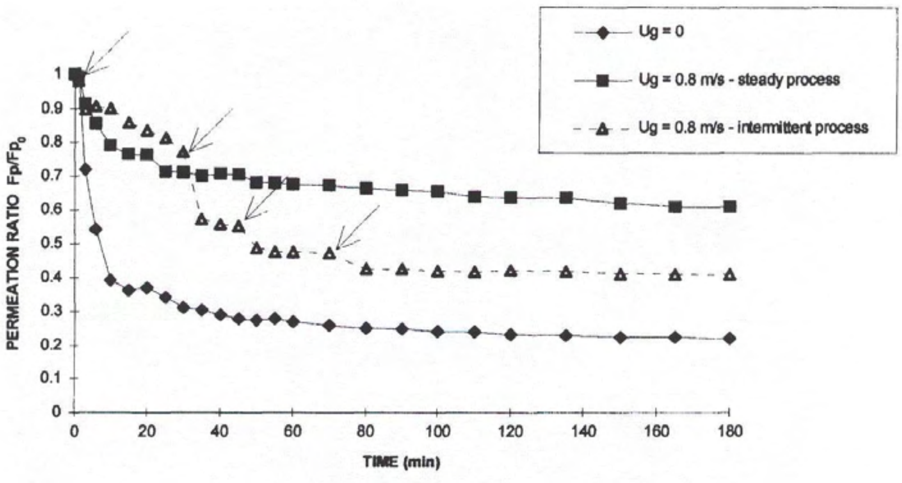

Figure 2.22. Effect of intermittent bubbling on flux (after Cabassud et al., 1997). Arrows indicate time at which gas was injected for one minute.

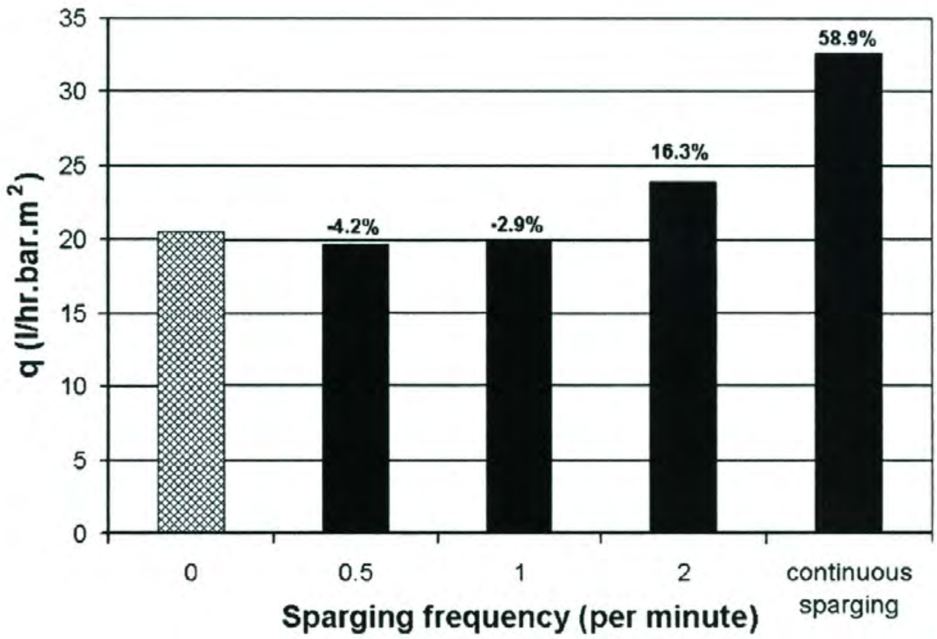

Figure 2.23. The effect of sparging frequency values with percentage enhancement over one-phase shown. (after Smith & Cui, 2004a).

2.4.2.9 Correlation of flux enhancement with wall shear stress

Several studies have attempted to link shear stresses generated in two-phase flow to flux enhancement. Employing an electrochemical method to measure shear stress on the membrane wall, Ducom et al. (2002b) demonstrated that the permeate flux can be linked to the wall shear stresses at the membrane surface and that it is possible to control fouling by applying appropriate wall shear stresses. Cabassud et al. (2001) were able to successfully link the total shear stress on the membrane to flux enhancement where a linear relationship was obtained for shear stresses greater than 10 kPa (Figure 2.24). They further illustrated mathematically that the total shear stress on the membrane is proportional to the mixture Reynolds number and so is flux enhancement.

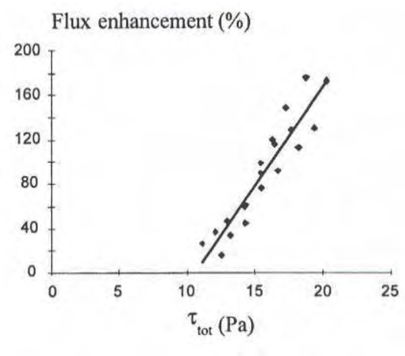

Figure 2.24. Variation of the flux enhancement with the total shear stress (source: Cabassud et al., 2001).

Laborie et al. (1999) and most recently Laborie and Cabassud (2005) utilized two methods to evaluate the shear stress generated by slug flow for 1 mm HF membrane. First, they calculated the shear stress using slug flow models and then used the electrochemical method to measure shear stress. A good agreement between calculated and measured shear stresses for the liquid slug was achieved but a discrepancy existed for the gas slugs. This was associated with the fact that shear stress on the gas slugs has a negative value and the electrochemical method does not determine the sign of the shear stress. Laborie et al. (1999) learnt that the permeate flux increases with the liquid shear stress. Comparing two different liquid velocities they found that, for the same liquid shear stress, the permeate fluxes are higher and increase more rapidly with the liquid shear stress for a liquid velocity of 0.9 m/s than for 0.5 m/s. This implies that the flux also depends on the value of shear stress of the gas slugs.

The effect of shear was also examined by Vera et al. (2000) who reported a linear relationship between two dimensionless parameters: the shear stress number (N'_S) and the resistance Number (N_f) which were plotted for gas sparging filtration of dextran solution, ferric hydroxide suspensions, and secondary effluent using an inorganic tubular membrane. The slope and the non-zero intersection with the N_s' axis of the straight line of the N_s' versus N_f plot were used to assess the effect of gas sparging on the deposit resistance. Their results showed that gas sparging could completely eliminate the resistance for filtration of hydroxide suspension and dextran solution in the slug flow region but only partly eliminated the filtration resistance caused by secondary treated wastewater.

When comparing performance with and without gas sparging, Mercier-Bonin et al. (2003) found that permeate fluxes were similar for single and two-phase flow if the shear stress was the same and if it was below a certain critical value. This strongly supported the notion that shear stress is the major hydrodynamic parameter involved in the enhancement of flux. They noted that when the wall shear stress exceeded a certain critical value; two different behaviours were observed: for two-phase flows, permeate flux kept increasing whereas, for single-phase flows, it tended to level off and then decrease (see figure 2.25) In the cross-flow microfiltration of skimmed milk, Mercier-Bonin et al. (2004) found further evidence to support their earlier claim that wall shear stress was the most important hydrodynamic factor regarding two-phase flow enhancement of flux.

On the contrary, Smith and Cui (2004b) disagree with this claim. They claim that flux enhancement by air sparging is primarily due to flow reversal and not shear stress enhancement. However, flow reversal can only be significant if bubbling occurs inside confined channels such as tubular or HF membrane modules. According to Howell et al. (2004), it is not clear how much shear stress at the membrane surface in a submerged membrane system is increased by increasing the air flow rate. This study will address this question.

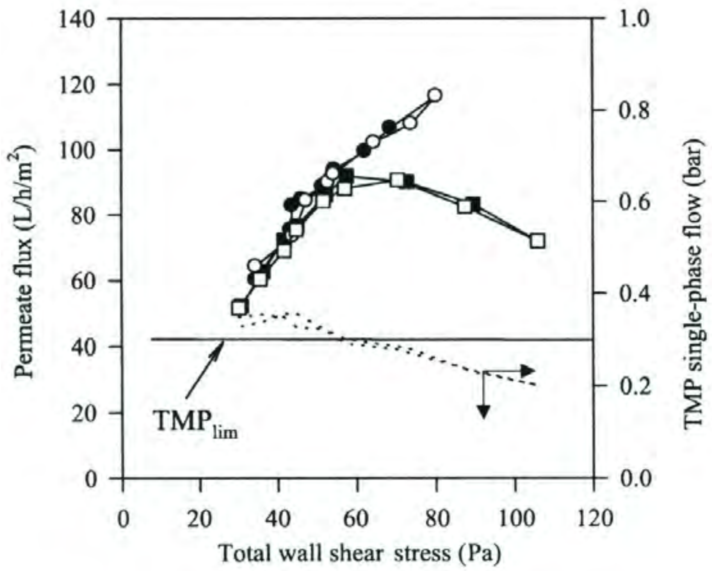

Figure 2.25. Variation of the permeate flux with the total shear stress under single-phase flow conditions (■, □) and two-phase flow conditions (●, ○). (Source: Mercier-Bonin et al., 2003).

Taha and Cui (2002b) conducted CFD simulations of slug flow through a 10 mm ID tube with the aim of understanding and quantifying the details of the flux enhancement process. The shear stress data calculated by the CFD model were correlated with mass transfer and permeate flux. The wall shear stress was observed to increase from the bubble nose to a maximum value corresponding to the bubble tail. There was considerable shear stress fluctuation near the bubble tail and in the wake due to a change in flow direction of the falling film that occurs in this region. Figure 2.26 depicts the calculated shear stress for four bubbles of different lengths. These authors obtained good agreement between the experimental flux and the flux calculated using the predicted shear stress data.

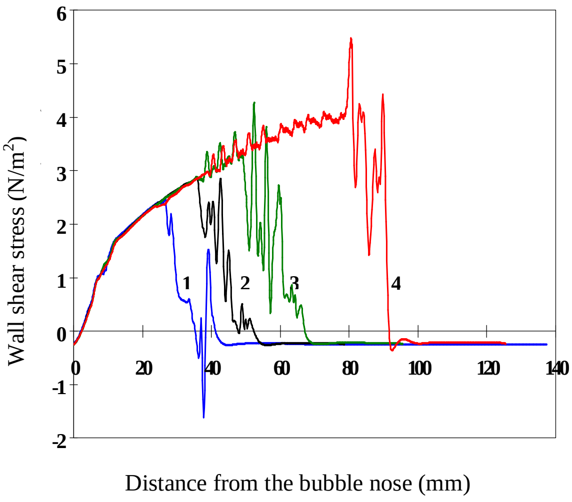

Figure 2.26. Variation of wall shear stress along the falling film (Source: Taha & Cui, 2002b).

2.5 CONCLUSION

From the above review of the studies of bubbling in membrane processes, it is evident that the degree of flux enhancement ($\phi = \dfrac{\text{Flux with bubbling}}{\text{Flux without bubbling}}$) depends on the type of membrane module, membrane orientation and operating parameters, such as trans-membrane pressure (TMP), feed concentration, bubble size and frequency, gas flowrate and liquid flowrate. The main implications from these studies can be summarized as follows.

1. The flux enhancement (ϕ) is more pronounced when concentration polarization is more severe, for example, at a high TMP, low liquid crossflow velocity, and a high feed concentration. This result suggests that air bubbles minimize fouling by disrupting the concentration polarization layer.
2. Membrane orientation, particularly for tubular membranes, is very important. Vertically installed tubular membranes performed much better than horizontal membranes, however, for flat sheet channels, horizontally aligned channels were better than vertical ones. For tubular membranes, downward two-phase flow gave superior performance to upward flow.

3. The flux enhancement is greater in larger channels than in small ones. For example, flux enhancement in tubular membranes is greater than for hollow fibres. The reason for this is that, in hollow fibres there is already high shear on the membrane due to the flow channel being narrow, therefore the introduction of the gas does not increase shear as significantly as it does in tubular modules. Also in larger tubes, the velocity of the liquid in the falling film region around the gas slug is higher than that in smaller tubes.
4. With gas sparging present, the permeate flux is relatively insensitive to the actual liquid flow over much of the laminar flow region. This is because the secondary flow induced by bubbles is dominant.

In the reviewed studies, several mechanisms by which gas-liquid two-phase flow enhances flux have been proposed. The following mechanisms have been identified to contribute to the observed flux increase with the dominant mechanism depending on the membrane configuration and the individual operation.

1. Bubble induced secondary flow*:* as the bubble moves through the liquid it induces secondary flows and liquid recirculation in the wake, which promote mixing, and destabilises the mass transfer boundary layer. This is similar to the enhancement of heat transfer in liquid convection by injected gas bubbles. In slug flow, the liquid falling film between the bubble and membrane wall imposes very high shear stress on the membrane wall which disrupts the concentration boundary layer.
2. Physical displacement of the concentration polarization layer*:* air slugs have the ability to scour the concentration polarization layer off the membrane surface. For example, the liquid film thickness between the membrane wall and the slug in small diameter tubes, including hollow fibres, is less than the calculated mass transfer layer thickness in single-phase liquid flow at the same liquid flow rate (Bellara et al., 1996).
3. Pressure pulsing caused by passing slugs*:* a moving bubble induces pressure variations in certain locations across the membrane. This occurs because the rising bubble has a high pressure around its nose and low pressure in the wake. This sudden change in local pressure as the bubble passes, produces an effect similar to that produced by pulsatile flow.

4. <u>Increase in the superficial cross-flow velocities:</u> high gas flow rate injection can increase the liquid cross-flow velocity significantly, which can result in a flux increase. This however, is only significant with high gas flow rate sparging.

Having conducted this comprehensive review of literature on the application of two-phase flow in membrane systems, it becomes apparent that there is still a lot of unknown information when it comes to the utilization of two-phase flow as a flux enhancing mechanism. Some of the information that is still unknown, which this study will investigate is as follows:

- Most studies have focused on "in-out" filtration systems where bubbling occurs inside the membrane module. In these cases, the flow channels are well defined, and hence two-phase flow in these channels can be characterized very well and be easily optimised. Studies on submerged "out-in" systems are very few and most of them have focused on submerged hollow fibre membranes. Only two studies were found (Chua et al., 2002; Howell et al., 2004) which have looked at submerged flat sheet membranes on a laboratory scale. The other studies on submerged flat sheet membranes were undertaken on industrial-scale commercial units (Churchouse & Wilgoose, 1999; Morgan et al., 2003) and were not running at optimized operating conditions.
- None of the studies on the submerged systems have investigated the effect of nozzle size and geometry. These parameters seem to have been decided arbitrarily and hence are not optimized. As a result commercial MBRs use nozzles of different shapes and sizes. For example, Zenon Environmental Ltd. uses rectangular slots in their MBR whilst Kubota uses circular nozzles and recently changed their nozzle size from 10 mm diameter to 4 mm (Morgan et al. 2003).
- Characterization of two-phase flow in submerged flat sheet modules has not been conducted, hence it is not known how factors such as air flow rate, nozzle size and geometry and channel gap width affect the nature of two-phase flow and which type of two-phase flow is most effective for flux enhancement. On the other hand, it is well known that for non-submerged "in-out" systems, slug-flow is the ideal two-phase flow for flux enhancement.

- There is still no agreement on the mechanisms by which two-phase flow enhances flux. Most authors seems to think that it is primarily wall shear stress enhancement by two-phase flow which causes fouling minimization whilst others dispute this and claim that it is flow reversal which is more important than shear stress enhancement.
- Generally, information on the operation of submerged flat sheet systems is limited due to the fact that this process is being used only on a limited commercial scale. There is therefore a need to collect experimental data for such systems for process optimisation.
- There has been no attempt to measure wall shear stress for a submerged flat sheet system. It is therefore not clear how the change in the air flow rate affects the shear stress on the membrane surface. Thus the flux enhancement data reported in literature for these systems are only quantitative. In this study CFD investigations will be carried out in order to gain some insight into this issue.

Chapter 3

EXPERIMENTAL INVESTIGATIONS INTO FLUX ENHANCEMENT BY GAS –LIQUID TWO-PHASE FLOW

3.1 INTRODUCTION

Approximately 90 % of commercial MBRs make use of submerged membrane modules in which the membranes are directly immersed into the bioreactor (Stephenson et al., 2000). The submerged membranes are usually either hollow-fibre or flat sheet modules. The purpose of using the membranes is to clarify the mixed liquor thereby eliminating the need of a settling tank. This study focuses on the use of submerged vertical flat sheet membranes for solid-liquid separation.

Fouling is a major factor hindering commercialisation of MBRs. Consequently there is significant research being undertaken in order to develop strategies that reduce fouling in MBRs some of which have been reviewed in chapter 2. In recent years, gas-liquid two-phase flow has been introduced as a viable alternative flux enhancing technique, which is very suited to MBRs. Application of gas-liquid two-phase flow has in the past been largely used to enhance performance in heat and mass transfer processes. It has been shown in these processes that turbulence created by two-phase flow, even at small gas injection ratios, improves the heat and mass transfer coefficients significantly (Kenning & Kao, 1972; Kumar & Fan, 1994).

In membrane processes two-phase flow has been used for three different purposes (Cabassud et al., 2001), which are: 1) To destabilise particle deposition by a gas back flush. This process can only be used in MF processes because other membrane types like UF are too tight to be back flushed by air. 2) To prevent or limit the formation of a particle deposit or concentration polarization. 3) To transfer a compound from the gas phase to the liquid phase, most commonly oxygen.

Despite an increasing number of publications on the use of two-phase flow as flux enhancing strategy, there is still very little known about the manner in which two-phase flow enhances membrane flux. Slug flow has been shown to be the most effective two-phase flow regime for bubbling inside tubular or hollow fibre modules. For submerged flat sheet systems, the most effective two-phase flow regime has not yet been fully identified and thus the use two-phase flow in these systems has not yet been optimised.

Preliminary investigations in this study revealed that the bulk of air flowed towards the centre of the column, resulting in an uneven distribution of the gas across the membrane surface. This phenomenon has been observed in bubble column studies such as those of Lapin & Lübert (1994a) and Jakobsen et al. (1997). It was speculated (and later proven) that this uneven distribution of air would result in some parts of the membrane being cleaner than others. In order to address this uneven distribution of bubbles, baffles were inserted in the space between the membrane and the tank walls and the efficiency of the baffles was elucidated experimentally as well by computational fluid dynamics.

The aim of this study is to add to the knowledge of how gas-liquid two-phase flow enhances flux in submerged flat sheet modules for cases with and without baffles. This could lead towards improving the performance of submerged flat sheet MBRs by optimising the use of two-phase flow. More specifically, the objectives of this chapter are to:

- Investigate the effect of air flow rate on suction pressure (TMP) rise, and flux,
- Investigate the effect of nozzle size on TMP and flux,
- Investigate the effect of air flow rate and nozzle size on critical flux,
- Investigate the effect of nozzle geometry on TMP and flux,
- Investigate the effect of feed concentration on TMP and flux,
- Investigate the effect of intermittent bubbling and intermittent filtration,
- Investigate the effect of membrane baffles on TMP and flux,
- Investigate the effect of the channel gap width between submerged membranes.

3.2 EXPERIMENTAL SETUP

A diagram of the experimental rig used for the experiments is depicted in Figure 3.1. A single submerged flat sheet membrane was used. The system was operated as a constant flux operation and therefore TMP increased with time. Permeate was compelled to pass through the membrane by applying a negative suction pressure. The process feed tank was open to the atmosphere.

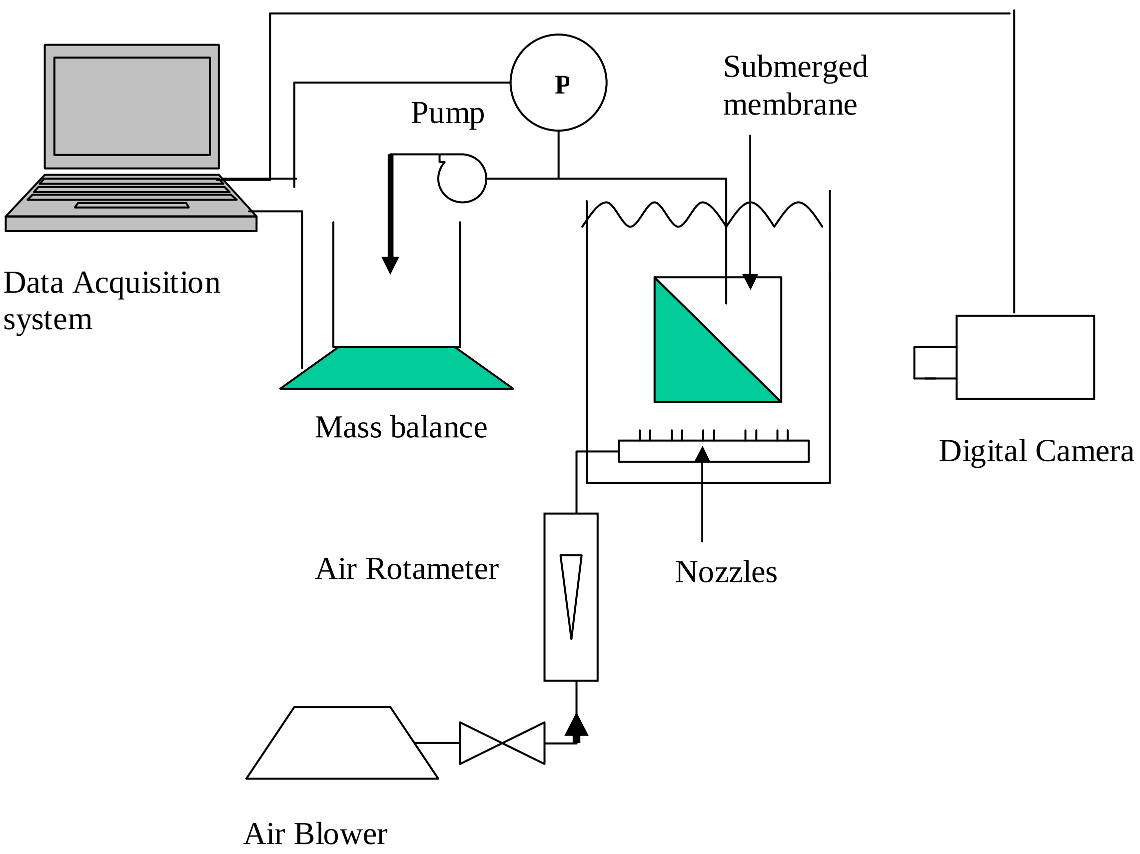

Figure 3.1. Schematic diagram of experimental setup.

3.3 EQUIPMENT DESCRIPTION

3.3.1 The Process Feed Tank

The feed suspension was contained in a 20 litre rectangular tank. The tank was designed with special slots to hold the membranes and it could fit up to a total of eight flat sheet membranes. However in this study only a single membrane was used, and the membrane was inserted in the first slot near the wall and then a partition covering the whole depth and width of the tank was inserted just next to the membrane to cut off the rest of the tank. The partition ensured that the gas bubbles stayed in the section of the tank where the membrane was located. However, the partition was not tightly sealed thus the liquid feed suspension filled the entire tank.

3.3.2 The Flat Sheet Membrane

The membrane used was a microfiltration flat sheet membrane manufactured by Yuasa Corporations of Japan with a nominal pore size of 0.4 µm. It had a total surface area of 0.1 m^2 with 0.05 m^2 on each side. The membrane was suspended 150 mm above the bottom of the aeration tank and the feed suspension was filled to 100 mm above the top of the membrane unit. Figure 3.2 shows the schematic diagram of the membrane element. The membrane is approximately the size of an A4 sheet (190 (w) × 290 (h) mm). The gap between the membrane and the tank sidewalls was approximately 7 mm on both sides of the membrane. This dimension is important as it defines the width of the flow channel available for bubble flow.

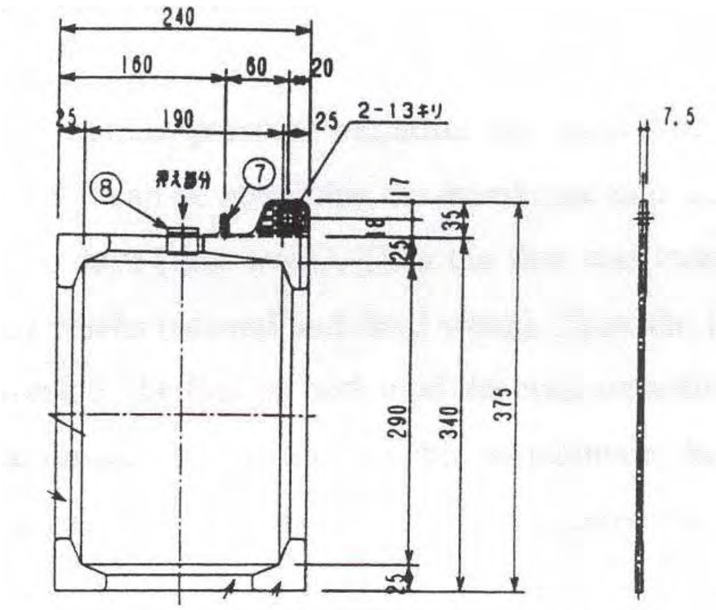

Figure 3.2. Schematic of a flat sheet membrane. Dimensions are in millimetres. (Source Cho, 2002).

3.3.3 The Nozzles

Air inlet nozzles were made by drilling holes in half-inch stainless steel tubes. Cylindrical and square nozzles were fabricated with ten nozzles of the same size and geometry on each tube. The holes were 20 mm apart. The stainless steel tube with nozzles was inserted into the tank at a point which was 100 mm below the bottom of the membrane. The nozzle tube was inserted directly beneath the membrane so that both sides of the membrane received approximately the same flow of gas bubbles. The cylindrical nozzles were 0.5, 1.0, 1.5, 2.0, 3.2 and 4.5 mm diameter. For the cylindrical nozzles of diameter 3.2 and 4.5 mm, corresponding square nozzles with equivalent open areas were made. The dimensions of these square nozzles were 3×3 mm and 4×4 mm. A schematic diagram of a typical nozzle arrangement is shown below in Figure 3.3.

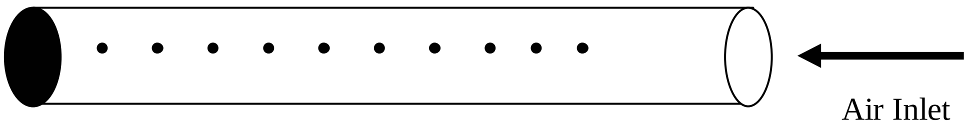

Figure 3.3. Schematic diagram of the diffuser

3.3.4 The Process Pump

A variable speed peristaltic pump from Cole Parmer was used to withdraw permeate from the membrane. Pump tubing made from Tygon material was used.

3.3.5 The Air Blower

A Hillblow air blower was connected to the nozzles on the feed tank via flexible tubing. An air rotameter manufactured by Gilmont was used to monitor the airflow rate. Typical values of air flow rates used in the experiments for this chapter ranged from 20 l/min per m^2 of membrane area to 80 l/min per m^2 of membrane area. This range spanned within the typical bubbling flow rates used in industry, which is about 20 to 60 l/min per m^2 of membrane of membrane area (Cho, 2002), although current developments with bubbling intermittency may be heading towards 10 l/min per m^2, or less (Guibert et al., 2002).

3.3.6 Pressure Transducers

The trans-membrane pressure (TMP) was measured via a Labom pressure transducer installed on the line between the membrane and the suction pump. In order to ensure that the pressure transducer remained correctly calibrated, a manual pressure gauge was installed to monitor the calibration of the pressure transducer. Although all the pressure readings were actually negative, in all the plots shown in this chapter the absolute values of pressure have been plotted as this represents the TMP.

3.3.7 The Feed Suspension

A suspension made from commercially available dry bakers' yeast was chosen as the model feed. This type of suspension was selected based on its ease of availability and also because it has properties which simulate those of mixed liquor, such as cellular materials, cell debris and extra cellular materials. A particle size analysis of the yeast feed suspension was carried out using a Malvern Mastersizer. The particle size distribution of yeast obtained is depicted in Figure 3.4. From this Figure, it can be determined that the mean particle diameter of yeast is about 5 microns. The nominal membrane pore size is 0.4 µm, this implies that a main mechanism of fouling will be due to cake formation.

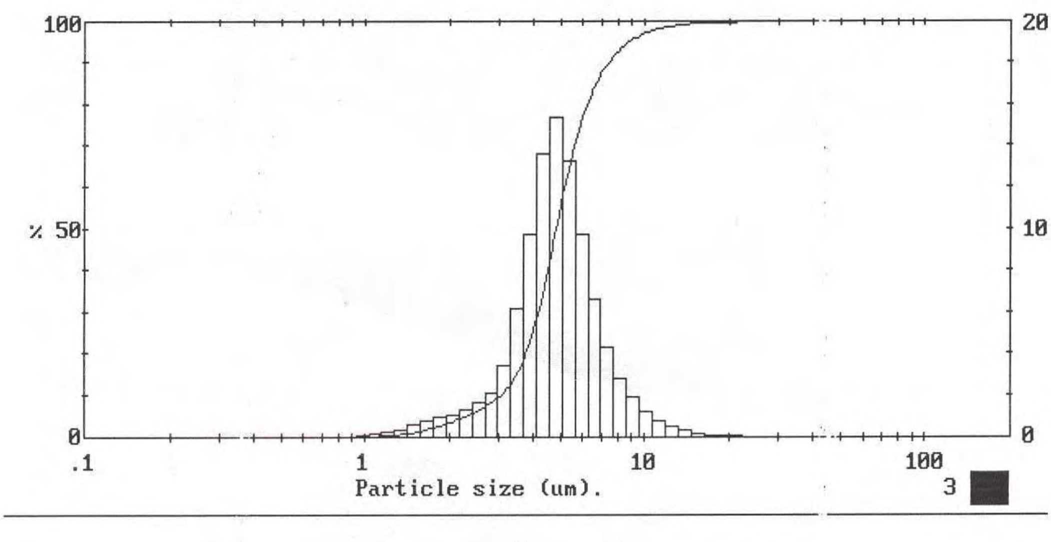

Figure 3.4. Yeast suspension particle size distribution.

3.3.8 Monitoring of the permeate flux

Flux was measured by monitoring the rate of change of weight collected over time in a plastic beaker which was placed on top of the measuring balance. Although all experiments were intended to be run at constant flux, it was found that in some experiments when the TMP had increased up to a certain level, it became impossible for the pump to deliver constant flux. As a result it was important to monitor flux during the experiments. The permeate collected in the beaker was limited to one litre and then returned to the feed tank in order to keep the concentration more or less constant.

3.3.9 The baffles

The design of the baffles was such that they form small rectangular channels over the membrane surface. An example of the baffles that were used is shown in Figure 3.5. The rectangular channels created by the baffles were 10 mm wide, and they were as long as the membrane and the depth was 7 mm. This design ensured that there was no room left for air to flow sideways but it had to flow upward through the narrow rectangular channels.

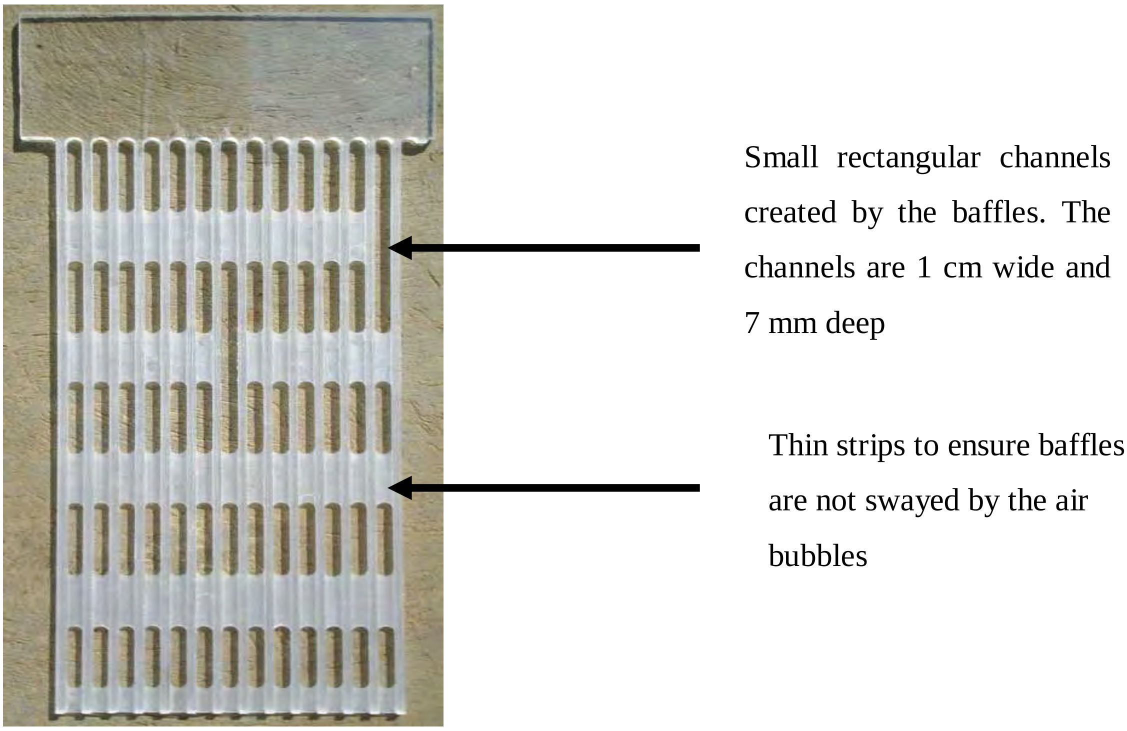

Figure 3.5. A photograph showing the structure of baffles inserted between the membrane and the wall.

3.4 EXPERIMENTAL PROCEDURE

The feed suspension was prepared by measuring a desired amount of yeast and then diluting it with water to a volume of one litre. This solution was then sonicated for 10 minutes; thereafter the solution was further diluted to fill up the process tank and was thoroughly mixed. The yeast was not washed during this process. The feed concentration was either 5, 10 or 15 g/L depending on the experiment. After the solution was prepared, the air-blower was switched on and the desired airflow rate selected on the rotameter using a regulator valve. The membrane was then inserted into the feed tank and firmly secured. Finally the experiment was initiated by starting the suction pump. The duration for most runs varied between two and three hours. All experiments were carried out under room temperature.

At the end of each experiment, the membrane was cleaned by gentle scrubbing of the surface with a solution of an appropriate detergent such as "Targ Enzyme A". Following cleaning, the membrane was thoroughly rinsed with Milli-Q pure water and then soaked overnight in a solution of 0.5% w/w Sodium Hypochlorite. This treatment effectively restored membrane permeability and ensured that the membrane was in similar conditions at the initiation of each experiment.

3.5 RESULTS

The success of gas-liquid two-phase flow in combating fouling depends on the combination of many factors. These factors include, air flow rate, nozzle size and geometry, operating strategies, such as intermittent bubbling or intermittent filtration, and feed concentration. In order to define an optimal combination of these factors for a submerged flat sheet system, the effect of each factor on flux and trans-membrane pressure was studied. The extent to which each factor was successful in minimising fouling was judged by the degree to which the rise in TMP was curbed. Unlike in most other studies which were reviewed in chapter 2, in which the gas-liquid two-phase flow has been investigated, there was no pumping of the feed in the system studied here. Gas was blown into a stagnant feed solution and induced some form of secondary movement in the liquid. This method of operation is very close to the manner by which commercial submerged MBRs operate. The type of system in which gas is used to produce movement in a stagnant liquid is often referred to as an airlift (Chang & Fane, 2000). However, the requirement of an airlift system is that the liquid must flow up on one side column and down on the other side of the column (Ben Aim, 2002). This is achieved by using a downcomer. In this study, there was no downcomer and the liquid was flowing up and recirculating on both sides of the membrane since the air bubbles were introduced on both sides of the membrane.

3.5.1 Repeatability

Prior to the commencement of experimental investigations, the reproducibility of the results from the experimental rig was tested. Runs were carried out at various conditions, each condition being repeated at random. From these tests the repeatability of the TMP data was found to be within a margin of 10 % or less which was considered to be acceptable. Consequently, all the results presented in the rest of the thesis are only reported for cases where the experimental conditions were within one standard deviation of the mean value.

3.5.2 The effect of air flow rate and nozzle size

The effects of air flow rate and nozzle size were studied simultaneously by investigating a range of air flow rates on nozzles of different sizes. For this purpose, nozzle sizes of 0.5, 1.0 1.5 and 2.0 mm were used with air flow rates of 2, 4, 6 and 8 l/min investigated at each nozzle size. The effect of air flow rate with and without baffles was also studied for nozzle sizes of 1.0 and 2.0 mm. In all experiments, the initial flux was set at close to 40 $l/m^2.hr$, which was above the critical flux under most operating conditions as discussed in section 3.5.5. Thus, for all experimental conditions considered, concentration polarisation and fouling of the membrane would result and the effect of airflow rate and nozzle size would be more clearly identified. During the experiments, the main indicator of the effectiveness of gas bubbling or nozzle size was the rate of increase of the TMP as the flux was maintained constant. If the membrane is fouling severely, TMP will increase very rapidly, but if the fouling is being retarded then TMP will increase at a reduced rate.

Figure 3.6 shows typical results of TMP versus time curves obtained for different gas flow rates when the nozzle size of 1.0 mm was used and the concentration was 5 g/L. Similar trends were obtained for nozzles of other sizes. From this figure it can be seen that, for both no air (0 l/min) and low airflow (2 l/min), the system showed a slow rise of the TMP followed by a significant TMP rise which slowed down approximately after 3 hours of operation. For the higher gas flow rates, TMP was still increasing after 3 hours. For the low gas flow rates, the TMP curve is composed of three distinct regions. Several researchers have also reported a slow rate of increase in the TMP (or resistance) followed by much more rapid rise in the TMP and then followed by a slower increase again (for example, Ueda et al. 1996; Nagaoka et al. 1998; Cho & Fane, 2002). During operation of a submerged MBR, Nagaoka et al. (1998) observed such a transition in TMP and modelled this by assuming that fouling resistance was due to extra-cellular polymeric substances (EPS) deposition and that the foulant was compressible with a specific resistance that increased with TMP. Cho and Fane (2002) studied the cross-flow microfiltration of an anaerobic reactor effluent at nominally subcritical flux. They attributed the slow TMP rise to gradual EPS fouling, the distribution of this fouling was found to vary locally leading to a distribution of local fluxes. They explained the sudden rise in TMP as due to local fluxes in some areas exceeding the critical flux of the dominant foulant.

As seen in Figure 3.6 for lower airflow rates, in the first 40 to 60 minutes the rise in TMP was very slow. After this period, TMP started to rise rather rapidly for approximately an hour. Then finally, the third part of the TMP curve was at a reduced rate of TMP rise. In the first part of the experiment, the membrane was clean, thus there was little resistance across the membrane wall. According to the resistance-in-series model (Davis & Grant, 1992a), if flux is kept constant, low resistance would result in low TMP. In fact a slow rise in TMP at the beginning of the experiment was observable in almost all experiments, at all flow rates, nozzle sizes and concentrations.

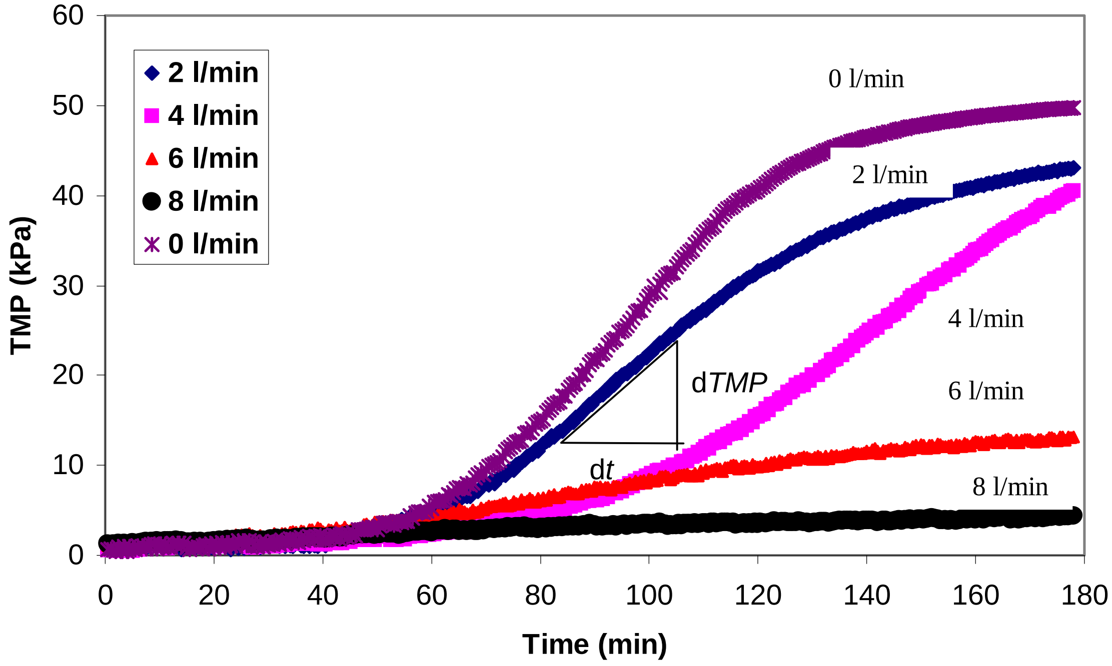

Figure 3.6. Variation of TMP with time at different airflow rates for the nozzle size of 1.0 mm and concentration is 5 g/L.

At this stage, deposits are just starting to occur on the surface of the membrane, the cake layer is thin and offers little resistance. Eventually the cake layer increases and the cake becomes more compact, leading to a higher resistance. This causes the TMP to start to rise rapidly as in the second part of the curve, as the resistance continues to increase with the build-up of the cake. In some of the experiments, particularly at zero and low air flow rates, the TMP reached 40 to 50 kPa after which the TMP rise slowed down (but was not zero). The explanation for this third stage is complex. One explanation is based on analogy with submerged hollow fibres where the rapid rise in TMP followed by a slower rise has been attributed to a shifting of the flux distribution as fouling occurs (Chang & Fane, 2001). Thus flux is initially located where the suction pressure is highest and then as this region fouls, with rapid TMP changes, the maximum driving force relocates so that eventually all zones of the membrane experience the surface averaged flux. The fact that TMP rise slows down once TMP is relatively high (recall the driving force is suction) also suggests that a point is reached where the permeate pump is unable to maintain the desired flow. This effect was clearly seen at feed concentrations of 10 and 15 g/L, and may have influenced the 5 g/L results at low gas flow rate. A similar flux decline for a submerged MBR system was also observed by Shimizu et al. (1996). When high bubbling rates were employed, there would have been a more effective removal of particles from the membrane surface which explains why the TMP rise was slower and after three hours of operation the steady-state TMP had not been reached yet.

Figure 3.7 shows typical TMP versus time data obtained from two runs, one with baffles and the other one without. This Figure shows that the development of the TMP was much slower when the baffles were employed; for example, the maximum dTMP/dt without baffles was 1.15 kPa/min compared with 0.44 kPa/min with baffles. If dTMP/dt can be taken as a measure of the rate of fouling, these results suggest that simply adding the baffles reduced the rate of fouling by almost a factor of 3.0. This effect was observed at all air flow rates for nozzle sizes of 1.0 and 2.0 mm and indicates that baffles are very effective in distributing the air bubbles over the membrane. Figure 3.8 illustrates the effectiveness of baffles in distributing the air bubbles by comparing two photographs taken from cases with and without baffles. Figure 3.8 (a) shows that in the absence of baffles most bubbles migrate towards the centre of column and continue to rise in that vicinity. Figure 3.8 (b) reflects that when baffles are present there is better distribution of bubbles across the membrane surface. The differences in the two-phase flow patterns are even much better illustrated by looking at short videos recorded for the two scenarios. These videos have been attached as Appendix B in a compact disc (CD). The video with a file name ‘Video 1’ shows the flow profile in a non-baffled case and the video entitled ‘Video 2’ shows the flow profile in a baffled case.

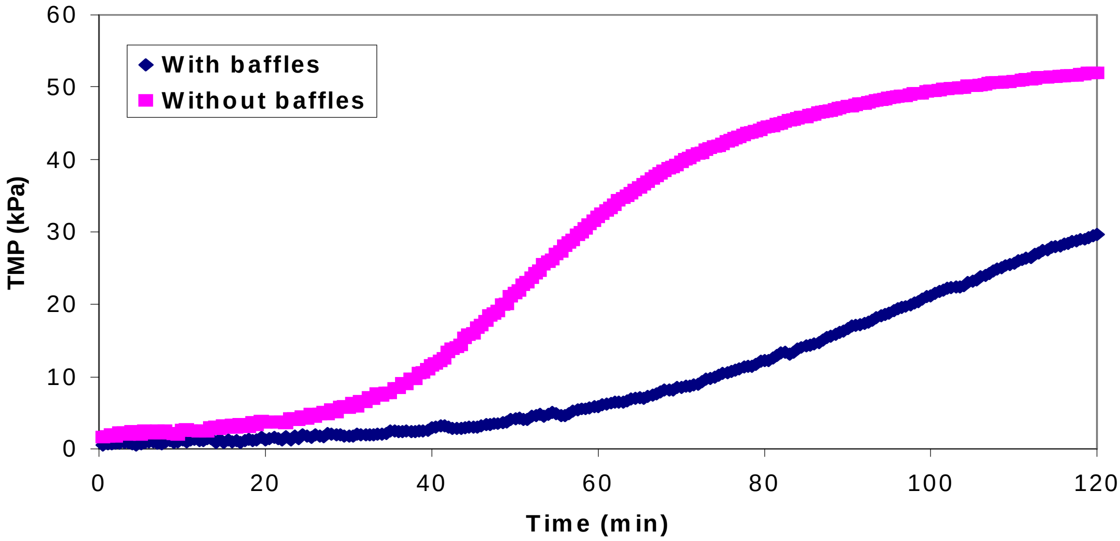

Figure 3.7. Variation of TMP with time for a run with baffles and without baffles. The nozzle size is 0.5 mm, the concentration is 5 g/L and the air flow rate is 2 l/min.

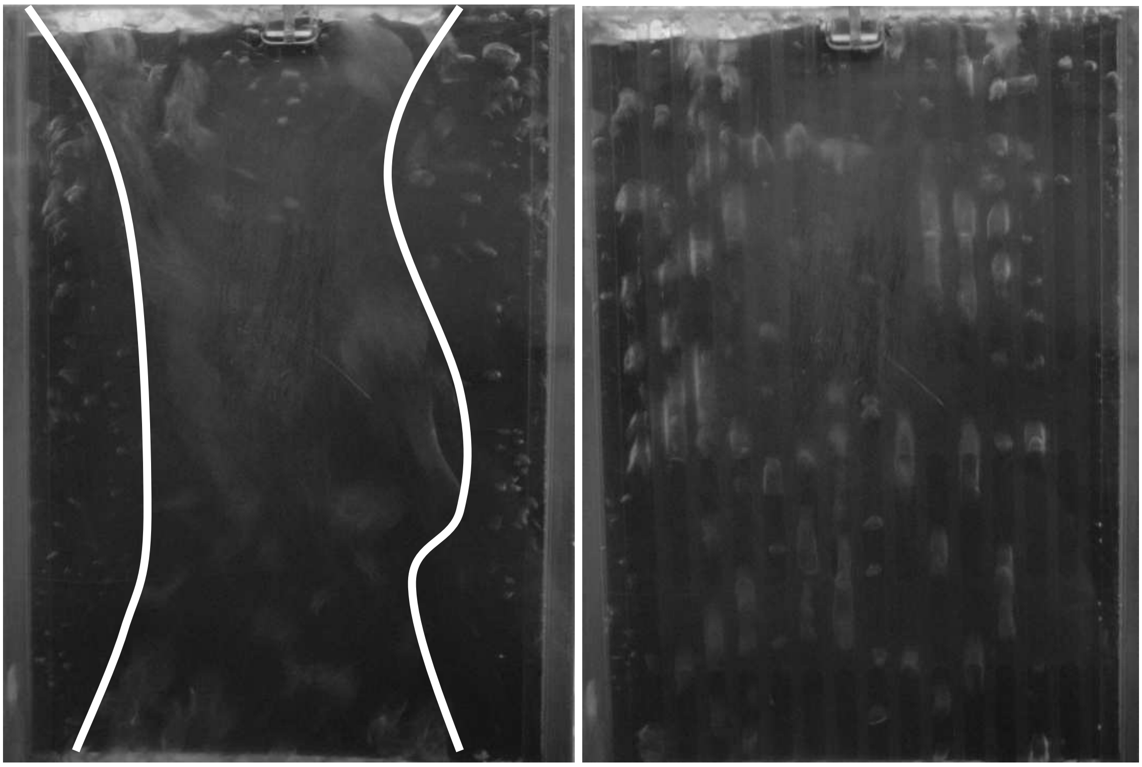

(a) (b)

Figure 3.8. Comparison of two-phase flow profiles in (a) non-baffled and (b) baffled cases. The air flow rate is 8 l/min through a 2.0 mm nozzle.

Although experiments in this study were designed to be at constant flux, at higher concentrations the flux started to decline at some point during the experiment. When the resistance across the membrane had increased to a certain value, the pump was no longer able to maintain constant flux thus leading to a decline in flux. Significant flux decline was not observed for the concentration of 5 g/L, but it was observed at concentrations of 10 and 15 g/L. Flux decline for a submerged MBR system was also observed by Shimizu et al. (1996) after TMP had reached a certain level.

There are a number of methods by which fouling reduction occurring on the surface of the membrane could be analysed. Methods that have been used in this study are:

(i) observing the final TMP attained at the end of each run or the final total resistance,

(ii) calculating a TMP reduction factor whose computation is shown in equation 3.2,

(iii) calculating the rate of change of TMP (dTMP/dt) at a particular fixed time for each run and

(iv) calculating the change in the specific cake resistance.

Figure 3.9 shows the final TMP obtained at the end of two hours for different nozzles and different bubbling rates for a concentration 5 g/L whilst Figure 3.10 compares final TMPs for runs with baffles and those without baffles. Figure 3.9 shows that the final TMP decreases with increasing air flow rate and nozzle size. Similar trends were observed at concentrations of 10 and 15 g/L. Since flux was constant in the experiments for 5 g/L, the plots of final resistance against air flow rate and nozzle size yielded the same trends as those shown by Figure 3.9 with the resistance decreasing with an increase in the air flow rate and nozzle size as shown in Figure 3.11. Figure 3.10 shows that the biggest reduction of the final TMP occurs with a smallest air flow rate of 2 l/min when baffles are used. At 8 l/min, the difference in the final TMP, for a case with and without baffles, is small. At an air flow rate of 2 l/min when baffles are used, the final TMP is 38% lower when compared to the case without baffles, and at 8 l/min it is reduced by 29%. This suggests that baffles are more effective at a smaller air flow rate, otherwise without baffles TMP reduction increases with air flow rate. However, if the data at 2 and 4 l/min (in figure 3.10) are compared it can be seen that the 2 l/min-baffled run had a lower fouling rate than the 4 l/min-unbaffled run.

The plot of final total hydraulic resistance and final TMP against gas flow rate yields essentially the same information, namely, benefit occurs from increasing gas flow rate and that bigger nozzles appear to be better than smaller ones. Another way of analysing the effect of two-phase flow was to look at specific cake resistance as opposed to total hydraulic resistance. The specific cake resistance was calculated using the following equation. The origin of Equation 3.1 is based on the analysis of microfiltration performance with constant flux processes conducted by Parameshwaran et al. (2001).

$$\frac{dR_{tot}}{dt} = \alpha_c m = \alpha_c (J - J_{crit}) * C_b \qquad (3.1)$$

where R_{tot} is the total resistance across the membrane, α_c the specific cake resistance, J the flux through the membrane, m is the cake load, J_{crit} the critical flux and C_b the bulk concentration. According to this equation, the net deposition of particles occurs when flux through the membrane is greater than the critical flux. The change in resistance is therefore only due to the new material being deposited. This change in resistance can be evaluated from the change in the TMP. Having evaluated the critical flux independently (as will be described in section 3.5.5), the specific cake resistance can then be evaluated at a particular moment in time. When the fluxes drop below the critical flux, equation 3.1 can no longer be used to calculate the specific cake resistance. For most runs conducted in this study, fluxes dropped below critical flux after about 90 minutes of operation (for feed concentrations of 10 and 15 g/L). The specific cake resistance was therefore only calculated up to the 90th minute. It is recognised that this estimation is an approximation because,

(a) it assumes homogeneous deposition on the membrane, and this is unlikely (see above), and
(b) early values may have incomplete deposition.

The trends in Figure 3.12 show α_c apparently increasing with time and lower values at higher airflow rates. The effect of air flow rate on α_c is similar to that reported by Cabassud et al. (2001) for filtration of clay particles by hollow fibre UF membrane with bubbly flow in the lumen. It suggests that the surface shear promotes a more open deposit at high gas flow. The observed increase in α_c with time could be partially related to the incomplete deposition [point (a) above], but this does not explain the longer term trends. Other reasons for α_c rise include cake collapse or compression and infiltration of fines into the deposit. Without further analysis it is not possible to pin point the mechanism. However the observations suggest that intermittent suction (to promote cake relaxation and removal) would be beneficial. This approach is discussed in section 3.5.8.

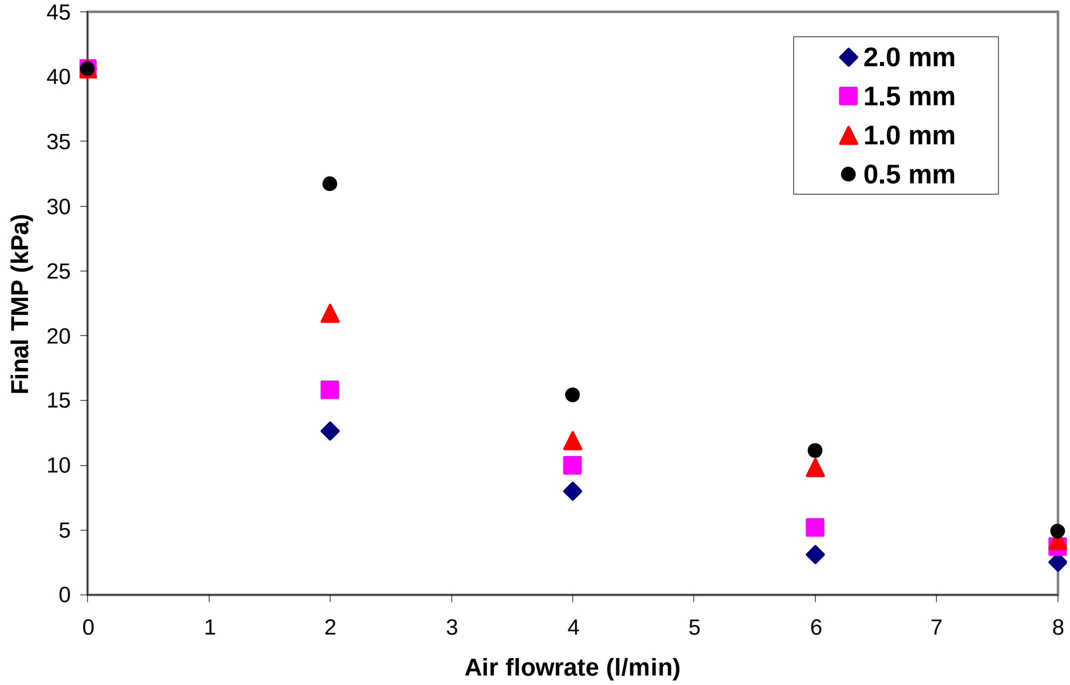

Figure 3.9. Final trans-membrane pressures (TMP) obtained at the end of each experiment for a concentration of 5 g/L and different nozzle sizes for runs with no baffles.

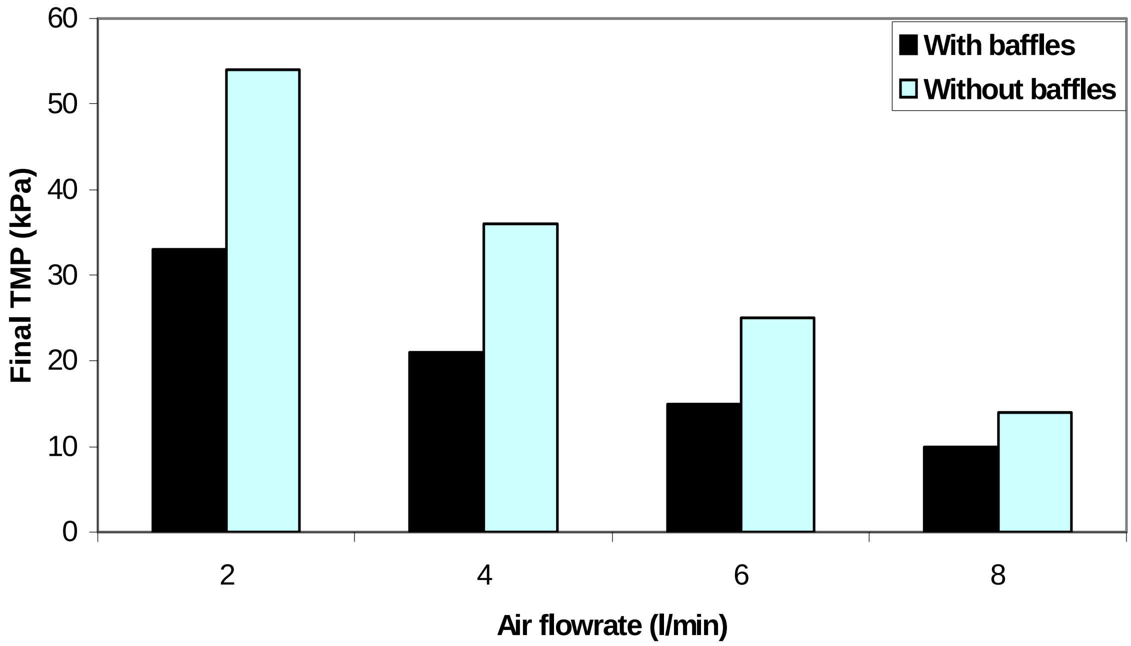

Figure 3.10. Final TMP obtained after two hours for runs with and without baffles for a concentration of 5 g/L and a nozzle size of 2.0 mm.

	2.0 mm	1.5 mm	1.0 mm	0.5 mm
0	4.23	4.23	4.23	4.23
2	1.32	2.1	2.9	3.56
4	0.6	1.1	1.7	2.2
6	0.369	0.566	0.9	1.3
8	0.11	0.32	0.52	0.78

Figure 3.11. Total hydraulic resistance calculated at the end of each experiment for runs without baffles for a feed concentration of 5 g/L.

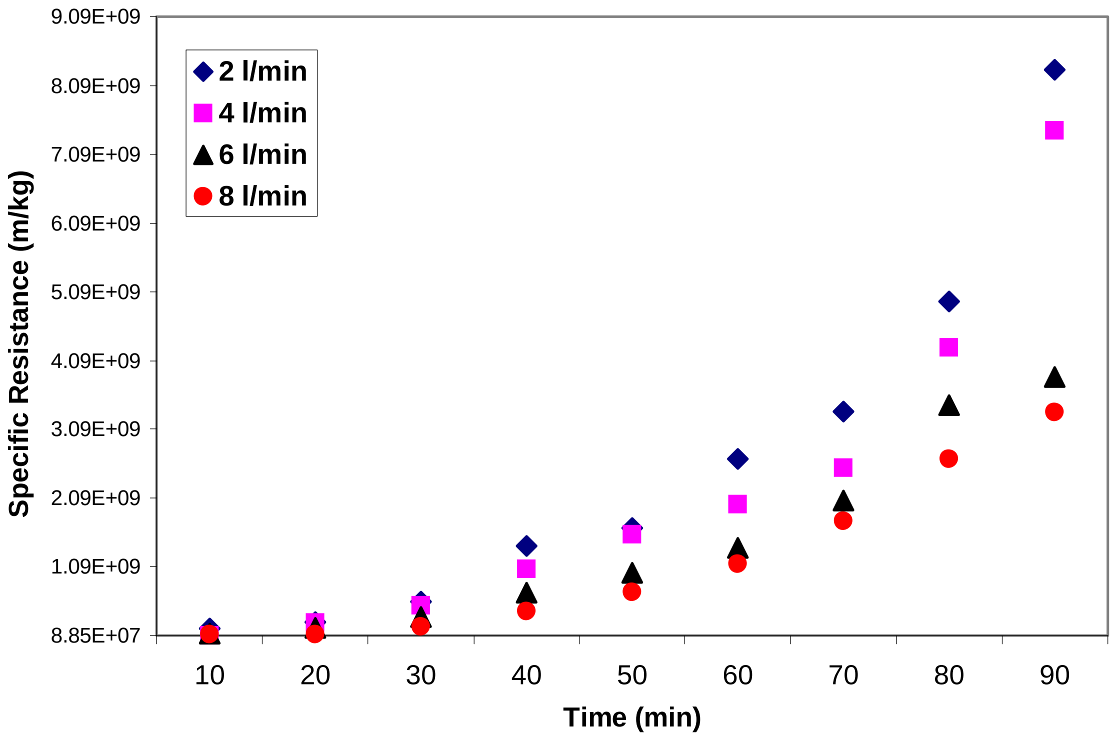

Figure 3.12. Evolution of the specific cake resistance with time for a concentration of 10 g/L and a 0.5 mm nozzle is used. There were no baffles in these experiments.

In order to obtain further insights into the fouling phenomena, TMP reduction factors were computed. In most previous studies in which gas-liquid two-phase has been studied, flux enhancement was used as a measure of the effectiveness of bubbling (Bellara et al., 1996; Cabassud et al., 2001; Cui et al., 2003). This criterion cannot be applied in this study as flux is mostly constant. Rather TMP reduction computed as follows was used as a measure of the effectiveness of bubbling.

$$\phi = \frac{Final\,TMP\,achieved\ without\ gas\ bubbling}{Final\,TMP\,achieved\ with\ gas\ bubbling} \tag{3.2}$$

Thus $\phi > 1$ indicates improvement. Figure 3.13 shows TMP reduction factors for the runs at 5 g/L calculated using equation 3.2. This Figure shows that the extent of TMP reduction increases with both the nozzle size and the airflow rate. This trend was also observed at concentrations of 10 and 15 g/L. This is somewhat contrary to findings in other studies (e.g., Cui & Wright, 1996; Sur et al., 1998), where the advantage gained by bubbling was found to be the greatest with a smaller bubbling rate and to decrease when the bubbling rate was increased. Still other researchers reported an optimal gas flow rate for bubbling inside tubular and hollow fibre modules (Laborie et al., 1998; Cabassud & Ducom, 2001). However, in this chapter an optimal gas flow rate was not realised over the range of airflow rates studied and the extent of fouling reduction increased with an increase in air flow. Part of the reason for the difference in results may be that the membrane modules studied by researchers such as Cui & Wright (1996), Laborie et al. (1998) and others were those in which bubbling occurred in the lumen of the membrane where a different regime of two-phase flow occurs. In the case of bubbles or slugs inside tubes, an increase in air flow may increase the slug length rather than the number of slugs (and slug wakes). The data here for submerged flat sheets can be compared to studies on submerged hollow fibres (Chang & Fane, 2001) where increase in bubbling also improves performance although the benefit reaches a ‘plateau’ where further gas rate increase has little effect. The same trend could be anticipated for submerged flat sheets, although not observed over the gas flows studied in this chapter.

Another way of analysing fouling reduction is to calculate the rate of change of TMP two hours after the start of the experiment. This method was preferred over calculating the maximum dTMP/dt for each experiment because, in some of the experiments after three hours of operation, the maximum slope may not have been reached, particularly when the gas flow rates were high. However, the shortcoming of this method is that, since it only looks at one particular moment in time and not an average over time, it may not be a true reflection of the fouling rate under those conditions. Calculated values of dTMP/dt at each flow rate for each nozzle are shown in Figure 3.14. The rate of change of TMP with time (dTMP/dt) represents the fouling rate. The higher the rate of change of TMP, the faster is the fouling rate. Figure 3.14 confirms that the greatest fouling rate occurs with the smallest nozzle and smallest gas flow rate.

Figure 3.15 shows typical dTMP/dt data calculated after 90 minutes of filtration for a run with and without baffles. As expected the dTMP/dt decreases with an increase in air flow rate and it is lower for the cases with baffles than the cases without them. It is also evident from this Figure that the difference in the dTMP/dt between cases with baffles and those without them decreases as the air flow rate increases. This supports further the indication that using baffles is more effective at lower air flow rates. This suggests that when baffles are used, a lower gas flow rate may be necessary to achieve the same effect achieved at a high gas flow rate without baffles. Therefore the use of baffles may also results in the saving of energy.

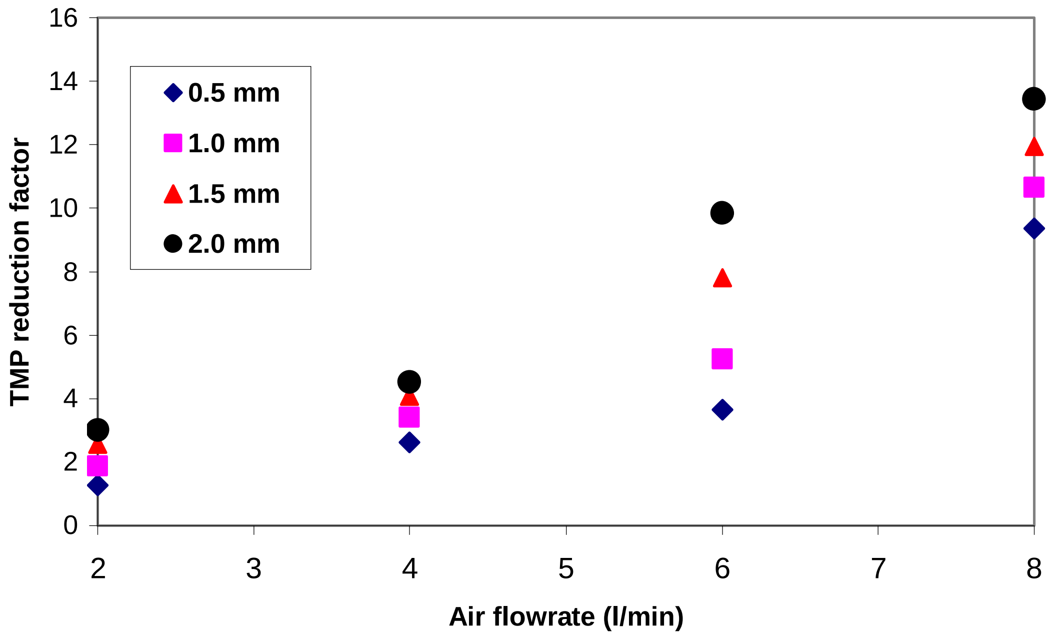

Figure 3.13 TMP reduction factors at two hours plotted against the air flow rate for runs without baffles.

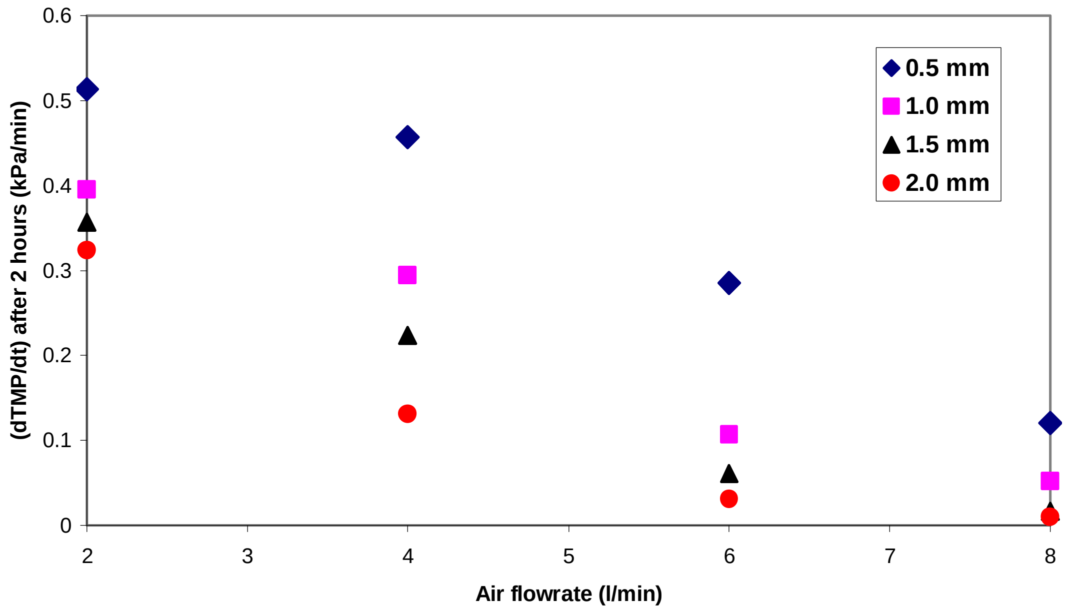

Figure 3.14. dTMP/dt values determined after two hours of filtration for non – baffled cases.

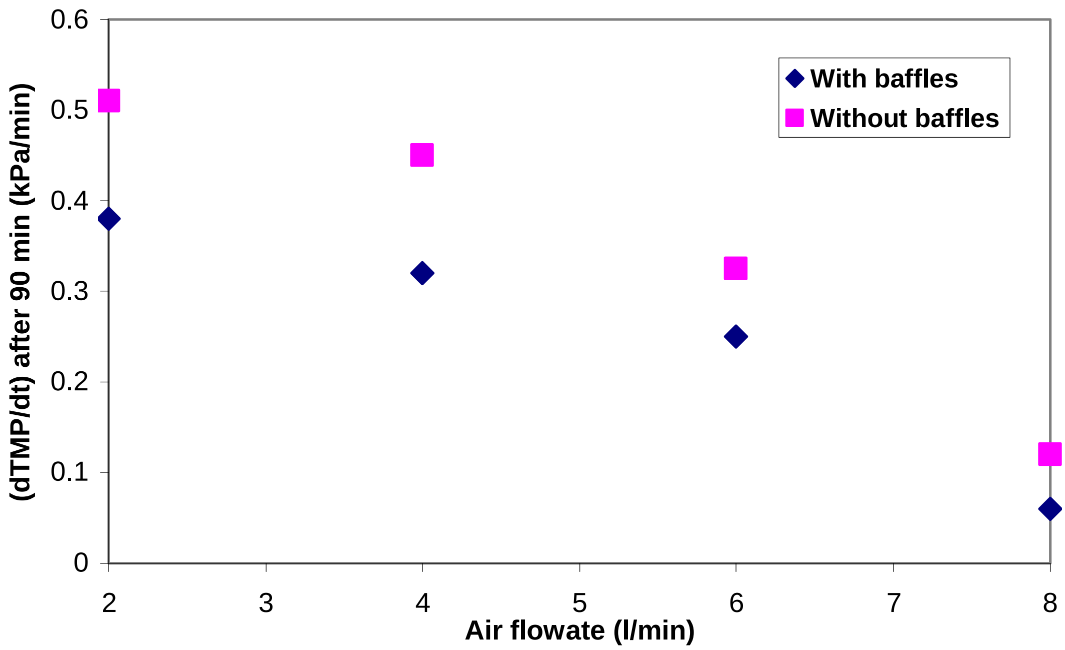

Figure 3.15. dTMP/dt values calculated after 90 minutes of filtration for runs with and without baffles for a 2.0 mm nozzle.

Figures 3.6 to 3.15 all show that the effectiveness of gas bubbling improved with an increase in the gas flow rate and nozzle size and that the use of baffles improves the efficiency of two-phase flow. Bubbling is clearly much better than no bubbling at all; even at low flow rates, such as 2 l/min there is considerable reduction in the TMP. The nozzle size also plays a significant role in the bubbling process. The efficiency of bubbling improved with an increase in the nozzle size with the 2.0 mm nozzle being the most effective. However, Figure 3.9 suggests that, as the air flow rate increases, the differences between the nozzle sizes diminish. This indicates that, if high gas flow rates are to be used, the efficiency of the two-phase flow will tend to be independent of the nozzle size. The beneficial effect of larger nozzle size observed here for the submerged flat sheet has not been observed for submerged hollow fibres, where marginally better fouling control appears to come from smaller size nozzles (Wicaksana et al. 2006). The reasons for these differences are not clear but may due to the different flow paths and effects bubbles can have between flat vertical walls and in and around flexible bundles of fibres.

As a strategy, the usage of high gas flow rate is not recommended as this is counter productive. The bubbling rate of 8 l/min used in this study is equivalent to 80 l/min.m^2 of membrane area and is above typical gas flow rates used in industry per meter square of membrane area which ranges from 10 to 60 l/min.m^2 (see section 3.3.5). Usage of very high air flow rates may have a negative effect in MBR applications because the agitation induced by the bubbles may cause disruption of the biofloc, which in turn would slow down the biodegradation process (Brockmann & Seyfried, 1996). Moreover, high flow rates require high energy inputs thus making the operating costs very high. Based on these considerations, it was concluded that air flow rates higher than 8 l/min are not practical industrially and so were not examined any further in this chapter.

The question that needs to be answered is why bubbles are effective. Possibilities include increased shear stress on the membrane, increased liquid superficial velocity and the development of back-pressure across the membrane surface. These will be addressed further in the discussion section when other investigations such as critical flux analysis and analysis of fouling deposit on the membrane have been presented.

The effect of imposed flux on dTMP/dt was also evaluated at different air flowrates. During this evaluation, the flux was held constant for about 30 to 40 minutes and then the overall dTMP/dt over that duration was evaluated. This was repeated for different fluxes at different air flow rates. The experiments were carried out only for the 0.5 and 2.0 mm cylindrical nozzle at 5 and 10 g/L. Typical results obtained for a concentration of 5 g/L and a 0.5 mm nozzle are shown in Figure 3.16(a). It is observed that dTMP/dt decreases with an increase in the air flow rate for all fluxes considered. For low fluxes, such as 15 l/m^2.hr, the dTMP/dt value is close to zero for all air flow rates which indicates that the rate of fouling is extremely low, thus this flux may be close to a critical flux.

At constant air flow rates, the dTMP/dt increases with an increase in flux which means that fouling is higher at higher fluxes. When the dTMP/dt are plotted versus flux for the lowest gas flow rate (2l/min) [Figure 3.16 (b)] it is evident that beyond a flux of about 20 l/m^{2}hr the TMP rise was rapid. This identifies the critical flux at this air flow rate. It shows that even at the lowest gas rate the system could be operated at a reasonably high flux. In practice the choice of flux and airflow rate would involve a balance of capital cost (flux related) and operating cost (airflow related).

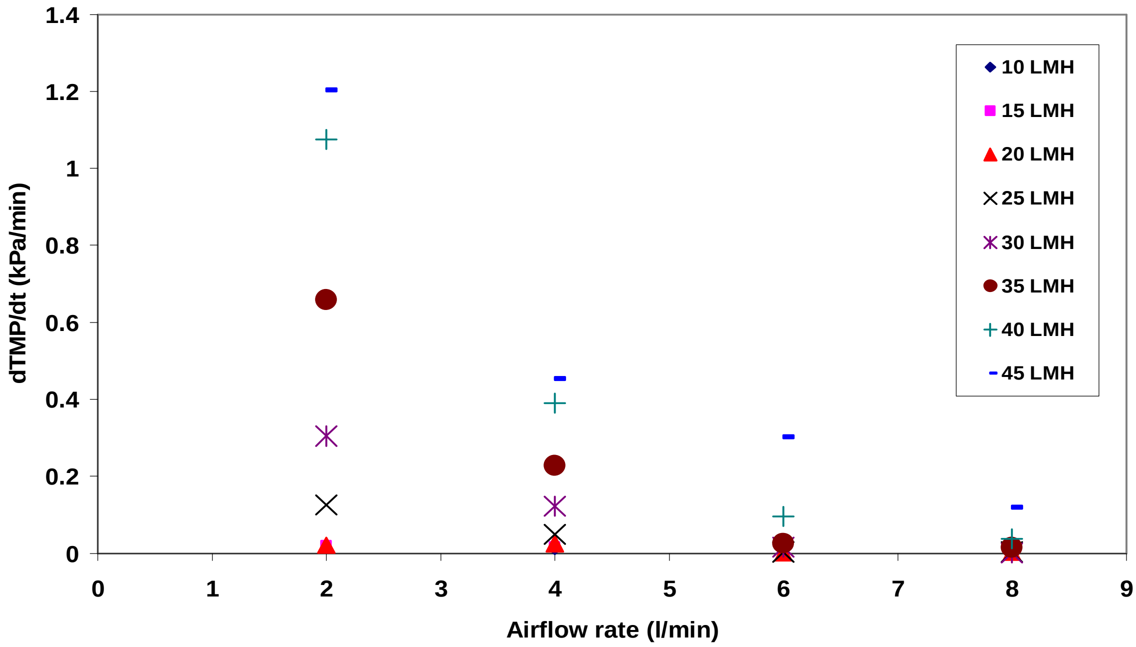

Figure 3.16 (a). Variation of dTMP/dt with air flow rate for each flux at a concentration of 5 g/L and 0.5 mm nozzle was used.

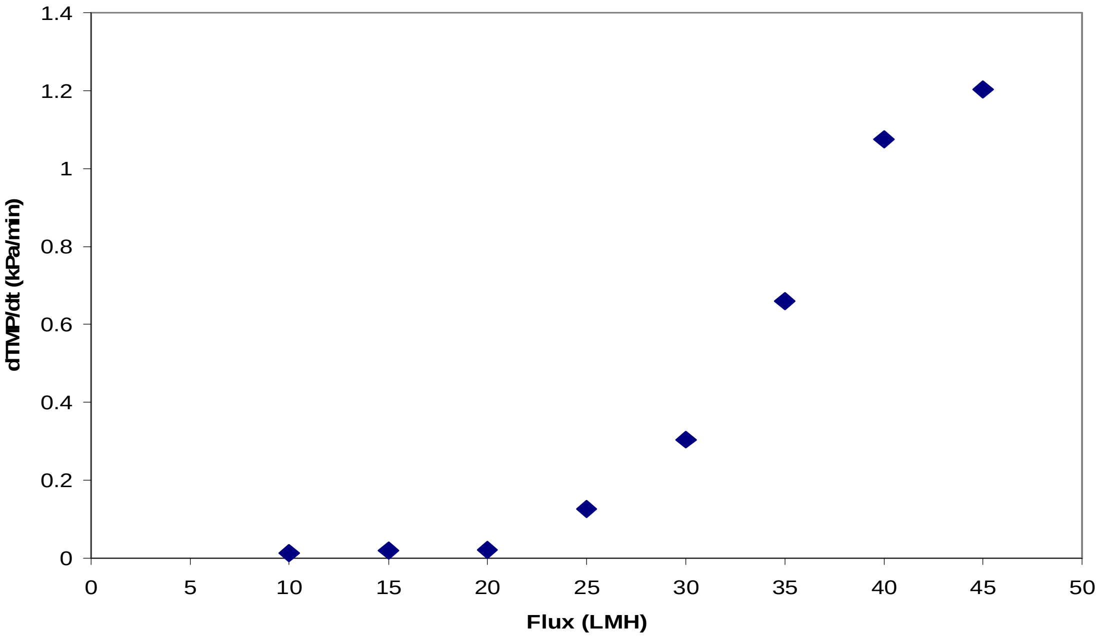

Figure 3.16 (b). Variation of dTMP/dt with flux for an air flow rate of 2 l/min.

3.5.3 The effect of concentration

From the literature, it has been stated that bubbling is more effective under conditions which are more prone to fouling such as high TMP and high concentration (Mercier et al., 1995; Cui et al., 2003). Thus it has been concluded that flux enhancement by air bubbling is due to the disruption of the concentration polarisation layer. In some studies, it has been observed that increasing the concentration can improve the flux because if there are more particles present, particles will collide more often and in this way coagulation between the particles is promoted (Cabassud et al., 1997). When the larger coagulated particles are deposited on the membrane surface, they will tend to form a cake with a higher voidage and hence less resistance and this will improve the performance. The results for specific cake resistance versus air flow rate (Figure 3.13) support this view.

In order to assess the effect of concentration on the effectiveness of bubbling, runs were carried out at three feed concentrations of 5, 10 and 15 g/L with an initial imposed flux of 40 l/m^2hr. However, in this study, as shown in Figure 3.17, increasing the concentration had a negative effect on TMP which means that fouling was more severe at a higher concentration. Trends similar to those shown in Figure 3.17 were observed at all gas flow rates. This result is not unexpected based on the well-known effects of feed concentration on the degree of polarisation and rate of cake formation. In other words any notional benefits in decreasing α_c with concentration would have been swamped by the increased cake load (*m* in equation 3.1) due to concentration. Churchouse & Wildgoose (1998) also observed that higher concentrations of the mixed liquor led to higher TMPs during evaluation of a submerged flat sheet MBR.

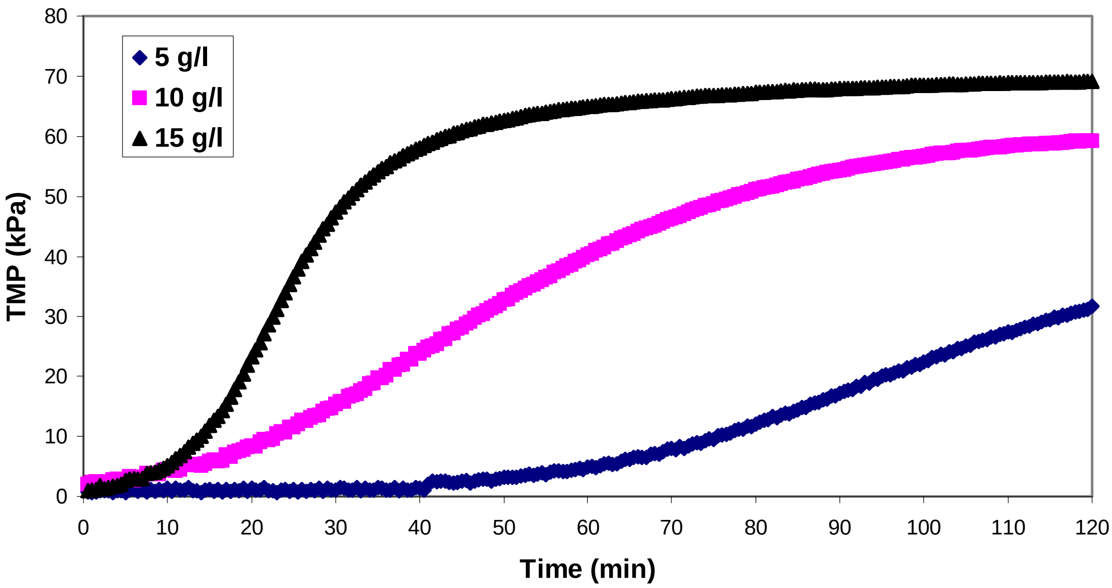

Figure 3.17. Variation of TMP with time for three different concentrations when the bubbling rate is 2 l/min and a nozzle size of 0.5 mm is used.

The final TMPs obtained after two hours of experimentation for different gas flow rates at different concentrations with a nozzle size of 0.5 mm are shown in Figure 3.18. The final TMP decreases with an increase in air flow rate for each concentration. The final TMP also increases with an increase in concentration.

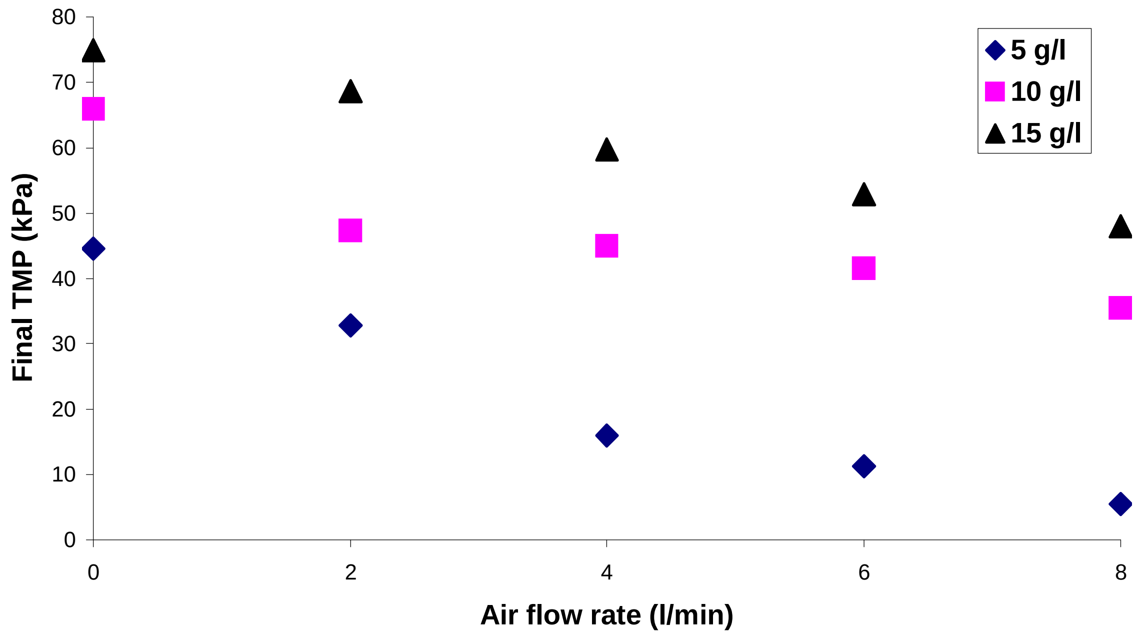

Figure 3.18. Final TMPs after two hours of experimentation for a nozzle size of 0.5 mm.

As for previous results reported in section 3.5.2, all experiments were intended to be at constant flux, however as mentioned earlier, significant flux decline was observed at higher concentrations of 10 and 15 g/L as illustrated by Figure 3.19. Similar effects of concentration on flux were reported by Bellara et al. (1997) and Mercier-Bonin et al. (2000a). The point where the flux starts to decline coincides with the point when the TMP starts to increase rapidly as reflected in Figure 3.20 at the concentration of 10 g/L and gas flow rate of 2 l/min for a 0.5 mm nozzle. This figure clearly shows that TMP increase is related to the build up of the filter cake. The extent of fouling reduction was evaluated using TMP reduction factor as shown in Figure 3.21 for the 2.0 mm nozzle. Similar trends were observed for nozzles of different sizes. As shown previously, the degree of TMP reduction increases with the air flow rate. However, at high concentrations of 10 and 15 g/L, the increase is small, varying from 1.3 to 1.8 (as the air flow rate increased from 2 to 8 l/min) compared to increasing from 2.5 to 11.6 at the low concentration of 5 g/L. Thus the apparent effectiveness of bubbles decreased as the fouling load increased. One possible reason for this is that suspension viscosity increases significantly with feed concentration, and at 15g/L the viscosity could be 2 to 3.0 times that of water. This would tend to reduce bubble rise velocity and dampen the effects of bubble-induced surface shear.

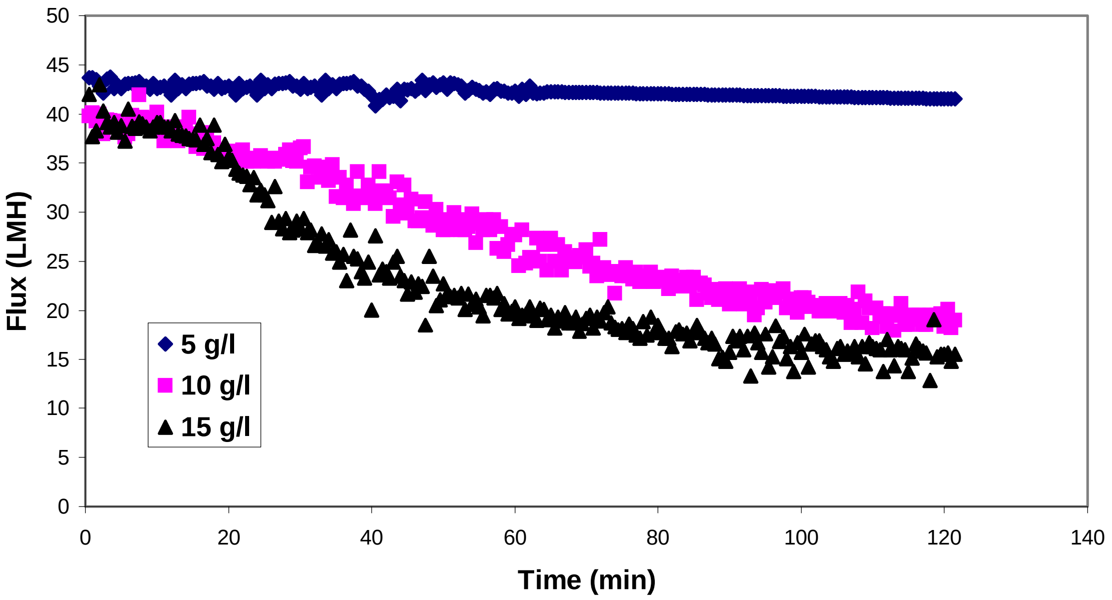

Figure 3.19. Variation of flux with time for different concentrations at an air flow rate of 2 l/min and a nozzle of 0.5 mm.

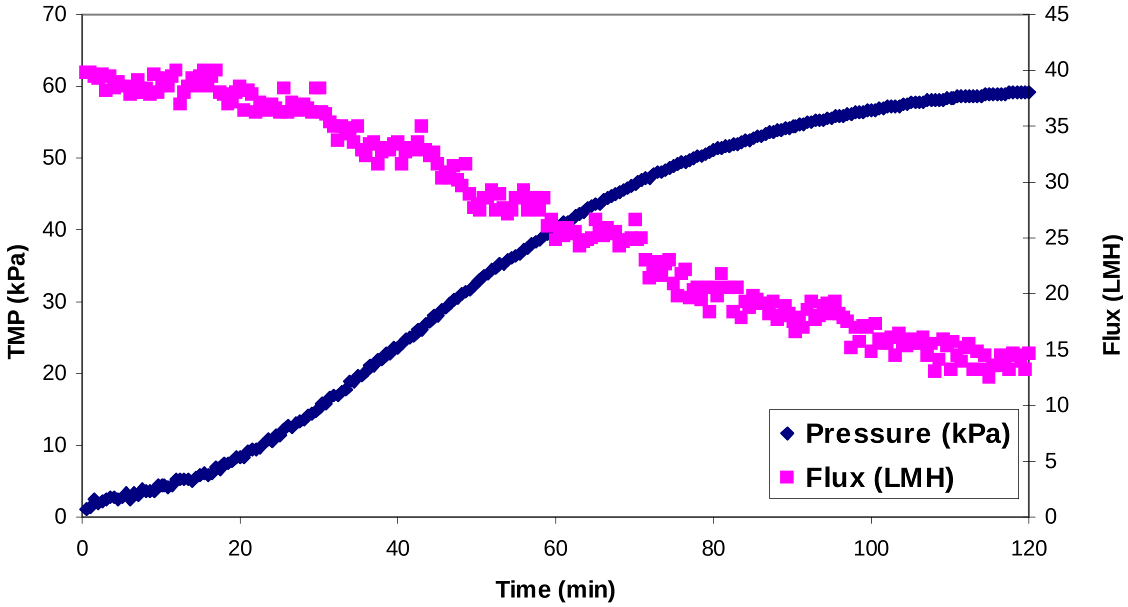

Figure 3.20. Variation of flux and TMP when the concentration is 10 g/L. The air flow rate is 2 l/min and a 0.5 mm nozzle is used.

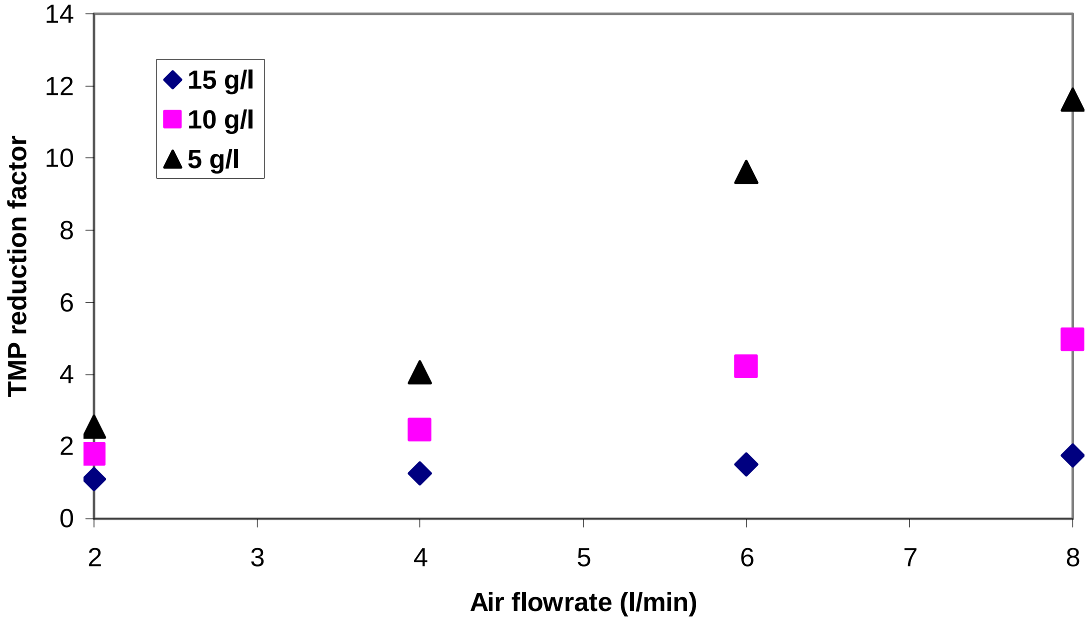

Figure 3.21. TMP reduction factors obtained at different concentrations for all air flow rates when a 2.0 mm nozzle was used.

3.5.4 Evaluation of fouling deposits

In section 3.5.2, it was shown that the initial rise in TMP is slow. It is possible that when foulants start to deposit on the surface of the membrane, they do not deposit uniformly. This would result in some areas of the membrane remaining 'cleaner' than others. These clean spots would offer low resistance to permeate flow and thus keep the TMP rise low. In order to analyse the validity of this idea, an analysis of the amount of total carbohydrates deposited at two different locations on the membrane was conducted.

Furthermore, from visual observations and videos of the two-phase flow, it was observed that there is greater gas flow near the centre of the membrane than near the edges as previously shown in Figure 3. 8 (see also Video 1 in Appendix B, the Compact Disc). Although the nozzles are evenly distributed at the bottom of the membrane, gas bubbles tend to prefer a particular path as they rise past the membrane, moving in a zigzag manner near the centre-line of the membrane. Bubbles emerging from the nozzles near the walls quickly move towards the centre of the membrane to form a large 'swarm' of bubbles, with very few bubbles passing close to the wall. The migration of bubbles away from the column wall towards the centre is a phenomenon which has also been observed commonly in bubble column reactors (Ranade, 1997; Jacobsen et al., 1997) but there has been no general agreement reached in literature regarding the probable causes of bubble migration.

Lopez de Bertadano et al. (1990) attempted to explain the migration of bubbles in turbulent bubble flows. They stated that phase distribution could be controlled by the liquid phase turbulence structure, also called turbulent migration. According to this theory, the gas phase has a tendency to accumulate in the regions of maximum turbulent kinetic energy of the liquid phase which tends to be near the column centre. Another possible source for lateral migration according to Spicka et al. (2001) could be the asymmetric flow around a bubble rising near the walls. Because of the no-slip boundary condition on the walls, there is increased pressure from the side of the wall that generates a net inward lateral force similar to the Bernoulli force. Tzeng et al. (1993) attributed the bubble migration to the uneven dissipation of turbulence generated by bubble wakes. Another possible cause for bubble migration according to Jacobsen et al. (1997) is the Magnus force, which is purely related to transversal forces acting on rotating bodies. If a rotating particle is placed in a uniform flow field, the particle rotation results in an increase in the velocity on one side and a decrease on the other. This gives an asymmetrical pressure distribution around the particle due to the viscous effects close to the particle interface which results in the particle migrating.

For our analysis of deposits, one location was selected near the centre of the membrane where there is strong upward two-phase flow and a second location was selected near the bottom right corner of the membrane where there are very few bubbles but strong recirculation of the liquid. The position of the analysis locations selected is illustrated in Figure 3.22. The filtration experiments were run for about 40 minutes and then stopped. This time of 40 min was chosen because after this period the TMP typically started to rise very rapidly which may indicate more uniform fouling across the membrane. After 40 minutes, the membrane was carefully removed from the feed tank with minimum agitation and cleaned only on the spots indicated in Figure 3.22. An O-ring of about 30 mm diameter was placed on the selected regions and a hollow cylindrical Perspex vessel with the same diameter was placed on top of the O-ring and firmly held. A volume of 80 to 120 mL of milli-Q was used to clean the membrane for 5 minutes. The cleaning solution was collected using a syringe and analysed for total carbohydrates using the method developed by Dubois et al. (1956). According to this method, a volume of 0.4 mL of the cleaning solution was mixed with 0.4 mL of 5 % (w/w) phenol in a test tube. 2 mL of H_2SO_4 was added and the mixture left at room temperature (18 – 26 ^{0}C) for 10 minutes. The contents of the test tube were transferred to cuvettes and analysed on a Carry UV-VIS spectrophotometer against a blank at a wavelength of 480 nm. Carbohydrate concentration (in mg/L) was determined from a calibration curve obtained with glucose standards.

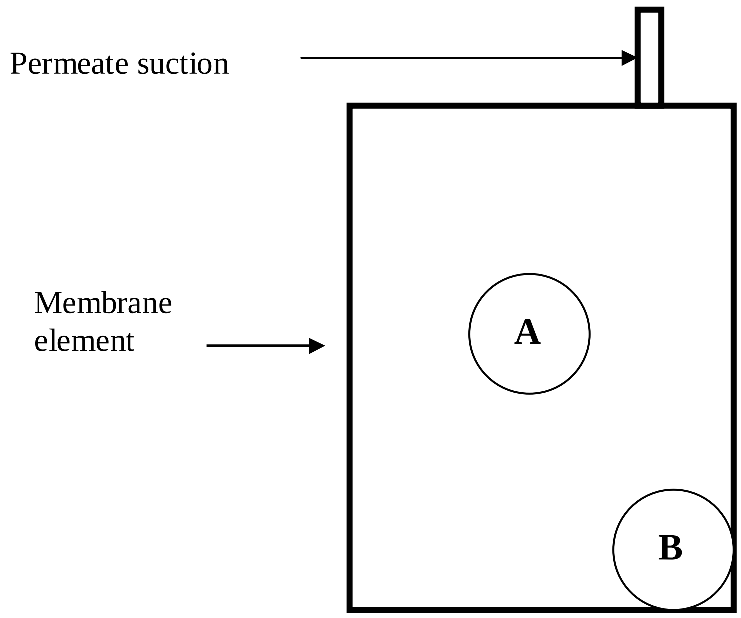

Figure 3.22. Location of spots on the membranes analysed for total carbohydrates deposited

The filtration and analysis of the foulant on the membrane was repeated seven times at a concentration of 5 g/L and an air flow rate of 4 l/min through a 0.5 mm nozzle. Although the total amount of deposits varied from one run to another as shown in Figure 3.23, location A, at the centre of the membrane (which lies in the path of most bubbles), always had a lower amount of total carbohydrates compared with location B at the bottom right corner. This result suggests that the gas bubbles are more effective in reducing deposition on the membrane surface than the recirculating liquid. Further analysis of the role of bubbles in reducing fouling will be presented in chapter 5, where the number and size of bubbles passing locations A and B have been measured. It should be noted that for constant average flux processing, the local fluxes may vary. In this situation the flux at location A would have tended to be higher because the membrane was cleaner in that location, presumably because of the higher bubble density in that region. This maldistribution of fluxes may not be sustainable if the bubble-starved regions gradually cease to permeate. Eventually the high flux region may reach a condition of critical flux, in spite of the bubble density. This is similar to the conceptual model proposed by Cho and Fane (2002) for TMP transients.

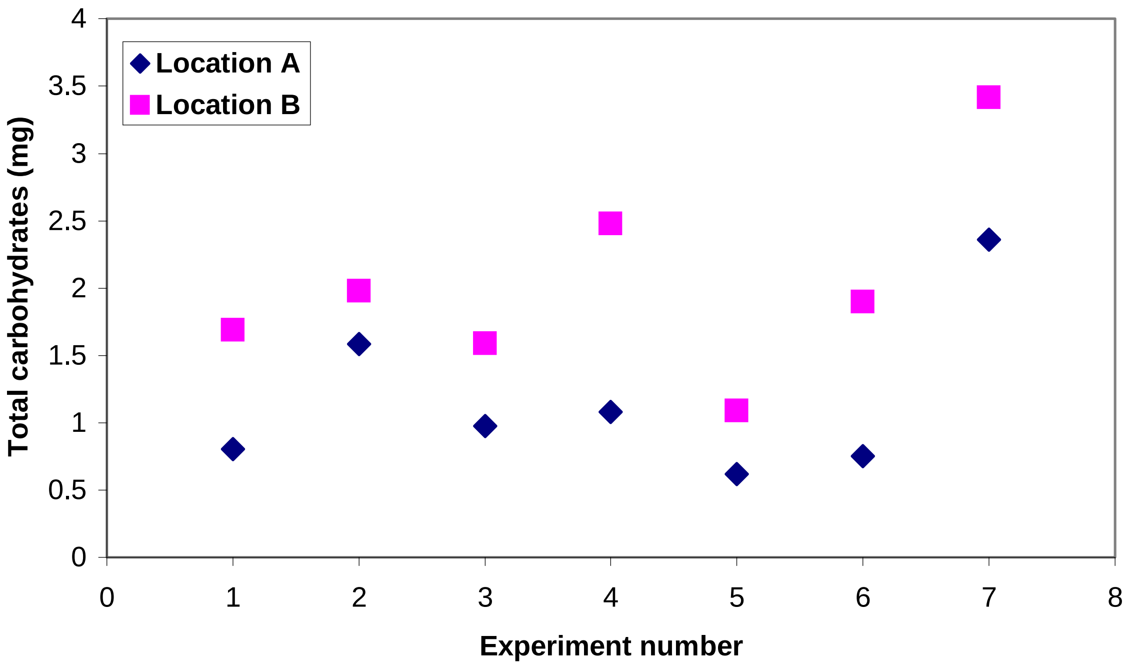

Figure 3.23. Total carbohydrates on the cleaning solution for location A and B.

3.5.5 Critical flux evaluation

The critical flux concept, which describes long-term stability of membrane processes, was first proposed by Howell and his group (1993). According to Field et al. (1995), critical flux can be defined as a flux below which no deposition occurs on the membrane surface, above this flux fouling occurs. In constant flux processes, critical flux is often defined as the flux above which TMP starts to increase rapidly with time. In constant pressure processes operating in cross flow filtration, the decline of flux with time is inevitable as the cake builds up. Thus flux declines rapidly initially and is then followed by a period where there is very small decrease of flux with time. This stable flux, which changes negligibly over a long period of time, is known as the steady-state flux and should not be confused with critical flux as stable flux is the limiting flux beyond which no further build up of the fouling layer occurs.

Knowledge of critical flux is important for commercial plants. Operating below critical flux implies that the membrane will be fouled less significantly and this will allow operation for a longer period of time before any chemical cleaning may be necessary. Obviously, operating below critical flux may mean that the production rate is low, but on the other hand prolonging the period between cleanings may mean reduced expenditure on cleaning chemicals and potentially prolong membrane life span.

There are several methods by which critical flux can be assessed. In this study, critical flux was determined by monitoring TMP while increasing the permeate flux in a step-wise fashion. Below critical flux, the TMP should remain constant with time after each flux step, because there is no net deposition. Critical fluxes were evaluated for concentrations of 5 and 10 g/L using the 0.5 and 2.0 mm nozzles. Figure 3.24 shows an example of typical data recorded during critical flux assessments. Because the flux was increased by increments of 5 l/m^2hr, the exact critical flux for each condition could only be identified to this level of accuracy as shown in Figure 3.25 for the 0.5 mm nozzle.

Figure 3.25 shows that critical fluxes increase with an increase in air flow rate but decrease with concentration. Similar dependency of the critical flux on air flow rate was also reported by Chang (2001). This trend in the critical flux agrees with performance trends obtained above critical flux in sections 3.5.2 and 3.5.3 where higher concentrations resulted in higher TMPs and lower TMP reduction factors. As noted in section 3.5.2, the trend for submerged hollow fibres is that the benefit from increasing air flow reaches a plateau and this also applies for critical flux. The data for submerged flat sheets in Figure 3.25 do not show a plateau, which presumably occurs at higher gas rates.

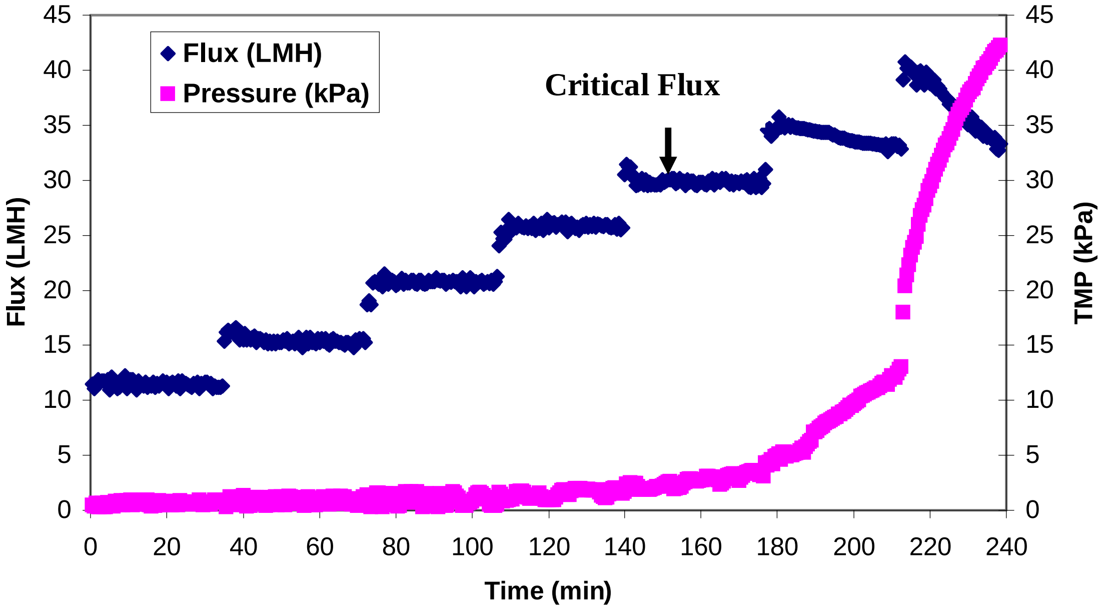

Figure 3.24. Critical flux evaluation by stepwise increase in flux method. Airflow rate is 8 l/min, nozzle size is 0.5 mm and the concentration is 5 g/L

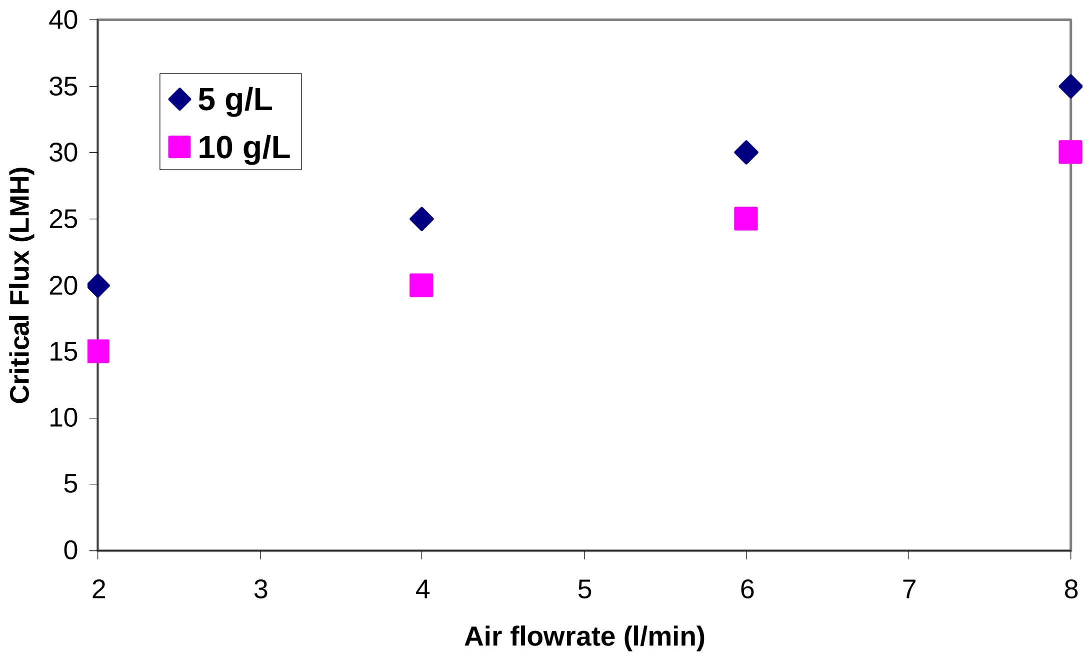

Figure 3.25. Critical flux evaluation for a nozzle size of 0.5 mm at two different concentrations.

Another method for more accurately identifying critical flux is based on monitoring the rate of change of TMP with time (dTMP/dt). When the membrane is fouling (supercritical flux conditions), TMP increases and dTMP/dt will have a positive slope. When the membrane is not fouling, TMP is constant and hence dTMP/dt is zero. The flux at which dTMP/dt changes from zero to a positive value is the critical flux [One example of this approach was shown in Figure 3.16(b)]. However in a typical experiment, the dTMP/dt curve increased up to a maximum and then decreased back to zero. The dTMP/dt decreased because flux also started to decrease (due to suction pump limitations), thus lowering the rate at which foulants were being transported to the membrane surface. The flux and dTMP/dt continued to decline until a steady-state was reached where dTMP/dt became zero and flux remained more or less constant at that particular value. Since dTMP/dt was now zero, it implies that there was no net deposition of material on the membrane, and thus the flux at this point can be interpreted as a measure of 'critical flux'. It should be noted that this method would define the average flux at which there is no longer any deposition occurring at any location on the fouled membrane. It is likely to give a lower value than the flux stepping protocol using a clean membrane. The flux at which dTMP/dt returns to zero for a fouled membrane can be defined as a type of critical flux condition, let us call it Critical Flux (F) to distinguish it from the clean membrane Critical Flux. Also under some conditions, for example, if the bubbling was very strong or the concentration was low, the dTMP/dt curve may not come back to zero, at least not within the experimental duration. Under such conditions a sustainable flux rather than a form of critical flux would be identified.

Figure 3.26 shows a typical variation of dTMP/dt with flux. In this Figure, the dTMP/dt curve returned back to zero when the flux had dropped to about 14 l/m^{2}hr implying that the flux of 14 l/m^{2}hr was a critical flux (F) for these conditions. The critical fluxes (F) identified using this method are plotted in Figure 3.27. It is clear from this Figure that critical flux (F) is a function of the airflow rate and nozzle size. Critical flux (F) seems to increase with both nozzle size and airflow rate. The identification of critical flux (F) using this method was only conducted at a concentration of 10 g/L. At a lower concentration of 5 g/L critical flux conditions were not attained by this method as the membrane fouled at a much lower rate and the dTMP/dt curve did not return to zero.

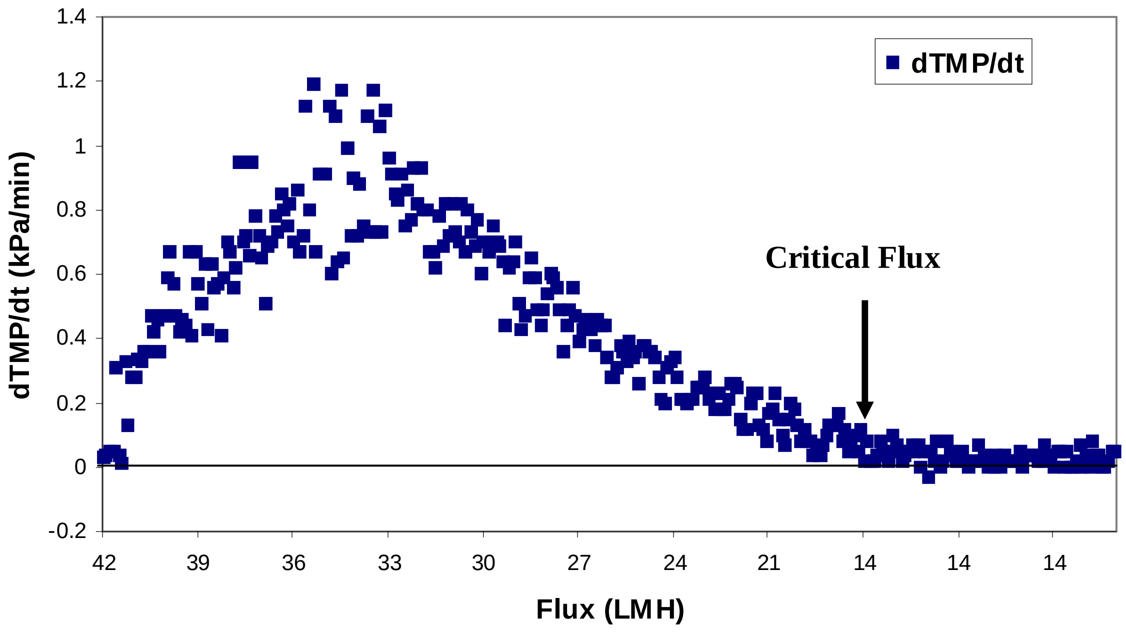

Figure 3.26. Variation of dTMP/dt with flux. The nozzle size is 0.5 mm, the airflow rate is 2 l/min and the concentration is 10 g/L.

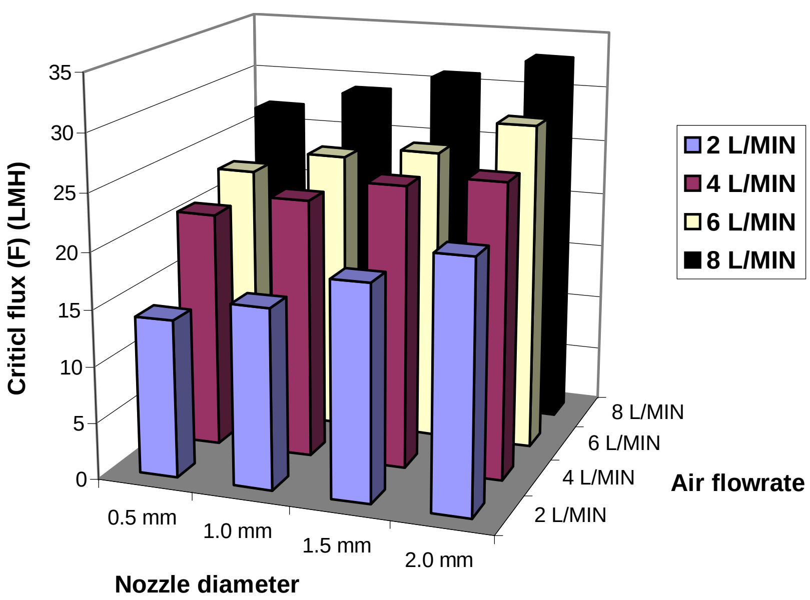

Figure 3.27. Critical flux (F) identified using the dTMP/dt method for a concentration of 10 g/L in the non-baffled runs.

A comparison was made between the critical fluxes identified by using the flux-stepping method on a clean membrane and the dTMP/dt method which identifies critical fluxes (F) after the membrane has been fouled. The comparison was made at a concentration of 10 g/L, for a nozzle size of 0.5 mm at different air flow-rate. This comparison is depicted in Figure 3.28. It can be seen from this Figure that the critical fluxes identified using the flux-stepping method are marginally higher by about 10% at most than those determined using the dTMP/dt method. This is to be expected because in the flux stepping method the membrane is still clean when the evaluation is done, whereas in the dTMP/dt method, the membrane may have been irreversible fouled.

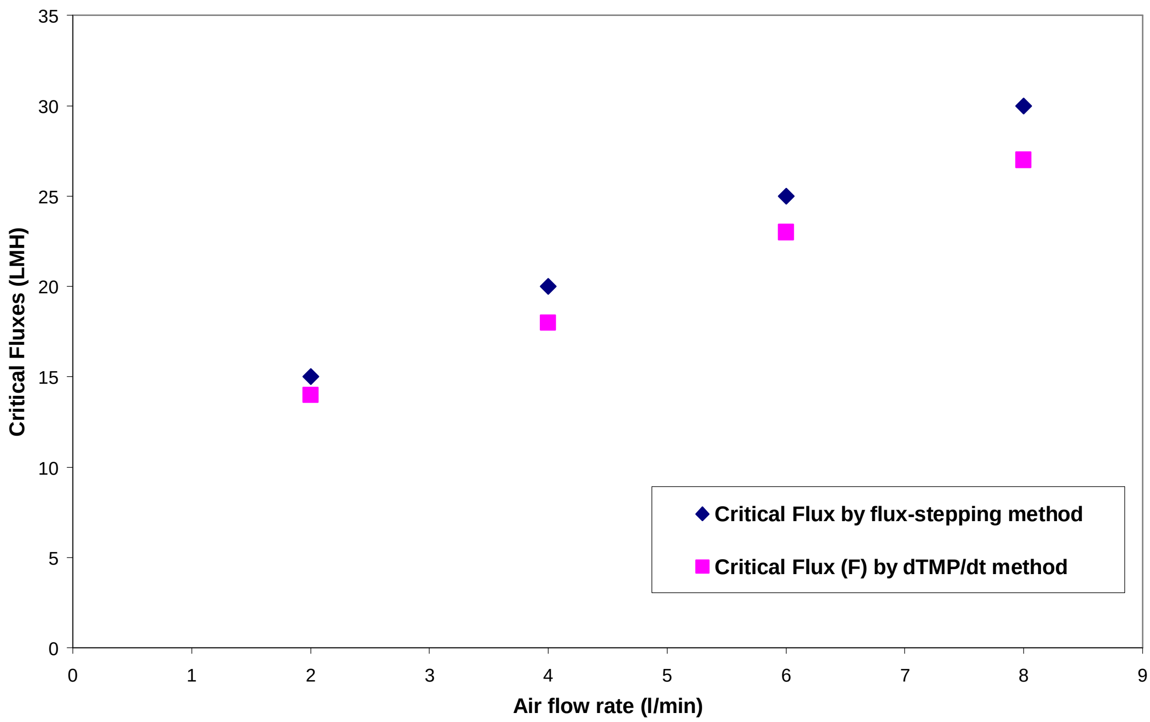

Figure 3. 28. A comparison of critical fluxes identified by two different methods. The concentration is 10 g/L and the nozzle size is 0.5 mm.

Critical fluxes were also evaluated in runs with baffles. The dTMP/dt method was used to identify the critical flux (F) for the concentration of 10 g/L with bubbling through a 0.5 and 2.0 mm nozzle. The use of baffles has already been shown to improve the effect achieved by gas bubbling and, as expected, the use of baffles also increased the critical flux (F) obtained when compared to those achieved with no baffles being used. Figure 3.29 compares critical fluxes (F) obtained with and without baffles and it can be seen that critical fluxes (F) were always higher when the baffles were used (by 10 to 30%). Also those for the 2.0 mm nozzle were greater than those of the 0.5 mm nozzle.

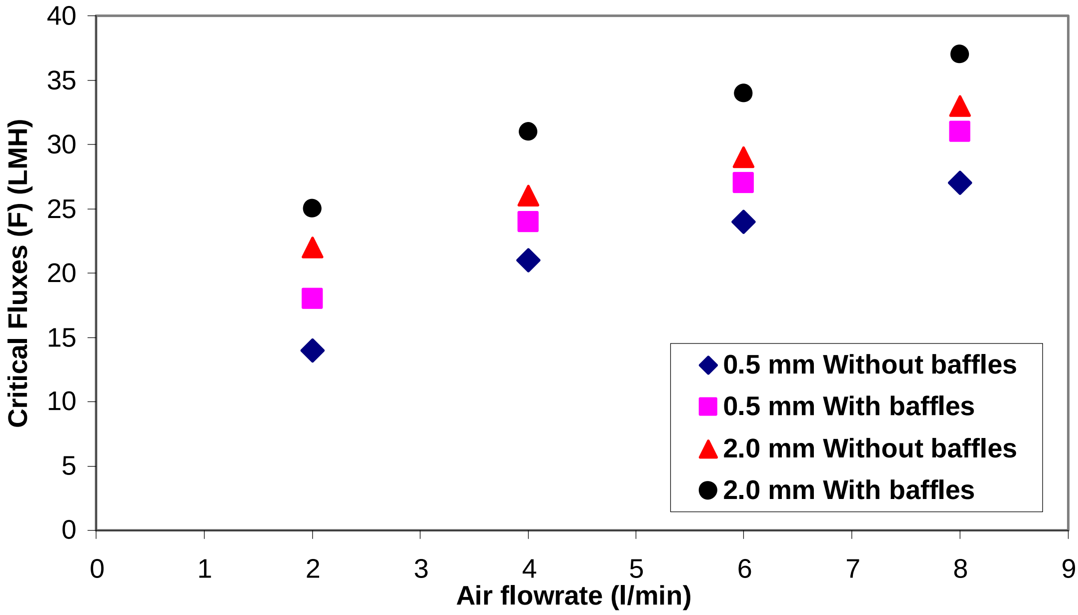

Figure 3.29. Critical fluxes (F) for runs with and without baffles at a concentration of 10g/L.

3.5.6 Effect of nozzle geometry

The geometry of the nozzle could play a significant role in determining the type of bubbles eventually formed. Different types of bubbles may induce different cleaning effects on the membrane. This is clearly a very large topic, presumably well researched by industry. However, no systematic studies have been reported in the literature on the effect of nozzle geometry in submerged membrane systems. The study reported here is also limited but points to important effects induced by different nozzle types. In this study, two types of nozzle geometry, circular as well as square nozzles were evaluated. The surface area of the nozzles was kept the same to ensure that there was an equal amount of air, and similar air velocity, being emitted from each nozzle. Four sets of nozzles with five nozzles on each tube were fabricated. The first two sets had an area of 9 mm^2 per nozzle and the second set of nozzles had an area of 16 mm^2 per nozzle.

Figure 3.30 shows TMP data obtained for the four sets of nozzles when the bubbling rate was 2 l/min at a concentration of 5 g/L. Similar results were obtained at other air flow rates. Figure 3.31 depicts the final TMP achieved after two hours of experimentation for the nozzles of 9 mm^2 surface area. The results clearly show that the circular nozzles were much better than the square nozzles for both 9 and 16 mm^2 nozzles. However, the difference between the circular and square nozzles tended to diminish slightly with an increase in air flow rate. For example, at the flow rate of 2 l/min, the difference in final TMP between the two sets of nozzles was 22% whilst at the air flow rate of 8 l/min the difference had decreased to 8%. This difference in performance by nozzles of different geometries may be due to the types of bubbles that each nozzle produces and this will be investigated further in chapter 5. Clearly it is difficult to draw firm conclusions from this limited comparison, and further work is recommended.

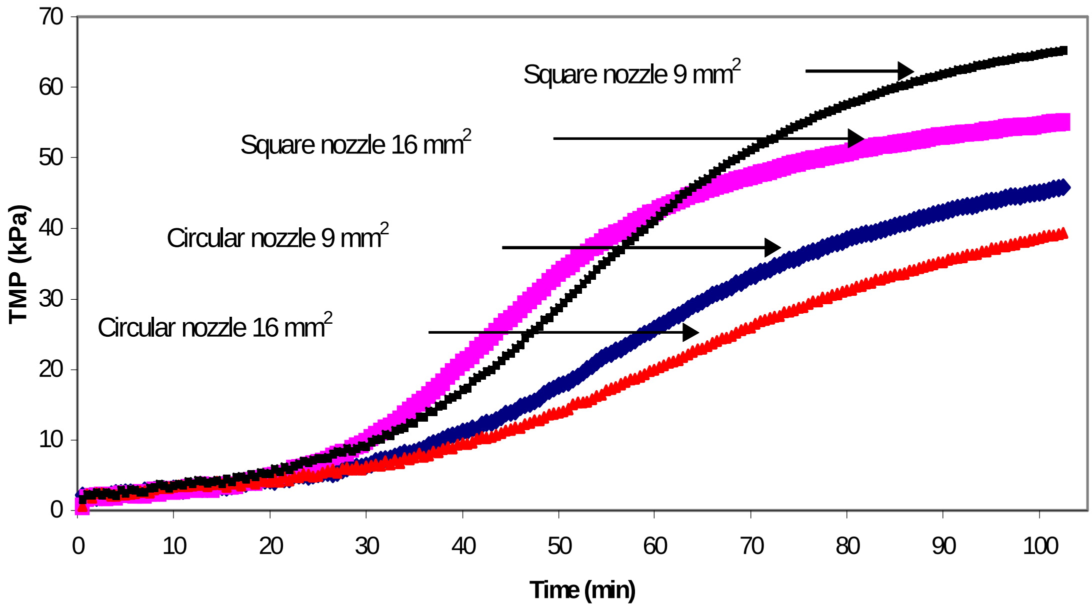

Figure 3.30. Variation of TMP with time for square and circular nozzles at a concentration of 5 g/L and an air flow rate of 2 l/min.

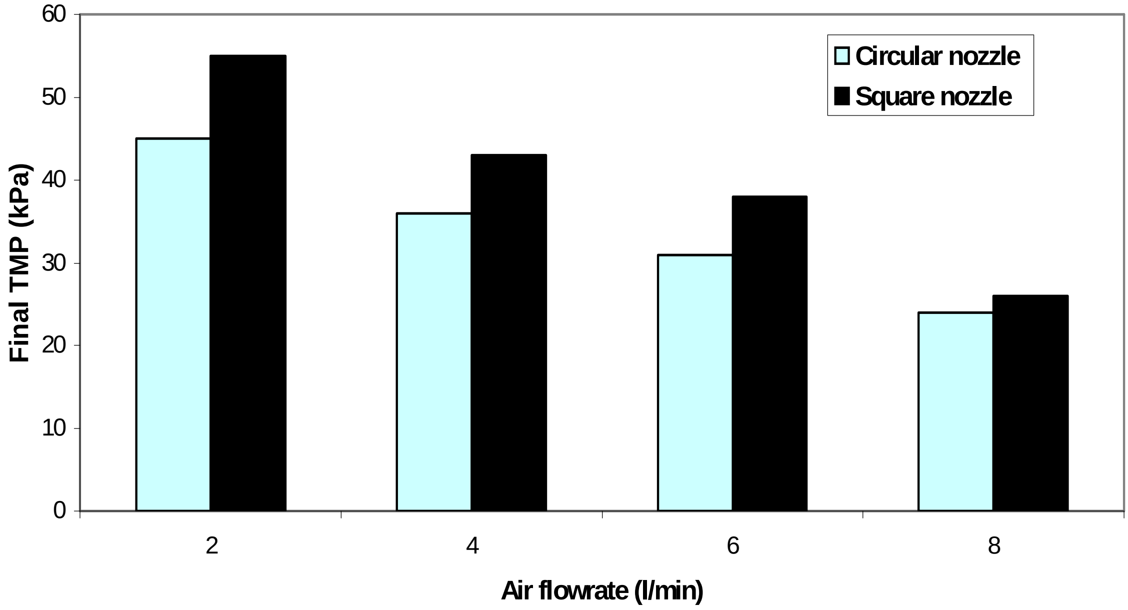

Figure 3.31. Final TMP obtained after two hours with square and circular nozzles of 9 mm^2 surface area.

3.5.7. Effect of membrane channel gap width

For submerged flat sheet membranes, the gap between adjacent membranes can have a significant effect on hydrodynamic conditions. The Kubota MBR system uses a gap of 7 mm (Churchouse & Wildgoose, 1999) between the flat sheet membranes whilst the Pleiade MBR uses a gap of 5 mm (Stephenson et al., 2000). No systematic study of the effect of the gap width has been reported. In this study, only one membrane was used therefore it was the gap between the membrane and the adjacent walls that was varied. Due to the tank design, the gap between the membrane and the walls could only be varied in increments of 7 mm. Therefore only two gap widths of 7 and 14 mm were studied. In both situations, the air diffuser was always located in line with and just underneath the membrane. These evaluations were done using nozzle sizes of 0.5 and 2.0 mm only.

Figure 3.32 shows typical results of TMP versus time obtained with an air flow rate of 2 l/min for the gaps of 7 and 14 mm while Figure 3.33 shows the final TMP for both gaps at all air flow rates and Figure 3.34 shows the dTMP/dt after two hours of experimentation. The TMP increased more quickly and to a much higher level when the gap was 14 mm. This indicates that air flow rate always plays some role in reducing fouling but that widening the gap had a negative effect on the shear stresses on the membrane. It has been found for tubular membranes that bubbles whose diameter is similar to the tube diameter (that is, slugs) are most effective in enhancing flux (Cui et al., 2003). Taking this into consideration, it may seem that by widening the channel gap, the number of bubbles whose diameter was larger than the channel gap was significantly decreased meaning that the actual number of bubbles that were in contact with the membrane surface was reduced. This had a negative impact on the TMP. This result seems to suggest that for two-phase flow to be more effective in submerged systems, the bubbles must at least be as wide as the channel gap. The additional liquid recirculation induced by the movement of bubbles does not seem to generate sufficient shearing on the membrane to keep the foulants off.

The differences in final TMP between the gaps of 7 and 14 mm decrease with an increase in the air flow rate (Figure 3.33). This may suggest that as the air flow rate is increased, the number of large bubbles increases as well and hence there are more bubbles that are scouring the membrane surface. This supports the notion that larger bubbles are more effective than smaller bubbles in submerged flat sheet membranes. This claim will be investigated further in chapter 5 and 7.

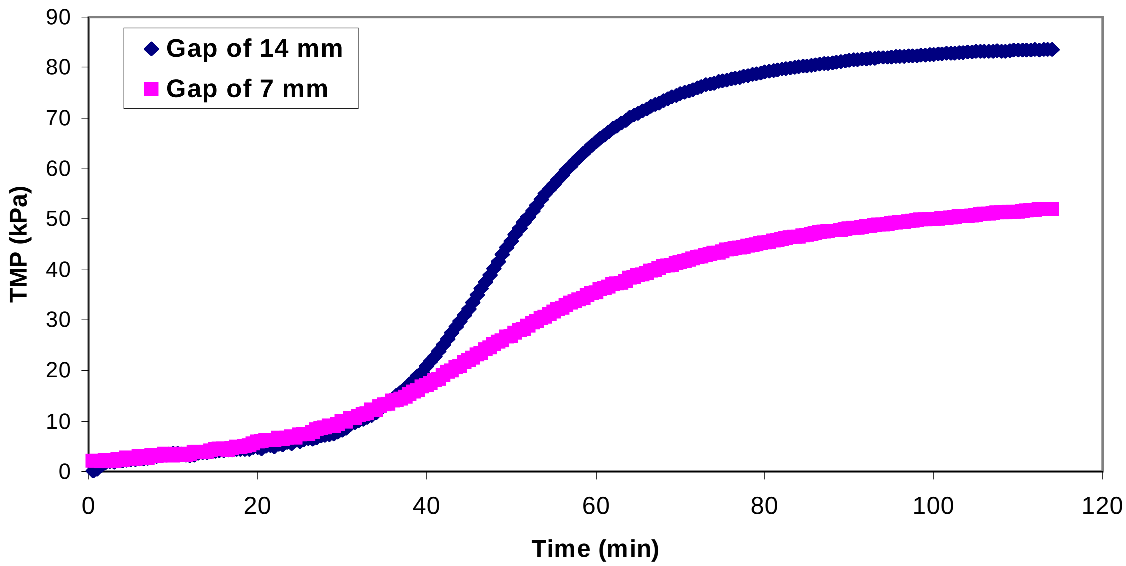

Figure 3.32. Variation of TMP with time for different gaps between the membrane and the wall. The concentration was 5 g/L, the air flow rate was 2 l/min and a 0.5 mm nozzle was used.

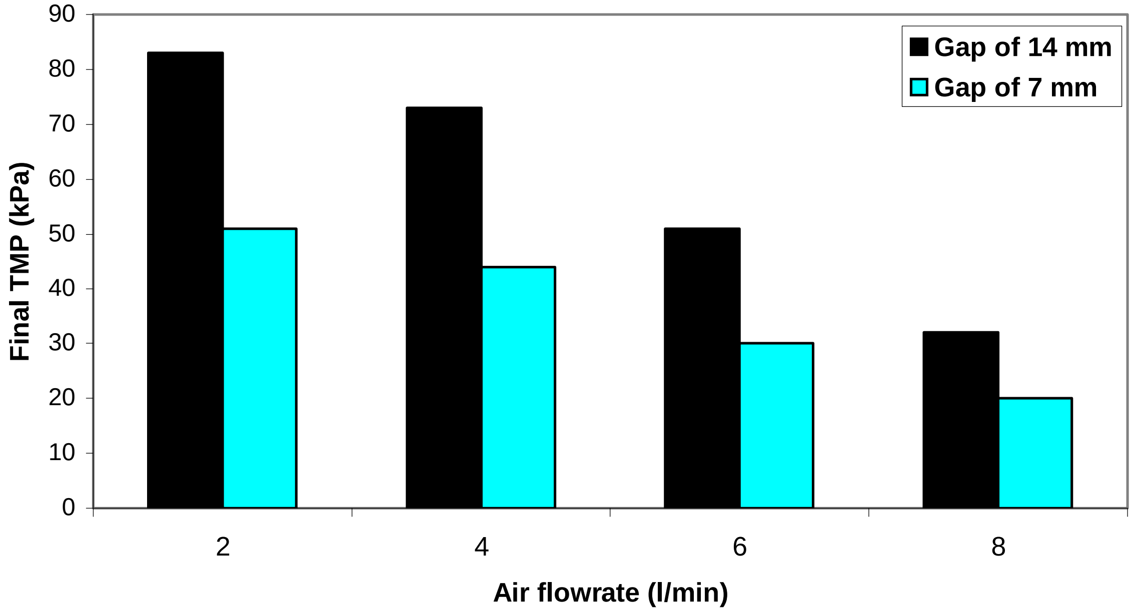

Figure 3.33. Final TMPs for runs with channel gaps of 7 and 14 mm at a concentration of 5 g/L and a 2.0 mm nozzle was used.

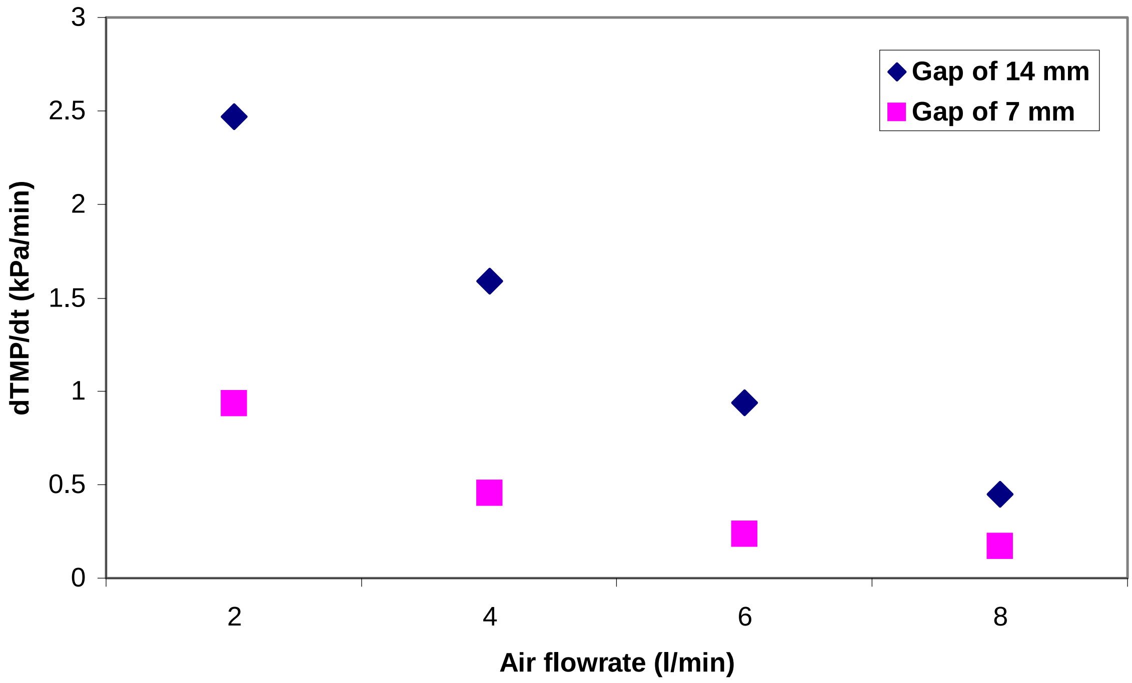

Figure 3.34. Variation of (dTMP/dt) with air flow rate for the gap of 7 and 14 mm at a concentration of 5 g/L and a 2.0 mm nozzle was used.

3.5.8 Intermittent filtration

Using gas-liquid two-phase flow can be very effective in combating fouling as most studies have revealed (Vera et al., 2000; Essemiani et al., 2001; Cui et al., 2003; Pospisil et al., 2004), however, it could be energy expensive if not operated at an optimum point. One way of minimising energy is to use intermittent filtration. In this method a period of filtration is followed by a period of non-filtration during which the suction pump is switched off and the TMP drops to zero. Intermittent filtration reduces compression of the cake layer, thus resistance is reduced and better flux is maintained (Yamamoto et al., 1989; Chiemchaisri et al., 1992). When the filtration is stopped, the process of gas bubbling and hence shearing on the membrane surface is allowed to continue. The combination of this shear stress and no suction force makes it easier for the deposited particles to be removed from the membrane surface. When the filtration cycle is resumed again, the membrane is relatively clean compared to what it was when the filtration cycle was stopped.

The effect of intermittent filtration was investigated at a concentration of 5 g/L at various airflow rates with a 1.0 and 2.0 mm nozzles. Experiments were conducted with and without baffles. The filtration cycle was allowed to run for a duration of 20 min then stopped for a duration of 5 minutes. Typical TMP versus time data are shown Figure 3.35 for runs with no baffles whilst Figure 3.36 shows a comparison for a case with and without baffles. The results for all airflow rates clearly indicate that intermittent filtration was far more effective than continuous filtration, even for the smallest airflow rate of 2 l/min. For example, with continuous filtration, the TMP after two hours of filtration increased up to 34 kPa but with intermittent filtration it only reached 8 kPa. Figure 3.36 further shows that TMP was always slightly lower for the case with baffles than the case without baffles. Thus, an economical way of operating a submerged flat sheet membrane system will be to use baffles with intermittent filtration at a lower gas flow rate.

Because the TMP remains fairly low with intermittent filtration, it is possible to sustain higher fluxes for a longer duration of time under this regime than with continuous filtration. Figure 3.37 compares the cumulative permeate production during a two hour duration. This Figure shows that there was more permeate produced during intermittent filtration than during continuous filtration because the intermittent filtration resistance increase was lower. Thus intermittent filtration not only saved energy but it was also more productive.

As can be seen from Figure 3.35 for the intermittent filtration run, each time the new filtration cycle starts, the TMP curve becomes steeper than the one in the previous cycle. This behavior can be explained as follows. At the end of the filtration cycle, there is a certain amount of foulants on the membrane. When the filtration is stopped, the air bubbles remove a certain portion of these foulants but not all foulants will be removed. Thus when the new filtration cycle starts, there is higher resistance on the membrane than there was during the start of the previous cycle. This causes the membrane to foul at a quicker rate than compared to the previous cycle thus the dTMP/dt becomes higher for each successive filtration cycle. In particular, the residual fouling on the membrane could cause increased 'local' fluxes to give a given average flux. The increased fluxes would lead to more irreversible fouling and less removal during the "off" time. This would cause the membrane to foul at a faster rate compared to the previous cycle thus the dTMP/dt would become higher for each successive filtration cycle.

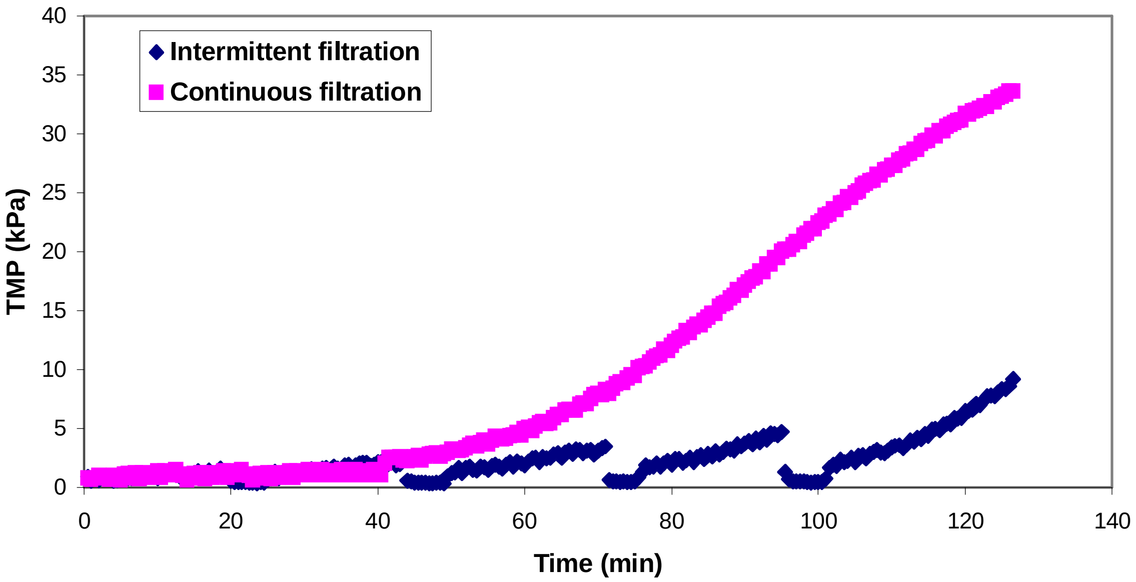

Figure 3.35. Variation of TMP with time during continuous and intermittent filtration. The air flow rate was 2 l/min and a 1.0 mm nozzle was used and the initial flux was 40 l/m^{2}hr.

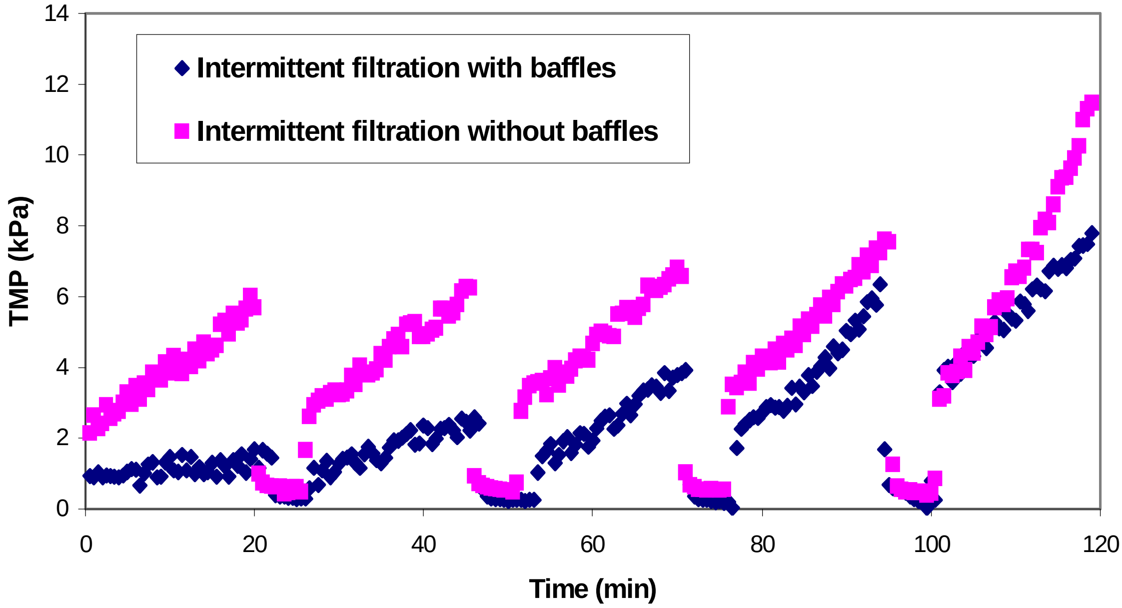

Figure 3.36. Variation of TMP with time during intermittent filtration for a run with and without baffles.

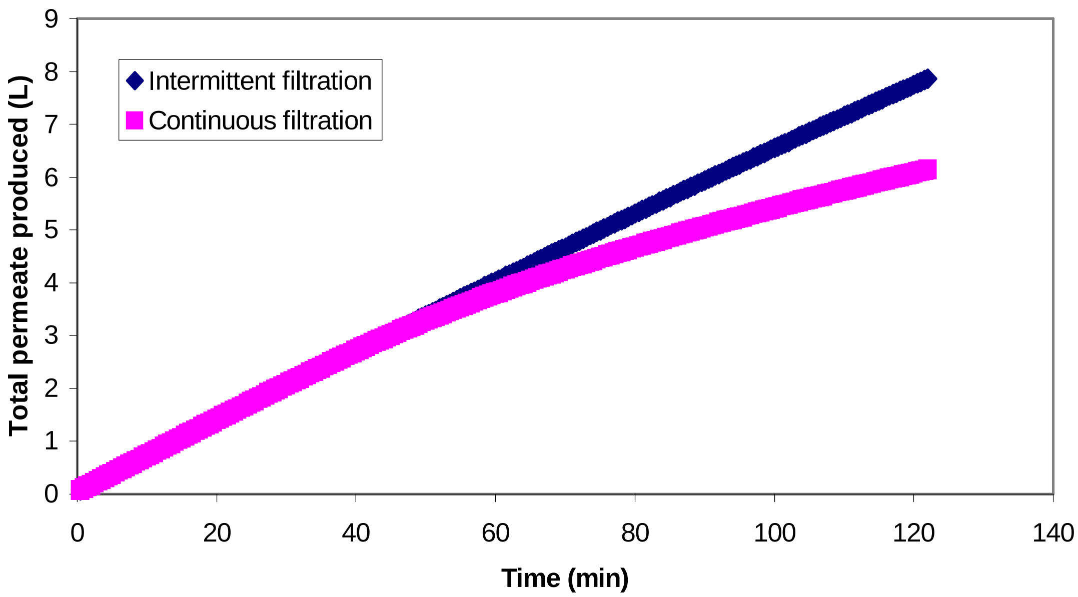

Figure 3.37. Cumulative permeate produced during continuous and intermittent filtration.

3.5.9 Intermittent bubbling

Having realised how successful intermittent filtration was, another operating strategy called intermittent bubbling, was investigated also with an aim to reduce energy requirements. In this process gas supply is switched off for some time and then switched on again. Yamamoto et al. (1989) observed that intermittent aeration was not detrimental to the biological process in an MBR which means that dissolved oxygen could not be depleted in such a short non-aeration time. Whilst intermittent aeration reduces the amount of gas used, it has not always been found to be better than continuous bubbling in terms of preventing the TMP increase or preventing flux decline (Lee et al., 1993; Mercier-Bonin et al., 2000a). However, it has always been found to be better than having no gas bubbling at all. In one case in which intermittent bubbling was found to be better than continuous bubbling, slug flow was used to enhance membrane performance (Bellara et al., 1996). With slug flow, the use of intermittent bubbling means that the Taylor bubble length is very well controlled and bubble wakes do not overlap. If they overlap, it may have a negative impact on the flux enhancement process. In other cases where slug flow is not involved, using bubbling intermittency may not be very effective. The story may differ for submerged hollow fibres where intermittent (alternate side) bubbling can be beneficial due to induced lateral flow through the fibre bundle (Guibert et al., 2002).

In this study, the effect of intermittent bubbling was investigated by switching the air supply off for 5 minutes after every 15 minutes. These frequencies were chosen to be similar to those used in intermittent filtration. Different airflow rates were examined using a 1.0 mm and a 2.0 mm nozzle. Figure 3.38 shows typical TMP versus time data and Figure 3.39 shows flux versus time data for conditions of no bubbling, continuous bubbling and intermittent bubbling. All the results show that, regardless of the air flow rate and the nozzle size used, the switching off of the air supply had a negative impact on the TMP. The TMP rose rapidly as soon as the air was switched off. When the air supply was switched on again, TMP recovered very slightly and then started to increase again. Although intermittent bubbling was always worse than continuous bubbling, it still gave much better results than no bubbling as is evidenced by Figure 3.38 and 3.39. Figure 3.40 shows the TMP reduction factors and the total volume of gas used during continuous bubbling and intermittent bubbling over a period of two hours for a bubbling rate of 8 l/min. By using intermittent bubbling, there is a saving of about 17% on the gas used. However this saving is detrimental to the TMP, as the TMP reduction is greater by about 15% with continuous bubbling than with intermittent bubbling. The results suggest that, in this system, air bubbles are effective in preventing cake formation but do not seem to be effective in destabilising an already formed cake. It should also be noted that only one intermittency condition was studied here and quite possibly there may be benefit from shorter cycles of on/off bubbling such as 20 seconds of bubbling followed by 5 seconds of no bubbling.

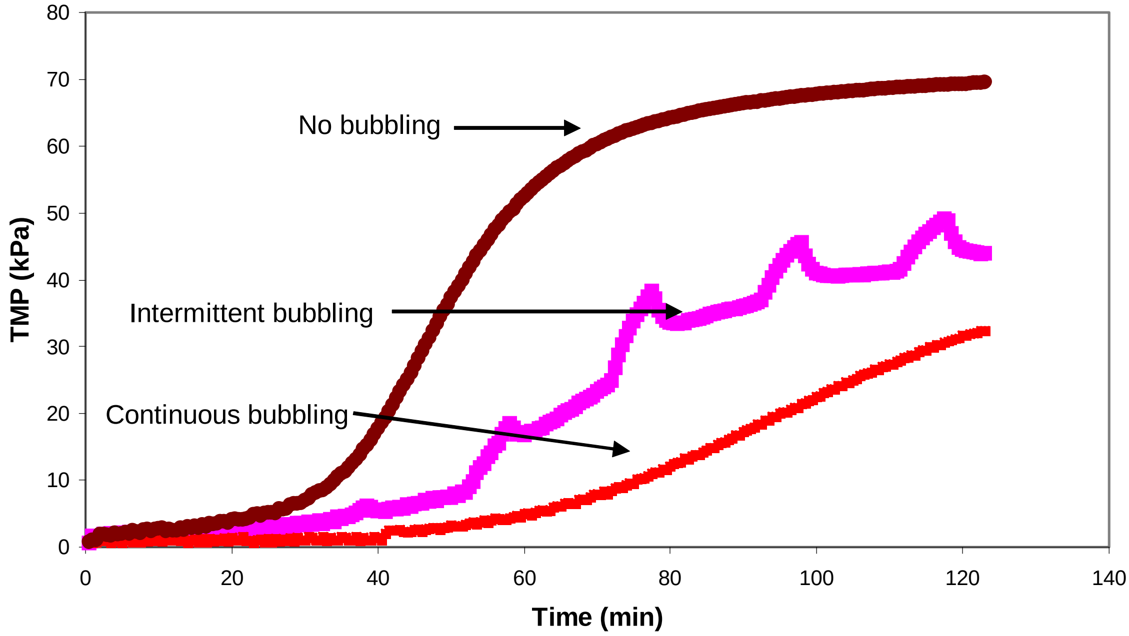

Figure 3.38. Variation of TMP with time under different modes of bubbling. The concentration was 5 g/L, airflow rate was 2 l/min and a 1.0 mm nozzle was used.

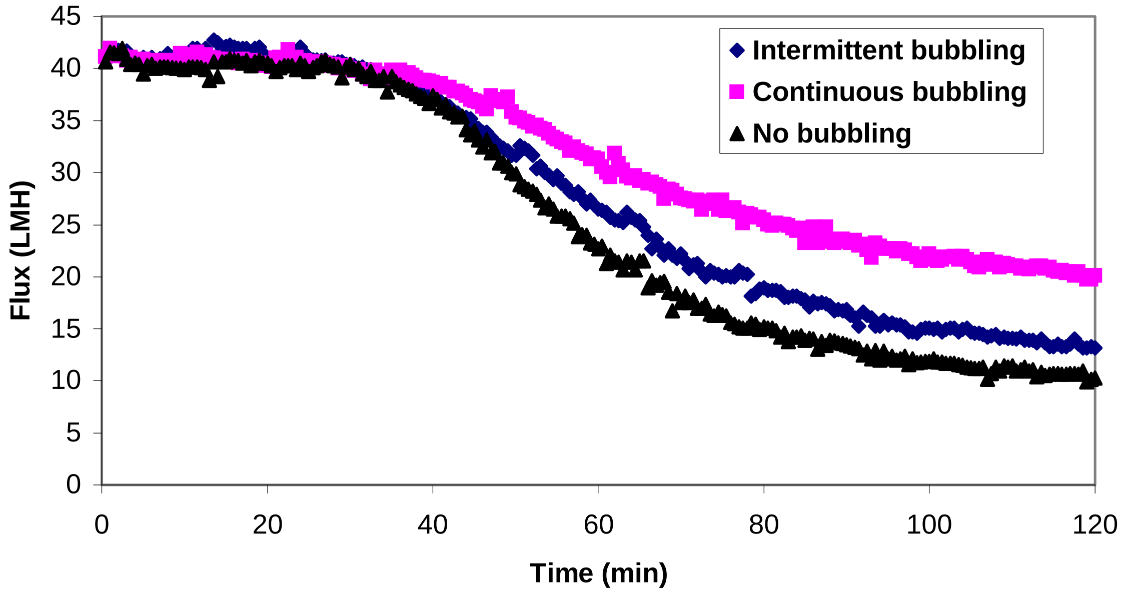

Figure 3.39. Variation of flux with time. The concentration is 10 g/L, the airflow rate is 2 l/min and a 1.0 mm nozzle is used.

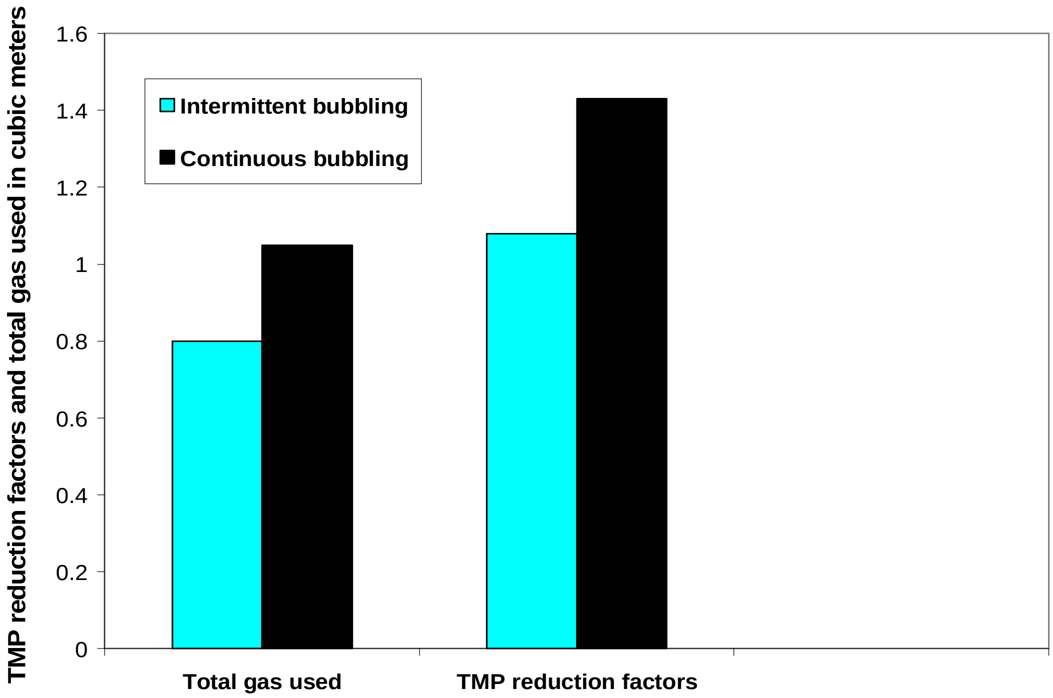

Figure 3.40 TMP reduction factors and total gas used for intermittent and continuous bubbling at a concentration of 5 g/L with an airflow of 2 l/min.

3.6 DISCUSSION AND CONCLUSIONS

The main objective of this chapter was to evaluate how various hydrodynamic factors that govern the structure of two-phase flow between parallel submerged flat-sheet membranes affect the fouling retardation process. The key parameters that have been investigated are air flow rate, nozzle size, nozzle geometry, feed concentration, membrane channel gap width, intermittent filtration, intermittent bubbling, and effect of baffles. Performance of two-phase flow was evaluated in terms of changes in TMP (dTMP/dt), TMP reduction factors, cake specific resistance, critical flux and total organic carbon deposits.

The important major findings of the research presented in this chapter can be summarised as follows:

- TMP reduction increases with the gas flow rate and nozzle size.
- The effectiveness of bubbling decreases with an increase in concentration.
- Bubbles are often unevenly distributed over the membrane surfaces.
- Use of baffles enhances the gas bubbling efficiency by improving gas distribution.
- Critical fluxes increase with gas flow rate and nozzle size and decrease with concentration.
- Intermittent filtration is superior to continuous filtration whilst continuous bubbling is better than intermittent bubbling, however, probably shorter frequencies than the ones studied here may improve intermittent bubbling.
- The size of the gap width between the submerged membranes has an important effect on the gas bubbling efficiency.

In section 3.5.2, the effect of air flow rate and nozzle size on fouling minimisation was examined. The degree by which fouling was minimised was measured by looking at the evolution of various parameters with time. These parameters were TMP, total resistance, specific cake resistance, dTMP/dt and TMP reduction factors. Results presented in section 3.5.2 all showed that the effectiveness of gas sparging improved with an increase in the gas flow rate and nozzle size. The probable reasons as to why this is happening which have been developed based on the evidence found in this chapter and in the following chapters will be discussed in more details chapter 8.

No systematic study was found in literature in which the effect of the nozzle size has been investigated for submerged flat sheet membranes. The results obtained in this study showed an increasing enhancement effect with an increase in nozzle size when the air flow rate was kept constant (Figure 3.9 and 3.13). These results are difficult to explain as the amount of gas introduced into the system is the same regardless of the nozzle size. Therefore these results suggest that it is not just the volume of gas that matters but also the bubble size distribution. This seems to indicate that different nozzle sizes give rise to different bubble population characteristics. This matter will be discussed in more detail in Chapter 5 when bubble size distribution analysis is conducted.

Another important finding of this chapter has been that the effectiveness of gas bubbling decreases with an increase in feed concentration. There are conflicting reports in literature with regards to the effect of concentration. In some studies, flux was found to increase with concentration (Cabassud et al., 1997), and in other studies flux declined with concentration (Mercier-Bonin et al., 2000a). In this study, TMP was found to rise more rapidly with an increase in concentration at all bubbling rates. Gas-liquid two-phase flow has been found by some researchers to be more effective under conditions when fouling would be most severe (Cui et al., 2003) such as at high concentration, however in this study this was not the case. Higher TMP reduction factors (Figure 3.21) were obtained at lower concentrations than at higher concentrations for all air flow rates considered. This observation puts into question the theory that two-phase flow works by disruption of the concentration polarisation layer, at least for the submerged flat sheet membranes. It is quite possible that the presence of the gas phase minimises the rate of formation of the concentration boundary layer rather than disrupting an already formed layer. Thus, at higher concentrations, the tendency for the concentration layer to form is much higher, which lowers the effectiveness of gas bubbles. It is also possible that the increase in concentration also increased the suspension viscosity and that this would tend to slow bubble rise and attenuate the effect of shear transients.

Another key finding in this study has been the uneven distribution of bubbles across the flat-sheet membrane. This phenomenon was also reported by Li et al. (1998) who noticed that some parts the membrane were bubble free. This uneven distribution resulted in uneven deposition of fouling on the membrane (Figure 3.23). The use of baffles rectified this problem to a considerable extent. Baffles seem to have increased the overall shear stress on the membrane surface, yielding lower TMPs than cases without baffles. The effect of baffles on the gas and liquid velocity profiles as well as on membrane shear stress will be further evaluated using CFD and the results are presented in chapter 7.

Critical flux is a vital concept in MBR processes because it allows for the operation of the MBR for a long period without any cleaning necessary. During sub-critical flux operation, it is thought that particles will not deposit on the membrane surface as long as the convection of particles caused by the permeate flux can be balanced by the back-transport of rejected particles from the membrane to the bulk feed (Howell, 1995). Critical flux in this study was determined by the flux-stepping method and by using the dTMP/dt versus flux data as shown in Figure 3.24 and Figure 3.26. The practical significance of the critical flux is that, with control of imposed flux below critical flux, the deposition dominated by convection can be avoided or minimised. The ideal result for critical flux operation is a completely cake free membrane. However, it has been found that with biomass filtration, even when operating under critical flux, some slow TMP rise occurs due to EPS and trace colloids deposition (Chang, 2001; Cho & Fane, 2002; Jefferson et al., 2003). In this study, critical flux was found to increase with the gas flow rate. Increasing the gas flow rate increases the wall shear stress (Ducom & Cabassud, 2003) which will then enhance particle back transport and thus lead to higher critical fluxes. Possible mechanisms of back transport include Brownian diffusion, shear induced diffusion and inertial lift model (Chang, 2001). All of these mechanisms predict slightly different increases in critical flux with the shear rate. Critical fluxes were also found to decrease with concentration, understandably because higher particle loading increases the probability of interaction between the membrane and the particles.

Two potential energy saving mechanisms, intermittent filtration and intermittent bubbling were investigated. In agreement with what Bouhabila et al. (1998) found, it was found in this study that two-phase flow was effective in minimising fouling when used at the start of the filtration process but was ineffective in restoring the TMP fully during an intermittent bubbling operation. Cabassud et al. (1997) also learnt that, with an interruption on the gas bubbling process, a particle deposit is created which is difficult to remove when the air injection is restored. This is contrary to what was observed by Bellara et al. (1996) who found that flux obtained by the use of two-phase flow was entirely recoverable if one was to stop the gas flow and restart it again. However, there are more studies which seem to show that the unsteadiness created by two-phase flow is unable to disrupt completely a previously deposited cake as was observed by Mercier-Bonin et al. (2000a) and Bouhabila et al. (1998). Therefore, the results obtained in this study agree with most of the literature which show that continuous bubbling is much better than intermittent bubbling whilst on the other hand it was established in section 3.5.8 that intermittent suction was a better operating strategy than continuous suction. Intermittent suction also reduced the energy requirements.

Results obtained from varying the gap width between the membrane and the wall showed that increasing the gap width has a detrimental effect on the TMP rise during gas sparging. Similar observations were made by Lee et al. (1993) during filtration of a cell suspension. They noted that a drastic reduction of the channel height in a cross-flow cell resulted in a high shear rate between the membrane surface and the air slug interface. Thus, a similar explanation could be adopted for the observations made in this study. A narrower gap results in high shear rates which results in a slower increase of the TMP. Cui and Wright (1996) found that, in narrower channels in cross-flow cells, only a small amount of gas is necessary to achieve flux enhancement, whereas on a wider channel, more gas would be required to achieve the same degree of flux enhancement. Thus, the gap width between the submerged membranes has an important role to play in the determination of shear stresses on the membrane.

It is clear from the findings of this study that for submerged flat-sheet membranes, physical factors such as air flow rate, nozzle size and geometry, membrane gap width and mode of operation play a crucial role in determining the effectiveness of two-phase flow in minimising fouling. Based on the observations made in this study and for membrane modules similar to the one studied here, optimal performance can be obtained by maintaining the gas flow rate at about 80 l. min^{-1}per m^2 of membrane area, however, with intermittency this value could be significantly reduced. Reasonably large circular nozzles of at least about 2.0 mm in diameter should be employed. In terms of operating strategy, intermittent suction is recommended and if practical, baffles should be used between the submerged flat membranes. The gap width between the membranes should be kept fairly small at about 7 mm and definitely not more than 14 mm, so that slug flow with high surface shear can occur.

What is perplexing about the results from this study is the effect of nozzle size and geometry. It was learnt that, if the air flow rate is kept the same, the enhancement effect exhibited strong dependence on the nozzle size and geometry. It is difficult to explain this type of behaviour without looking at a detailed analysis of the two-phase flow inside the channel. This investigation of two-phase flow characterisation will be conducted in chapter 5. CFD simulations were also conducted to gain a better insight into the gas and liquid velocity profiles inside the channel as well as to look at shear stress distributions on the membrane surface. The CFD results will be presented in chapters 6 and 7. Baffles were also shown to improve the enhancement effect of two-phase flow but the real mechanisms behind this improvement are not yet fully understood. Once again CFD simulations incorporating baffles were conducted to gain fundamental knowledge of the enhancement effect and these results will be discussed in chapter 7. Also more work needs to be done on optimising the design of baffles. This work fell beyond the scope of this project and is recommended for future studies.

Chapter 4

MICROFILTRATION OF ACTIVATED SLUDGE USING A SUBMERGED MEMBRANE WITH AIR BUBBLING

4.1 INTRODUCTION

In chapter 3 a series of experiments were conducted in which the effects of air bubbling on fouling retardation were investigated under different conditions. However, these experiments were conducted using an artificial suspension of commercially available bakers' yeast. Although the results obtained may yield some insights into how two-phase flow works in submerged flat-sheet membranes, in terms of optimising the usage of two-phase flow in membrane bioreactors (MBRs) which is a principal aim of this study, these results may not be directly applicable in practical situations. To supplement this shortcoming, experiments almost similar to those conducted in chapter 3 were completed using a typical MBR feed of activated sludge mixed liquor.

In this study we have only focused on the optimisation of the two-phase flow cleaning process which is a partial contribution towards the optimisation of the MBR process as a whole. To optimize the MBR process, many parameters have to be considered. These include solid concentrations, solid retention time (SRT) or sludge age, the hydraulic retention time (HRT), aeration rate (aerobic processes), material costs, and the energy cost of the membrane separation (Hasar et al., 2001). All of these parameters are interrelated which makes optimization difficult. There have been many studies (for example, Hasar et al., 2001; Le-Clech et al., 2003a; Lee et al., 2003; Howell et al., 2004) which aimed to optimize these parameters but only a few studies have concentrated on optimization of aeration rates, particularly for submerged flat sheet membranes, which is why this study has focused on this aspect.

4.2 OBJECTIVES

The specific objectives of this chapter are to:

- Investigate whether an optimum bubbling rate exists in the case of a submerged flat sheet membrane by experimenting with a wider range of gas flow rates than in chapter 3.
- Verify whether the effects of baffles, nozzle size, nozzle geometry and intermittent filtration with the activated sludge suspension are similar to those found with the model yeast suspension.
- Compare the fouling potentials of the activated sludge and yeast suspensions by examining fouling rates (dTMP/dt) and critical fluxes.
- Assess the membrane performance by measuring the quality of the permeate.

4.3 EXPERIMENTAL SETUP AND METHODOLOGY

4.3.1 Equipment description

The experimental setup used in this chapter is identical to that used in chapter 3 and depicted in figure 3.1 and hence will not be reproduced or discussed further here. The only difference is that in chapter 3 a yeast suspension was used whilst in this chapter, waste activated sludge was used. The waste activated sludge was collected on a daily basis from the Northerns Wastewater Treatment Works, situated in the city of Durban, South Africa. This plant has an SRT of 15 days to 20 days, an HRT of about 10 hours and an average MLSS concentration of about 4 to 6 g/L.

Figure 4.1 shows the particle size distribution of aerated waste activated sludge measured with a Malvern 2000 Mastersizer after 3 hours of a bubbling experiment. The measured mean particle size of the aerated sludge was found to be 77 μm. This represented a slight reduction of the mean particle when compared to before the bubbling experiment where the mean particle size of the sludge was measured to be 81 μm. Since the membrane used in this study had an average pore size of 0.4 μm it means that pore plugging by the biomass would be small, and that fouling would result mostly from pore blocking and cake formation which should be easily counteracted by two-phase flow. However in real MBR systems which run much longer than the short experiments (three hours at most) conducted here, there is growing evidence which seems to suggest that fouling by EPS and colloids become more dominant than fouling by the flocs. Also these MBRs run at fluxes which are lower than the critical flux of the flocs. All the experiments conducted in this study were run at fluxes higher than the critical flux of the dominant foulant (the floc). The main purpose of this chapter was to compare the observed effects of hydrodynamic parameters on a model fluid (yeast) with a real complex suspension (activated sludge), therefore the system reported here was not an MBR as such.

As in chapter 3, flux and TMP were monitored during each experiment. The rate of membrane fouling under different conditions was judged by the increase in TMP over time (dTMP/dt). For all experiments, unless otherwise stated, the initial flux was set at 40 l/m^2hr as in chapter 3. All experiments were designed to run at constant flux even though this was difficult to achieve under most conditions. The reasons for this are described later. Apart from a few exceptions, all experiments were about 2 hours long. Thus the protocol adopted would have assessed the control of fouling by the dominant fouling species, in this case the bacterial floc. It would be usual operating practice to operate at a flux below the 'critical flux' of this dominant foulant.

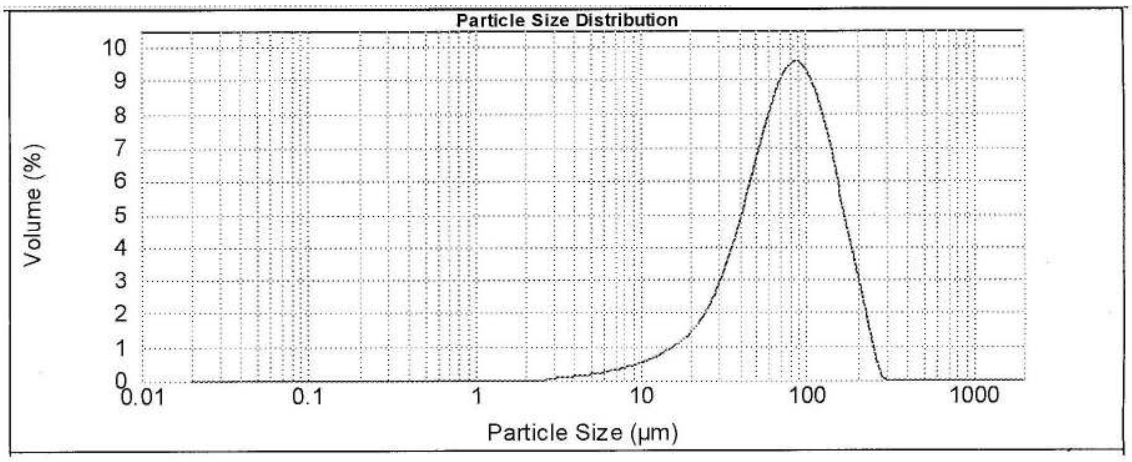

Figure 4.1. Particle size distribution of aerated waste activated sludge.

4.3.2 Analytical methods

In chapter 3 the quality of the effluent was not monitored but as the water quality is a primary concern in MBRs, the membrane performance in terms of water quality was monitored in this chapter using three parameters, namely, chemical oxygen demand (COD) removal, suspended solids removal, and turbidity. The analysis of the permeate quality was not conducted for all the runs but for some runs selected randomly. COD was measured by the micro-COD method proposed by HACH in which COD vials, a COD reactor and a spectrophotometer are used. Turbidity was measured by a potable HACH turbidimeter and the units of the measurements were in Nephelometric Turbidity Units (NTU). However this turbidimeter had a maximum detection limit of 1200 NTU and it was found that in all the experiments the feed turbidity was always higher than this value and hence could not be measured. Only the permeate turbidity is reported. The suspended solids concentration was measured by weighing a sample of permeate after filtering with a GF/C filter (0.22 μm) and drying in an oven for one hour at 105 ^{o}C.

4.4 RESULTS AND DISCUSSIONS

4.4.1 Effects of aeration rates

The effects of air bubbling rates on combating fouling were studied for cases incorporating membrane baffles and for cases without baffles to establish whether baffles were as effective with the activated sludge suspension as they were on the yeast suspension. In chapter 3, air flow rates investigated were up to 8 l/min or 80 l/min per m^2 of membrane area. It was found that the efficiency of two-phase flow continuously increased with the air flow rate and no optimum bubbling rate was established. In this chapter higher air flowrates (up to 20 l/min) were investigated with the aim to determine whether an optimum bubbling rate exists. For these investigations only the circular nozzle size of 2.0 mm was used since, based on the results of chapter 3, it yielded the best performance compared to the smaller nozzles. Figure 4.2 represents TMP versus time data for various gas flow rates for cases without baffles, Figure 4.3 shows typical steady-state or final TMPs achieved with the activated sludge suspension at various gas flowrates and Figure 4.4 shows flux versus time data corresponding with TMP data in Figure 4.2.

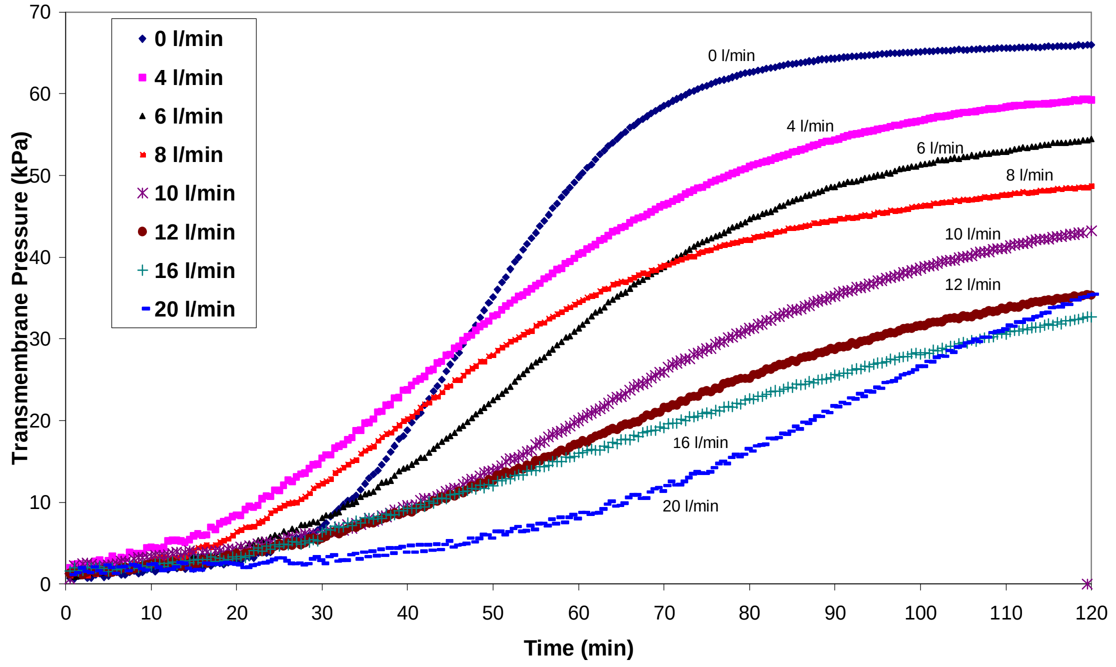

Figure 4.2. Variation of TMP with time under various air flowrates for a nozzle size of 2.0 mm.

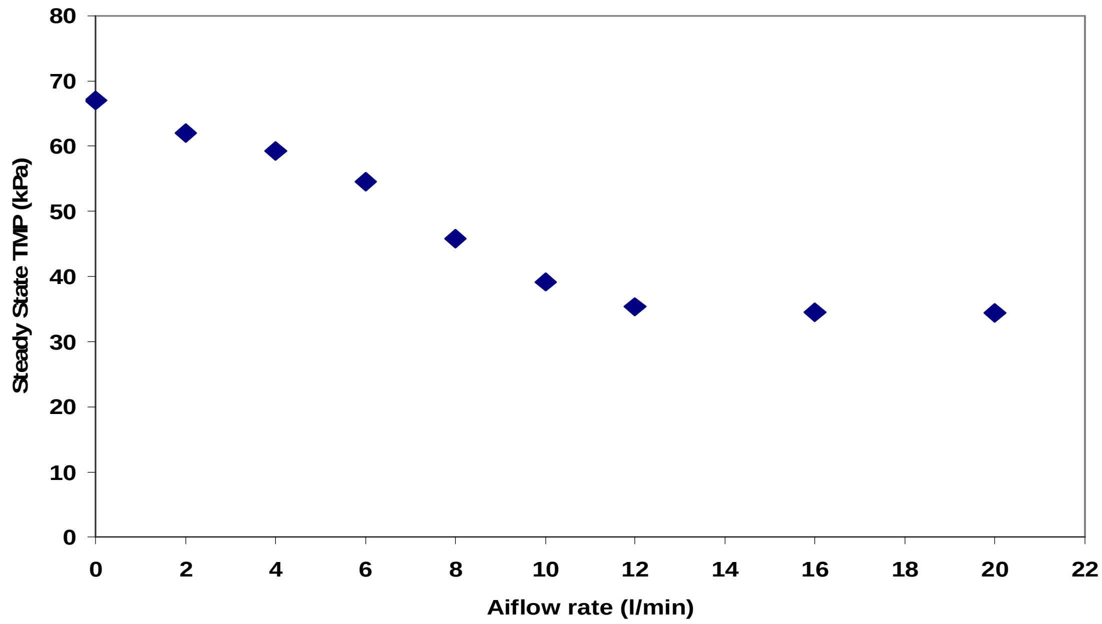

Figure 4.3. Final or steady-state TMPs achieved with the waste activated sludge filtration at different airflow rates for a nozzle size of 2.0 mm.

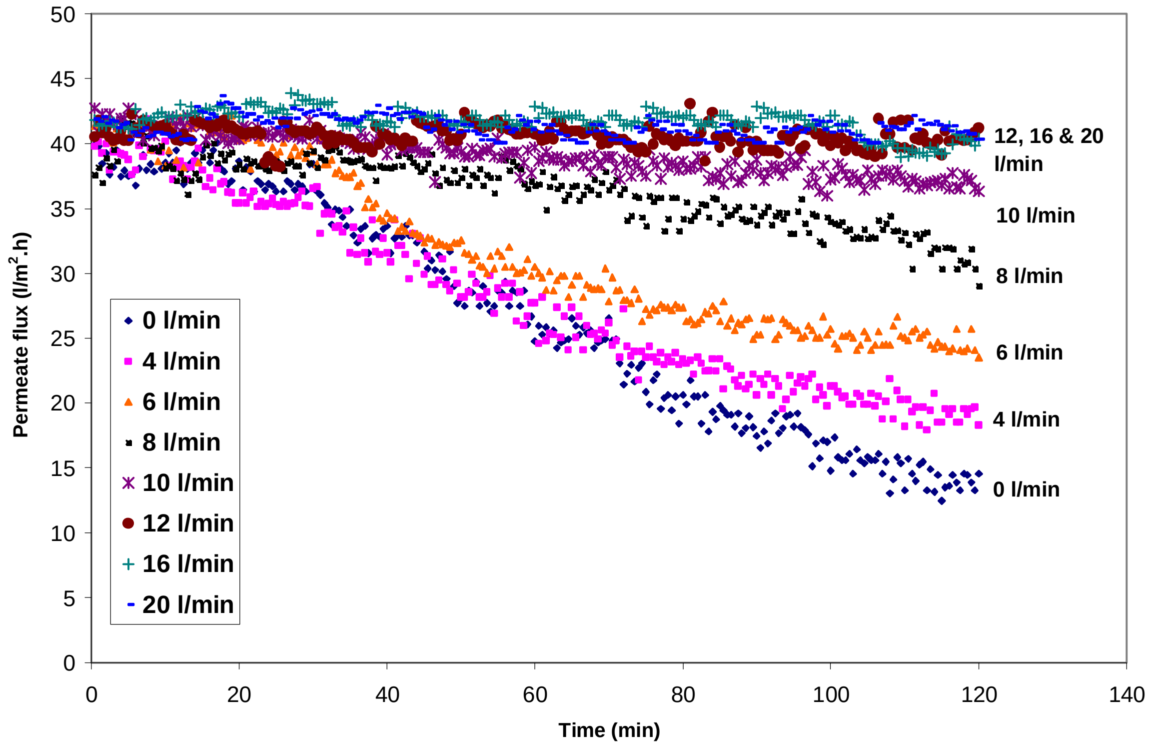

Figure 4.4. Flux versus time data for various air flowrates with a nozzle size of 2.0 mm.

It is clear from figure 4.2, 4.3 and 4.4 that gas bubbling, no matter how small, plays an important role in reducing the increase of TMP over time which indicates the fouling of the membrane. The behaviour of the TMP trends for air flow rates up to 10 l/min, is similar to that observed in chapter 3 where the increase of the TMP is small over the first 30 minutes, followed by a sharp increase for the next hour or so, finally attaining an almost steady-state value. The possible reasons for this TMP behaviour have been discussed in chapter 3.

Noticeable from figure 4.2 is that the TMP trends for the air flow rates of 12, 16 and 20 l/min are almost similar and from figure 4.3, the final TMPs are more or less the same. Figure 4.4 shows that the extent of flux decline decreased with an increase in the air flowrate and from 12 l/min upwards, flux remained relatively constant throughout the experiment. The repeatability of the experiments at these air flow rates was good with the difference in the final TMP after two hours being less than 8%. This suggests that the flow rate of 12 l/min might be an optimum gas flow rate for this system. One way of explaining the optimum bubbling rate is that above a certain gas flow rate, a balance is reached between the rate at which particles are transported to the membrane wall due to the permeate flux and the rate at which they are carried away from the membrane due to shear induced by bubbling. Once this balance is reached any further increase in the gas flow rate does not have any significant effect on reducing fouling if the flux is kept constant. It is also possible that, during filtration, irreversible internal fouling of the membrane occurs which cannot be removed by any further increase in the gas flow rate. Another factor maybe due to the effect of bubbling on the floc size distribution, with small floc sizes developing due to breakup as the bubbling is increased. Hong et al. (2002) suggested that an optimum bubbling rate exists because an increase in the bubbling rate may increase the fluid resistance to the bubble flow which then affects the cleaning mechanism.

Experiments were also conducted with baffles inserted in the riser sections between the membrane and the tank walls. To provide a comparison, TMP variation with time for one case with baffles and one without is shown in figure 4.5. The bubbling flow rate for the cases shown is 12 l/min. This figure confirms that the baffles were also effective with the activated sludge suspension. The TMP after two hours only increased to 32 kPa for the run with baffles whilst it reached 37 kPa for the run without baffles. This superior performance of the baffles was observed at all air flow rates. It was also further observed that with the baffles the optimum gas flow rate was reduced from 12 to about 8 l/min.

The TMP reduction factors as computed using equation 3.2 in chapter 3 are shown in figure 4.6 for cases with and without baffles at various air flow rates. TMP reduction factors are an indication of the effectiveness of the gas flow rate. The more effective the gas flow rate, the higher will be the TMP reduction factor.

The TMP reduction factors depicted in figure 4.6, increase with the gas flow rate up to an optimum of 8 l/min for runs with baffles and 12 l/min for runs without baffles. The TMP reduction factors are always higher for runs with baffles than for those without. Whilst this result suggests that the use of baffles would be beneficial, the effect baffles would have on the biological activity (if any at all) is not clear (for example the baffles could provide a support for biofilm growth). This effect was not investigated in this work which was a hydrodynamic investigation only.

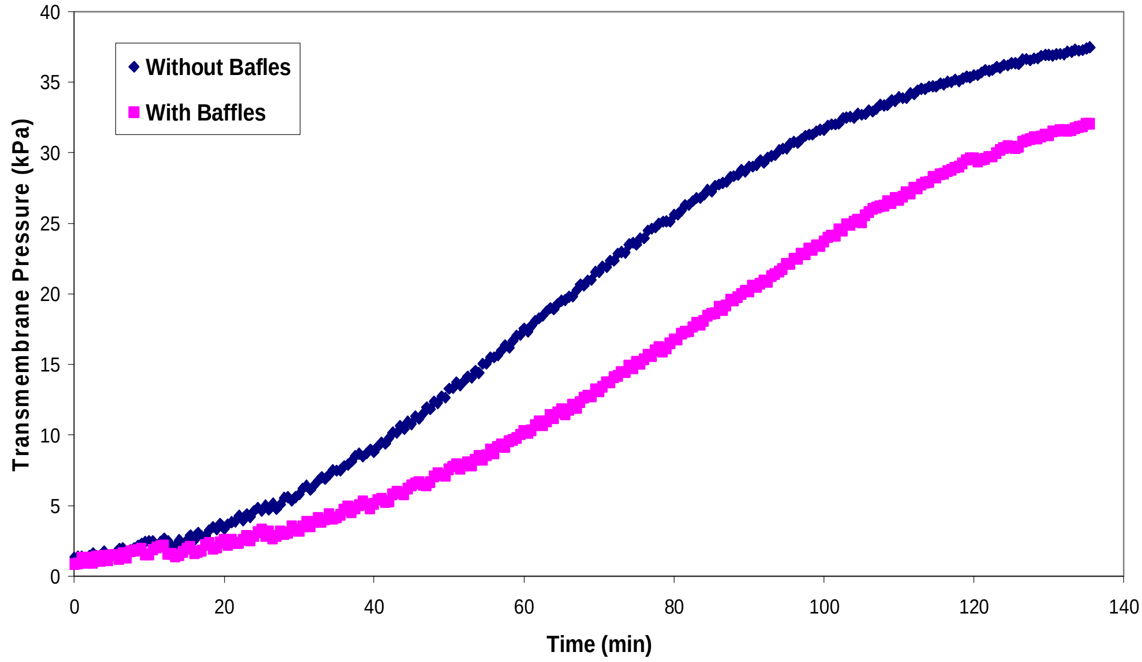

Figure 4.5. Variation of TMP with time for runs with and without baffles. The gas flow rate was 12 l/min and the nozzle size was 2.0 mm.

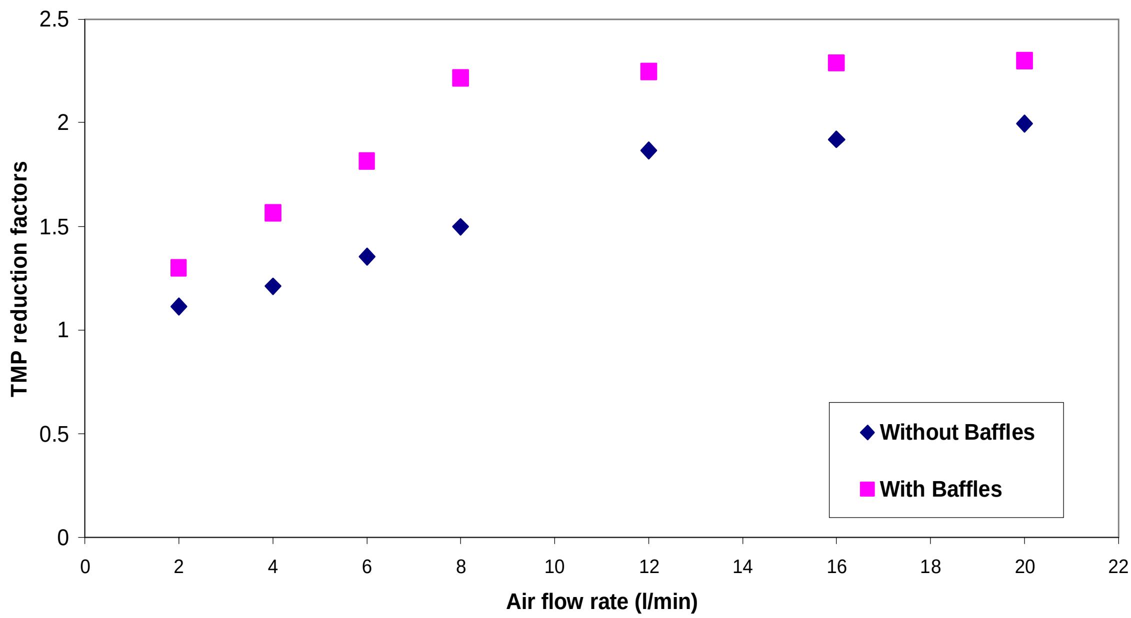

Figure 4.6. TMP reduction factors at various gas flow rates for the nozzle size of 2.0 mm.

Another way of assessing the effectiveness of air bubbling is by looking at the rate of TMP increase (dTMP/dt) at a specific point in time. dTMP/dt is a commonly used parameter to indicate the fouling rate (Judd et al., 2001; Howell et al., 2004). The average dTMP/dt over the last fifteen minutes of each experiment is shown in figure 4.7.

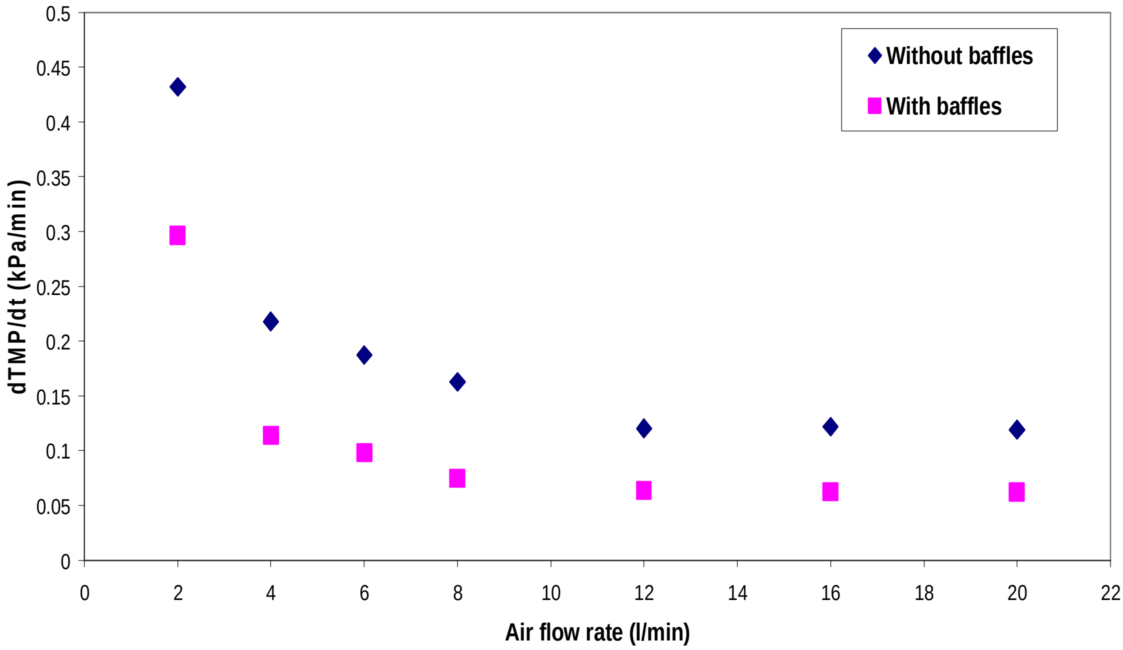

Figure 4.7. Variation of dTMP/dt with air flow rate for runs with and without baffles.

From figure 4.7 we can see that the fouling rate decreases almost exponentially with an increase in the gas flow rate. Similar observations were made by Howell et al. (2004) for a submerged flat sheet membrane. Fouling rates were always lower when baffles were used. Once again, beyond the optimum gas flow rates for baffles (8 l/min) and non baffle cases (12 l/min), there is no further significant reduction in the dTMP/dt. The exponential relationship between the gas flow rate and the membrane fouling rate indicates the importance of operating under appropriate conditions. Operating at a very low gas flow rate will evidently result in a rapid fouling of the membrane. Operating at optimum gas flow rates should improve productivity while lowering energy costs.

For the results presented in figure 4.7, the starting flux was 40 l/m^{2}hr. Figure 4.8 shows how dTMP/dt varied with different initial imposed fluxes.

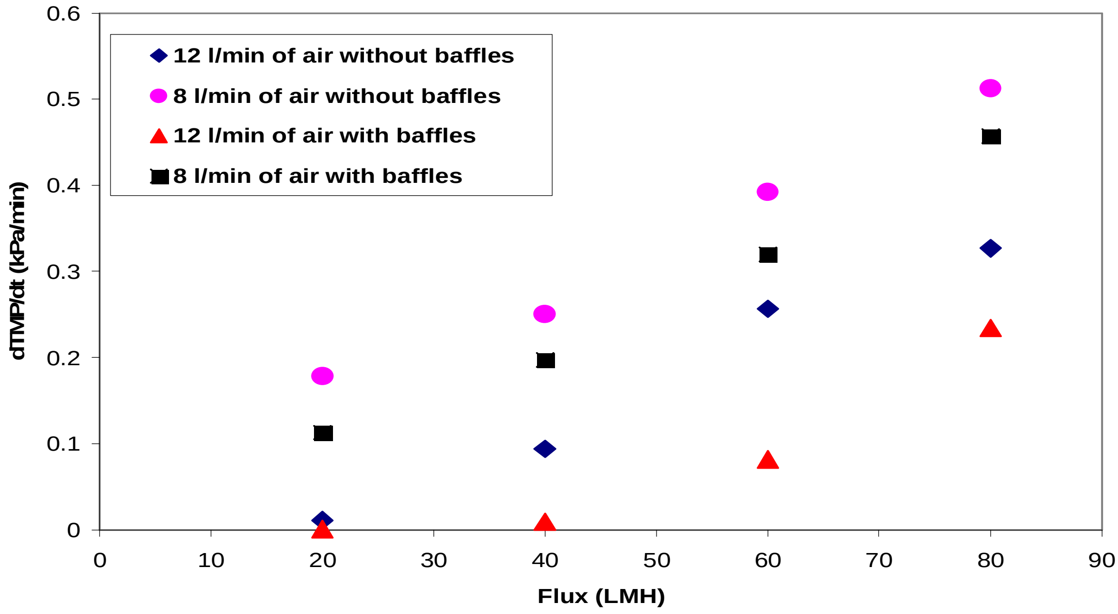

Figure 4.8. Variation of dTMP/dt with flux at air flow rates of 8 and 12 l/min for runs with and without baffles.

From figure 4.8, it can be seen that the rate of fouling increased significantly with the imposed initial flux. Observed fouling rates are once again lower when baffles are used. This further stresses the importance of operating at the correct initial flux as a high flux will result in rapid fouling of the membrane. For the case with baffles and an air flow rate of 12 l/min, the dTMP/dt was almost zero up to a flux of 40 l/m^{2}hr and then started to increase. Below the critical flux, dTMP/dt was zero as the membrane was not fouling. Therefore this means that for the case with baffles and an air flow rate of 12 l/min, the critical flux lay somewhere around 40 l/m^{2}hr; without baffles the critical flux was about 20 l/m^{2}hr. More details about the determination of the critical fluxes will be presented in section 4.4.4.

Unlike in chapter 3, where flux was constant most of the time (for the yeast concentration of 5 g/L) and therefore TMP and resistance curves gave essentially the same information as one was the re-scaling of the other, here it was found difficult to maintain constant flux due to the higher concentrations of the MLSS and the more complex foulant mixture. After a certain period of time, cavitation started occurring with large air bubbles seen in the permeate line. Once this started to happen flux decline was inevitable. Flux declined until a certain steady-state flux was reached. The extent of this flux decline was found to depend on the bubbling rate.

The effects of aeration were also assessed by looking at the hydraulic resistance developed which is a combination of the membrane resistance and the cake resistance. The total resistance R_t may be calculated by using Darcy's law:

$$J = \frac{\Delta P}{\mu R_{tot}} \tag{4.1}$$

$$R_{tot} = R_f + R_m$$

where R_m is the membrane resistance, R_f is the fouling resistance, J is the filtrate flux, μ is the dynamic viscosity of the permeate and ΔP is the trans-membrane pressure.

The membrane resistance was calculated by filtering with triple distilled water. Once R_m was known, at the end of each experiment R_{tot} was evaluated using equation 4.1. Then the ratio R_t / R_m was computed and plotted against the air flow rate. This is shown in figure 4.9. The hydraulic resistance decreased with the air flow rate but did not disappear even when the air flow rate had reached its "optimum" value for both cases with and without baffles. To investigate whether the changes in hydraulic resistance were due to internal fouling of the membrane, a separate set of experiments was completed where, at the end of each experiment, the membrane was cleaned using the detergent 'Targ Enzyme A' and then the pure water flux was measured. The membrane was then used in another filtration experiment, cleaned with the detergent, and the pure water resistance measured again. The membrane for this investigation was not chemically cleaned with 0.5% (w/w) Sodium Hypochlorite (which removes internal fouling) as was the case with the membranes used in the other experiments. The results of this investigation are shown in figure 4.10.

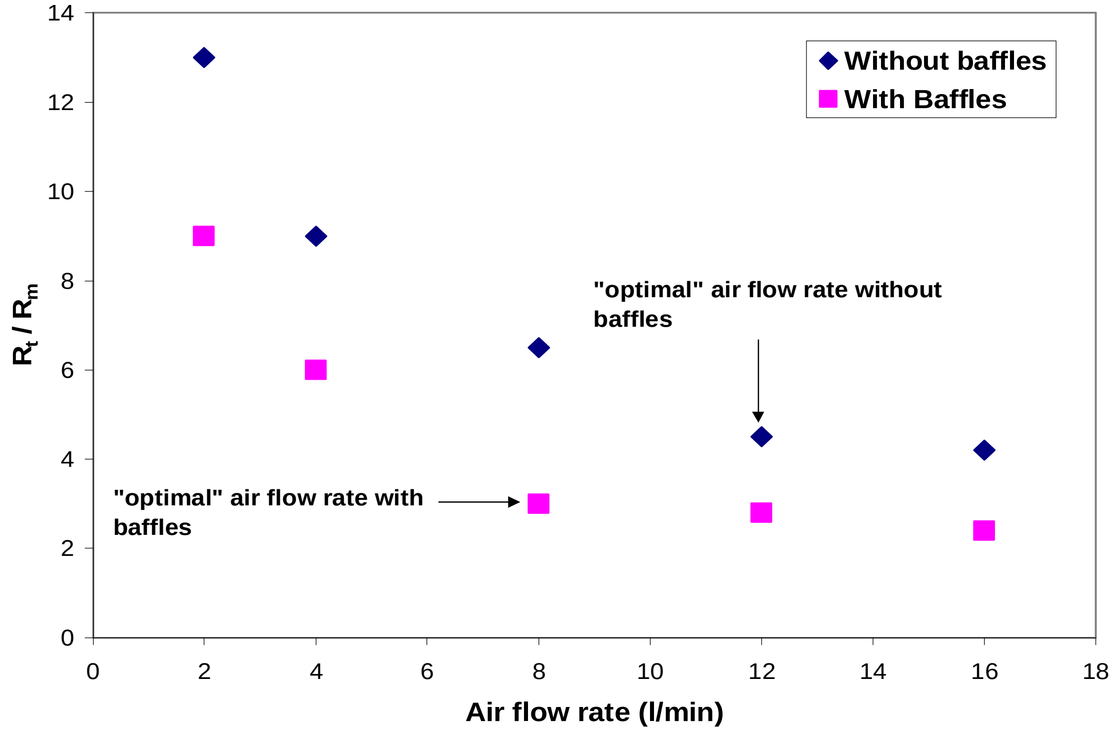

Figure 4.9. Effects of air flow rate on R_{tot} / R_m ratio for cases with and without baffles.

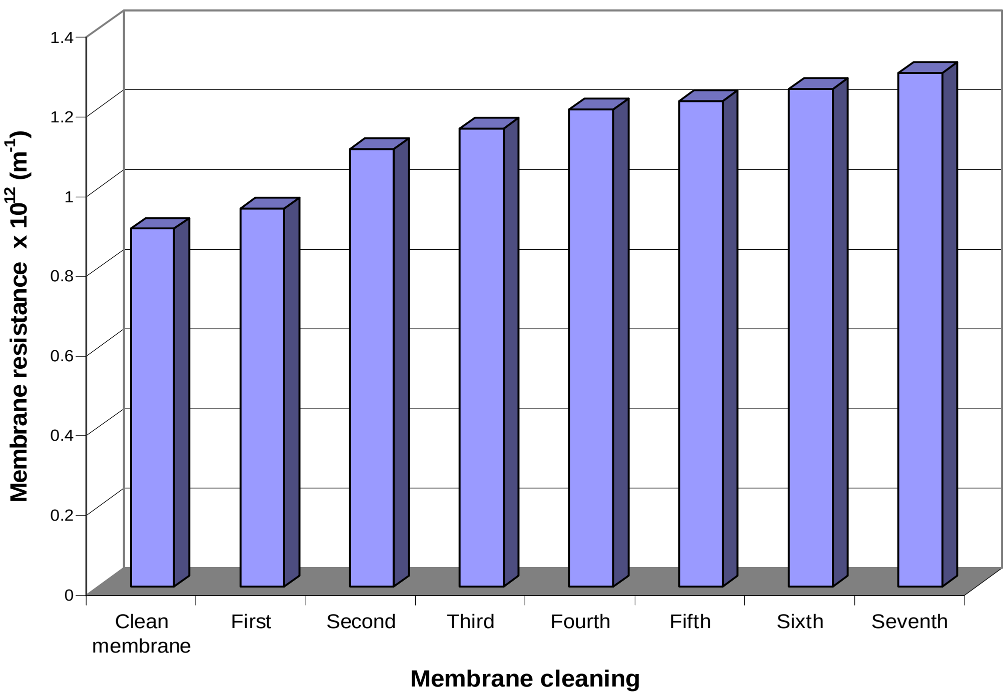

Figure 4.10. Membrane resistance after each normal clean with the detergent only.

Figure 4.10 shows that the membrane resistance gradually increases after each experiment if the membrane is not chemically cleaned. This indicated the existence of internal fouling, probably from colloids (Parameshwaran et al., 1999), which could not be removed either by air bubbling or normal cleaning after the experiment. This provides a reason why bubbling is effective only to a certain extent. The existence of internal fouling also stresses the importance of chemically cleaning the membrane after a certain period of time to recover fluxes. To reduce the frequency of chemical cleans it is normal practice to operate at modest fluxes and with intermittency.

Bouhabila et al. (2001) and Chang et al. (2002) have also examined the effect of bubbling rates by looking at instantaneous permeability. The instantaneous permeability, $L_{i,}$ is computed as follows:

$$L_i = \frac{J}{\Delta P} \tag{4.2}$$

where the symbols carry the same meaning as in equation 4.1. It is a useful measure if ΔP and/or J are changing during a test.

Instantaneous membrane permeabilities were evaluated from the results of this chapter for various air flow rates and plotted against time in figure 4.11. The instantaneous permeability initially declines very rapidly for all gas flow rates in the first 40 min of the experiment. This rapid decline is followed by a slow long term decline. Instantaneous permeabilities are higher for higher gas flow rates and also attain a steady-state which increases with an increase in the gas flow rate (Figure 4.112). Bouhabila et al. (2001) have associated the initial rapid decline with the presence of colloids in the MLSS but it could also be associated with cake formation particularly at low gas flow rates.

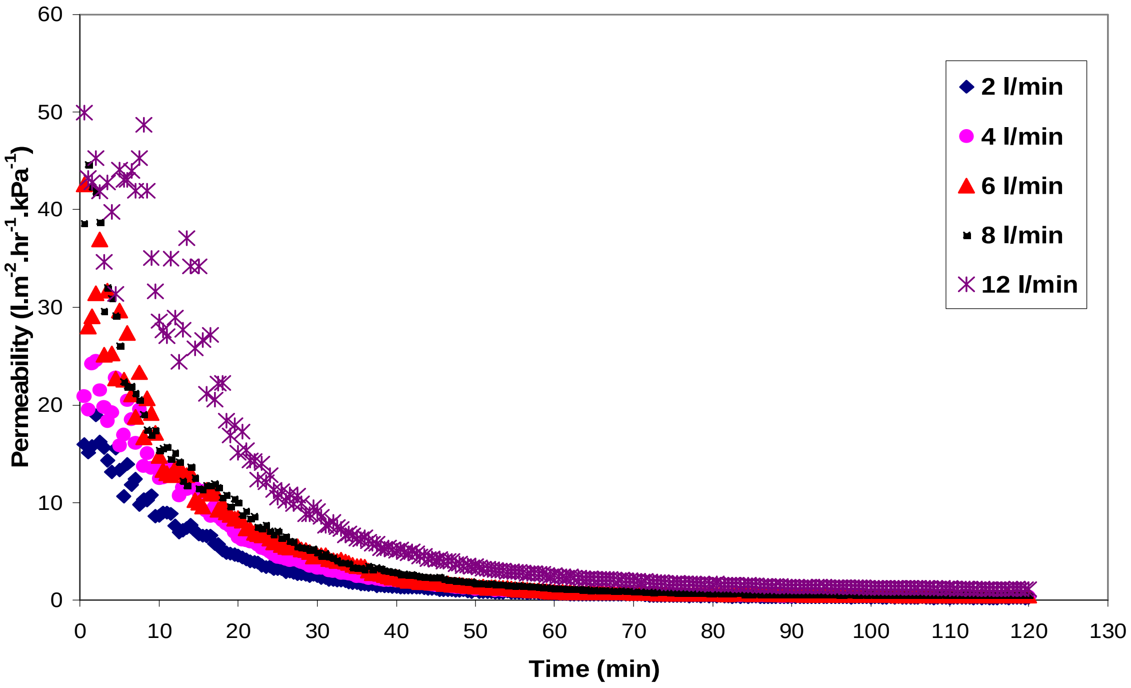

Figure 4.11. Variation of membrane permeability with time for various air flow rates for an initial flux of 40 l/m^{2}hr.

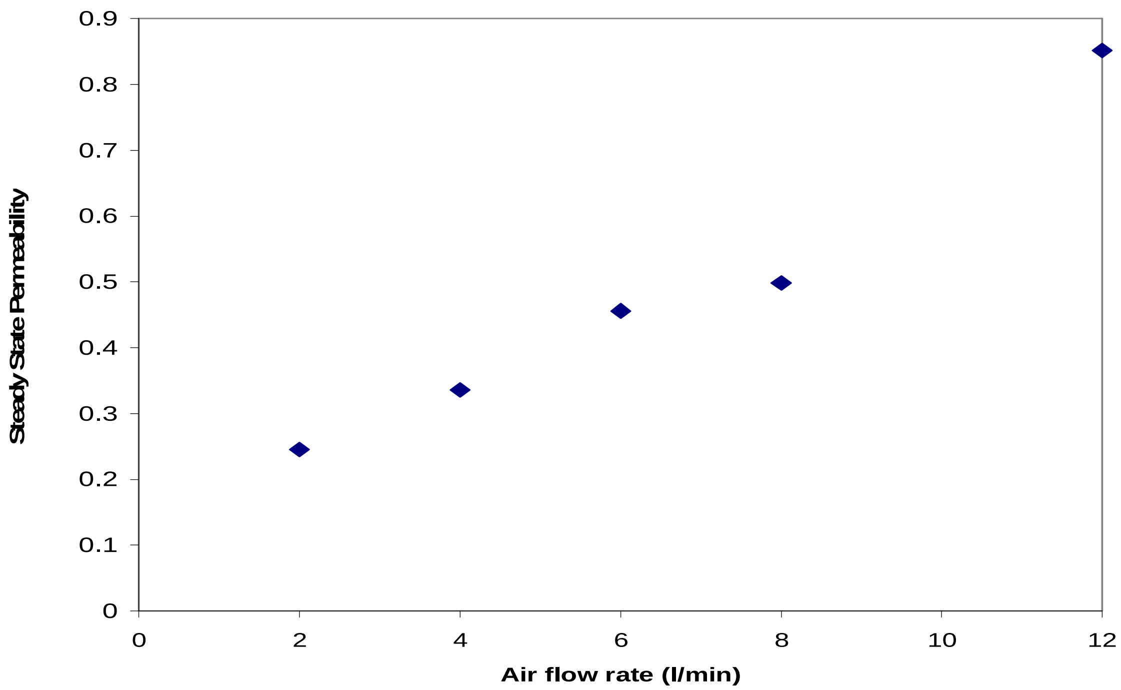

Figure 4.12. Membrane steady-state permeabilities after two hours of filtration.

Because microfiltration is a complex process, Vera et al. (2000) developed two new dimensionless quantities in order to better understand the effects of two-phase flow in sparged tubular membranes. They called these dimensionless quantities the shear stress number (N_s) and the resistance number (N_f). The shear stress number for a sparged system is given by:

$$N's = \frac{\rho'(U_g + U_l)^2}{P} \tag{4.3}$$

where U_g and U_l are the gas and liquid superficial velocities respectively calculated as if each phase was circulating alone, P is the trans-membrane pressure and ρ' is average mixture density given by:

$$\rho' = \frac{U_g \rho_g + U_l \rho_l}{U_g + U_l} \tag{4.4}$$

where ρ_g and ρ_l are respectively the gas and liquid densities.

The shear stress number compares the shear stress against the membrane wall to the TMP. The fouling or resistance number (N_f) which is given by equation 4.5 below compares the convective cross-flow transport flux (U_l) to the permeation flux (J_f), through a layer whose resistance is the overall resistance (R_f) induced by all the processes that can limit the mass transfer, for example, particle deposition, concentration polarisation, adsorption and/or internal pore closure.

$$N_f = \frac{\mu R_f U_l}{P} = \frac{U_l}{J_f} \tag{4.5}$$

where the symbols have the same meaning as explained above and μ is the viscosity of the permeate.

According to Vera et al. (2000), in the N's versus N_f plot, a straight line of positive slope means that the mass transport is mostly limited by a compression of the deposit and weakly enhanced by the cross-flow velocity. A straight line of negative slope followed by a steady-state N_f value implies that fouling cannot be completely eliminated by liquid cross-flow velocity.

In this study shear stress and fouling numbers were evaluated at different bubbling rates (from 2 – 8 l/min) for the 2.0 mm nozzle. The superficial gas and liquid velocities (U_g and U_l) were obtained via CFD simulations (see Chapter 7) and average velocities were taken. A plot of shear stress number versus fouling number was then computed and is shown in figure 4.13. This figure shows a straight line of negative slope, followed by a somewhat steadier N_f. Adopting the explanation of Vera et al. (2000), this means that the nature of fouling observed in this study could not be completely eliminated by gas-liquid two-phase cross-flow. This is probably due to the adsorption and pore closure that occurs on the membrane surface (adsorption test data are presented in section 4.4.7) and can explain the existence of optimal bubbling as seen in figure 4.2 and 4.3.

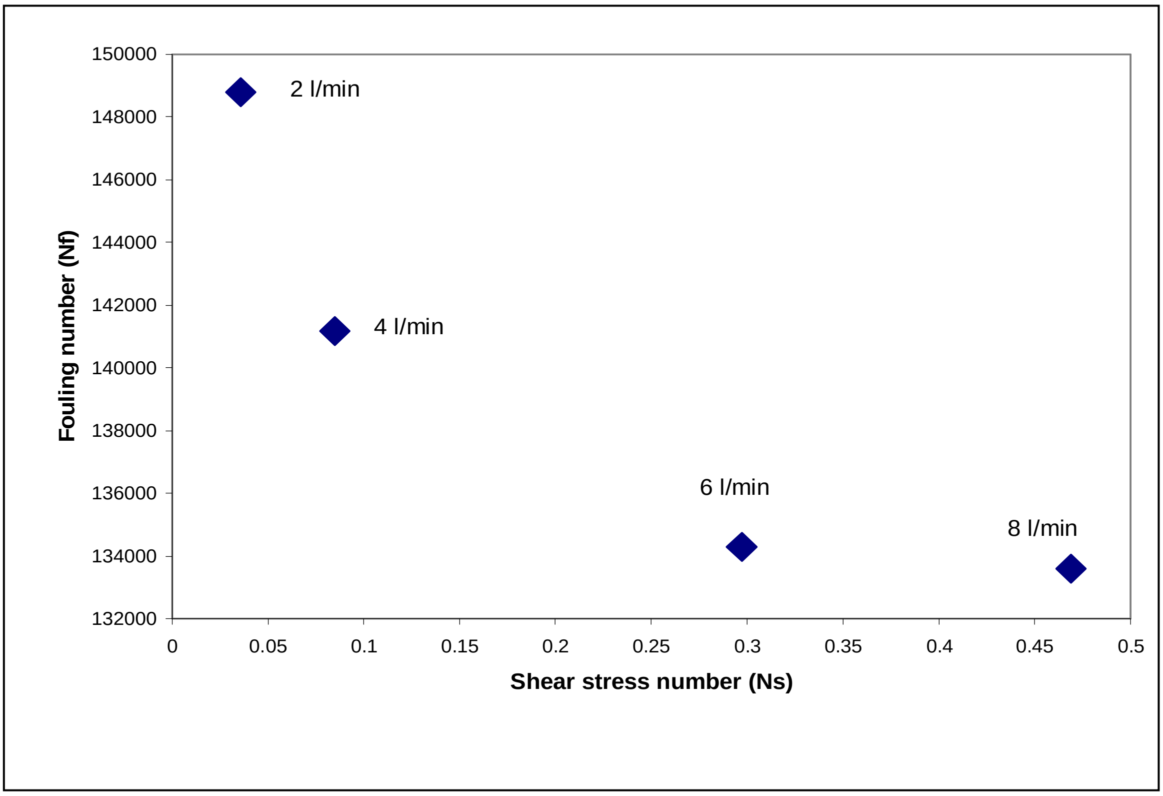

Figure 4.13. Fouling number versus shear stress number for different bubbling rates.

4.4.2 Effect of nozzle size and geometry

In this chapter, a short study has also been undertaken in order to ascertain whether the findings of chapter 3 still hold when the feed suspension has been changed. All the results presented in the previous section 4.4.1, were completed with the nozzle size of 2.0 mm as this was found to be the best nozzle size in chapter 3. A few experiments were then performed with the 0.5 mm nozzle in order to compare with the results of the 2.0 mm nozzle. The repeatability of these experiments was good, within 10% margin of error. Typical comparative results of TMP versus time for the two nozzles are shown in figure 4.14. For these runs, the air flow rate was kept at 12 l/min after having established that this is close to optimum bubbling flow rate for non-baffled cases. From figure 4.14, it can be seen that the TMP increase is substantially higher for the smaller nozzle of 0.5 mm. This result confirms that the nozzle size does have an important role to play and, more importantly, it also suggests that the observed optimal bubbling rate depends on the nozzle size used. A higher gas flow rate of 20 l/min through the 0.5 mm nozzle resulted in a slight improvement in TMP but was still not better than the 2.0 mm nozzle. A short comparison of the effect of nozzle geometry was also undertaken. Square and circular nozzles of 3.14 mm^2 surface area (based on a circular nozzle of 2.0 mm diameter) were used and the air flow rate was 12 l/min. These results are depicted in figure 4.15 and confirm the trends reported in Chapter 3.

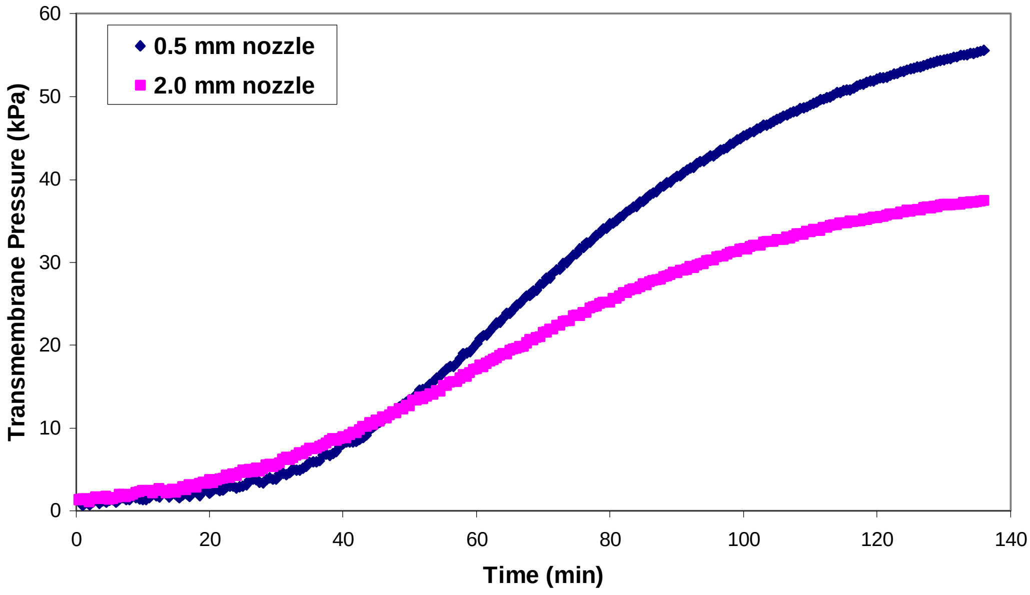

Figure 4.14. Variation of TMP with time for the nozzle size of 0.5 and 2.0 mm. The air flow rate is 12 l/min.

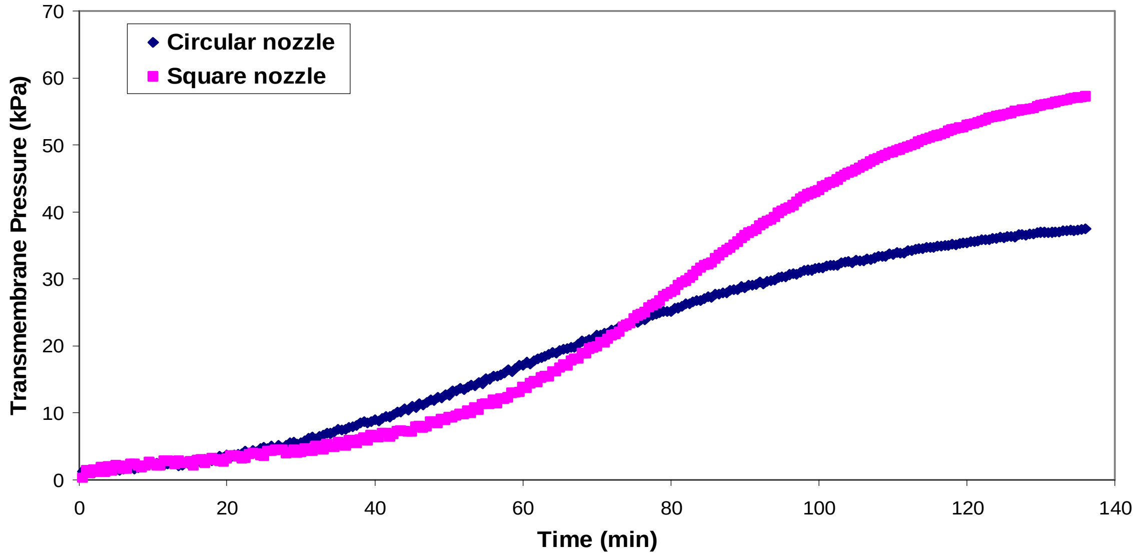

Figure 4.15. Variation of TMP with time for a square and a circular nozzle. The air flow rate is 12 l/min.

The circular nozzle outperforms the square nozzle by yielding a much lower TMP increase. Possible reasons for this behaviour are considered in more detail in chapter 5.

4.4.3 Intermittent filtration

Intermittent filtration, as discussed in chapter 3, is a viable alternative operating mode for MBRs which can reduce energy demands. According to Howell et al. (2004) intermittent filtration can be a very useful tool if an MBR is to be operated with a variable throughput. A variable throughput MBR is actually desirable since the influent to most wastewater treatment plants is not constant; it varies with time during the day. Thus at peak times the throughput of the MBR could be increased by reducing the time during which the suction pump is shut off.

Intermittent filtration in this chapter was conducted at four different gas flow rates of 2, 4 8, and 12 l/min. The permeate suction pump was switched off for 2 min after every 20 min. These time intervals were selected arbitrarily. Measurements were then made of the rate of increase of TMP during each cycle time that the permeate pump was on. Figure 4.16 represents the TMP versus time data for various air flow rates during intermittent filtration. Evidence of irreversible fouling of the membrane could be seen very early on for all gas flow rates with the exception of 12 l/min. This irreversible fouling causes the rise of TMP to be much steeper with every successive cycle. However Figure 4.16 shows that intermittent filtration can indeed be very effective. For example, with 12 l/min of air flow, the TMP had only risen to 4 kPa, whereas with continuous filtration, TMP reached 35 kPa for the same duration.

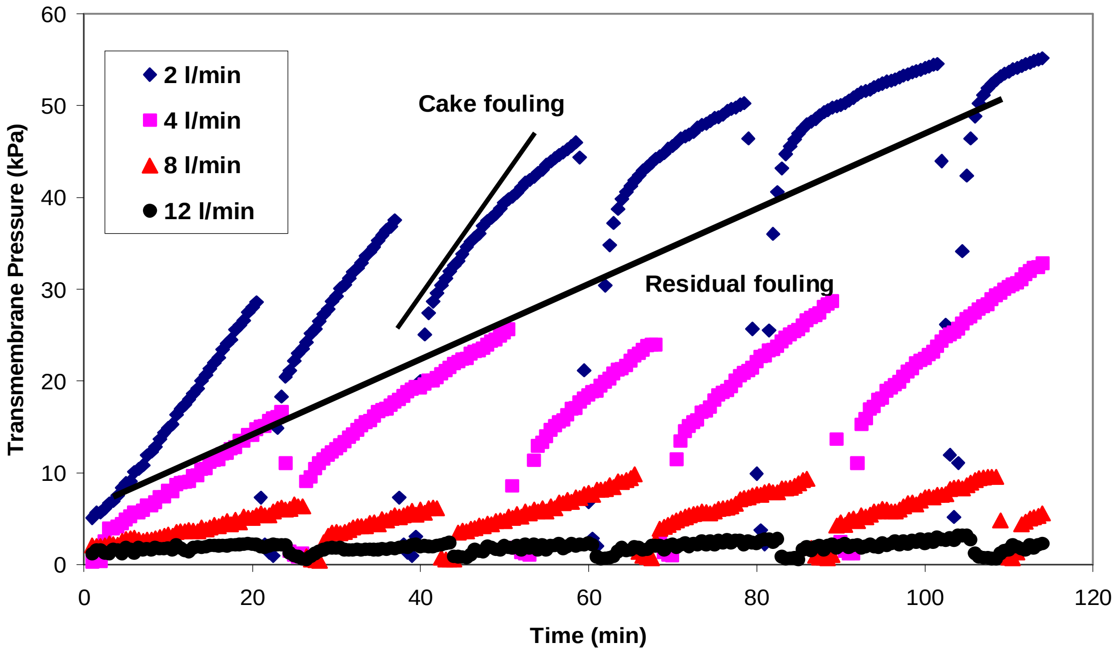

Figure 4.16. Variation of TMP with time during intermittent filtration at different air flow rates. The initial imposed flux was 40 LMH. Intermittency: 20 min on / 2 min off.

During intermittent filtration, the TMP increase becomes steeper with each cycle as can be seen in figure 4.16. This increase of TMP is known as residual fouling (Howell et al., 2004). Also shown in this figure is the slope for cake filtration for one of the cycles. The residual fouling rate differs for the different gas flow rates. The residual fouling slopes were measured and plotted against the gas flow rate in figure 4.17. The residual fouling rate decreases with the air flow rate in almost a linear fashion. Similar observations were made by Howell et al. (2004).

The slopes of the cake fouling lines as depicted in figure 4.16 were then plotted against the cycle number for various gas flow rates in figure 4.18. The cake fouling rate was found to increase with the cycle number except for the air flow rate of 12 l/min. For this flow rate, the cake fouling was almost zero. Thus with intermittent filtration, the sustainable flux (that is the long term stable flux) was increased substantially from about 20 l/m^{2}hr to about 35 l/m^{2}hr, allowing long term operation of the membrane at raised fluxes.

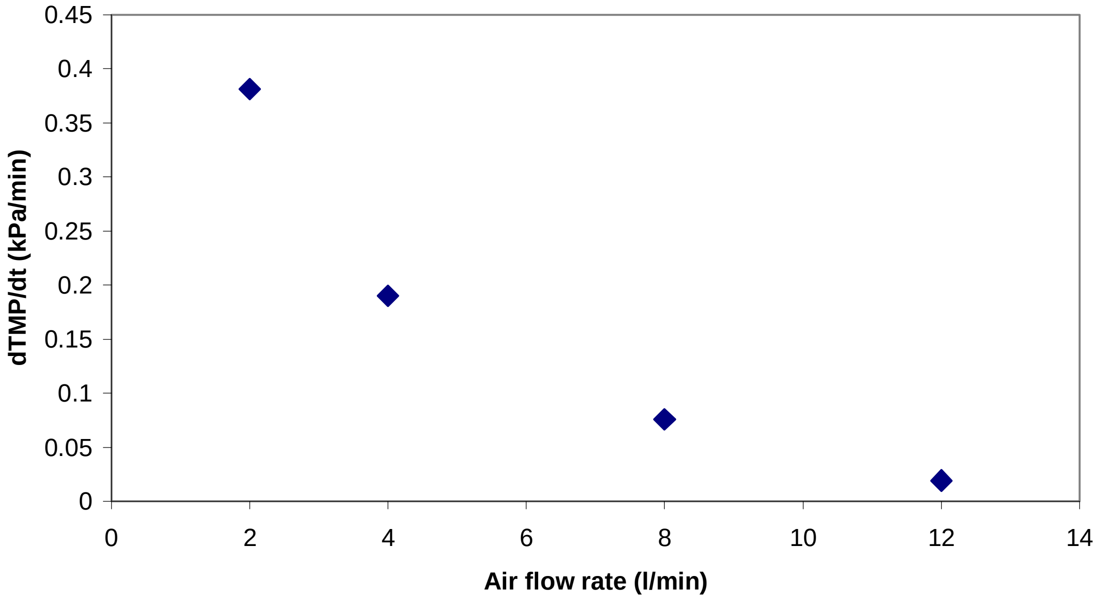

Figure 4.17. Residual fouling rates plotted against the air flow rates. Initial imposed flux was 40l/m^2/hr.

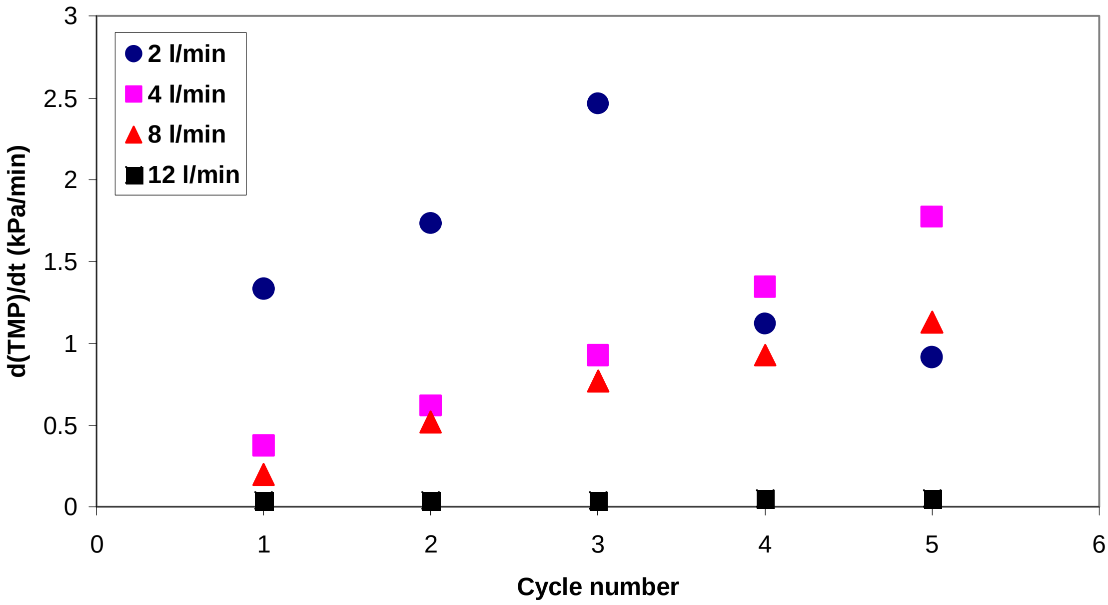

Figure 4.18. Cake filtration as a function of cycle number at various gas flow rates.

Interestingly, the cake fouling rates were found to first increase and then decrease sharply for the air flow rate of 2 l/min. This occurs because; at this air flow rate it is more difficult to maintain the imposed flux. Thus the TMP reaches steady-state, where the fouling rate becomes zero again when the flux has declined to such an extent that it is below critical flux.

4.4.4. Critical flux evaluation

The effective critical flux of the dominant foulant was determined using the stepwise method (Defrance & Jaffrin, 1999; Ognier et al., 2002; Le-Clech et al., 2003a). The permeate flux was stepwise increased in increments of 5 l/m^{2}hr with each step lasting for approximately 30 min. Below the critical flux, the TMP either rises gradually or quickly reaches a stable value and above critical flux the TMP starts to rise very rapidly. The gradual increase of TMP with flux indicates that some degree of fouling is present below effective critical flux but changes dramatically when the critical flux of the dominant foulant is reached, leading to a steep rise on TMP probably due to pore blocking or cake formation. The effect of air flow rate and membrane baffles on this effective critical flux was determined.

Le-Clech et al. (2003a) used the flux-stepping method to determine critical flux and made use of critical parameters that define the fouling behaviour at each flux step. These parameters are demonstrated in figure 4.19 and can be calculated according to the following equations:

Initial TMP increase: $$\Delta P_0 = TMP_i^n - TMP_f^{n-1} \tag{4.6}$$

Rate of TMP increase: $$\frac{dTMP}{dt} = \frac{TMP_f^n - TMP_i^n}{t_f^n - t_i^n} \tag{4.7}$$

Average TMP: $$P_{ave} = \frac{TMP_f^n + TMP_i^n}{2} \tag{4.8}$$

Permeability of the system: $$K = \frac{J}{P_{ave}} \tag{4.9}$$

Le-Clech et al. (2003a) defined critical flux as the maximum flux at which $K > 0.9K^0$, where K^0 is the permeability measured for the first flux step. Typical TMP data obtained during the determination of critical flux in this study are shown in figure 4.20 and the critical parameters determined using equations 4.3 to 4.6 are shown in table 4.1. For the data shown in Figure 4.19, K^0 = 1.92, and the maximum flux at which K > 1.728 ($0.9K^0$) is 35 l/m^{2}hr. Therefore, under these hydrodynamic conditions, the critical flux is estimated to be 35 l/m^{2}hr. From figure 4.20 it can be seen that, above 35 l/m^{2}hr, the TMP starts to rise rapidly thus indicating that supercritical conditions have been reached. Table 4.1 also reveals that all the critical parameters (K, ΔP_0 and $dTMP/dt$) were within 20% of the mean value until the critical flux was reached, at which point significant changes in the parameters were then observed. This confirms that the critical parameters are also a good indication of the flux at which fouling starts to become significant.

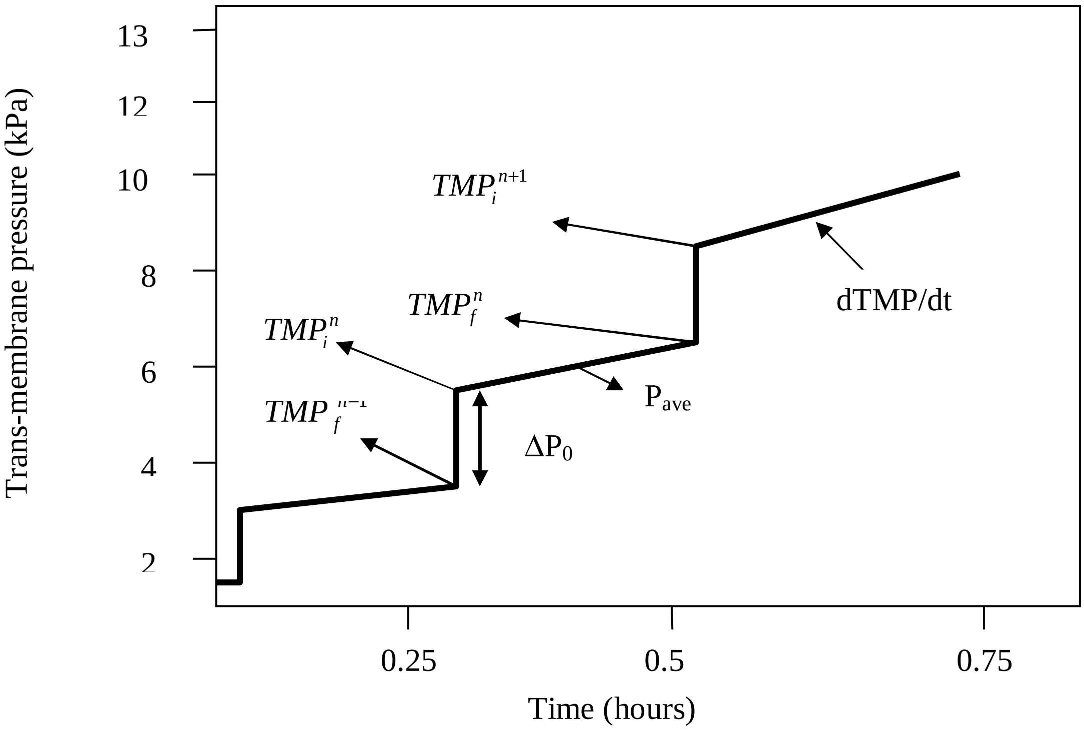

Figure 4.19. Illustration of critical flux determination with the flux-step method, and calculation of the derived TMP parameters (see also Eqns. 4.6 - 4.9).

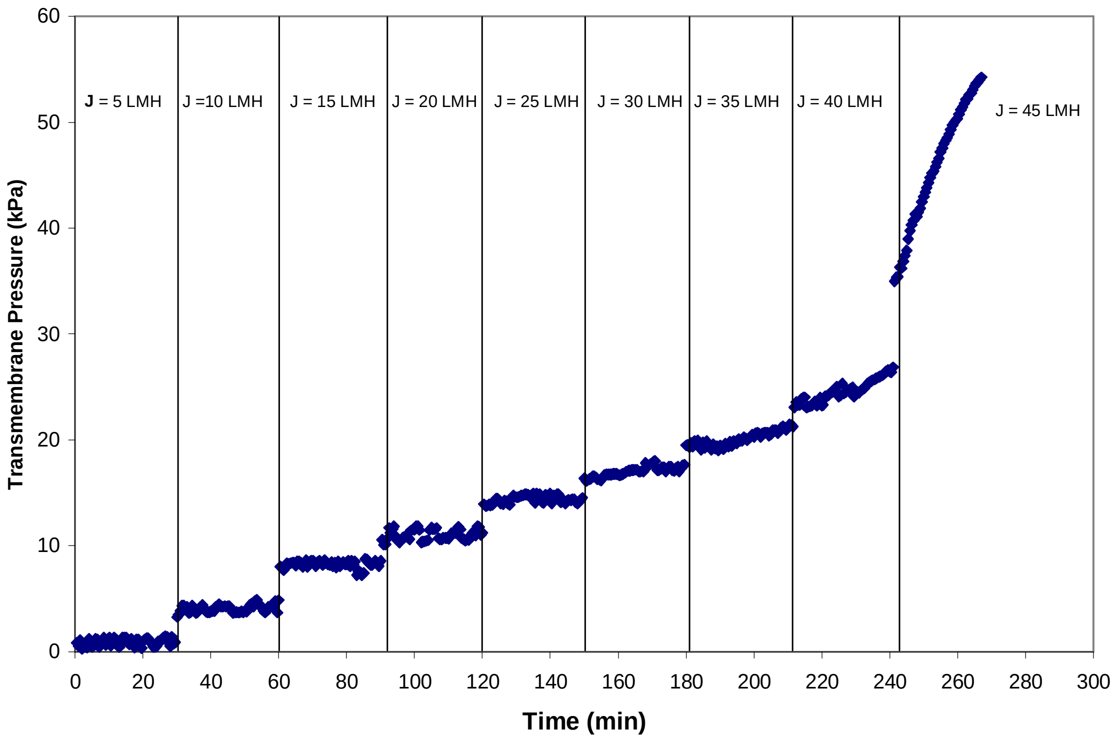

Figure 4.20. Critical flux determination with the flux-step method. The air flow rate is 12 l/min.

Table 4.1. Example of calculation of critical parameters for the data shown in fig. 4.20.

Flux	*Pave*	*K*	ΔP_0	Dp/dt (Kpa/min)
0				
5	2.6	1.92	1.2	0.02
10	4.76	2.1	1.8	0.023
15	8.305	1.81	2.25	0.019
20	10.86	1.84	1.97	0.022
25	14.23	1.75	1.86	0.021
30	17	1.76	1.83	0.024
35	20.23	1.73	1.85	0.029
40	*24.83*	*1.61*	*1.87*	*0.125*
45	*44.6*	*1.008*	*8.152*	*0.94*

Numbers in italic are defined as super-critical.

For the data shown in figure 4.19, average TMPs were calculated at each flux step. The same experiment was then conducted using pure water with again the average TMPs evaluated at each time step. These average TMPs were then plotted against flux (figure 4.21). It can be seen that below critical flux the TMP rose linearly with flux and above critical flux (in this case ≈ 35 l/m^2hr), the TMP started to rise exponentially for the MLSS run whilst that of pure water still remained linear. The rapid rise of the TMP is a strong indication that fouling in the form of cake deposit had started to occur. This figure also shows that even below critical flux, the TMP for the MLSS run was slightly higher than that of pure water. This was probably due to an instantaneous fouling phenomenon which took place at the beginning of the filtration process (Ognier et al., 2002) or is due to particles being temporarily deposited on the membrane and then being swept away again as observed by Neal et al. (2003) using Direct Observation Through the Membrane (DOTM) technique.

Figure 4.22 presents critical fluxes identified using the stepwise method at different gas flow rates for runs with and without baffles. This figure shows that for both arrangements an increase in the aeration rate increased the critical flux. Therefore an increase in the air flow promotes the back-transport of particles away from the membrane, minimising fouling and increasing the critical flux. For both cases the increase in critical flux with air flow rate seems to be approaching a limiting value implying that, above a certain gas flow rate, the critical flux becomes independent of the bubbling rate. Howell et al. (2004), working in a submerged flat sheet MBR configured almost similarly to the one in this study, noted that it was difficult to raise the critical flux beyond 23 l/m^2hr despite increasing the gas flow rate substantially. This is much less than the optimum critical fluxes observed in this study of around 40 l/m^2hr when baffles were used. Howell et al. (2004) postulated that this limiting critical flux is a function of the MLSS concentration in the bioreactor. The differences in the critical fluxes reported by Howell et al. (2004) and those found in this study can be linked to a number of factors. Firstly, Howell et al. (2004) used a synthetic sludge and not real waste activated sludge. The MLSS concentration in their reactor was in the range of 6.78 to 21.7 g/l. This range is much wider than the range in this study which was between 4 – 8 g/l. Therefore they could have had more solids in their reactor which would lower critical fluxes. Finally, Howell et al.

(2004) also did not make use of baffles in their study which could have improved the critical fluxes.

In this study the critical fluxes were always higher in the runs with baffles than those without baffles. The effects shown in Figure 4.22 are significant. At an airflow of 8 l/min the critical flux was increased by 60% by the use of baffles. Another comparison shows that the critical flux at 16 l/min without baffles was achieved at 50% of the airflow (8 l/min) with baffles. These results confirm the potential benefit of baffles in the submerged flat sheet system. Further optimisation of baffle geometry may be possible, but was beyond the scope of this thesis.

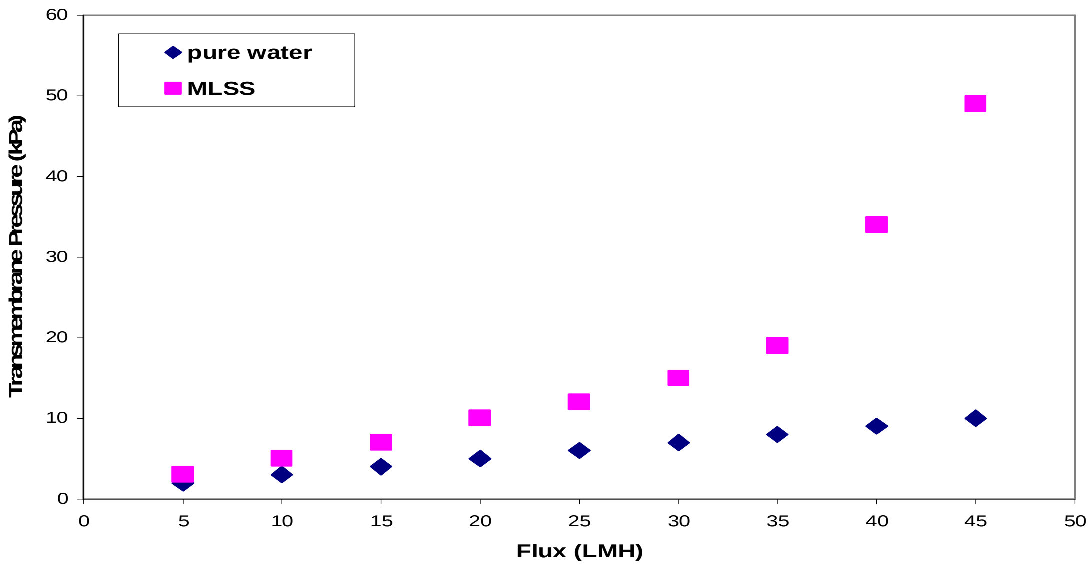

Figure 4.21. Average TMP versus flux. For the MLSS run, the air flow rate was 12 l/min.

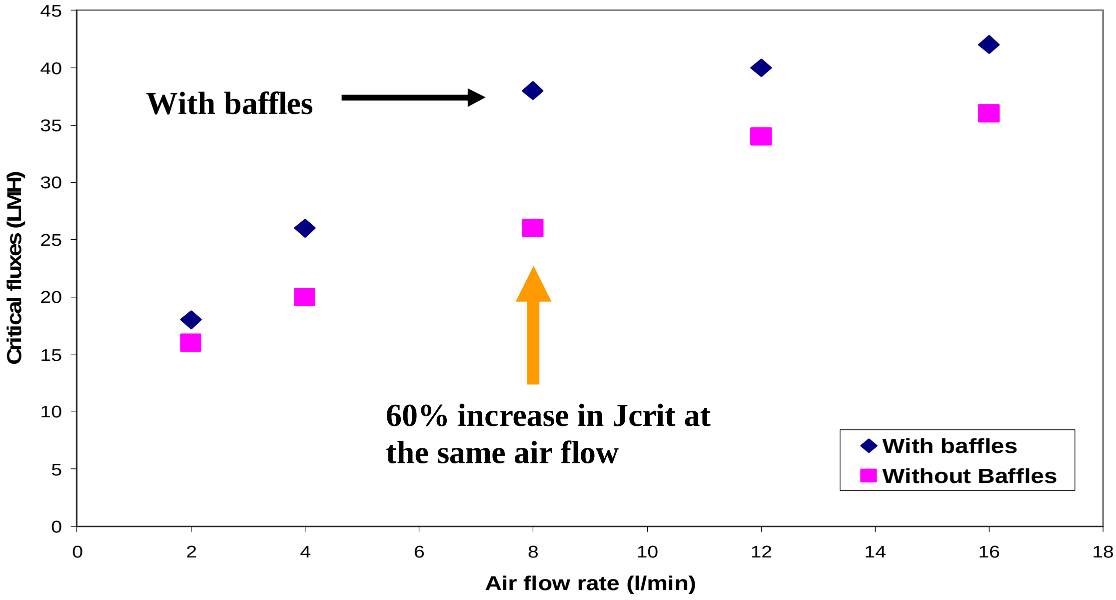

Figure 4.22. Critical fluxes determined at different gas flow rates for cases with and without baffles.

During the determination of critical fluxes, a flux stepping method was used. This enabled the calculation of hydraulic resistances at each flux step under different bubbling conditions. Results for the cases without baffles are shown in figure 4.23 below. For most cases, critical flux was below 40 l/m^{2}hr, therefore results are shown up to a flux of 35 l/m^{2}hr. The hydraulic resistance increases with flux for all bubbling rates and for a given flux, decreases with the bubbling rate. Most importantly, it can be observed that, as the flux continues to increase, the increase in resistance becomes smaller for all gas flow rate. This implies that the cake build up can only occur up to a certain point, beyond which any further increase in flux does not contribute to a significant increase in resistance. This figure also shows that at very low fluxes (below 10 l/m^2.hr), the influence of air flow rate is very small. According to Yeom et al. (1999), at low fluxes, adsorption fouling, which is insensitive to the hydrodynamic conditions, predominates.

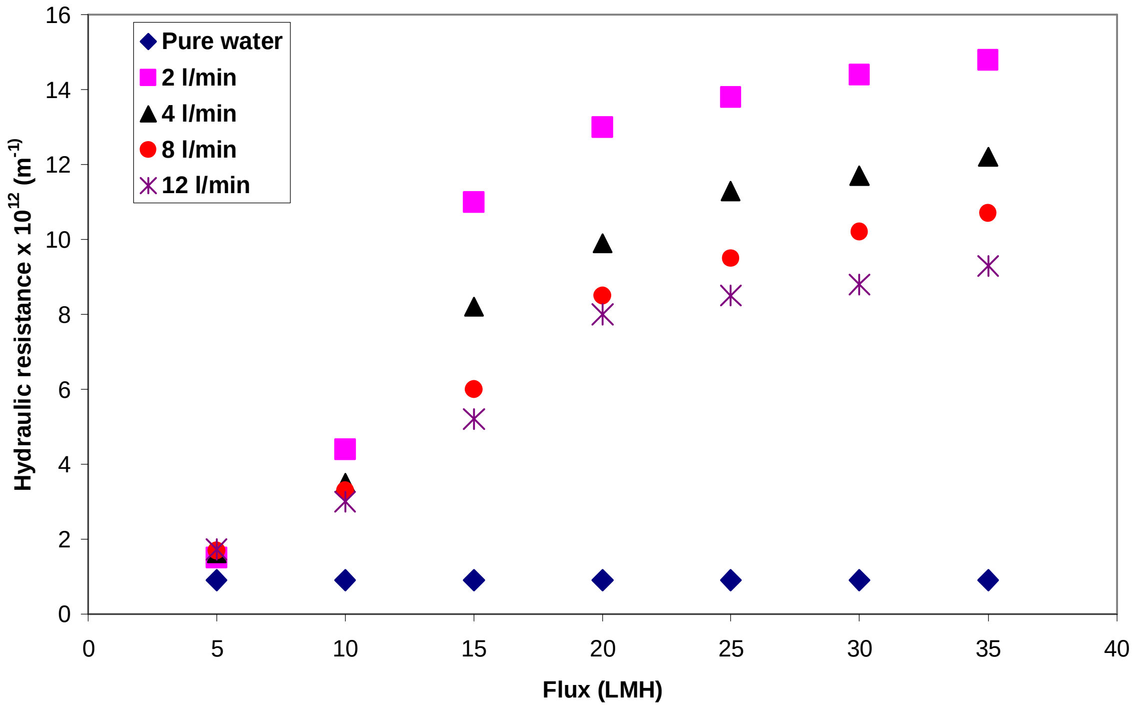

Figure 4.23. Variation of hydraulic resistance with flux at various gas flow rates.

4.4.5 Flux prediction model for aerated submerged membrane systems

Flux prediction models are a useful tool for the design and construction of membrane systems. Most flux prediction models that exist are for non-submerged membranes or the so-called "in-out" filtration systems. The submerging of membranes in the suspensions to be clarified is a fairly new approach and mostly used for MBRs, hence it is difficult to find flux prediction models for this configuration. One such model has been developed by Shimizu et al. (1996) for an aerated waste activated sludge suspension. According to this model, the steady-state flux obtained under any hydrodynamic conditions for a submerged membrane filtering aerated waste activated sludge is related to the two-phase flow velocity across the membrane, the geometric hindrance of the membrane, and the MLSS concentration in the following way:

$$J_{ss} = V_L = K^{'} \phi \, \mathrm{u}^{*a} \ \mathrm{MLSS}^{b} \tag{4.10}$$

where J_{ss} is the steady-state flux, V_L is the lift velocity, $K^{'}$ is the filtration constant, ϕ is the geometric hindrance factor of the membrane, u^* is the two-phase flow velocity and MLSS is the mixed liquor suspended solids concentration. The geometric hindrance factor ϕ, depends on the packing density and how easily fluid can pass over the surface of the membrane. It usually has a value of one for rigid tubular and flat sheet membranes and less than one for flexible hollow fibre membranes. Shimizu et al. (1996) evaluated the filtration constant $K^{'}$, and found it to have a value of 2.6×10^{-5} $kg^{0.5}$ $m^{-1.5}$. This value was found to be almost identical to the value obtained for a conventional "in-out" filtration system. It is evident that the above model is empirical and does not allow for the effect of membrane type (e.g. MF/UF) or biological factors, such as SRT and organic loading. However it is of interest to compare the Shimizu model with this study.

The model assumes that the steady-state flux J_{ss} is attained when the velocity of the permeate through the membrane V_L is exactly balanced by the lift velocity by which particulates are transported away from the membrane surface. The lift velocity is generated by the shear stress originating from the flow velocity gradient over the membrane surface and is a function of the operating parameters such as the two-phase flow velocity (u^*), which is induced by air bubbling, and fluid characteristics expressed by MLSS.

The exponents a and b in equation 4.10 are determined experimentally by plotting J_{ss} against u^* and J_{ss} against MLSS concentration. In each case, the value of the slope is the value of the respective exponent in the model. Since MLSS concentration could not be controlled in this study, the value for exponent b could not be determined experimentally and the value that was used was the one found by Shimizu et al. (1996) for aerated waste activated sludge. This value is -0.5. The value for exponent a was determined experimentally as shown in figure 4.24 and it was found to be 1.05. The two-phase flow velocities (u^*) used in figure 4.24 were not determined experimentally but were obtained from CFD simulations as will be described in chapter 7. The value of a obtained is almost the same as the one obtained by Shimizu et al. (1996) of 1.0.

Figure 4.25 shows a comparison between the experimental and predicted fluxes with the value of K taken from the work of Shimizu et al. (1996). The predicted fluxes are higher than the experimental fluxes by an average of about 15%. Possible reasons for this could be the following. Firstly, the exponent *b* was assumed to be the same as that of Shimizu et al. (1996) based on the range of MLSS concentrations that they covered. However, had it been possible to evaluated this value experimentally, a different value may have been found. Secondly, u^* values were obtained from CFD simulations; however these simulations were completed for a pure water – air mixture with the viscosity of water tripled so that it is closer to that of activated sludge because in literature activated sludge viscosities ranging from 7.5 to 85 mPa.s have been reported (Rosenberger et al., 1999) Lastly, the filtration constant $K^{'}$ depends on the membrane properties. Probably the value of Shimizu et al. (1996) for their submerged tubular membrane is different to that for the flat sheet membrane that was used in this study, even though the mean pore sizes of the two membranes were the same. So uncertainty in the value of $K^{'}$ would also contribute to the discrepancy between the predicted and experimental fluxes.

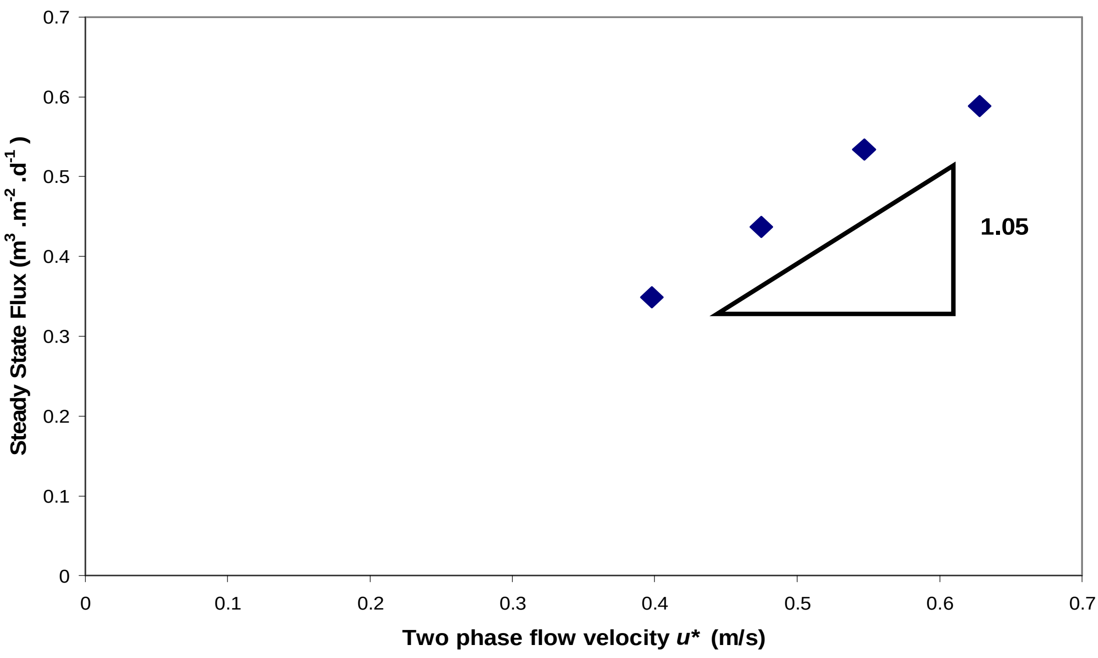

Figure 4.24. Effect of predicted two-phase flow velocity on steady-state flux for an aerated activated sludge suspension.

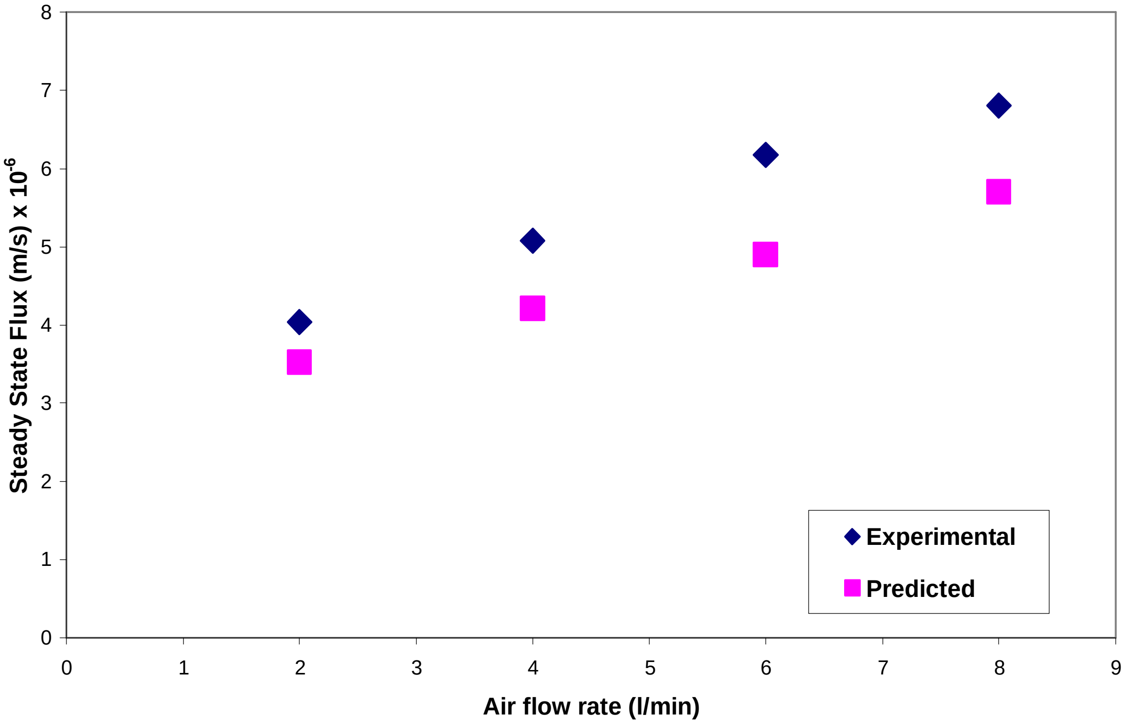

Figure 4.25. Comparison between predicted and experimental steady-state fluxes.

4.4.6 Membrane performance assessment

One of the main advantages of MBRs over conventional wastewater treatment processes is the exceptionally high quality of the effluent they produce. Therefore, in this study, the membrane performance was assessed in terms of three parameters, namely: permeate COD, permeate turbidity and suspended solids removal. The permeate COD was determined using methods described earlier and these values were compared with published COD data from a submerged MBR plant that uses similar types of flat sheet membranes (Kubota membranes). This comparison is depicted in figure 4.26. Although COD values observed in this study were somewhat higher than those reported by Churchouse (1998), they were consistently less than 100 mg/l which has been considered to be very good in other MBRs (Peters et al., 2000; Hasar et el., 2001; Lee et al., 2003).

The MLSS concentration for the feed used in this study varied within 4 to 8 g/L from run to run (figure 4.27). No suspended solids were detected in the permeate. The turbidity of the feed was found to be always greater than 1200 NTU which was the detection maximum for the turbidimeter used for analysis. The turbidity of the permeate varied between 0.25 and 0.9 NTU (figure 4.27) and it was always below 1 NTU. Most of the removals are below the standard set by US EPA for drinking water of 0.5 NTU (Parameshwaran et al., 1999).

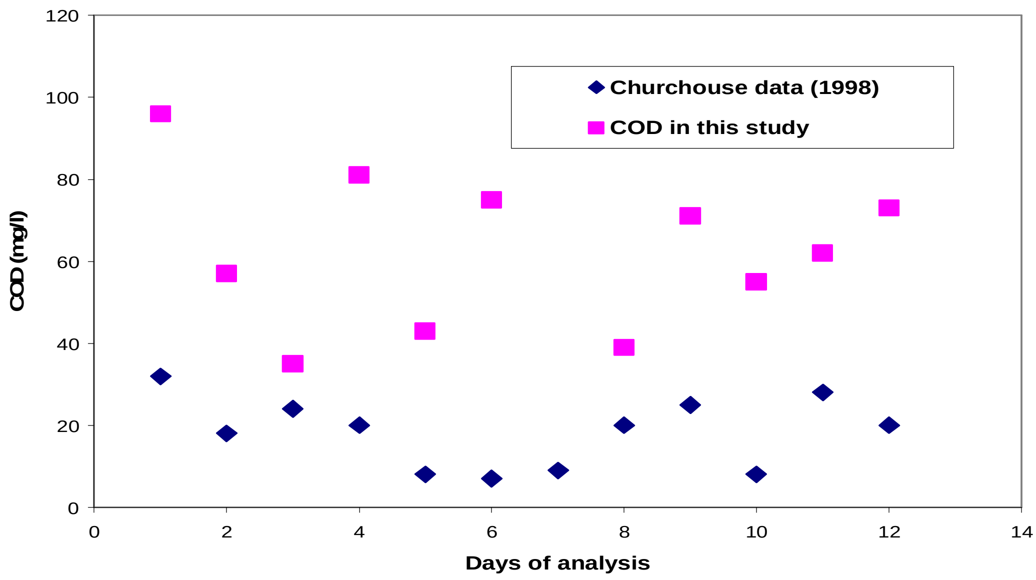

Figure 4.26. Feed and Permeate COD.

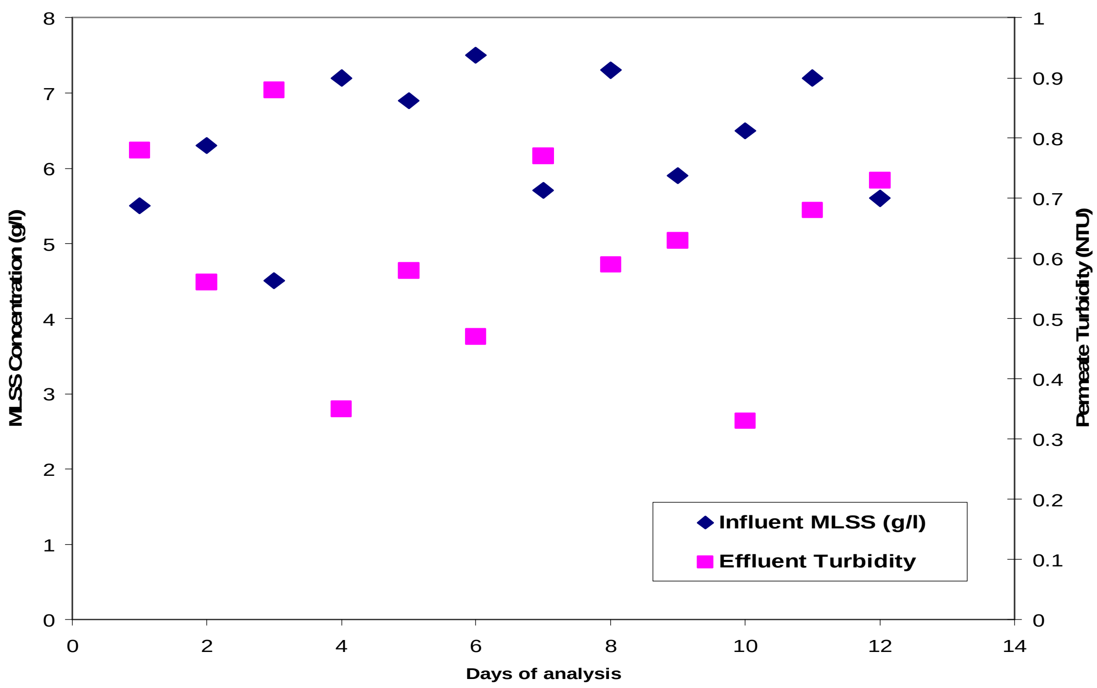

Figure 4.27. Variation of MLSS concentration and permeate turbidity.

4.4.7 Comparison with the results of chapter 3

Since the nature of the experiments conducted in this chapter was the same as those conducted in chapter 3, a brief comparison between the results of this chapter and those of chapter 3 can be made. For this comparison, only two aspects have been considered, the rate of fouling at a specific time (dTMP/dt) and the critical fluxes at various gas flow rates. In both chapters it was learnt that baffles gave better performance, thus only the cases with baffles have been used for comparison. The results used from chapter 3 are those of a yeast concentration of 5 g/L and the concentration of activated sludge in this chapter varied between 4 and 8 g/L. The results have been compared at air flow rates up to 8 l/min and for a nozzle size of 2.0 mm as these are the common conditions used in the two chapters. Figure 4.28 shows the dTMP/dt versus air flow rate for the yeast and activated sludge suspensions whilst figure 4.29 shows the critical fluxes at different bubbling rates for the two suspensions.

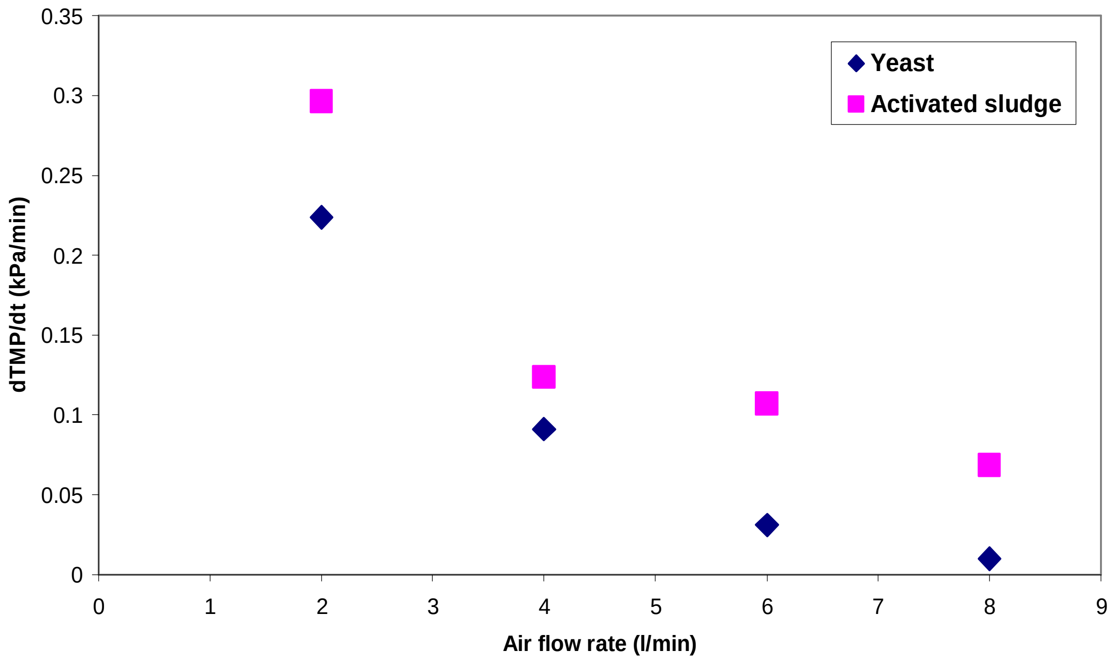

Figure 4.28. Variation of dTMP/dt after two hours at various air flow rates.

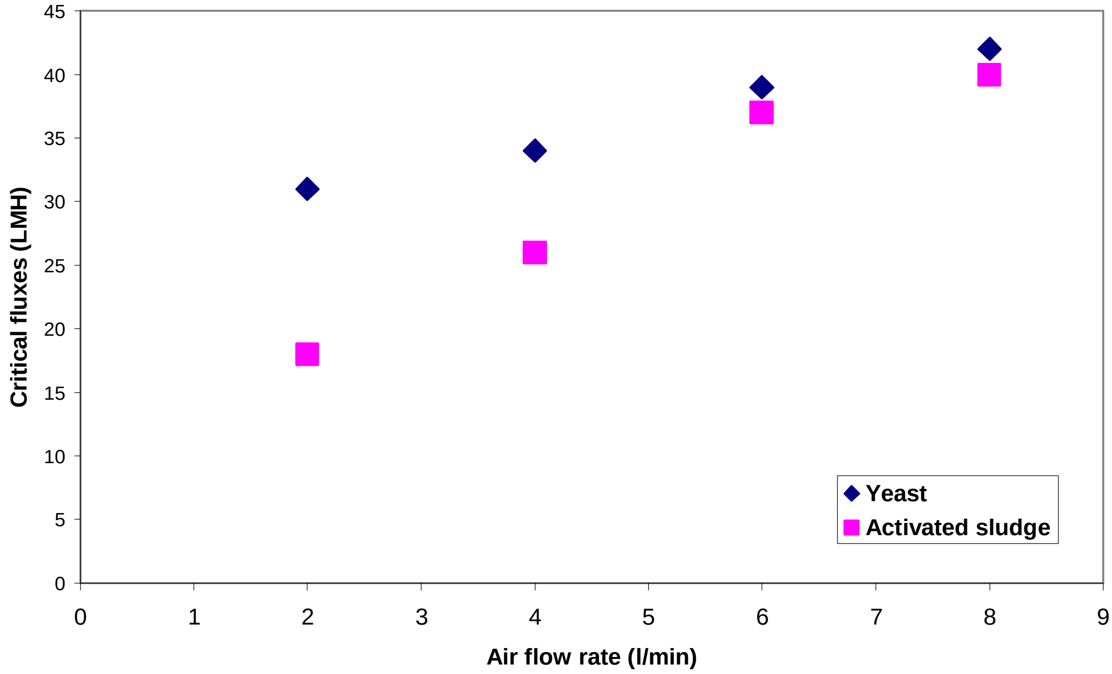

Figure 4.29. Critical fluxes of the yeast and activated sludge suspensions at various air flow rates.

The two figures show similar trends with air flow rate and demonstrate that the waste activated sludge suspension fouled the membrane more than the yeast suspension. For example, at a bubbling flow rate of 2 l/min, the dTMP/dt for activated sludge is 24% higher than that of the yeast suspensions. This result was not unexpected due to the more complex nature of the MLSS. A separate investigation was then carried out in order to illustrate how the waste activated sludge could be more fouling than the yeast suspension. This investigation involved determining the effect of adsorption that occurs when the two feeds are in contact with the membrane without filtration. In these tests the pure water flux was measured through a clean membrane; then the membrane was dipped into a suspension either of yeast or sludge for 30 minutes which was followed by measurement of the pure water flux again for 30 min. However, since the peristaltic pump was operated at a constant flux, it was the TMP that was monitored. Two adsorption tests were done for each feed and the results are shown in figure 4.30 below. In this figure the TMP for pure water before adsorption is also shown. Due to adsorption, the membrane permeability was reduced as shown by the higher TMP after adsorption for both suspensions.

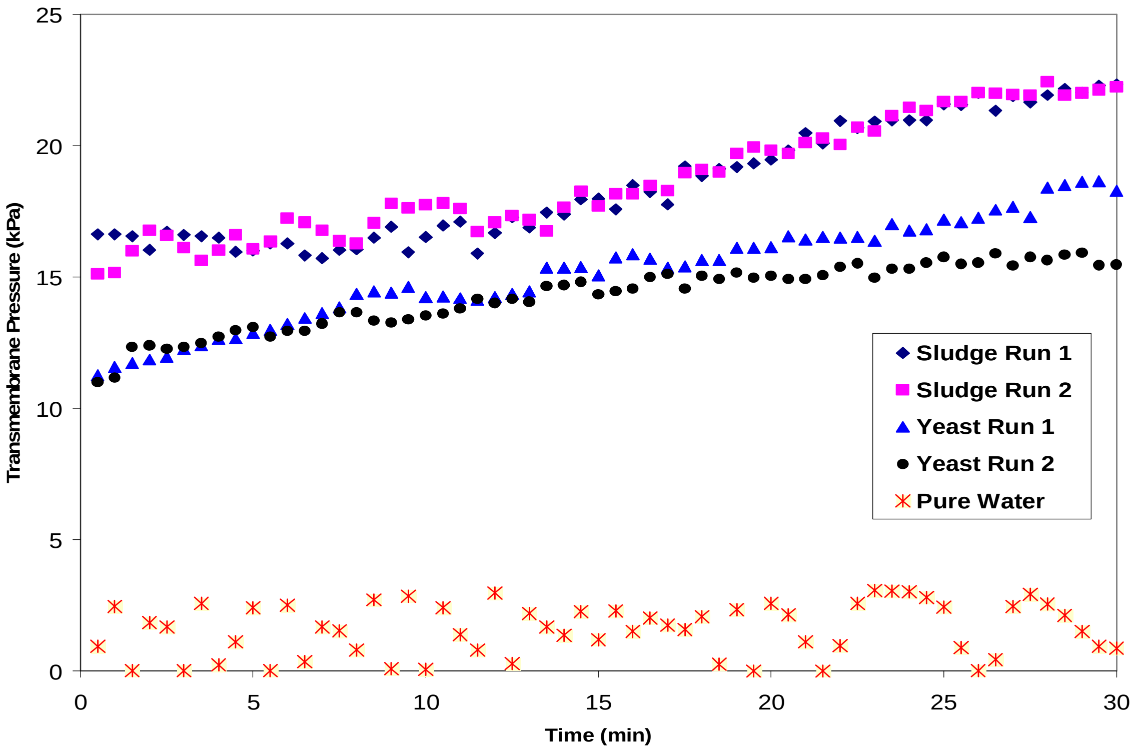

Figure 4.30. Variation of TMP with time during pure water filtration after adsorption period of 30 min.

Activated sludge is a complex and variable suspension. It is composed of three main fractions: the floc, which contains particles ranging from 1 µm to hundreds of microns; the colloidal fraction, which contains particles ranging from 0.001 µm to 1 µm; and the soluble fraction which contains macrosolutes and species smaller than 0.001 µm (Tardieu et al. 1998). The extra cellular polymeric substances (EPS) are a feature of mixed liquor and include some of the colloidal fraction and macrosolutes, such as polysaccharides, proteins and lipids. During the adsorption test, physico-chemical interactions occur between the membrane and the soluble and colloidal fractions of the yeast and the sludge and the particulate matter has less of a role to play. Figure 4.30 reveals more fouling from contact with MLSS and this implies that there is more adsorption occurring with the sludge suspension which suggests that the contents of the soluble and colloidal fractions of the sludge are higher in concentration than those of the yeast. According to Vera et al. (2000), during filtration of biologically treated wastewater, adsorption of macromolecules which occurs at the onset of filtration can lead to irreversible fouling. Besides the adsorption tests conducted here, further evidence can be found from the literature which suggests that it is the composition of the liquid phase of the sludge that contributes more to long term fouling than the particulate solids. Rosenberger et al. (2002) found that fouling was more sensitive to the concentration of extracellular polymer substances (EPS) in the liquid phase than to the MLSS concentration. Thus, just based on the composition of the liquid phases of the yeast and sludge solutions, possible reasons can be found which explain why sludge is the more fouling suspension.

Other reasons as to why activated sludge was the more fouling suspension can be found by looking at the particulate matter itself. The particle size distribution of the activated sludge is wider than that of yeast (see figure 3.4 and 4.1) and the mean particle size of the yeast (4.2 µm) is smaller than that of the aerated activated sludge (77 µm). A smaller particle size may suggest that a denser cake will be formed with yeast suspension resulting in higher resistances and reduced flux as Cabassud et al. (1997) found. However, the activated sludge suspension has a wide range of particles and Mercier-Bonin et al. (2000a) found that the presence of extracellular macromolecules (e.g. proteins, cell debri, complex substrates) caused the cake to be more adhesive and led to more irreversible fouling. The concentration of these extracellular components is likely to be higher in the activated sludge suspension than in the yeast suspension. Mercier-Bonin et al. (2000a) also observed that two-phase flow was unlikely to solve the problems of adsorption and membrane clogging by colloids and macromolecules likely to occur in complex biological suspensions. With yeast having a narrow range of particles, the filling of the voids in the yeast cake probably occurs to a lesser extent than in the activated sludge cake, thus resulting in a more porous and less resistant yeast cake. Comparing washed and unwashed yeast, Sur and Cui (2005) found that the removal of extracellular substances by washing the yeast resulted in much higher fluxes. For the comparison in this study, the presence of extracellular substances is much higher in the activated sludge suspension, thus the yeast suspension would be expected to yield higher fluxes. Although the yeast suspension yielded higher fluxes it showed qualitatively similar trends to the MLSS, in terms of response to air flow rate and baffles. This confirms the use of the yeast suspension as a ‘model’ feed in experiments on submerged flat sheet membranes.

4.5. CONCLUSIONS

Membrane fouling in a submerged flat sheet process filtering MLSS (similar to an MBR for wastewater treatment) is influenced by a number of hydrodynamic factors such as bubbling rate (figure 4.2), the use of baffles (figure 4.5), and nozzle size and geometry (figure 4.14 and figure 4.15). It has been demonstrated that aeration rate is a significant factor governing the filtration conditions and decreasing the fouling resistance. An increase in the air flow rate stimulated cake removal from the membrane, but there was a limit value beyond which the air flow rate increase had negligible effect on the cake-removal efficiency, an observation which was not made in the yeast experiments (in chapter 3). Aeration rates were also found to increase the critical fluxes up to a certain flux, beyond which any further increase in aeration has no effect.

Intermittent filtration has, once again, been shown to be a very effective technique that allows stable, long term operation of the membrane system by ensuring that the permeate flux remains below the critical flux, above which fouling is inevitable. This mode of operation would result in large savings in the amount of energy consumed.

Baffles were found to be equally effective in the activated suspension as they were in the yeast suspension. Baffles increased the observed critical fluxes by a margin of 10 to 50%, depending on the gas flow rate. Also, when baffles were inserted, a reduction in the optimum gas flow rate was observed by up to 50%. Thus baffles should allow for operation at higher fluxes with a reduced usage of air which would save energy.

For the runs in which membrane performance was monitored, effluent COD was always less than 100 mg/l. The turbidity was reduced from over 1200 NTU to no more than 0.94 NTU. No suspended solids were detected in the effluent. These values compare favourably with those reported by other researchers for submerged flat sheet MBR using the Kubota type membrane module (Churchouse, 1998; Churchouse & Wildgoose, 1999; Howell et al. 2004).

It has also been found in this chapter that the activated sludge suspension fouls the membrane at a greater rate than the commercial yeast suspension. This has been linked to the complex constituents of the activated sludge suspension which was shown to consist of components with a much higher adsorption affinity than the yeast suspension (figure 4.30). Gas-liquid two-phase flow has little effect on the removal of adsorbed compounds.

The results from this chapter show that the model suspension of yeast can be successfully used to obtain reliable information about the effects of various hydrodynamic conditions in a real submerged flat sheet MBR. The observations made in chapters 3 and 4 clearly demonstrate that two-phase flow is very efficient in reducing fouling and the investigations conducted point in the directions by which two-phase flow can be optimised. However, the information acquired thus far, does not really answer the question: why does two-phase flow work? Two of the remaining chapters of this thesis (chapters 5 and 7) will investigate this question, using both CFD simulations and further experimental analysis.

Chapter 5

CHARACTERISATION OF GAS-LIQUID TWO-PHASE FLOW

5.1 INTRODUCTION

In submerged flat sheet membrane bioreactors (MBRs), the gas is introduced into the tank containing the membranes by means of nozzles located on a diffuser which is placed underneath the membranes. The nozzle size could have an impact on the bubble size distribution and thus on the gas-liquid two-phase flow profile. Commercial submerged flat sheet MBRs use nozzles of different sizes, for example, the Kubota MBR initially made use of circular nozzles of 10 mm in diameter and then changed to 4 mm diameter nozzles (Morgan et al., 2003) and the Zenon Environmental Ltd hollow fibre MBR uses large rectangular slots (Stephenson et al., 2000). Another factor which governs the two-phase flow profile is the gas loading rate. The higher the gas loading rate, the greater the number of bubbles produced and this, in turn, affects the behaviour of the two-phase flow stream. It is the aim of this chapter to develop an understanding of how the nozzle size and the gas loading rate affects the bubble size distribution and the bubble rise velocities.

Although numerous studies have been published on two-phase flow profiles in bubble columns (Sokolichin & Eigenberger, 1994; Lapin & Lubert, 1994a; Ranade & Tayalia, 2001), none of these studies have focused on the effect of the nozzle size and geometry in membrane systems particularly in membrane bioreactor applications. Some of the questions that need to be answered include: what is the effect of nozzle size on bubble size distribution and are small bubbles or large bubbles more effective for enhancing the flux? What is the effect of air flow rate and nozzle size on bubble rise velocity and does this velocity have a significant role to play in the flux enhancement process? What is the effect of nozzle geometry on bubble size distribution? It has been established in chapter 3 and 4 that higher gas flow rates and larger nozzles have a better effect on flux enhancement but the reasons for this are not yet fully clear. Thus this chapter will attempt to develop a link between bubble size distribution and bubble rise velocity to flux enhancement.

Nozzles of different sizes have been used in this study in order to determine the extent to which the size of the nozzle affects two-phase flow and ultimately the flux enhancement. In chapter 3, it was established that the nozzle size of 2.0 mm in diameter is much more effective in combating fouling than nozzles of smaller diameters; however, this difference between the nozzle effectiveness diminishes when the gas flow rate is increased (see figure 3.9). With regards to nozzle geometry, the circular nozzle tended to be more effective than the square nozzles of the same surface area in combating fouling. This is puzzling because the same volume of gas is pumped into the system in each case regardless of the nozzle size or geometry. One way to explain this observed difference in performance by various nozzles is by analyzing the type of two-phase flow produced by each nozzle. In this study, this was achieved by analyzing still digital images and short videos of two-phase flow produced by different nozzles at different air flow rates. The still images and videos were taken using a digital camera and were analysed using particle imaging software. The structure of two-phase flow was also analysed using CFD and these results are presented in chapter 7.

5.2 OBJECTIVES

The specific objectives of this chapter are to:

- Study the effect of nozzle size and geometry on bubble size distribution,
- Study the effect of airflow rate on bubble size distribution,
- Study the effect of baffles on bubble distribution across the membrane surface,
- Evaluate the effect of airflow rate and nozzle size on bubble rise velocity.

5.3 EXPERIMENTAL SET-UP

The experimental set-up is similar to that used in chapter 3 and was shown in figure 3.1. The position of the diffuser and the membrane in the tank is shown here with respective distances in figure 5.1. The process feed tank for the investigations of this chapter was filled with clean Milli-Q water instead of the yeast suspension. Although the presence of the yeast particles in the actual experiment may, to a certain extent, influence the behaviour of the gas bubbles (Wu & Gharib, 2002), it has been assumed that this influence is not significantly lost when Milli-Q water is used. In addition, pictures of the two-phase flow could not be taken when the yeast suspension was used as the bubbles became obscured. A Nikon Coolpix995 digital camera, positioned about 300 mm from the feed tank was used to take digital images and to record short 40 second videos of the two-phase flow pattern for analysis.

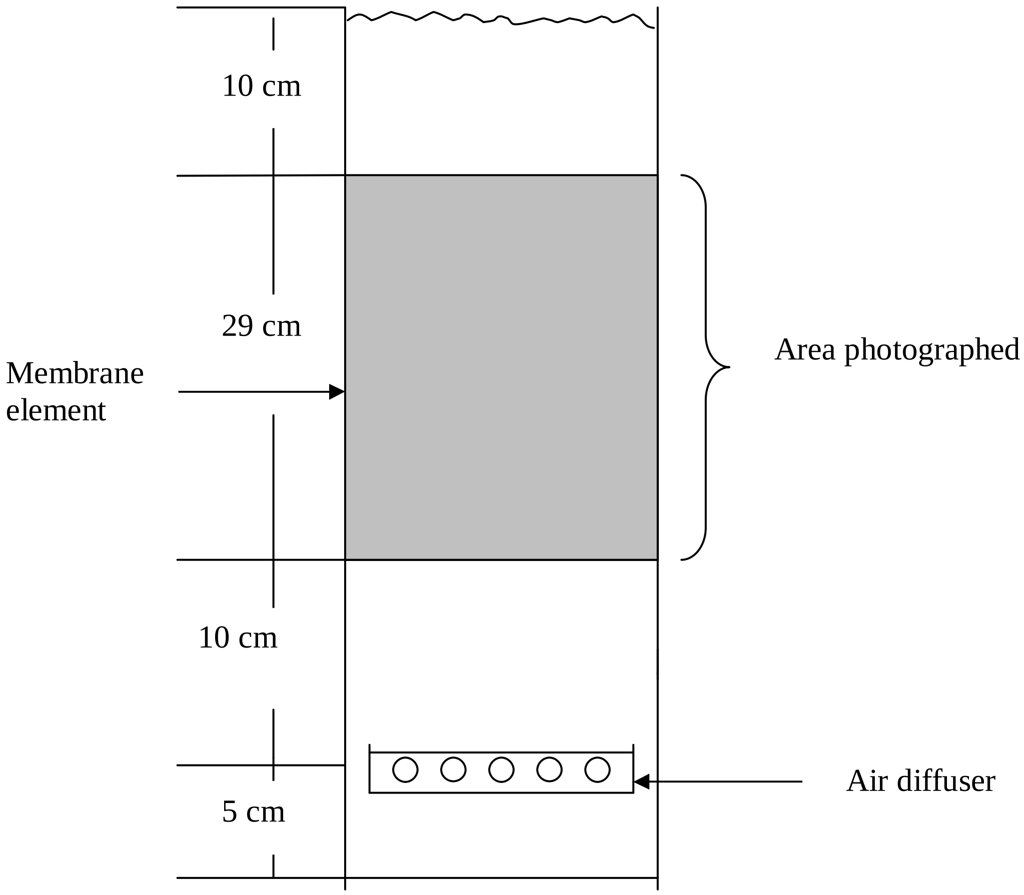

Figure 5.1. Illustration of the setup showing the area photographed for analysis.

5.4 EXPERIMENTAL PROCEDURE

The main activity involved was recording pictures with a digital camera under different conditions. The desired set of nozzles was fitted to the tank. The nozzles used were circular nozzles of diameters 0.5, 1.0, 1.5, 2.0, 3.2 and 4.5 mm and square nozzles 3 × 3 and 4×4 mm. After fitting the nozzles, the feed tank was filled with pure Milli-Q water. The membrane was then inserted into the tank and secured. The air blower was switched on and the desired air flow rate selected on the rotameter using a regulator valve. Numerous pictures were taken with the digital camera for each air flow rate and for each nozzle size. The range of airflow rates investigated was similar to those used in the yeast filtration experiments which were 2, 4, 6, and 8 l/min. Once the process of recording the pictures was completed, pictures were downloaded onto a personal computer using Nikon software. The digital pictures were originally in black and white JPEG format and had to be transformed into grayscale TIFF format using Adobe Photoshop before they could be processed further. The pictures were then analysed using AnalySIS® software which was available at the Electron Microscope Unit at the University of New South Wales. For each picture analysed, the software could produce information such as the total number of bubbles, the surface area of each bubble, the mean diameter of the bubble and the perimeter of each bubble.

5.5 RESULTS

5.5.1. Effect of nozzle parameters on bubble characteristics

For nozzle sizes of 0.5, 1.0, 1.5 and 2.0 mm, pictures were taken for air flow rates of 2, 4, 6 and 8 l/min or from 20 to 80 $l.min^{-1}.m^{-2}$ of membrane area. It was found that this range covers typical air flow rates which are used in membrane bioreactors for bubbling in submerged flat sheet membranes which range from 20 to 65 $l.min^{-1}.m^{-2}$ of membrane area (Cho, 2002). Some pictures taken for the 0.5 mm nozzle at different air flow rates are shown in figure 5.2 while some pictures for different nozzle geometries are shown in figure 5.3. The pictures show an increasing bubble population density as the air flow rate increases. This is expected because an increase in the amount of gas blown in should result in an increase in the number of bubbles. A closer inspection at the pictures shows that the bubbles can be grouped under three categories. There are small (less than 2 mm), medium sized (2 – 10 mm) and large (greater than 10 mm) bubbles. The large bubbles appear to be more predominant when the air flow rate is increased. The higher air flow rates also appear to have more small and medium sized bubbles. The still pictures seem to show that bubbles are well distributed over the membrane surface. What they do not reveal is that the bubbles towards the centre of the column are flowing up whilst those near the edges are flowing down or held almost stationary due to the re-circulation of the fluid in that region. This effect is better shown in a video. See ‘Video 1’ in a CD attached as appendix B. A closer examination of the bubbles in figure 5.3 for different nozzle geometries reveals that the occurrence of larger bubbles is qualitatively greater for the circular nozzle than for the square nozzle.

Table 5.1 shows a typical result file obtained after analyzing a picture with the AnalySIS® software. This table gives the total number of bubbles in the picture under the Particle ID category and then for each bubble, important information such as the area, perimeter, and diameter is given. Usually this type of results file is very long as there may be hundreds of bubbles in a single picture and hence only a portion of the file is shown here. For each picture that was analysed, the mean diameter and the total area of each bubble could be obtained. There was a minor problem encountered with the software when it comes to differentiating between overlapping bubbles. The software was unable to distinguish bubbles that overlapped and instead it treated them as one big bubble. Therefore a cluster of small bubbles would instead be treated as one big bubble. This meant that the true size and the actual number of the bubbles would be incorrect. This problem was averted by a painstaking process of manually editing the picture being analysed in order to separate overlapping bubbles. As a result of this procedure, some bubbles ended up being slightly smaller than their actual size but this approach was judged to be much better than losing the whole bubble.

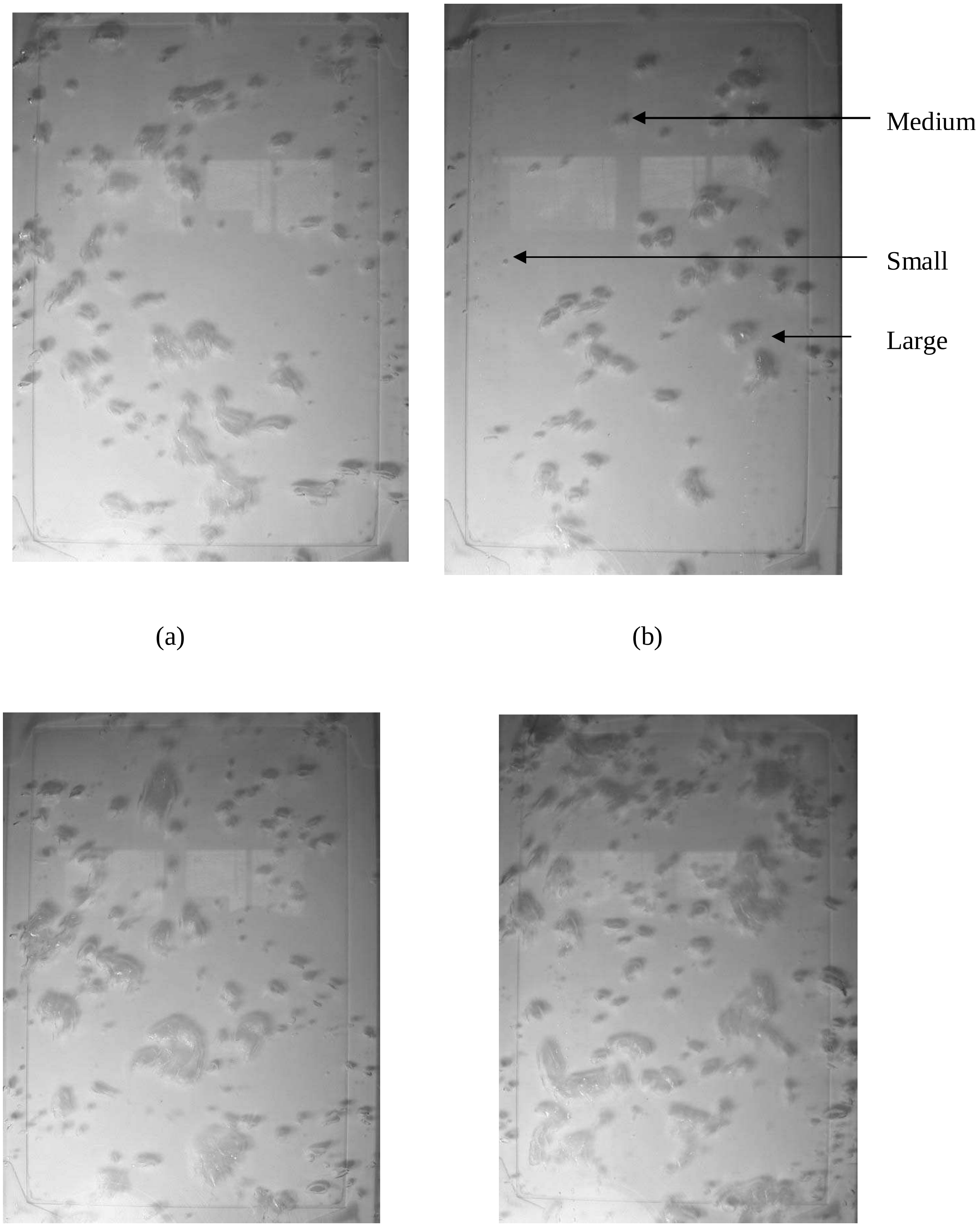

(c)

(d)

Figure 5.2. Pictures of two-phase flow at different air flow rates of (a) 2 l/min, (b) 4 l/min, (c) 6 l/min and (d) 8 l/min.

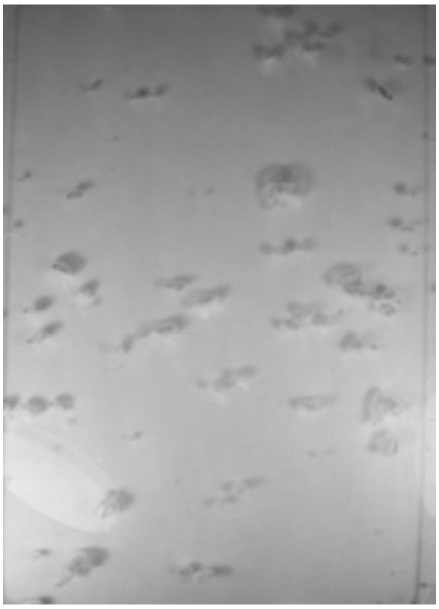

(a) Square – 2 l/min

(b) Circular – 2 l/min

(c) Square – 8 l/min

(d) Circular – 8 l/min

Figure 5.3. Pictures of bubbles from circular and square nozzles at air flow rates of 2 l/min (a and b) and 8 l/min (c and d) through a 0.5 mm nozzle.

For the purposes of this study, three parameters were investigated to evaluate their importance to flux enhancement: the bubble area; the bubble mean diameter; and, the total number of bubbles per picture. For each condition, four pictures were analysed and the results combined in order to obtain an average. The total number of bubbles produced at each flow rate for each nozzle is shown in figure 5.4, while figure 5.5 shows the average mean bubble diameter and figure 5.6 shows the average bubble area at each airflow rate and nozzle size. A table showing how many of the small, medium and large bubbles are present under each condition is given in table 5.2. Table 5.3 shows the average mean bubble diameter and the total number of bubbles for each nozzle and air flow rate. The results were also analysed for the average mean, median and mode bubble diameter as shown in table 5.4. The average mean diameter is calculated by adding the mean diameters for all the bubbles and dividing by the total number of bubbles. The median represents the bubble diameter for which 50% of the bubble population has a mean diameter greater than, and the mode represents the mean bubble diameter with the highest frequency under each condition.

Having obtained the total number of bubbles and the area of each bubble in each figure, the total volume occupied by the gas in the photographed section of the tank was assessed after assuming a spherical shape for each bubble. We are aware that the depth of the liquid in the photographed section was 7 mm and therefore bubbles whose diameters were larger than 7 mm effectively became slugs and thus limiting the applicability of the aforementioned assumption. After calculating the volume of liquid in the photographed section of the tank, the void fraction (V_{gas}/V_{liquid}) occupied by the gas was then calculated. The void fractions calculated at each flow rate for each nozzle size are shown in figure 5.7. Figure 5.8 shows the number of bubbles for each nozzle geometry at each flow rate while figure 5.9 shows the average bubble area for nozzles of different geometries. Bubbles for the square and circular nozzles were also classified under small, medium and large categories as shown in table 5.5.

Table 5.1. A typical results file from the analySIS® software (the table is incomplete)

ID Particle	ID Class	Area	Shape Factor	Diameter Max	Diameter Mean	Diameter Min	Perimeter
		mm²		mm	mm	mm	mm
1	6	23.73	0.32	9.36	7.90	5.10	30.32
2	9	32.53	0.43	11.41	10.07	7.46	30.79
3		70.28	0.14	30.41	27.74	13.09	78.33
4		148.55	0.61	16.28	15.08	14.03	55.25
5	3	9.73	0.35	5.12	4.66	4.10	18.67
6		173.55	0.26	32.50	28.08	11.36	92.32
7		252.05	0.17	34.02	29.13	20.83	135.70
8		52.10	0.55	11.19	10.35	8.18	34.50
9		178.42	0.38	20.26	18.30	14.48	76.92
10	2	6.37	0.31	4.42	3.91	3.42	16.00
11	5	19.10	0.45	9.08	7.73	4.10	23.15
12		85.79	0.43	16.22	14.62	8.85	50.00
13	5	17.60	0.34	9.26	7.94	3.62	25.59
14		47.12	0.45	12.96	11.18	6.27	36.17
15	1	3.01	0.64	3.42	2.95	1.70	7.68
16		155.96	0.57	20.34	18.29	10.57	58.40
17		42.95	0.68	10.66	9.54	5.45	28.17
18		69.24	0.80	12.22	10.58	8.53	32.95
19		72.59	0.47	15.85	14.52	11.11	44.22
20		57.31	0.49	13.56	11.74	7.61	38.51
21		76.65	0.51	16.36	14.43	7.15	43.25
22		57.08	0.46	15.78	13.32	7.49	39.48
23		78.04	0.49	18.40	15.98	7.15	44.68
24		55.34	0.53	15.37	13.35	5.78	36.10
25		129.56	0.44	22.24	19.45	12.96	60.85
26		55.23	0.63	13.03	11.27	6.50	33.19
27		42.49	0.63	12.37	10.76	5.95	29.18
28		53.49	0.35	16.68	14.85	6.13	43.56
29		57.43	0.48	16.34	13.69	7.08	38.94
30		108.49	0.58	17.10	14.91	10.21	48.41
31		66.81	0.31	17.03	14.93	6.12	51.83
32		209.68	0.27	32.28	27.92	12.61	99.37
33		95.63	0.44	18.09	15.78	9.58	51.98
34		117.98	0.16	30.60	26.77	10.96	96.14
35		62.29	0.61	13.04	11.00	7.86	35.68
36	2	4.75	0.54	3.66	3.34	2.74	10.51
37		86.84	0.45	20.52	18.31	6.13	49.03

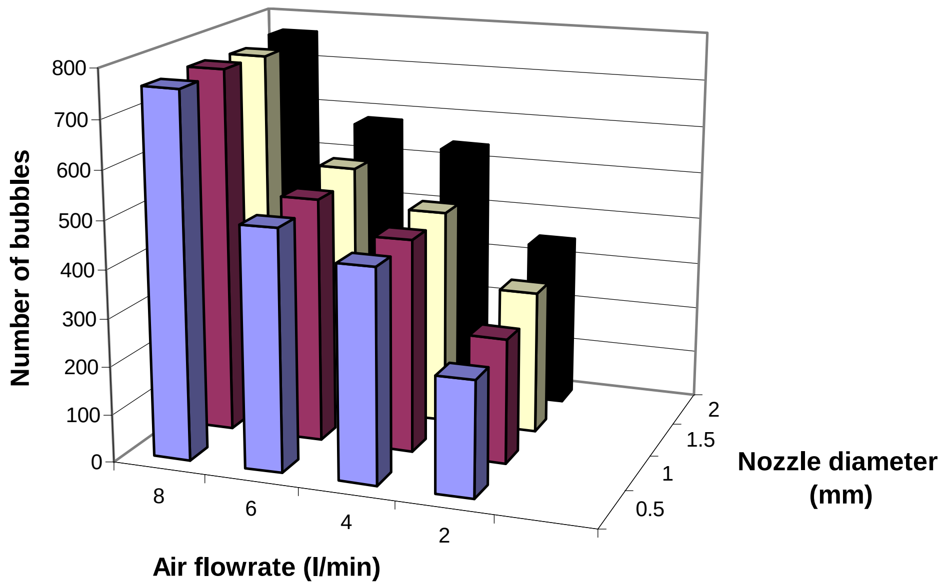

Figure 5.4. Total number of bubbles per picture for each set of conditions.

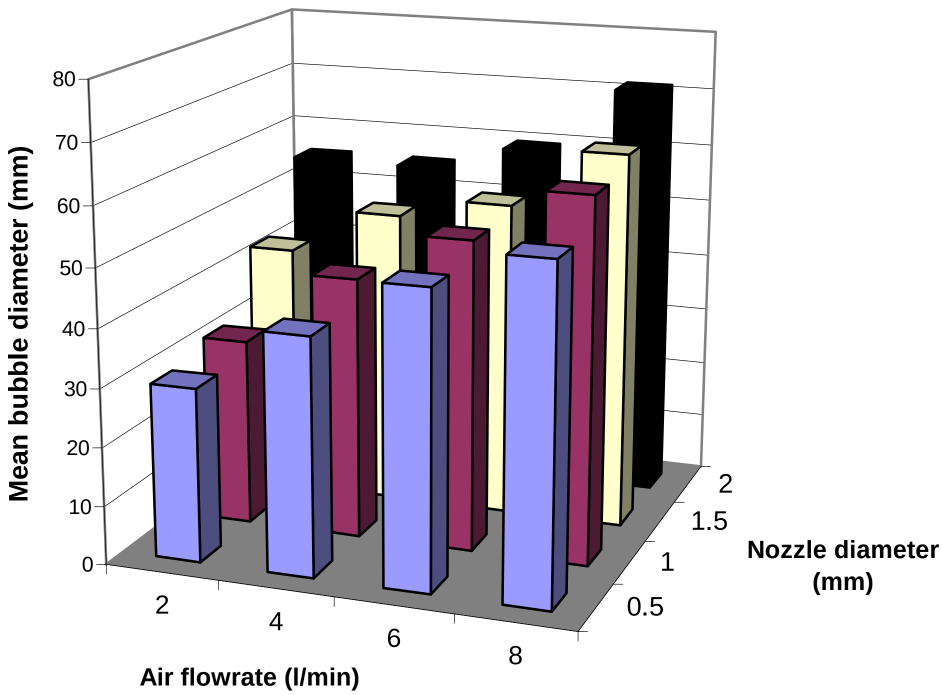

Figure 5.5. Variation of bubble mean diameter with nozzle size and air flow rate.

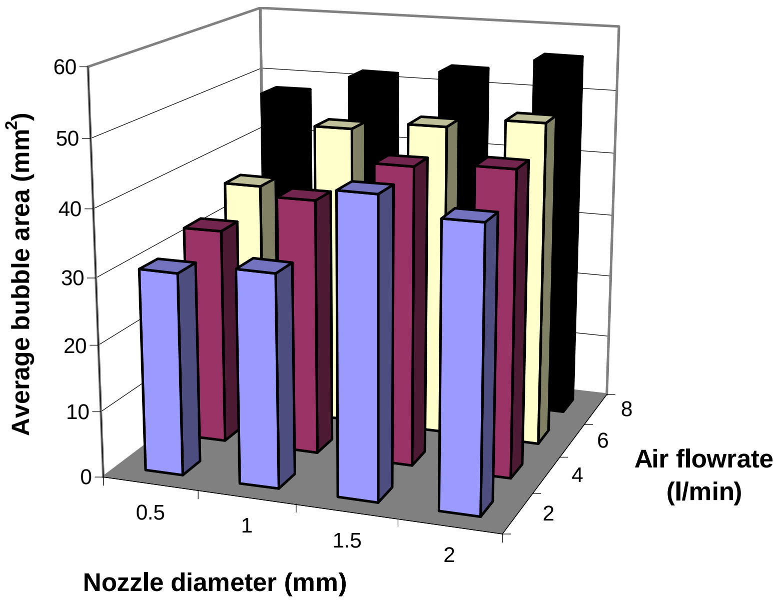

Figure 5.6. Variation of the bubble average area with nozzle size and air flow rate.

Table 5.2. Classification of bubbles under different categories.

Nozzle size (mm)	**Bubble category***	**Number of bubbles in each category**			
		2 l/min	**4 l/min**	**6 l/min**	**8 l/min**
0.5	**Small**	14	26	29	57
	Medium	102	262	339	546
	Large	61	155	192	223
1.0	**Small**	11	15	52	72
	Medium	137	290	431	479
	Large	108	201	206	230
1.5	**Small**	18	36	51	57
	Medium	198	348	375	437
	Large	84	170	211	264
2.0	**Small**	21	39	47	78
	Medium	204	346	371	554
	Large	128	113	208	218

* Small < 2 mm, medium 2 – 10 mm, large > 10 mm

Table 5.3. Average bubble mean diameter and number of bubbles for each nozzle

	2 l/min of Air		**4 l/min of Air**		**6 l/min of Air**		**8 l/min of Air**	
Nozzle size (mm)	**Average mean bubble diameter (mm)**	**Number of bubbles**	**Average mean bubble diameter (mm)**	**Number of bubbles**	**Average mean bubble diameter (mm)**	**Number of bubbles**	**Average mean bubble diameter (mm)**	**Number of bubbles**
0.5	6.96	327	7.3	443	8.21	560	8.87	826
1.0	7.14	256	8.63	506	9.47	686	9.67	781
1.5	7.9	300	8.87	554	9.51	637	9.77	758
2.0	8.22	347	9.43	498	9.74	626	9.92	850

Table 5.4. Analysis for mean, median and mode bubble diameter.

Nozzle size (mm)	**Bubble diameter (mm)**	**2 l/min**	**4 l/min**	**6 l/min**	**8 l/min**
0.5	**Mean**	6.96	7.3	8.21	8.87
	Median	7.73	6.17	6.6	6.78
	Mode	2.44	2.5	2.64	2.88
1.0	**Mean**	7.14	8.63	9.47	9.67
	Median	8.07	8.31	6.01	8.76
	Mode	1.88	2.08	2.18	2.4
1.5	**Mean**	7.9	8.97	9.51	9.77
	Median	5.31	6.67	5.88	6.36
	Mode	2.02	2.54	2.66	2.74
2.0	**Mean**	8.22	9.43	9.74	9.92
	Median	5.07	5.21	5.55	5.74
	Mode	2.07	2.15	2.31	2.43

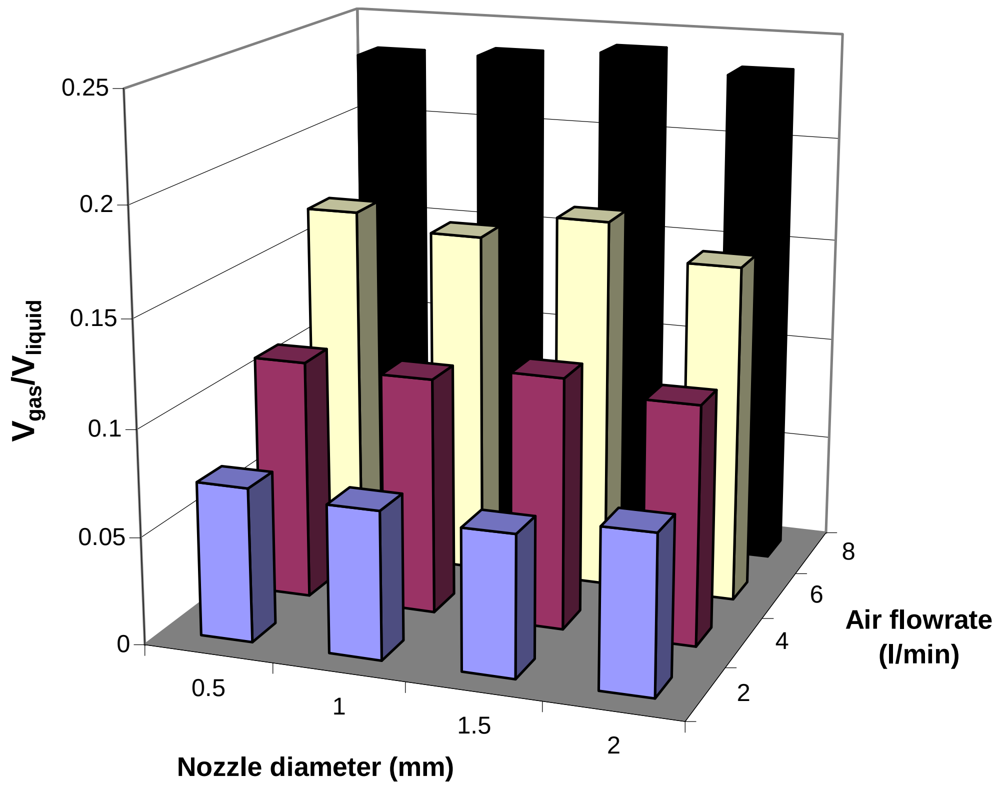

Figure 5.7. Variation of the void fraction with the air flow rate and nozzle size.

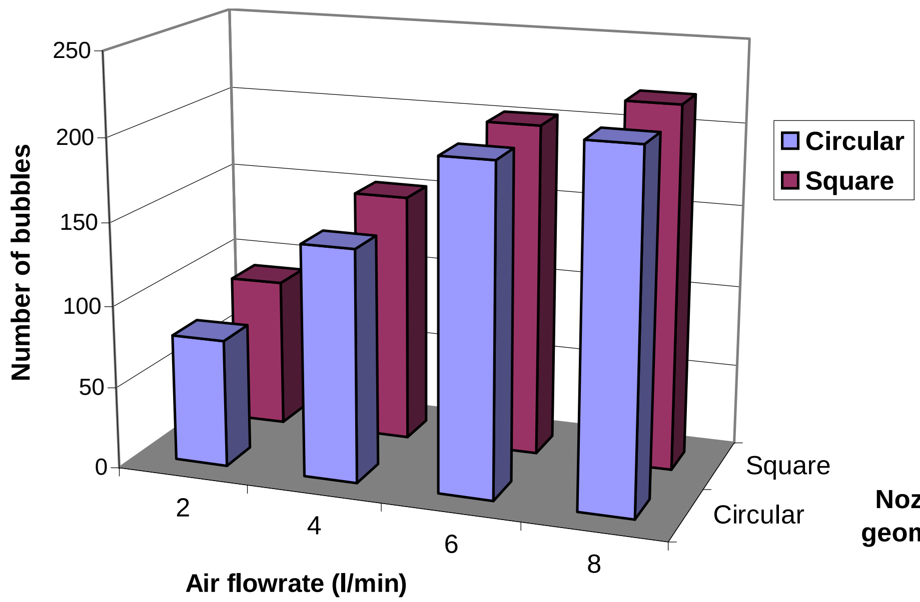

Figure 5.8. The total number of bubbles for the square and circular nozzle at different air flow rate nozzle.

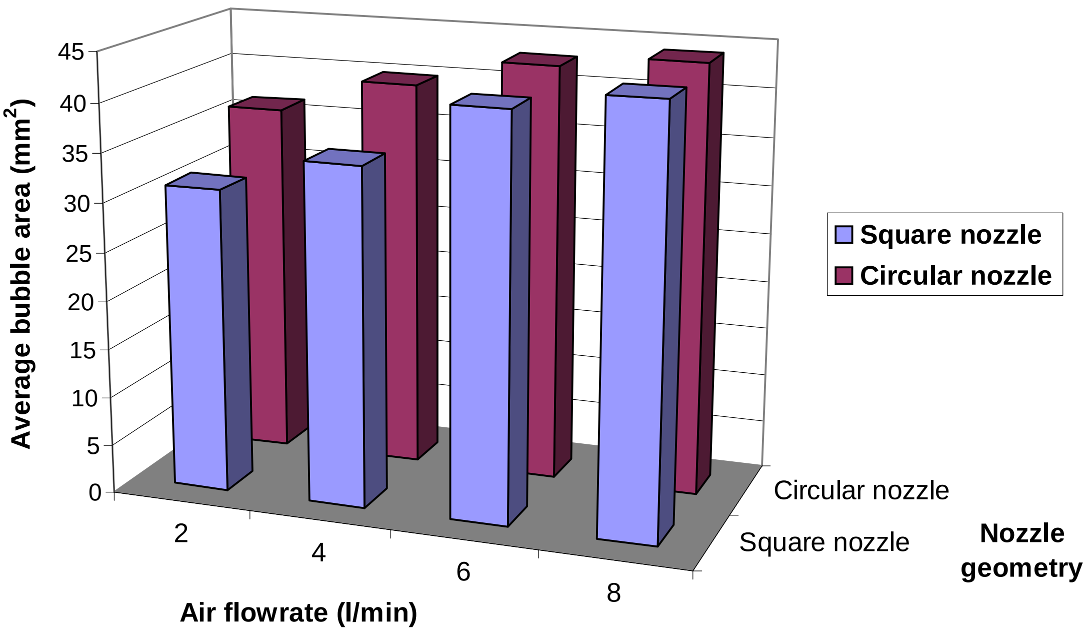

Figure 5.9. The average bubble area for the square and circular nozzle at different air flow rate.

Table 5.5. Classification of bubbles under different categories

Nozzle geometry	**Bubble categories***	**Number of bubbles**			
		2 l/min	**4 l/min**	**6 l/min**	**8 l/min**
Square	**Small**	21	34	28	20
	Medium	45	94	142	151
	Large	25	24	32	49
Circular	**Small**	7	11	10	15
	Medium	24	72	129	136
	Large	47	58	60	63

* Small < 2 mm, medium 2 – 10 mm, large > 10 mm

From figure 5.4 and table 5.3 the number of bubbles and the mean bubble diameter increases with the air flow rate as does the average bubble area in figure 5.6. On the other hand, the total number of bubbles does not seem to be a function of the nozzle size, although the number of bubbles increases with an increase in the air flow rate. Table 5.2 shows that the number of bubbles in each category increases as the air flow rate increase. There are also more bubbles in the medium category than in the other categories for all nozzle sizes and all flow rates. The number of bubbles in the large category is much greater than those in the small category and there are also more large bubbles for the larger nozzles than the smaller nozzles. From table 5.4, the median diameter does not show any dependence on the air flow rate or the bubble size. The mode, which represents the bubble size with the highest frequency, seems to increase slightly with the air flow rate but does not show any trend with regards to the nozzle size, whilst the average mean bubble diameter increases with the air flow rate and the nozzle size. Figure 5.7 shows that the volume fraction occupied by the gas is relatively small, the highest being about 25%. The void fraction increases with the air flow rate but does not show any pattern with regards to the nozzle size. This suggests that the nozzle size does not have an effect on the amount of air entering the tank as long as the air flow rate is the same across all nozzles. Figure 5.8 shows that the total number of bubbles is independent of the nozzle geometry under constant air flow rate whilst figure 5.9 and table 5.5 reveals that the occurrence of larger bubbles is higher with the circular nozzle than the square nozzle. The presence of more large bubbles with the circular nozzle could be the reason why the circular nozzle was more effective at reducing fouling than the square nozzle.

Having classified bubbles in the pictures as either small, medium or large, we took a step further and calculated the fraction of the incoming air flow forming small, medium or large bubbles. This was achieved by calculating the total volume (V) of gas in each of the three categories using data from particle imaging software and then calculating the average rise velocity of bubbles in each category (U). Bubble rise velocities were determined using the technique discussed in section 5.5.5. Knowing the height of the tank (H), the residence time (θ) of the gas in each category was calculated as H / U. Therefore the volumetric flow rate of the gas in each category was then calculated as V / θ and then this was expressed as percentage of the total gas flow. These data are shown in figure 5.10.

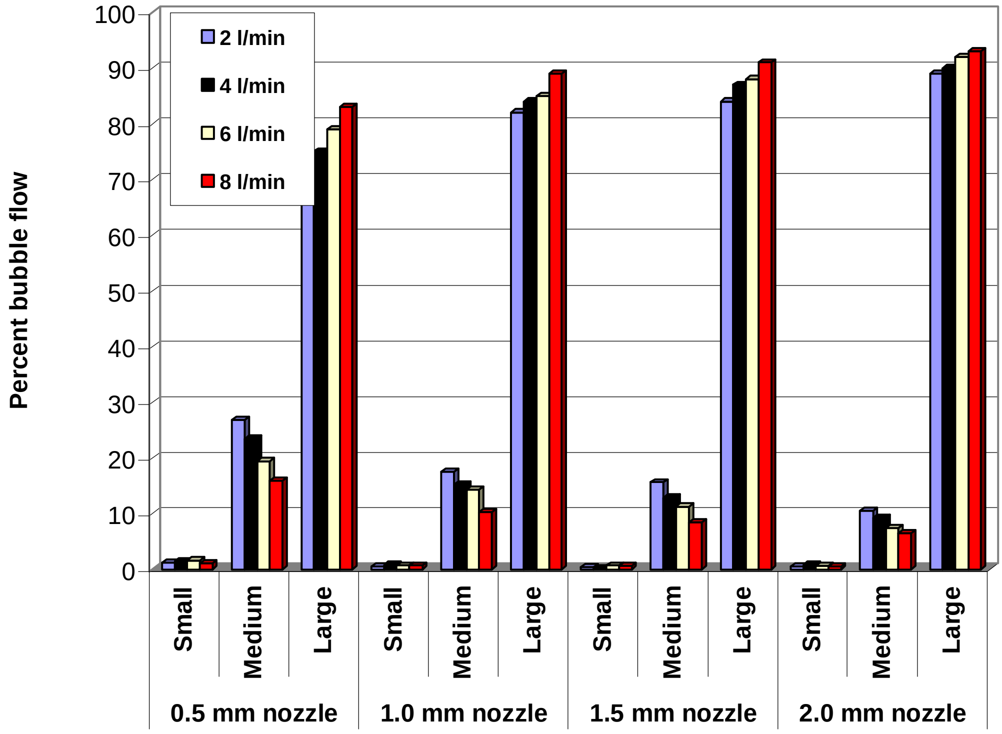

Figure 5.10. Distribution of flow into small, medium and large categories.

Figure 5.10 shows that the percentage of flow that ends up as small bubbles is very small being less than 1% of the total air flow for all nozzles except for the 0.5 mm nozzle where it went up to as high as 1.6%. The figure also clearly shows that most of the air ends up large flow, that is, comprising of bubbles greater than 10 mm. The percentage of flow in the medium category decreases with both nozzle size and air flow rate whilst the percentage of the large flow increases with both.

5.5.2 Effect of nozzle characteristics on bubble size distribution

In this section, the effect of air flow rate on bubble size distribution was analysed in detail. For the purpose of plotting the graphs, because the bubble mean diameter and area varied from very small to very large, bubbles were grouped in categories and the total number of bubbles was calculated in each category for either bubble mean diameter or bubble area. Since there are more bubbles less than 5 mm than any other category, bubbles under 5 mm in diameter were grouped into categories of 0 – 2 and 2 – 5 mm categories. Bubbles greater than 5 mm were then grouped into categories with a 5 mm range, for example, 5 – 10, 10 – 15, 15 – 20, up until the bubble size of 70 mm. There was no bubble found to be larger than 70 mm in any of the pictures. The bubble size distribution for the different air flow rates are shown in figure 5.11 to 5.14, while the distributions for different nozzle sizes at constant air flow rates are shown in figures 5.15 to 4.18.

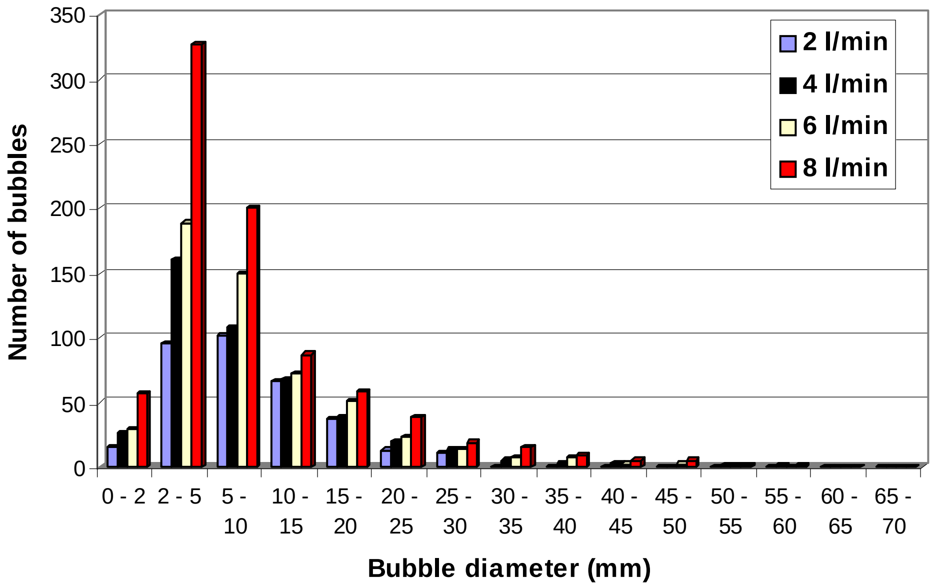

Figure 5.11. Bubble size distribution for the 0.5 mm nozzle.

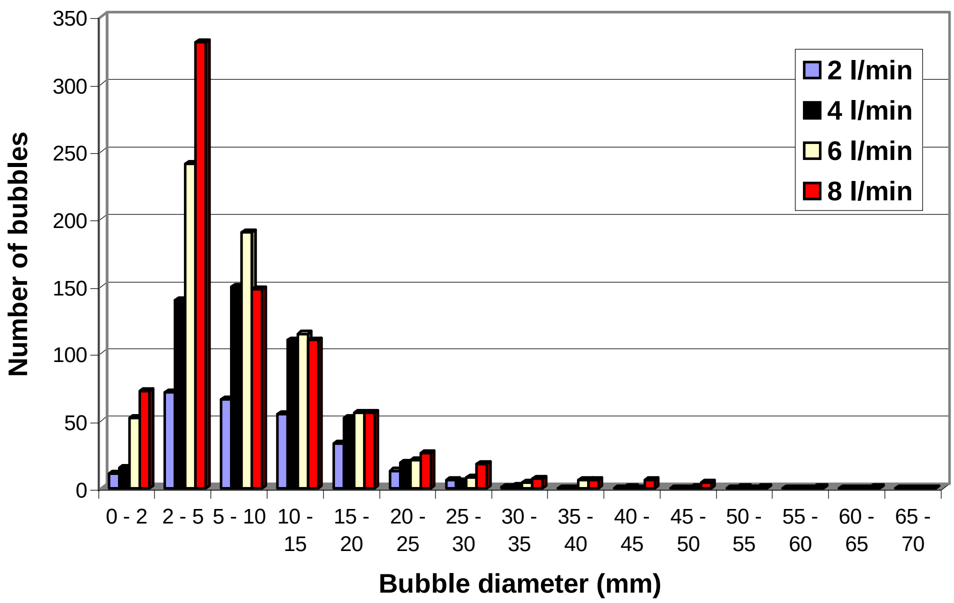

Figure 5.12. Bubble size distribution for the 1.0 mm nozzle.

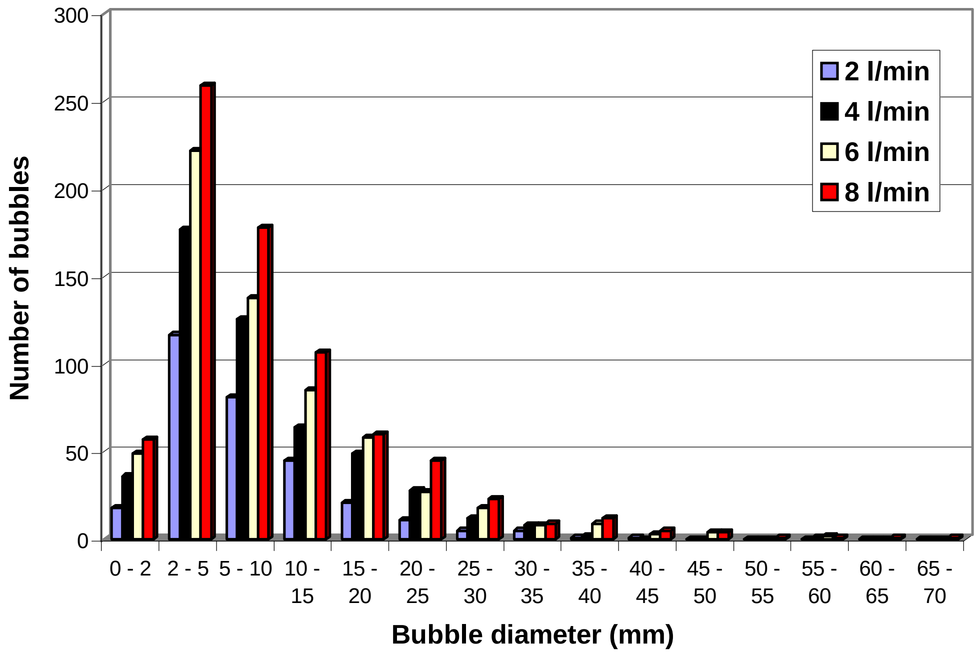

Figure 5.13. Bubble size distribution for the 1.5 mm nozzle.

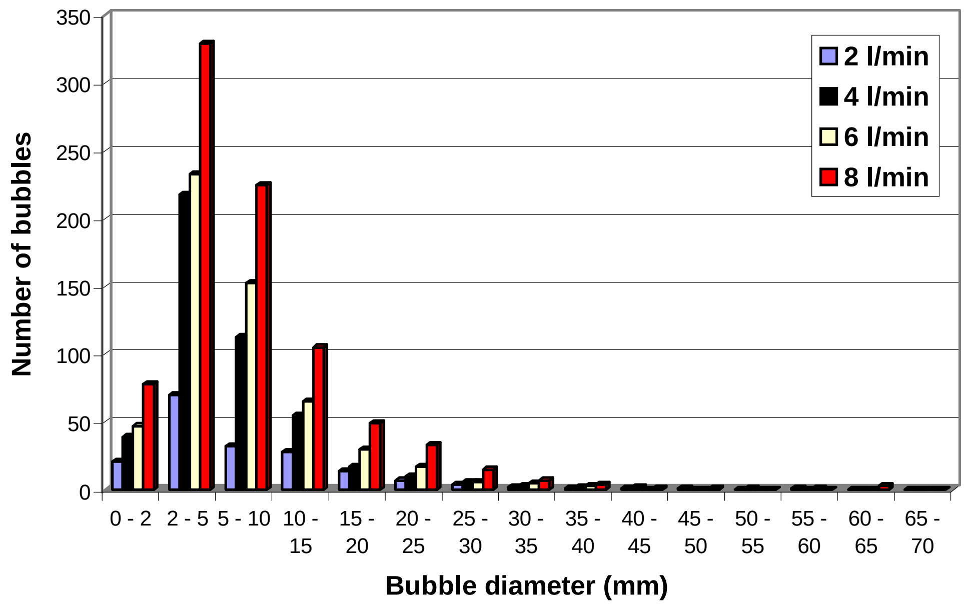

Figure 5.14. Bubble size distribution for a 2.0 mm nozzle.

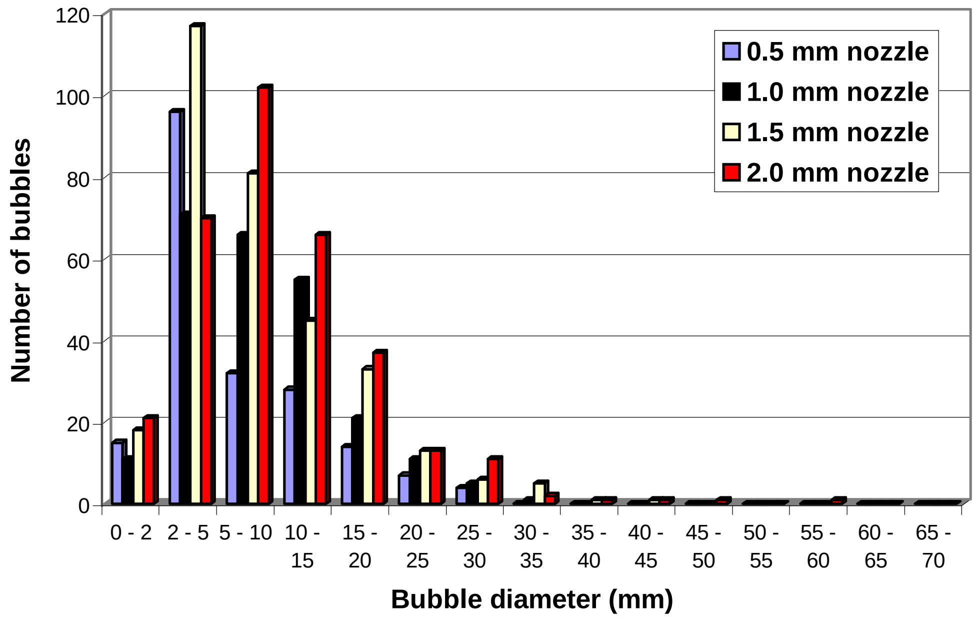

Figure 5.15. Bubble size distribution for the air flow rate of 2 l/min.

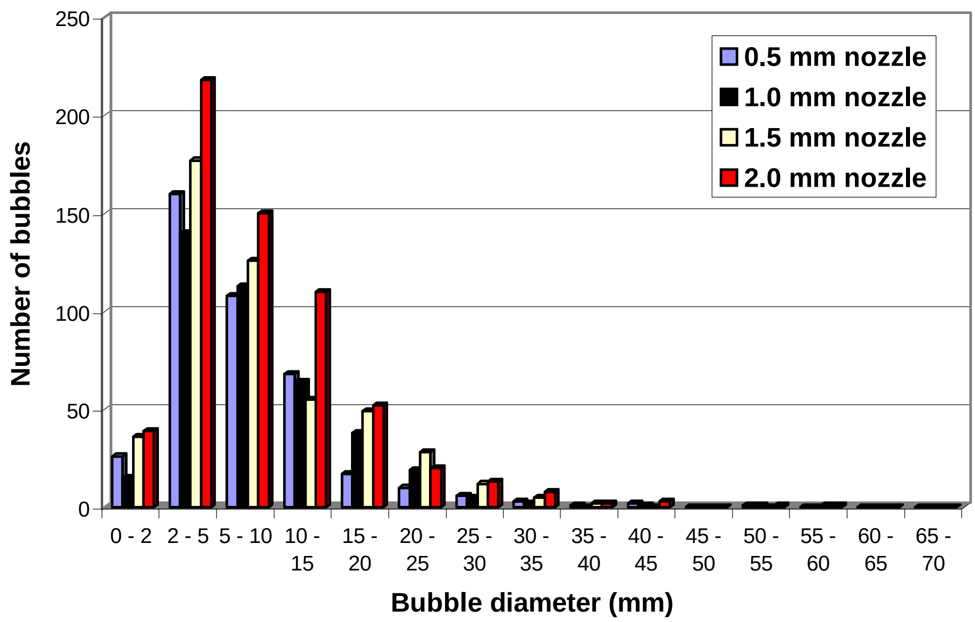

Figure 5.16. Bubble size distribution for the air flow rate of 4 l/min.

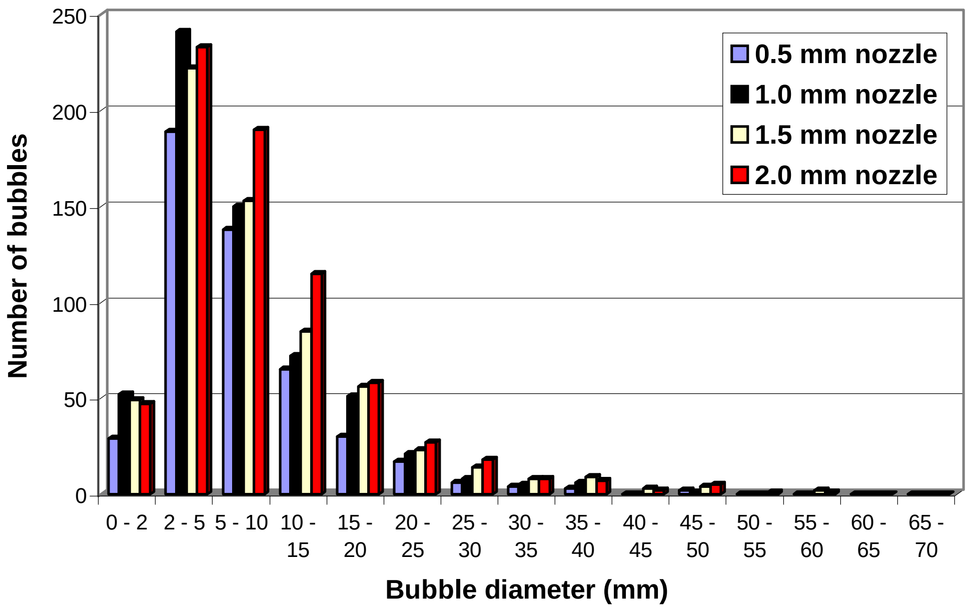

Figure 5.17. Bubble size distribution for the air flow rate of 6 l/min.

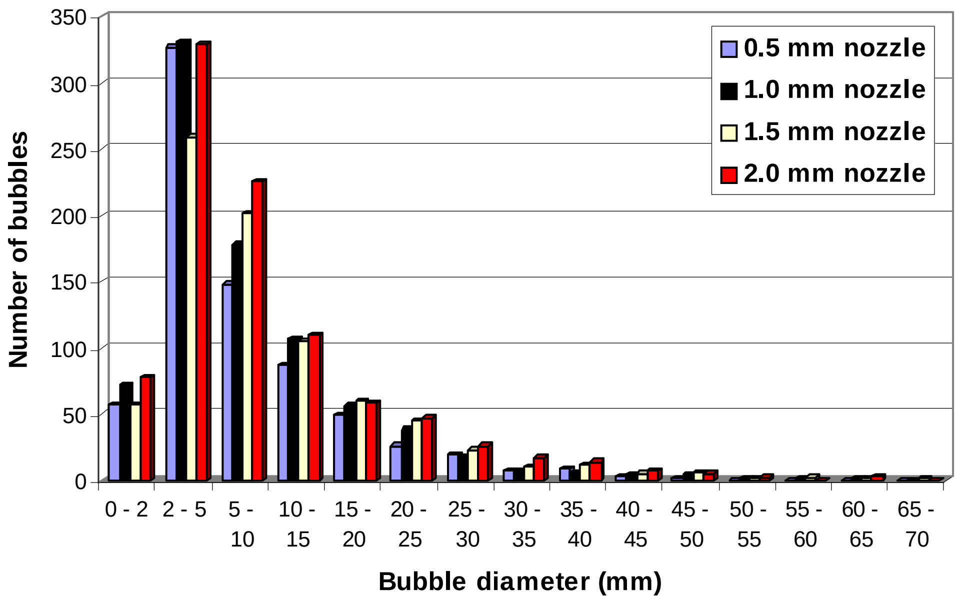

Figure 5.18. Bubble size distribution for the air flow rate of 8 l/min.

From the figures 5.11 to 5.14, it is clear that the higher the air flow rate, the higher is the number of bubbles in almost all categories of bubble sizes. In the category of very large bubbles, the small air flow rate (2 l/min) does not have a single bubble present although one or two large bubbles appear from time to time. The exception is the larger nozzle of 2.0 mm which produces very large bubbles continuously even at very low gas flow rates. The production of these large bubbles could be the reason why the 2.0 mm nozzle was found to be the most effective at reducing fouling.

In figures 5.15 to 4.18, it can be seen that the number of bubbles do not show a strong and consistent dependence on the nozzle size at a fixed air flow rate, particularly for the smaller bubbles less than 5 mm in size. The bubble size distribution results imply that the amount of bubbles produced depends more consistently on the air flow rate than on the nozzle size, but larger nozzles do produce more large bubbles than the smaller nozzles under constant air flow rates. At the highest air flow rate (8 l/min) the bubble distributions from all nozzle sizes are relatively similar, possibly due to coalescence of bubbles. This observation would also explain the reduced nozzle effect at high air flow rate reported for fouling control in chapter 3 (section 3.5.2, Figure 3.9).

Figures 5.19 to 5.22 present the bubble size distribution at different air flow rates for the two different nozzle geometries. These figures confirm that, for categories of bubbles less than 5 mm, the square nozzle produces more bubbles, but for most of the categories greater than 10 mm, the circular nozzle has more bubbles present. Therefore, the circular nozzle seems to be producing more large bubbles than the square nozzle. Thus the choice of nozzle geometry would depend, inter alia, on whether small or large bubbles give an advantage in fouling.

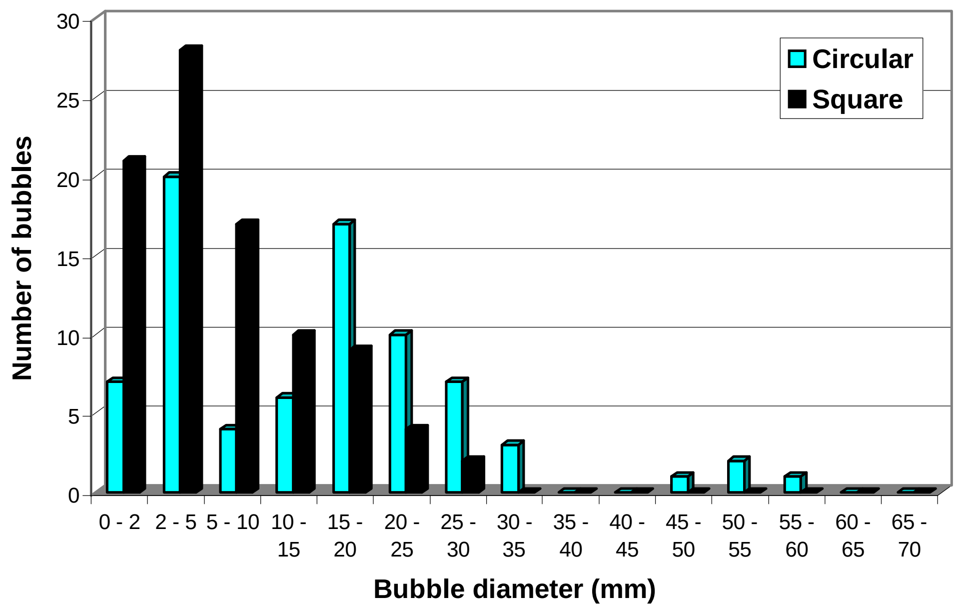

Figure 5.19. Bubble size distribution for square and circular nozzle at 2 l/min.

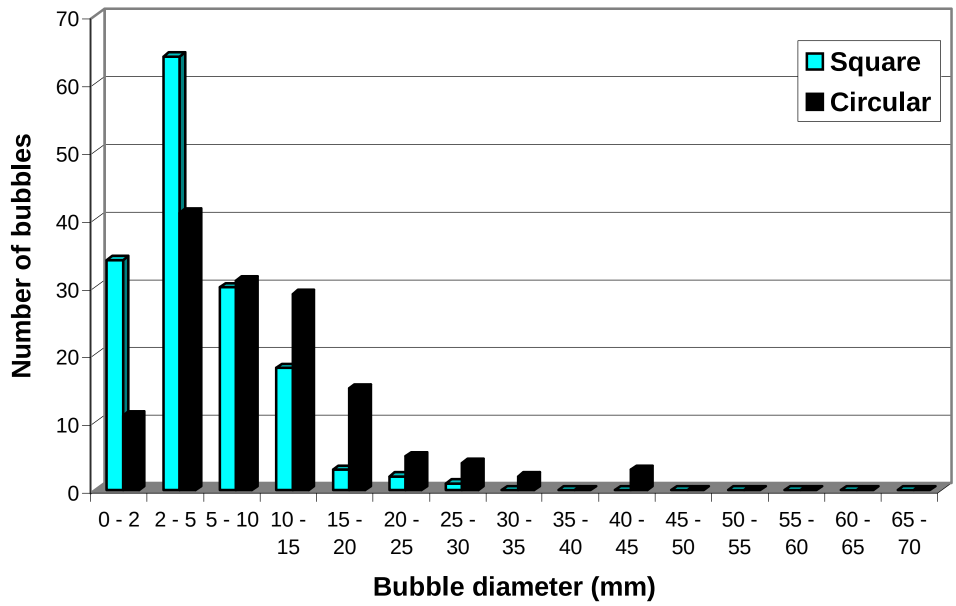

Figure 5.20. Bubble size distribution for square and circular nozzle at 4 l/min.

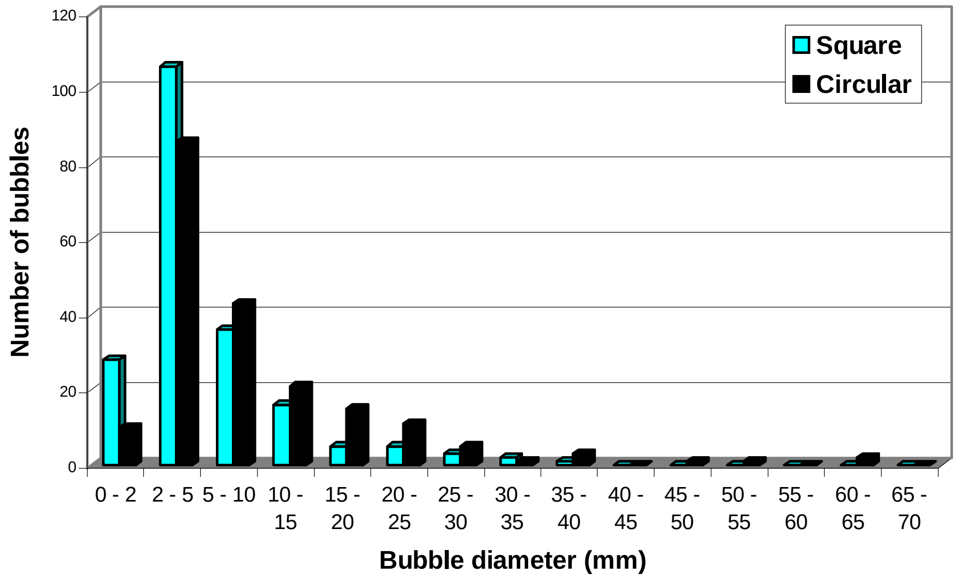

Figure 5.21. Bubble size distribution for square and circular nozzle at 6 l/min.

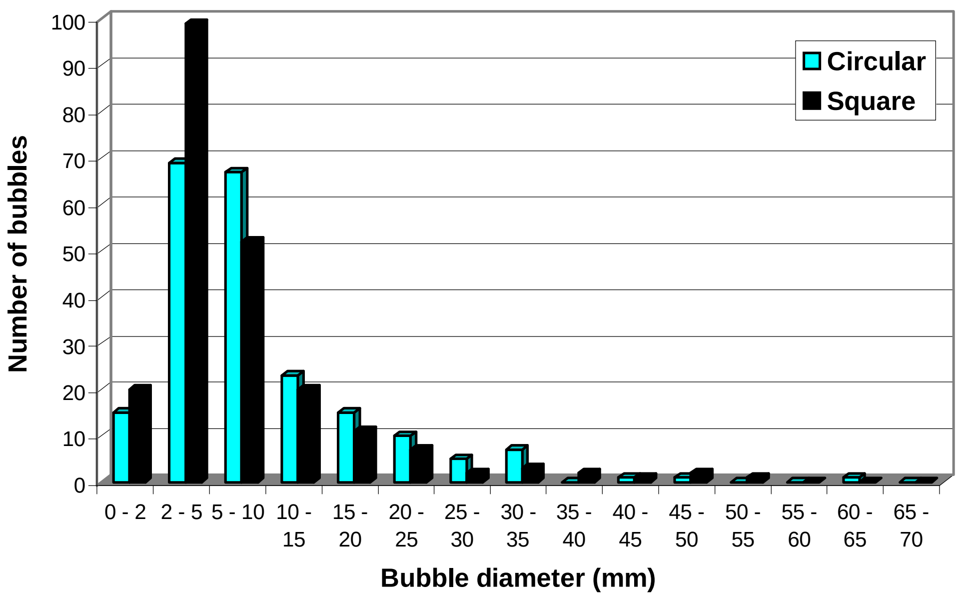

Figure 5.22. Bubble size distribution for square and circular nozzle at 8 l/min.

5.5.3 Distribution of bubbles across the membrane surface

In the experimental setup used in this study, the system is designed such that the air enters the diffuser on only one side of the tank. This process for air introduction is illustrated in figure 5.23. With the air entering on only one side of the diffuser, it could be possible that most of the air escapes through the first few nozzles and not evenly through all of the nozzles. Thus, there could be more air coming out of the nozzles nearer to the air inlet and less air coming out of the nozzles that are far away from the air inlet. Hamann et al. (2003) reported experiencing this kind of problem on a one metre wide tank and decided to introduce air on both sides of the nozzle so that the membrane was evenly aerated. Any pressure drop along the diffuser would produce higher pressure nearer to the air inlet, pushing more air out in this section of the pipe. If this occurs, it would result in an uneven distribution of bubbles across the membrane surface which could mean that the membrane would be cleaner on one side than the other. This uneven distribution may be more severe on the lower part of the membrane because, as the bubbles rise, they may tend to be distributed evenly eventually.

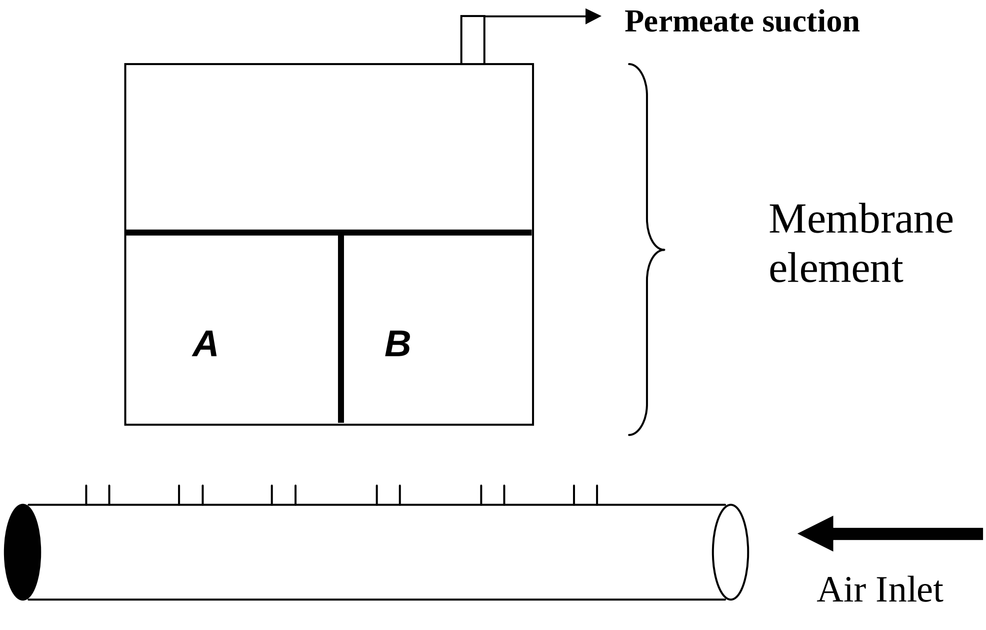

Figure 5.23. Air distribution over the membrane

Calculations were performed to estimate the pressure drop along the nozzle pipe, which is only 300 mm long, in order to gauge whether the pressure drop was significant or not. For these calculations the flow was assumed to be isothermal and the following equation was used to calculate the pressure drop for a compressible fluid (Perry & Green, 1999).

$$\left(\frac{G}{A}\right)^2 \ln\frac{P_1}{P_2} + \frac{P_2 - P_1}{v_m} + 4\phi\frac{l}{d}\left(\frac{G}{A}\right)^2 = 0 \qquad (5.1)$$

where G is the mass flow rate, A is the pipe cross section area, P_1 is the upstream pressure, P_2 is the downstream pressure, v_m is the specific volume of air, ϕ is the friction factor, l is the length of pipe and d is the diameter of the pipe. The upsteam pressure P_1 was measured using a normal pressure gage during experiment and then equation 5.1 was used to calculate the downstream pressure P_2. Typical values of calculated pressure drop versus air flow rate are depicted in figure 5.24. The pressure drop increases with the air flow rate but the pressure drop itself is very small. The flow rate of 8 l/min has the highest pressure drop of 69 Pa and this only represents a pressure drop of 6.9 %. It should be noted that this estimate could be higher than experienced because under operation the flow rate in the tube diminishes along the length of the tube (for example at the halfway point the flow will be of the order of 50% the input flow). These considerations suggest that the pressure drops in the experiments were too small to cause a significant maldistribution of air bubbles across the membrane.

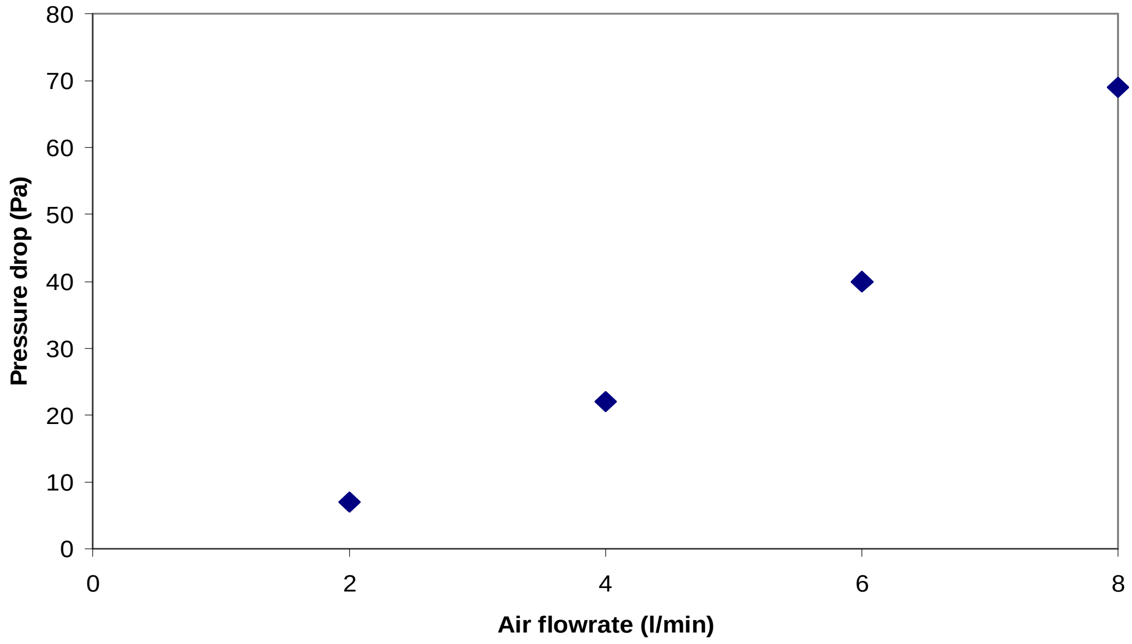

Figure 5.24. Estimated pressure drop along the nozzle at different air flow rates.

In order to ascertain whether the pressure drop was really too small to cause a maldistribution of bubbles, an analysis was carried out to determine the distribution of bubbles on the lower part of the membrane on the left and right hand side. The areas that were analysed for bubble distribution are shown as A and B in figure 5.23. These areas coincided with the location of the membrane in the pictures. Only pictures obtained from two sets of nozzles (0.5 and 2.0 mm) were analysed. Air flow rates of 2 to 8 l/min were considered. Figure 5.25 and 5.26 show the total number of bubbles for the two nozzles. The results of bubble size distribution are shown in figure 5.27 to 5.30. These results do not show that there are more bubbles in section A which is nearer to the air inlet. Even though the bubble size distribution varies from side to side, and there are sometimes more bubbles in section B than section A, overall the bubbles seem to be evenly distributed on both sides of the membrane. This confirms that the pressure drop along the diffuser was not significant.

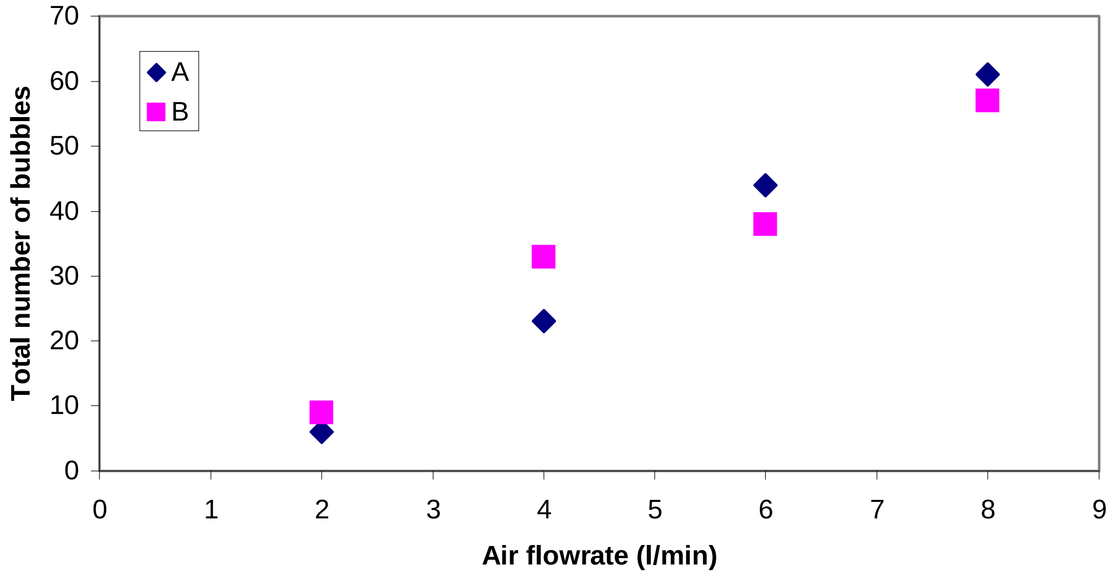

Figure 5.25. Total number of bubbles for side A and B for the 0.5 mm nozzle.

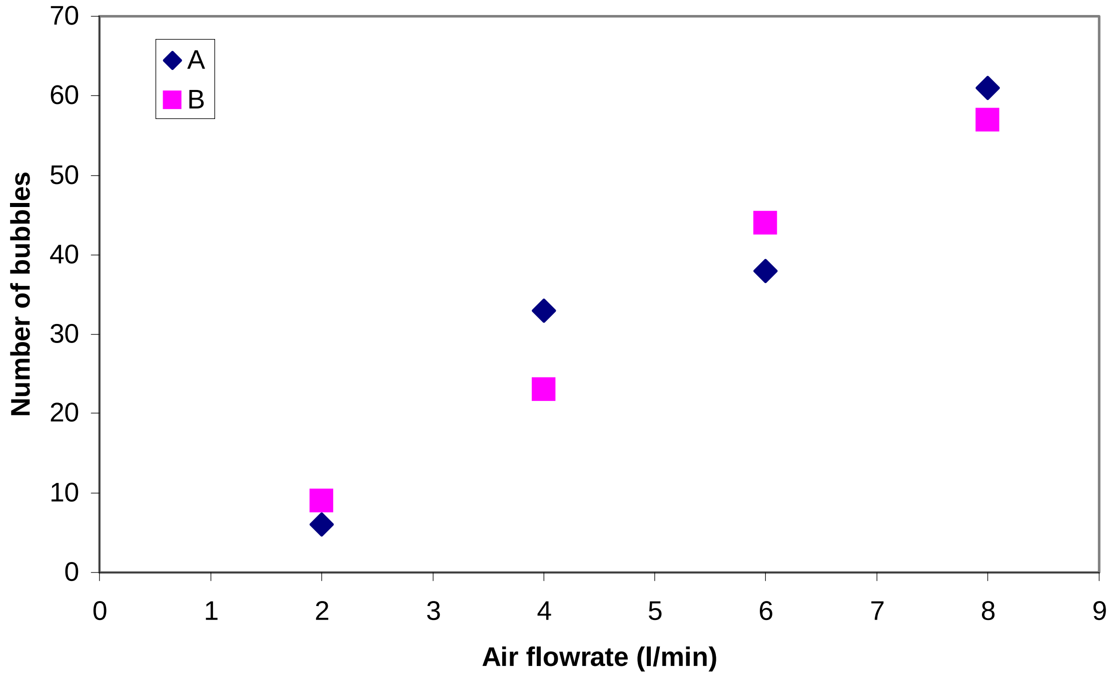

Figure 5.26. Total number of bubbles for side A and B for the 2.0 mm nozzle

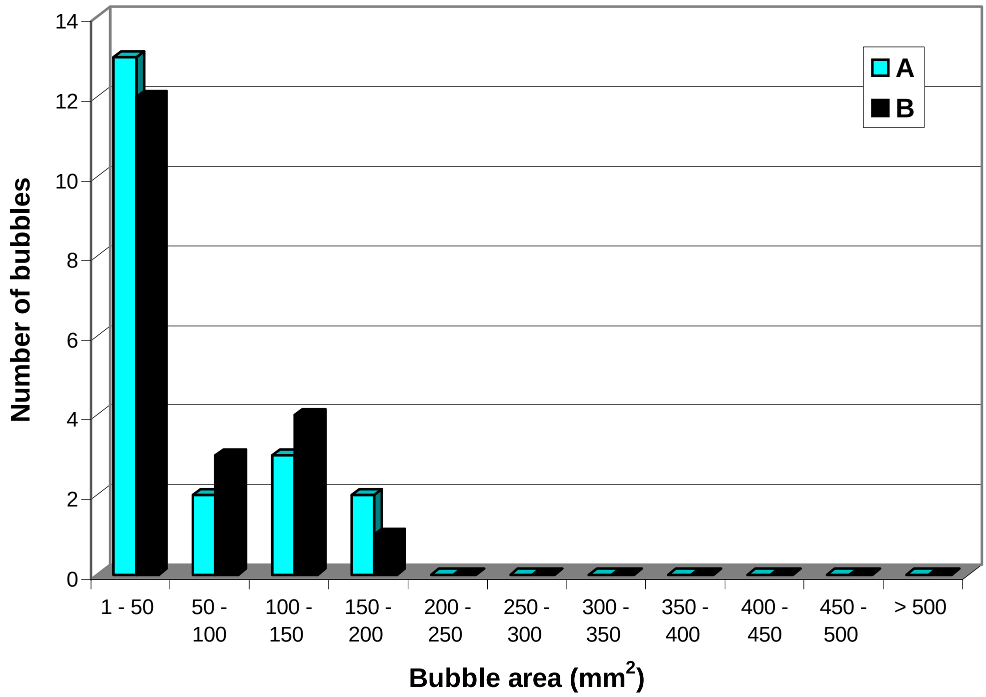

Figure 5.27. Bubble size distribution for side A and B at an air flow rate of 2 l/min.

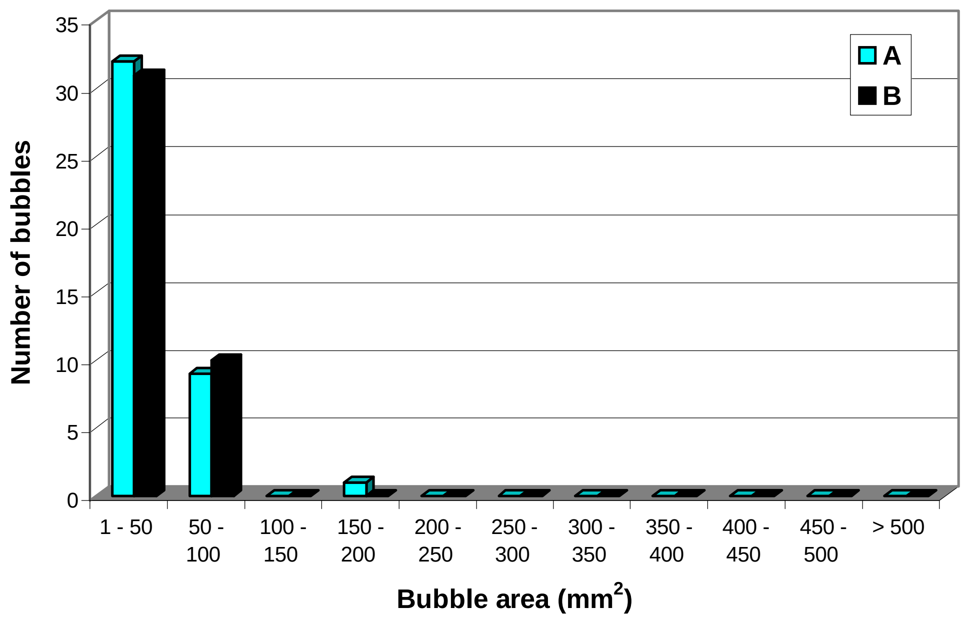

Figure 5.28. Bubble size distribution for side A and B at an air flow rate of 4 l/min.

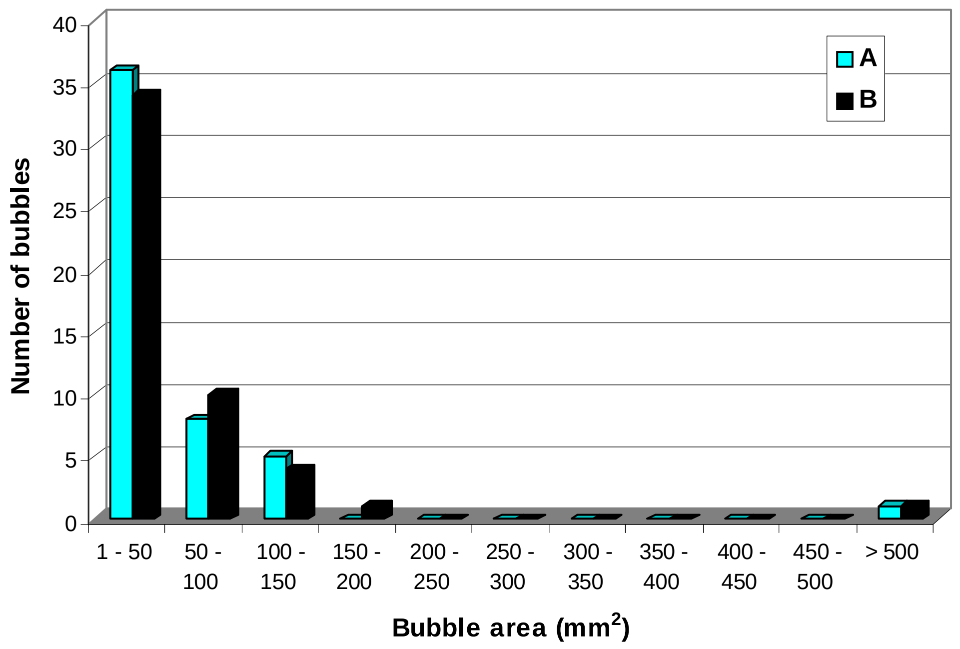

Figure 5.29. Bubble size distribution for side A and B at an air flow rate of 6 l/min.

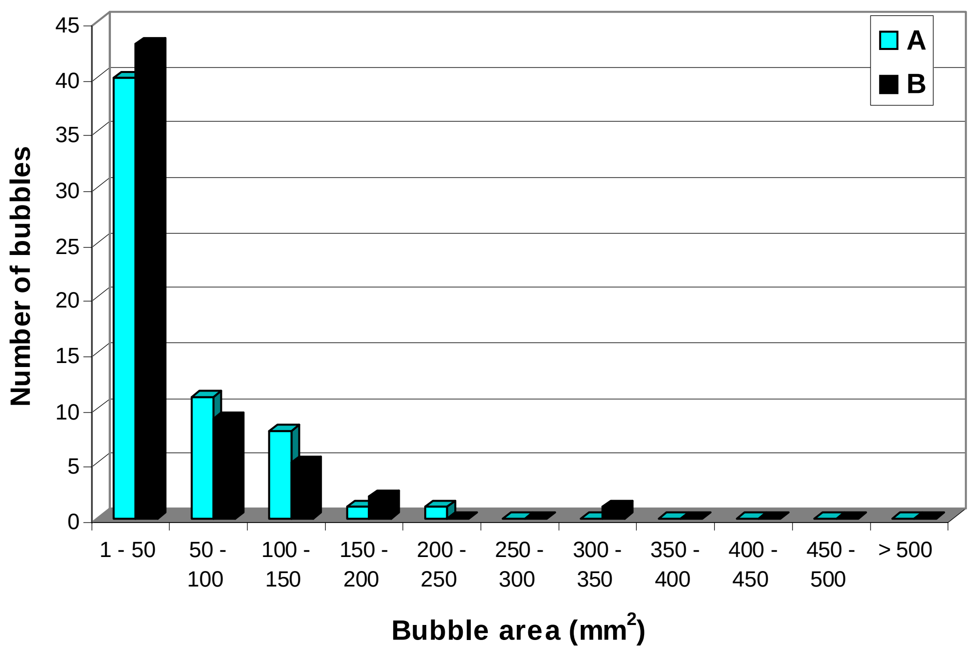

Figure 5.30. Bubble size distribution for side A and B at an air flow rate of 8 l/min.

5.5.4 Effect of baffles on bubble distribution over the membrane surface

As was explained in chapter 3 and 4, one of the reasons for inserting baffles between the membrane and the wall, was the visually observed maldistribution of bubbles over the membrane surface with most bubbles migrating and rising towards the centre of the membrane in the absence of baffles. In order to determine to what extent baffles improved the distribution of bubbles, an analysis was undertaken during which the membrane areas (scoured areas) covered by the bubbles and those that were not (unscoured areas) were calculated for both baffled and non-baffled cases. These data are shown in figure 5.31. It can be seen from this figure that the percent scoured area is always higher in cases with baffles than those without at all air flow rates. This figure also reveals that the benefit obtained by using baffles diminishes with the air flow rate. For example, at 2 l/min, the scoured area increases from 17% (non-baffled case) to 32% when baffles are inserted and yet at 12 l/min the increase is from 72% (non-baffled case) to 78% when baffles are present. This could provide a possible explanation for the findings of chapter 3 (figure 3.10) where it was observed that the differences in the final TMP decrease with the air flow rate when baffles are present.

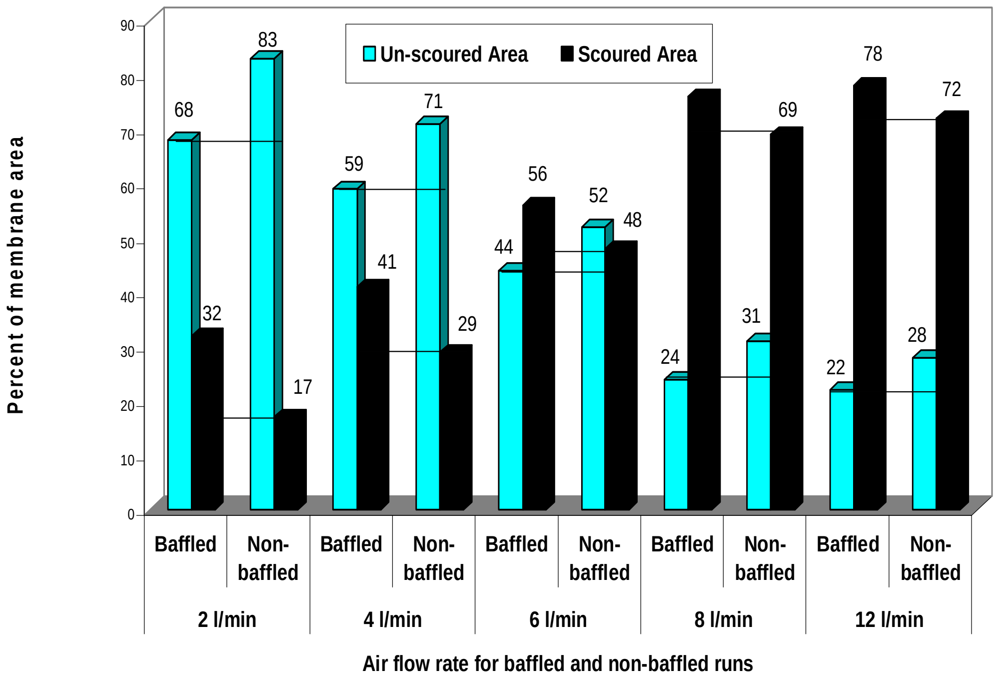

Figure 5.31. Comparison of scoured and unscoured areas in baffled and non-baffled cases.

By assuming that 50% of the initially imposed flux of 40 l/m^{2}hr passes through the air scoured membrane areas, the local fluxes under each condition could be estimated for baffled and non-baffles cases. These data are shown in figure 5.32 below. This figure shows that the difference between the baffled and non-baffled cases decreases as the air flow rate is increased. Local fluxes in the non-baffled runs are higher and this means that the membrane will foul much faster than in the baffled cases. If the membrane is fouling more rapidly then the critical fluxes will be lower. These data are supported by the critical flux data which were presented in chapter 4 in figure 4.21. In figure 4.21, the critical flux in the baffled cases at 8 l/min is almost double that at 2 l/min and in figure 5.32 below, it can be seen that the local flux at 2 l/min for the baffled cases is 2.4 times that at 8 l/min. Therefore there is some sort of correlation which exists between the total scoured area of the membrane and the observed critical fluxes.

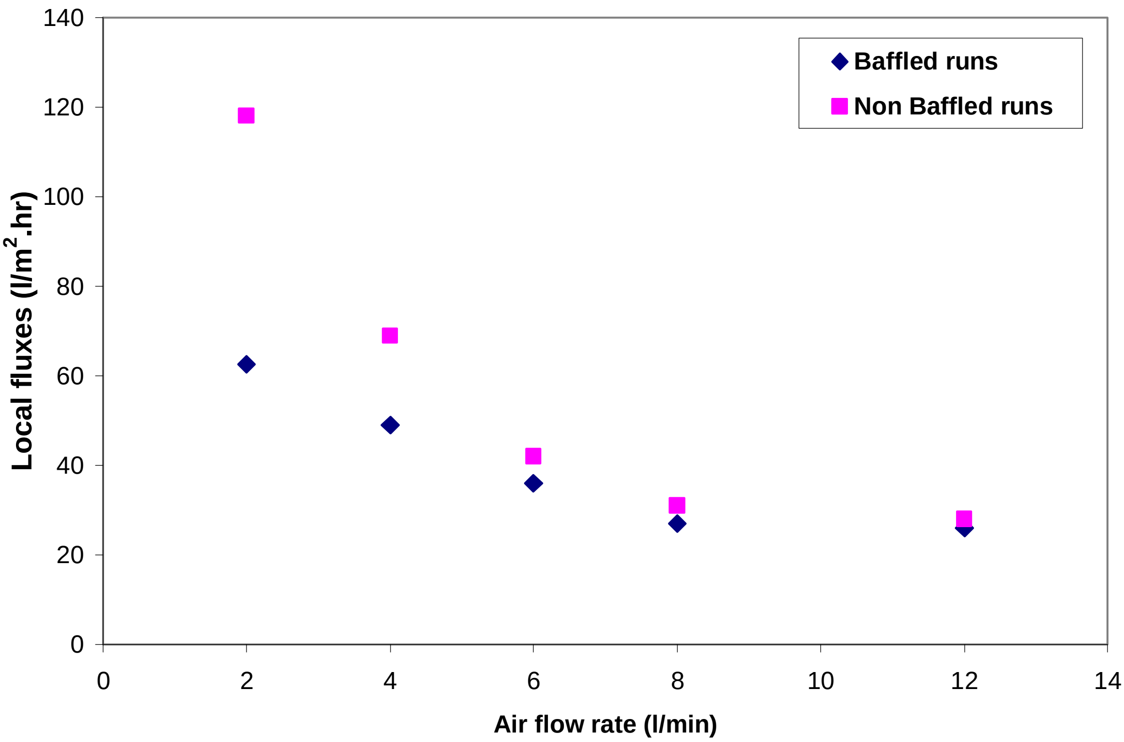

Figure 5.32. Estimated local fluxes for baffled and non-baffled cases based on the air scoured area of the membrane.

5.5.5 Determination of the bubble rise velocity

The rise velocity of a bubble in a stationary liquid depends on its size (Clift et al., 1978). Larger bubbles experience less drag force (per unit volume) than smaller bubbles and will thus rise faster than smaller bubbles. In this study, bubbles of different sizes were present, from those very small in diameter (1 – 2 mm) to those very large in diameter (40 – 70 mm). All these bubbles tend to rise at different terminal velocities. In some parts of the column, the rise velocity of the bubbles may have been slowed or accelerated by the re-circulating liquid. Therefore, in order to study the effect of air flow rate and nozzle size on the bubble velocity, only the bubbles having almost the same diameter were chosen and only bubbles rising in the central part of the column were considered. This is because towards the centre of the column, there seems to be a smaller amount of liquid coming down between the two flat sheets. The bulk of the fluid seems to flow down towards the edges of the column. The bubbles which were considered for analysis of rise velocity were about 5 mm in diameter and mostly very close to spherical in shape.

The bubble rise velocity was determined by using a combination of two software packages, Adobe Premiere 5 and Corel Draw 12. Videos of about 40 seconds in length were recorded using a digital camera. Using Adobe Premiere, the videos were broken down into frames which were 0.08 seconds apart. The exact position of the bubble and the diameter of the bubble in the first frame were determined using Corel Draw. The position of the bubble in the second frame and subsequent frames was also determined in a similar manner. Knowing the time interval between the frames and the distance the bubble had moved during this interval, enabled calculation of the bubble rise velocity. The measurements given by Corel Draw needed to be converted into real time measurements. This was achieved by measuring a distance between two points on the membrane, taking a photograph of the membrane and then using Corel Draw to measure the same distance. The camera setting had to be the same as those used to record the videos so that the magnification of the images was the same. The ratio obtained from these two measurements was than used to convert all the Corel Draw measurements into real time measurements. A difficulty which was encountered in determining the bubble rise velocity was that most of the bubbles do not rise in a straight line. For this reason only the bubbles whose path was very close to a vertical line were considered, as determining the diagonal distance that the bubble had moved between two different frames proved to be very difficult. Figure 5.33 (a) and (b) show an example of how the bubble rise velocity was calculated. In this example, the air flow rate was set at 2 l/min and a 0.5 mm nozzle was used. The bubble chosen for the analysis is shown in a black circle.

Figure 5.34 shows the effect of air flow rate on the bubble velocity. For the 5 mm bubble analysed in this study, the bubble rise velocity increases with the air flow rate. For example, for the 2 mm nozzle, the bubble rise velocity is 460 mm/s when the air flow rate is 2 l/min and the rise velocity is 710 mm/s when the air flow rate is 8 l/min. Thus for a fourfold increase in air flow rate, the bubble rise velocity increases by almost 36%. Figure 5.34 also reveals that the bubble rise velocity increases with the nozzle size for all air flow rates examined, with the 2.0 mm nozzle producing the highest bubble velocity and 0.5 mm the lowest. This is contrary to what has been found in some literature in which the bubble rise velocity decreased with the nozzle size (Valencia et al. 2002) whilst Le-Clech et al. (2003b) obtain the same rise velocity for nozzles of different sizes. This discrepancy could be due to the fact that these other studies were looking at an individual bubble instead of one bubble rising in a cluster of bubbles as in this study.

If the column is long enough, bubbles of the same size should theoretically reach the same terminal rise velocity. The terminal velocity of air bubbles with a diameter of 5 mm rising in water, can be predicted from the following equation (Eqn 5.2) developed by Beek and Muttzall (1975). This equation predicts a terminal velocity of about 0.24 m/s for a 5 mm bubble. This velocity is almost 40% lower than the smallest velocity that was predicted in this study. This discrepancy could be due to the fact that equation 5.2 was developed for single bubbles rising in stationary liquids. In our case there are swarms of bubbles rising, inducing a large amount liquid recirculation. The re-circulating liquid seems to have increased individual bubble velocities. The larger the bubble, the larger the amount of liquid recirculation induced and hence the observed effect of increased velocity with air flow rate and nozzle size.

$$U_b = \sqrt{\frac{2\sigma}{\rho d_b} + \frac{(\rho - \rho_b)}{\rho}\frac{g\, d_b}{2}} \qquad (5.2)$$

where, U_b is the terminal bubble rise velocity, σ, is the surface tension, ρ, is the density, g is gravitational acceleration, and d_b is the diameter of the bubble.

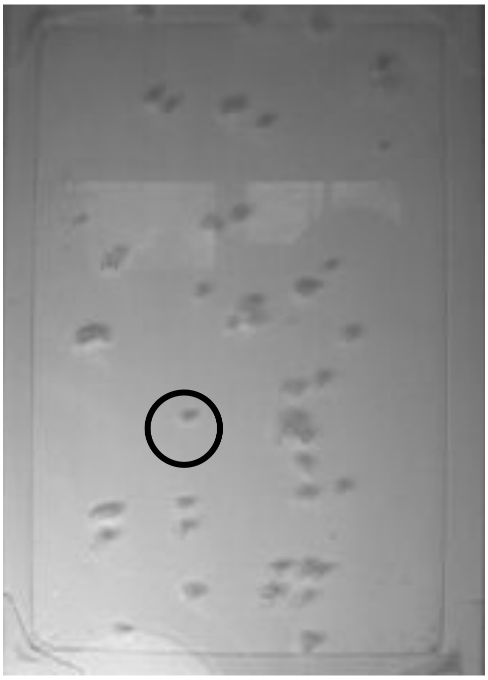

(a)

The bubble selected for analysis is shown in the black circle. The vertical position of the bubble was determined to be 114 mm from the bottom of the membrane.

(b)

This subsequent frame shows that the bubble has moved up a certain distance. The new vertical position of the bubble was determined to be 155 mm. The two frames are 0.08 sec apart.

Figure 5.33. Determination of bubble rise velocity from two subsequent frames (a) and (b)

The analysis of bubble rise velocity shows that the air flow rate and the nozzle size have a significant role to play in determining the rise velocities of the bubbles as bubble rise velocities seem to increase with both air flow rate and nozzle size. In chapter 3, the air flow rate of 8 l/min was found to yield better results for flux enhancements than lower air flow rates. This performance could be linked to the fact that bubbles are rising faster and thus inducing higher secondary flows in the liquid. Strong liquid secondary flows mean higher shear stresses on the membrane surface and thus better fouling control. This further explains why the effectiveness of the nozzle improves with the nozzle size, since large nozzles have been found to produce larger bubbles which rise faster inducing much higher liquid secondary flows.

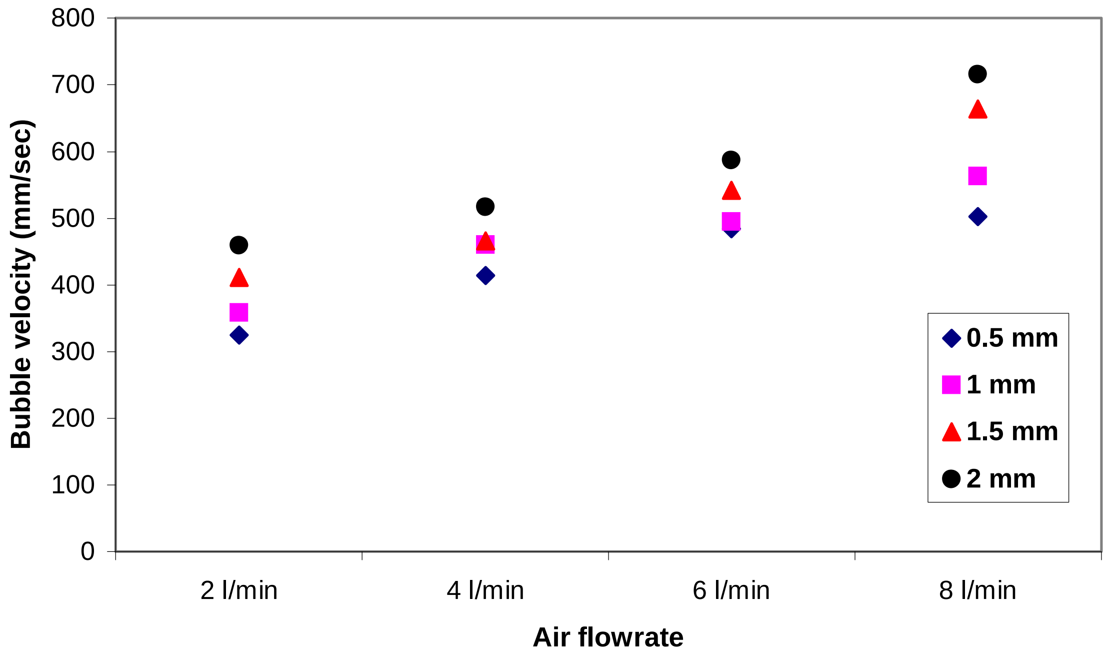

Figure 5.34. Calculated bubble rise velocities for a bubble of about 5 mm diameter.

5.6 DISCUSSION AND CONCLUSION

The use of the particle imaging software AnalySIS® has been helpful in providing some information regarding the effectiveness of gas-liquid two-phase flow in reducing fouling rate for submerged flat-sheet membranes. The information obtained in this chapter has explained some of the trends observed in chapter 3 and 4.

Based on the evidence presented in this chapter the following key findings are presented.

- The nozzle size has a significant influence on the bubble size distribution with the larger nozzles producing larger bubbles more frequently than the smaller nozzles.

- Nozzles of different geometries but same surface area have different bubble size distribution profiles.
- Fouling reduction depends on both the amount of gas injected and the bubble size distribution.
- Most of the injected gas (at least 70%) ends up as large flow with bubbles larger than 10 mm in diameter and this fraction increases with both the air flow rate and nozzle size.
- Both the gas injection rate and nozzle size have an influence on the bubble rise velocity.

Generation of bubbles from submerged orifices has been studied by a number of people (Davidson & Shüller 1960; Walters & Davidson, 1963; Yang et al., 2001; Valencia et al., 2002; Shyu et al., 2002). Most of these studies concentrated on studying the formation of a single bubble from a single orifice which is very different from this study where bubble formation was a continuous process through multiple orifices. Some of the important findings from these earlier studies are that, for each nozzle, bubbles of different sizes are produced but there exists a bubble with a maximum volume (Longuet-Higgins et al., 1991) and the maximum bubble size depends on the air flow rate to the bubble and the nozzle size.

Davidson and Shüller (1960) developed the following relationship between the bubble size and the gas flow rate.

$$Q(t) = \frac{dV}{dt} = Ko\left[P - \frac{2\sigma}{(3V/4\pi)^{113}}\right]^{\frac{1}{2}} \qquad (5.3)$$

where *Q(t)* denotes the volumetric flow rate of gas into a bubble, *Ko* is an orifice constant determined experimentally, σ is the surface tension, *P* is the gauge pressure at the inlet of the orifice and *V* is the volume of the spherical bubble respectively. Since *Ko* is a constant, this equation shows that the volume of the air bubble will increase with the air flow rate which agrees with the data presented in table 5.3 and figure 5.5. *Ko* could not be elucidated experimentally in this study which makes it difficult to generate data to compare with that of Davidson and Shüller (1960).

Valencia et al. (2002) also developed a relationship between gas flow rate, nozzle size and bubble size. According to their relationship given in equation 5.4, below a certain critical gas flow rate, the time of formation of the bubbles is constant regardless of the air flow rate, and, above a critical gas flow rate, bubbles are formed whose volume increases with the gas flow rate.

$$t_{Bl} = \frac{V_{Bl}}{Q} = \frac{2d_{Bl}^3}{3d_{or}^2 u_{or}} \tag{5.4}$$

where t_{Bl} is the time for bubble formation, V_{Bl} is the volume of the bubble, Q is the gas flow rate, d_{Bl} is the bubble diameter, d_{or} is the orifice diameter and u_{or} is the air inlet velocity. The critical gas flow rate can be obtained by using the following equation.

$$Q_T = 0.38 g^{1/2} \left[\frac{6\sigma d_{or}}{g\Delta\rho} \right]^{5/6} \tag{5.5}$$

where Q_T is the gas flow rate (m^3/s), g is gravitational acceleration (m/s^2), σ is the surface tension coefficient, d_{or} is the diameter of the orifice $\Delta\rho$ is the density difference between the gas phase and the liquid phase. According to equation 5.5, the critical gas flow rate with regards to the experiments in this study is about 5.2×10^{-7} m^3/s. The lowest air flow rate of 2 l/min used in this study corresponds to a volumetric flow rate of 3.33×10^{-6} m^3/s. This value is higher than the estimated critical gas flow rate thus for all the experiments conducted in this study bubbles were formed whose volume increased with the gas flow rate. This analysis supports the data presented in figure 5.5 where the mean bubble diameter increased with gas flow rate.

The very large bubbles observed in this experiment are not entirely due to the size of the nozzle but are also a result of coalescence of smaller bubbles. Particularly at higher flow rates, it was observed that many small bubbles would emerge from the nozzle and then merge to form larger bubbles that rose through the column. This phenomenon was also observed by Buwa and Ranade (2002). An example of coalescence is shown in figure

5.35. Evidence of bubble coalescence has also been reported by Zun et al. (1993) in a rectangular bubble column which is similar to the channel studied here.

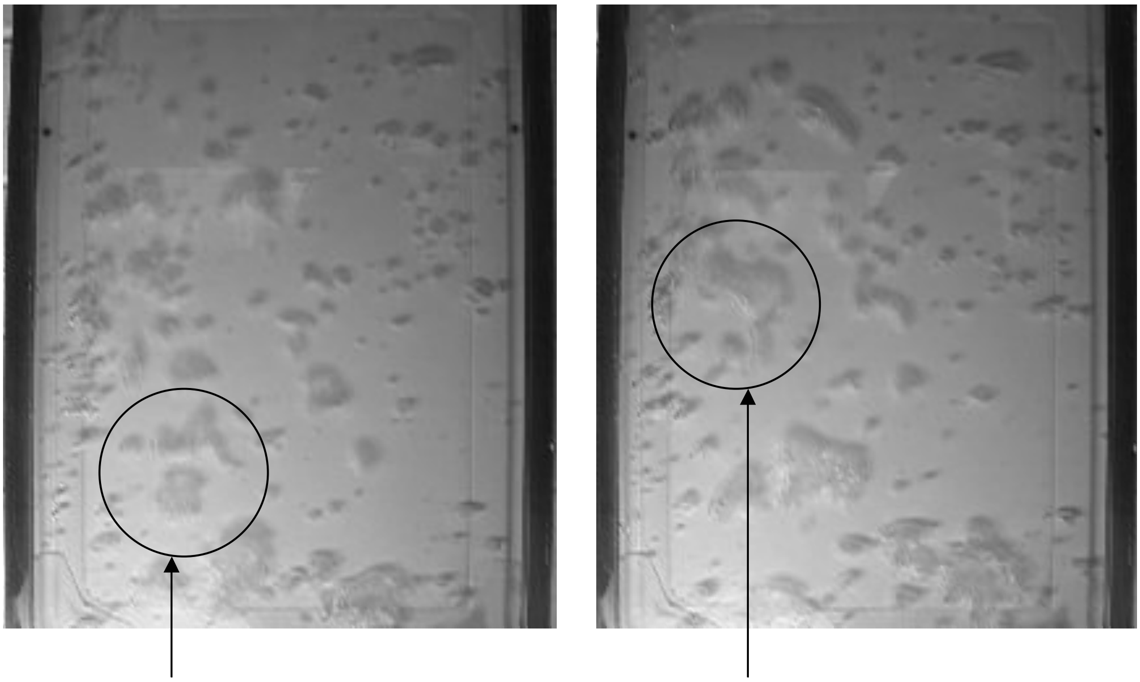

(a) Bubbles before merging (b) Merged bubbles

Figure 5.35. Evidence of bubble coalescence with (a) showing bubbles before they merge and (b) showing one big bubble formed after coalescence.

In the analysis of the pictures it was observed that the frequency of medium and large bubbles is higher for the higher air flow rates (6 and 8 l/min) and larger nozzles (1.5 and 2.0 mm). However, the number of small bubbles also increased with the gas flow rate and nozzle size. Further analysis into the distribution of flow into small, medium and large categories revealed that although there were more bubbles in the medium category, the actually amount of air in these bubbles is significantly less than the air contained by bubbles in the large category. Thus looking at the number of bubbles alone does not tell a complete picture. From this analysis it was clear that as the air flow rate and nozzle size increased, the fraction of air in the large category also increased. Having determined in chapter 3 and 4 that the extent of fouling reduction increases with nozzle size and air flow rate, therefore these results suggest that large bubbles play a much more dominant role in combating fouling than small bubbles. The channel gap width between the membrane and the wall was 7 mm. Therefore bubbles greater than 7 mm effectively became slugs or Taylor bubbles. For these types of bubbles there exists a thin falling film between the bubble and the membrane. Shear stresses in this film are known to be very high (Taha & Cui, 2002b; Ndinisa et al., 2005). Also behind the Taylor bubble, the falling film reverses flow direction and this creates a turbulent wake behind the bubble. This could therefore shed some light into the increasing fouling reduction obtained as bubbles became larger and the number of large bubbles increased.

At low gas loading rate, there is relatively little disturbance caused by the bubbles on the liquid phase. The bubbles are seen to be rising almost in a straight path (see the video entitled ‘Video 3’ in Appendix B, the CD). The bubbles rise smoothly through an almost stagnant liquid without causing much agitation and liquid recirculation. However, as the gas flow rate is increased, the system becomes more and more unstable. The majority of the bubbles start to migrate to the centre of the column and move vigorously in a zigzag manner (see Video 1 in Appendix B). There is strong up-flow of liquid in the centre of the column following the bubbles and strong down-flow near the walls. The down-flow of liquid near the walls is evidenced by bubbles either flowing down or held almost stationary in that vicinity. This flow pattern was also observed by Torvik and Svendsen (1990) and Delnoij et al. (1997) in bubble columns almost identical to the one studied here. Thus, with higher gas flow rates, there is a greater mixing in the system which helps to explain the improvement in flux.

More evidence which seems to suggest that larger bubbles contribute to making two-phase flow more effective can be obtained by examining bubble size distribution for different nozzles at the same gas injection rate. A careful examination of the bubble distribution presented in figure 5.15 to figure 5.18 shows that, with regards to the smaller bubbles (less than 5 mm), their production is independent of the nozzle size, however for bubbles larger than 5 mm, there seems to be more of these bubbles for the larger nozzles (1.5 and 2.0 mm). Thus, larger nozzles produce more larger bubbles which is in accordance with equations developed by Davidson and Shüller (1960) and Valencia et al. (2002).

Data presented in this chapter have shown that the area of the membrane scoured by the air bubbles increases when baffles are inserted thus showing that better distribution of the bubbles is achieved by using baffles. Also from previous chapters, 3 and 4, the presence of baffles was shown to increase fouling retardation by gas-liquid two-phase flow. This increase in the fouling retardation can therefore be linked to the fact that more of the membrane is scoured by air when baffles are presented. Another possible reason why baffles are seen to be more effective could be that when baffles are inserted, small rectangular channels (7 mm deep × 10 mm wide) are created through which the air can flow. Bubbles larger than 7 mm in diameter become slugs. Thus with baffles present the most dominant type of two-phase regime in the channel become slug flow. Slug flow is known to be the most effective two-phase flow regime for tubular and hollow fibre membranes (Cui et al., 2003). With slug flow, increasing the gas flow rate can lead to the decrease in the liquid slug and the bubble wake, and this can cause the cleaning effect of the two-phase flow to be reduced. A large increase in the air flow rate can eventually lead to bubbles overlapping and the bubble wake eliminated completely. This could perhaps explain why with baffles inserted, the maximum benefit of fouling minimization was obtained with lowest air flow rate of 2 l/min and decreased when the air flow rate was increased.

The analyses conducted in this chapter have shown that there is strong evidence which suggest that the efficiency of two-phase flow increases with both air flow rate and nozzle size and is strongly influenced by the bubble size for submerged flat sheet membranes. From filtration experiments with waste activated sludge, the optimal gas flow rate was found to be around 12 l/min. It is however difficult to determine the optimal bubble size due to the fact that bubble size could not be controlled when bubbles are generated. Therefore the effect of bubble size was studied only via CFD simulations and these results are presented in chapter 7.

Chapter 6

COMPUTATIONAL FLUID DYNAMICS SIMULATIONS OF TAYLOR BUBBLES IN TUBULAR MEMBRANES – MODEL VALIDATION AND APPLICATION TO LAMINAR FLOW SYSTEMS

This chapter is a reproduction of the paper that was published in the journal called "Chemical Engineering Research and Design". The full reference of the paper is as follows:

Ndinisa, N. V., Wiley, D. E. & Fletcher, D. F.; Computational Fluid Dynamics Simulations of Taylor Bubbles in Tubular Membranes – Model Validation and Application to Laminar Flow Sytems; *Chem. Eng. Res & Design*, 2005, 83(A1): 40 – 49.

The numbering of the headings and figures in the paper has been changed in order to be consistent with the rest of the thesis.

Chapter 6

COMPUTATIONAL FLUID DYNAMICS SIMULATIONS OF TAYLOR BUBBLES IN TUBULAR MEMBRANES – MODEL VALIDATION AND APPLICATION TO LAMINAR FLOW SYSTEMS

6.1 ABSTRACT

The use of gas-liquid two-phase flow has been shown to significantly enhance the performance of some membrane processes by reducing concentration polarization and fouling. However, the understanding of the mechanisms behind gas-liquid two-phase flow enhancement of flux is still limited. This paper reports on the validation of computational fluid dynamics simulations of a Taylor bubble, using a variety of numerical approaches. Good agreement between the experimental and numerical data is shown for an Eulerian two fluid model that uses a solution adaptive bubble size to avoid numerical mixing. This model is then used to study the effect of liquid extraction at the membrane wall on the wall shear stress, since it is the enhanced wall shear stress caused by the bubble passage that is important. This effect is shown to be negligible for typical operating conditions in membrane systems. Moreover, we show that the wall shear stress can be well represented by a “top hat” profile for the system considered here.

6.2 INTRODUCTION

The use of gas sparging through tubular membranes is increasing in importance because of its ability to reduce fouling and/or reduce concentration polarization effects (Cui et al., 2003). Several researchers have evaluated the effect of bubbling on the performance of membrane filtration by injection of air into the lumen of tubular and hollow fibre membranes. These studies include ultrafiltration of dextran with tubular membranes (5 mm i.d.) and hollow fibres (0.2 mm i.d.) (Cui & Wright, 1996; Bellara et al., 1996); filtration of bentonite suspension with tubular membranes (15 mm i.d.) and hollow fibres (0.93 mm i.d.) (Cabassud et al., 1997; Mercier et al., 1997); ultrafiltration and microfiltration of yeast suspensions using 15 and 6 mm i.d. tubular membranes (Mercier et al., 1998); and ultrafiltration and microfiltration of bacterial suspensions using flat sheet membranes (Lee et al., 1993). All of these experiments show that air injection can result in an improvement in flux but the extent of the enhancement depends on the type of module (tubular or hollow fibre) and the membrane type. For tubular membranes, the enhancement was about two to three-fold, while for hollow fibres the gain was 1.0 to 1.3. The effect of air slugs on flux was more pronounced with ultrafiltration membranes than with microfiltration membranes (Lee et al., 1993; Mercier et al., 1998).

Crossflow microfiltration in tubular membranes is often carried out under turbulent flow regimes in order to minimize concentration polarization and fouling. This usually requires high cross-flow velocities, which inevitably lead to high energy consumption. The use of two phase flow lowers the required velocities, allowing systems to be operated under laminar flow conditions. However, the introduction of gas causes the transition from laminar to turbulent flow to occur much faster (Ghosh & Cui, 1999). Several researchers have investigated the effectiveness of two-phase flow under laminar and turbulent flow conditions in tubular membrane modules (Cui & Wright, 1996; Cabassud, et al., 1997; Vera, et al., 2000; Taha & Cui, 2002a). All of these researchers found that the flux enhancement by two-phase flow decreased as the Reynolds number was increased. For example, Cui and Taha (2003) found a flux enhancement of 160% with a Reynolds number of 490, whilst at a Reynolds number of 3150 the flux enhancement was only 5%. These studies therefore suggest that it is optimal to operate in the laminar regime.

It is believed that the enhanced wall shear stress created as the liquid flow is squeezed passed the bubble is the primary enhancement mechanism, as it removes foulants from the walls. Wall shear stress profiles around Taylor bubbles have been determined using electrochemical methods for systems with a non-porous wall in place of a membrane (Cabassud et al., 2001; Mercier-Bonin et al., 2000b; Ducom et al., 2002b). Taha and Cui (2002b) have used CFD to predict the wall shear stress profile of a Taylor bubble in a 10 mm tube without extraction (see section 6.3 for more details). They then used the predicted shear stress to calculate mass transfer and hence permeate flux for a tubular membrane of the same diameter. However, in their CFD simulation they used a non-porous tube and so the predicted shear stresses did not account for the porous wall.

Wang et al. (1994) cite Howell et al. (1992) as concluding that in their experiments wall suction of up to 1% of the inlet flow did not distort the macroscopic flow field. The paper by Howell et al. (1992) reports CFD simulations of flow patterns and particle motion which occur during oscillatory flow in a baffled channel with and without porous walls. They concluded that "There is not much effect of 1% wall flux on flow patterns except near the wall region" but as their system is very different to the present one and no details of the modelling are given, their work cannot be used to justify the assumption that in general extraction has no effect on bubbling flows.

Therefore the main objective of this study is to validate a CFD model of Taylor bubble flow in a tubular column and to examine what effect wall flux has on the liquid flow field. The numerical model was validated using experimental data obtained by Bugg and Saad (2002) using Particle Image Velocimetry (PIV) for a bubble rising in a stagnant liquid. Then wall suction rates as high as 20% of the flow extracted over 16 tube diameter lengths have been investigated. For membranes, the flux is typically 15% of the flow extracted over a length of more than 250 tube diameters (Wang et al., 1994), so the current results more than cover the entire practical range of operation.

6.3 PREVIOUS WORK ON TAYLOR BUBBLE SIMULATION

Before describing the modelling work it is important to cite White and Beardmore (1962), who conducted a series of experiments on Taylor bubbles rising in stagnant liquids in vertical tubes. Their work is used extensively in model validation, and they determined the important dimensionless groups to characterize Taylor bubbles. They identified the Eötvös number ($\rho g D^2/\sigma$), the Froude number (U_t^2 /gD) and the Morton number ($g\mu^4/\rho\sigma^3$) as the important dimensionless groups. In these groups U_t is the terminal speed of the bubble, g is the acceleration due to gravity, D is the tube diameter, ρ is the liquid density, σ is the surface tension, and μ is the dynamic viscosity of the liquid. Other dimensionless groups which have been used are the Weber number

($\rho U_t^2 d_{bl}/\sigma$) and the bubble Reynolds number ($\rho U_t d_{bl}/\mu$), where d_{bl} is the equivalent diameter of the bubble. Combining their work with the work of others, White and Beardmore (1962) produced a comprehensive graphical correlation of Froude number as a function of the Eötvös and Morton numbers. They concluded that viscous forces are negligible if $\rho^2 g D^3/\mu^2 > 3 \times 10^5$, interfacial forces are negligible if $Eo > 70$, and inertial effects are negligible if $Fr < 0.05$.

Slug flow is encountered in many industrial applications. It occurs in hydrocarbon production and transportation, chemical and nuclear reactors, and phase change heat transfer. Two-phase flow has also been shown to enhance heat and mass transfer coefficients. Although slug flow has been widely studied experimentally, simulation of two-phase flow is a relatively new subject. The first computer codes for the simulation of two-phase flow were pioneered by the nuclear industry and adopted as a primary tool for simulating the possible loss of coolant accidents in nuclear reactors. These codes have been modified for use in the oil industry to simulate transient two-phase flow in pipelines (Taitel et al., 1989). Tomiyama et al. (1993) were amongst the first to study bubble behaviour using the Volume-of-Fluid (VOF) methods and showed that this technique produced qualitatively correct bubble shapes for a variety of conditions. They also studied the effect of an imposed field on the bubble trajectory and the dependence of this trajectory on the bubble and fluid properties.

There are many hydrodynamic models which have been developed to study slug flow but most of them have not been validated experimentally. Kawaji et al. (1997) were among the first to validate numerical simulations of slug flow with experimental data. The RIPPLE code that uses a VOF interface tracking method was used to simulate the hydrodynamics of a Taylor bubble rising through stagnant liquid in a vertical tube. The simulation was performed in a frame of reference moving with the bubble, so that the liquid and the tube wall moved downward at the bubble terminal velocity. The simulations were axisymmetric, transient and two dimensional. Bubbles of different lengths were simulated and the terminal speed was found to be the same for all bubbles. The Eo and Mo numbers in their simulations were 232 and 3.06×10^{-9}, respectively. According to the graphical correlation of White and Beardmore (1962) the bubble hydrodynamics in this region is independent of viscous and interfacial forces and is inertia-dominated. The flow in the falling film was found to be laminar and for shorter bubbles it penetrated deeper into the wake than for longer bubbles. The VOF model under-predicted the wall shear stress and velocity near the tube wall, while the differences diminished towards the interface. Based on the simulations, they conjectured that the residual eddies far below the wake of the leading bubble cause perturbations in the pressure and liquid flow field that in turn cause the trailing bubble to move laterally or deform its shape, which can lead to reduced drag force and an increase in the rise velocity.

Bugg et al. (1998) investigated the motion of bubbles in tubes using a two-dimensional, transient, finite difference model with volume fraction specification to track the movement of the gas-liquid interface. The simulations were axisymmetric and used a fixed frame of reference. Taylor bubbles rising through a stagnant liquid in a vertical tube were simulated for a wide range of Eötvös numbers between 10 and 100, and Morton numbers between 10^{-12} and 10. The main purpose of their investigation was to predict the final steady-state shape of the bubble for various flow profiles around the Taylor bubble. For all conditions, the initial shape of the bubble was the same but the final shape differed depending on whether viscous or inertial forces were important. All the simulated bubbles had the expected spherical nose and the trailing edge had a flat or rounded shape depending on the Froude number (Fr). For all cases with $Fr > 0.3$, it was observed that the bubbles had flat or concave bottoms. This was seen to be a better criterion for predicting the bubble shape at the bottom compared with earlier criteria proposed by White and Beardmore (1962) and Fabre and Liné (1992). For the cases in which viscous forces were unimportant, based on the White and Beardmore (1962) criterion, it was found that the falling film continues to thin all the way to the trailing edge of the bubble. In the cases where viscous effects were important, a portion of the falling film had a constant thickness, indicating that the falling film had reached equilibrium.

The numerical code used by Bugg et al. (1998) was recently validated against experimental data by Bugg and Saad (2002). The code uses a VOF method to track the gas liquid interface. In the experiments, a Taylor bubble rising through olive oil in a 19 mm ID tube was investigated. In this simulation the Eötvös number was 100 and the Morton number was 0.015. Experimental data were obtained using the PIV technique.

PIV measurements were validated by using a mass balance equation to calculate the terminal velocity of the bubble. The resulting terminal velocity was within 3% of the terminal velocity measured using the phase transition detectors. The terminal velocity predicted by the numerical method was within 7% of the experimental value. Velocity profiles were measured for the region ahead of the bubble, in the developing film, in the fully developed film as well as in the wake region. There was excellent agreement between experimental and numerical velocity profiles in all regions, except in the wake region where the maximum axial velocity was under-predicted by about 15%. This was attributed to the fact that the bottom edge of the bubble is not as rounded in the predictions as in the experiments.

Mao and Dukler (1991) developed a numerical model of the flow around a Taylor bubble using a curvilinear co-ordinate system attached to the bubble and fitted to the bubble shape. No *a priori* assumptions were made about the shape of the gas bubble. The model adjusted the shape of the interface so that normal stress at the interface satisfied the condition of constant pressure inside the bubble. The simulations were transient, axisymmetric and two-dimensional using a frame of reference moving with the bubble. The terminal velocity of the bubble was adjusted until the bubble was locally spherical at the nose. The solution domain extended only to the trailing edge of the bubble and not into the wake region. A modified RNG k-ε turbulence model was used when the liquid flow was turbulent. The computed Froude number was 0.346, which is very close to the experimental value of 0.351. The terminal velocity was found to be independent of viscosity and surface tension. The predicted wall shear stress increased along the side of the bubble and showed a wavy pattern towards the bottom, reflecting a wavy interface.

Clarke and Issa (1997) used a finite volume computational procedure to analyse for liquid flow field around a Taylor bubble rising in a vertical tube. A non-orthogonal block structured mesh which can map the entire flow field around the Taylor bubble and in the liquid slug behind it was used. The flow inside the bubble was ignored. Turbulence was modelled using the standard k-ε model. The rise velocity of the bubble was determined by a trial and error method, with the final correct velocity producing a bubble nose which is locally spherical at the stagnation point. Although the model calculated the shape of the bubble, the bottom part of the bubble was assumed to be flat. The simulations were two-dimensional axisymmetric and used a frame of reference moving with the bubble. This model also accounts for the presence of small dispersed bubbles in the liquid slugs by assuming homogeneous two-phase flow in this region. However, the homogeneous model was found to be inadequate in resolving two-phase flow in the liquid slug and hence the authors indicated that future models need to use the two-fluid model in order to account for dispersed bubbles correctly.

Issa and Ubbink (1999) developed a new algorithm for solving the volume fraction equation based to preserve a sharp interface between the two fluids and applied this to Taylor bubble simulations. The interesting feature of this algorithm is that the advection scheme was constructed to have minimal numerical diffusion without dispersive errors by making the convection scheme depend on the flow orientation relative to the cell face in the discretized equations. They carried out an extensive series of simulations to determine the bubble rise velocity for a variety of Eötvös and Morton numbers and obtained good agreement with the data of White and Beardmore (1962), except in cases where the surface tension force was dominant.

As discussed in section 6.2, slug flow has been shown to enhance the performance of membrane systems. In an attempt to understand the flux enhancing mechanisms of slug flow Taha and Cui (2002b) used a VOF method to model slug flow in a tubular ultrafiltration (UF) process. The model was used to calculate the shape and velocity of the slug, as well as the velocity distribution and local wall shear stress at the membrane surface. The predicted wall shear stress was then linked to the local mass transfer coefficient that was used to predict the permeate flux. The commercial CFD code FLUENT was used for the simulations which were transient, 2D and axisymmetric, with a frame of reference moving with the bubble being used. The RNG k-ε turbulence model was used. The shape of the Taylor bubble was predicted with reasonable accuracy. The predicted terminal rise velocity of the bubble in a 10 mm ID tube was 0.0692 m/s which was very close to the experimental value of 0.068 m/s.

It is apparent from the review of numerical methods that almost all the codes used have been specifically created for the simulation of slug flow, with the exception of that of

Taha and Cui (2002b) who used the general purpose, commercial CFD code FLUENT. However, Taha and Cui (2002b) did not present velocity profile distributions around the Taylor bubble and their method of validation was indirect. Bugg and Saad (2002) conducted an excellent validation of their numerical model for the case of slug flow but they used a purpose written code specifically developed for this application. It is also clear from the literature that most researchers have used a frame of reference moving with the bubble, which is less complicated than simulating a bubble rising from rest, but requires the terminal velocity of the bubble to be known *a priori* or to be adjusted iteratively. Therefore the aim of this paper is to study various two-phase flow models available in a general purpose commercial CFD code, CFX 5.6. The simulations are also conducted in a manner that closely resembles experimental conditions, in that a bubble is allowed to rise from rest.

6.4 THE NUMERICAL SOLUTION METHOD

In this section the various approaches used here to model two-phase flow (slug flow) are presented and their application to this problem is described.

6.4.1 The Euler two-fluid model

In this approach, the fluids are treated as two inter-penetrating continua, each having their own velocity field, each occupying separate regions in space but sharing a common pressure field. The two-fluid model is best suited for situations where there is a continuous and a disperse phase and where the continuous/disperse phase interface is smaller than the grid-size. However, use of appropriate closure correlations also allows for the simulations of two-phase flow phenomena where the characteristic length of the interface is large compared with the grid size. The interaction between the fluids is through the shared pressure field, the exchange of momentum via interfacial drag and other forces. Both fluids share space in proportion to their volume fractions which satisfy the condition

$$\alpha_G + \alpha_L = 1 \tag{6.1}$$

The two-fluid model is developed by writing conservation equations for each phase separately. Through the use of appropriate averaging techniques, these conservation equations can be used to represent macroscopic flow fields for each phase. However, during the process of averaging, important characteristics of the flow fields are lost and must be reintroduced into the model via appropriate closure laws. For isothermal two-phase laminar flow, the governing conservation equations are:

$$\frac{\partial \rho_k \alpha_k}{\partial t} + \nabla \cdot (\rho_k \mathbf{u}_k \alpha_k) = 0 \tag{6.2}$$

$$\frac{\partial \alpha_k \rho_k \mathbf{u}_k}{\partial t} + \nabla \cdot (\alpha_k \rho_k \mathbf{u}_k \otimes \mathbf{u}_k) = -\alpha_k \nabla p + \nabla \cdot \alpha_k \boldsymbol{\tau}_k + \sum_{l=1}^{N} \mathbf{M}_{kl} + \alpha_k \rho_k \mathbf{g} \tag{6.3}$$

where ρ_k, $\mathbf{u}_k$, α_k and $\boldsymbol{\tau}_k$ are the macroscopic density, the velocity, the volume fraction and the viscous stress tensor of the k_{th} phase, p is the pressure and $\boldsymbol{M}_{kl}$ is the inter-phase momentum exchange term between phase k and phase l. The important term that requires modeling is $\boldsymbol{M}_{kl}$ which for a continuous phase k and a disperse phase l takes the form

$$\mathbf{M}_{kl} = \tfrac{3}{4} \alpha_l c_d \rho_k |\mathbf{u}_l - \mathbf{u}_k| (\mathbf{u}_l - \mathbf{u}_k) / d_l \tag{6.4}$$

where c_d is the drag coefficient (set to 0.44 here), ρ_k is the density of the continuous phase and d_l is the disperse phase length-scale. As we will see later, the behaviour of the system of equations can be changed significantly by manipulating the disperse phase length-scale.

6.4.2 The Volume of Fluid model

The volume-of-fluid (VOF) model is suitable for describing two-phase problems where the characteristic length scale of the interface is larger than the grid size. The VOF method, originally developed by Hirt and Nichols (1981), tracks the motion of the gas-liquid interface and accounts for topological changes in the interface by using a transport equation for f, the fraction of space occupied by the liquid phase. The governing mass and momentum equations are derived from the two-fluid model by assuming no slip between the phases and that all properties are volume fraction weighted averages, giving

$$\frac{\partial \rho}{\partial t} + \nabla \cdot (\rho \mathbf{u}) = 0 \tag{6.5}$$

$$\frac{\partial \rho \mathbf{u}}{\partial t} + \nabla \cdot (\rho \mathbf{u} \otimes \mathbf{u}) = -\nabla p + \nabla \cdot \boldsymbol{\tau}_k + \rho \mathbf{g} + \mathbf{F}_{SF} \tag{6.6}$$

where the fluid properties are function of space and time and are given by

$$\rho(\mathbf{x},t) = f(\mathbf{x},t)\rho_L + [1 - f(\mathbf{x},t)]\rho_G \tag{6.7}$$

$$\mu(\mathbf{x},t) = f(\mathbf{x},t)\mu_L + [1 - f(\mathbf{x},t)]\mu_G \tag{6.8}$$

The subscripts L and G indicate the liquid and gas phases, respectively. The model solves the scalar advection equation for one of the volume fractions, f, via

$$\frac{\partial f}{\partial t} + \nabla \cdot (\mathbf{u} f) = 0 \tag{6.9}$$

with the other volume fraction being determined using equation 6.1.

In its simplest form, the VOF method relies on the use of a fine mesh and high order numerical schemes (see Issa and Ubbink, (1999) for an example of this approach) to resolve the interface over a distance of several cells. More sophisticated methods introduce algebraic reconstruction methods after each timestep, as discussed in for example Harvie and Fletcher (2000).

Finally, surface tension effects need to be included in the above models. The continuum surface force (CSF) of Brackbill et al. (1992) is used to model the force due to surface tension ($\boldsymbol{F}_{SF}$) acting on the gas-liquid interface.

6.4.3 Simulation Conditions

The governing equations for both models were solved using the commercial CFD code CFX 5.6 from ANSYS. This code solves the equations on an arbitrary grid using a finite volume method and a coupled solver. In this study a two-dimensional structured grid was used to represent the vertical tube used in the experiments. The fluids were assumed to be incompressible and isothermal and to have constant fluid properties. Transient simulations assuming laminar flow in a two-dimensional wedge were performed. The simulations were based on the experimental conditions of Bugg and Saad (2002). The fluid density was set to 911 kg/m^3, the viscosity was 0.084 Pa.s and the surface tension was 0.0328 N/m. These chosen fluid properties and tube diameter yield the following dimensionless numbers: Eo = 100, Mo = 0.015 and Re = 27. The regime map of White and Beardmore (1962) indicates that for the simulations conducted here the surface tension forces are unimportant.

The tube diameter was 19 mm and the tube height was 160 mm. The tube was modelled as a closed system with walls on the top and the bottom. The initial shape of the bubble was assumed to be cylindrical, with a height of 50 mm and a diameter of 14 mm, located centrally in the tube at 5 mm above the bottom wall. The bubble rises from rest and develops an invariant shape. For the VOF method, a no-slip boundary condition was applied to the walls, whilst in the two-fluid model, the wall boundary conditions were no-slip for the liquid and free-slip for the air.

Mesh variation studies showed that a grid size of 0.25 mm in the radial and 0.25 mm in the axial direction gave grid independent solutions. A constant time step of 1.0×10^{-4} s was used for all models. Note that both the spatial resolution and the temporal resolution need to be very fine to generate a properly converged solution, independent of the numerical solution parameters.

The VOF model is the classical method of solving a free surface problem. In CFX5.6 this method makes use of second order numerical schemes for both space and time with a compressive scheme (for both space and time) being applied to the volume fraction (f)

equation in order to reduce numerical diffusion to a minimum. No surface reconstruction scheme is used to sharpen the interface.

In the simulations performed using the Eulerian two fluid model, slip is allowed between the two phases. This only affects the solution in computational cells where there is a fluid mixture. Initially, the disperse phase length-scale, (d_l) was set to 5 mm to allow significant slip between the gas and the liquid. This size was chosen on the basis of trial and error, and was found to give the solution the desirable property that cells containing a mixture of gas and liquid would tend to separate. This was needed because significant mixing of the gas and liquid occurred in the wake region in the VOF simulations (see later), most likely because of the difficulty of choosing a physically acceptable set of initial conditions from which to start the simulation. However it has the undesirable effect of thickening the interface in regions where the gas is below the liquid, i.e. at the leading edge of the bubble, and increasing the computational time considerably.

To combat the loss of a sharp interface, a combined model was developed using a variable bubble size. A small bubble size (0.1 mm) was used throughout the domain except in cells where there was a mixture of gas and liquid, and the gas volume fraction gradient was in the opposite direction to gravity. In these cells, a gas bubble size of 5 mm was used, again to allow the gas to rise and rejoin the main bubble. This combined model then behaves like the VOF model (as d_l = 0.1 mm gives a very low slip velocity) except in regions where gas and liquid are mixed with liquid above gas, where the high slip velocity means that it behaves like the two fluid model, and the "gas bubbles" rise to rejoin the bulk of the gas.

6.5 MODEL VALIDATION

6.5.1 The bubble shape

The total simulated time for all the models was around 0.95 s, which was sufficient to allow the bubble to reach its terminal velocity. Figure 6.1 shows air volume fraction plots of the bubble at the end of the simulation for the three models. In the VOF case, the bubble has a sharp interface at the top but a badly mixed wake. The two fluid model with a constant disperse phase length-scale of 5 mm gives a well defined wake but a much more diffuse interface. Finally, the combined model has the best properties of both simulations. The figure shows a bubble with a prolate spheroidal leading edge and concave trailing edge. For the chosen conditions inertial forces dominate and Fabre and Liné (1992) state that in this regime bubbles have flat or concave bottoms, as observed here. Therefore the shape predicted by the two-fluid models is qualitatively correct. This shape also matches reasonably well with that observed experimentally by Bugg and Saad (2002).

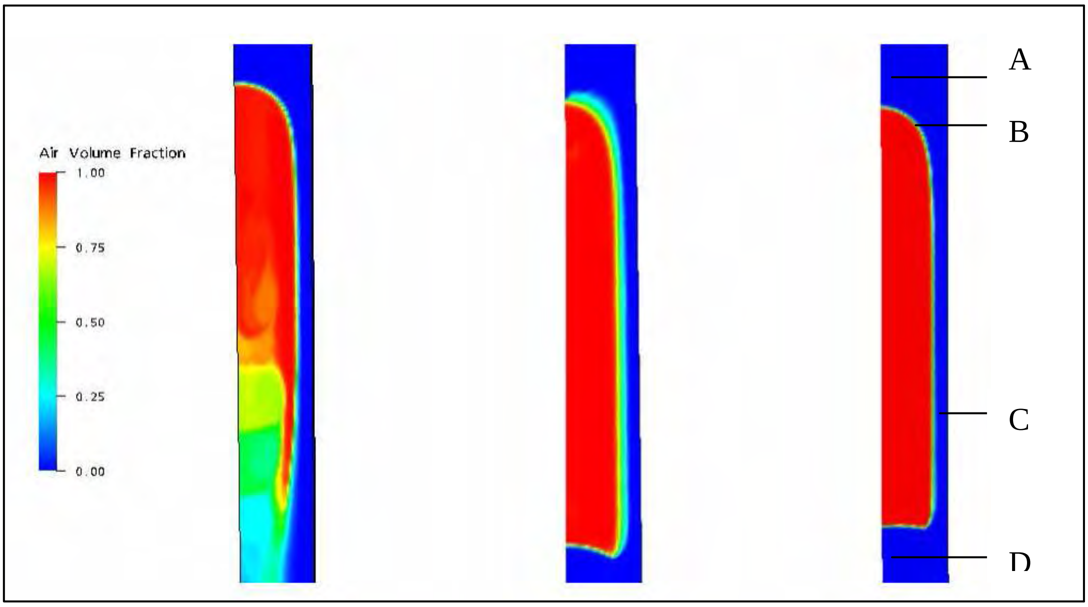

Figure 6.1. The bubble shape at the end of the simulation for (a) the VOF model, (b) the two-fluid model using a constant disperse phase length-scale of 5 mm, and (c) the combined model in which the disperse phase length-scale was adapted by the solution. The cross-sections A, B, C and D indicate the planes at which the radial and axial velocities were extracted.

6.5.2 The terminal velocity

For the VOF model the terminal speed of the bubble was found to be 0.14 m/s, for the two-fluid model it was 0.119 m/s and for combined model it was 0.11 m/s. The experimental value of the terminal velocity was 0.131 m/s (Bugg and Saad, 2002). The predicted values are within 8% of the experimental value which is comparable with the agreement achieved by Bugg and Saad (2002). Note that the terminal velocity has to be estimated from the movement of the slightly smeared interface and so its value is subject to some uncertainty. This affects subsequent comparisons where all velocities are normalized by the calculated terminal velocity but the effect is judged to be no more than 10%.

6.5.3 Axial velocities along the tube axis

As the bubble rises in the stagnant liquid, it accelerates the fluid ahead of it and this fluid is pushed sideways to allow the bubble to rise. Axial velocities ahead of the bubble were extracted along the tube axis from the bubble nose up to a distance of about 0.5*D*. The velocities from the three models, together with experimental data, are shown in Figure 6.2. This figure shows that the bubble does not have much influence on the liquid ahead of it, as the axial velocity decays to zero at about 0.3*D*. There is very good agreement between the numerical and the experimental data in all cases.

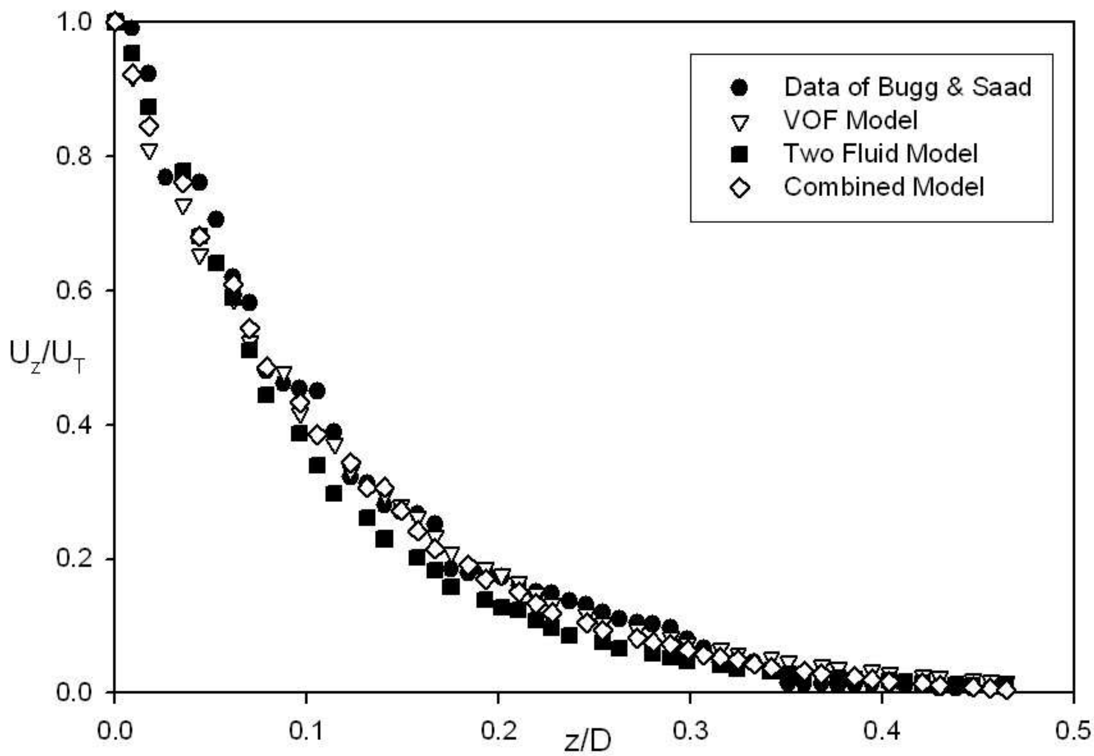

Figure 6.2. The normalized axial component of velocity along the tube axis above the bubble nose.

6.5.4 Axial and radial velocity profiles ahead of the bubble

As the bubble moves upwards, fluid ahead of it is pushed sideways (see Figure 6.3). As a result, a strong radial velocity component can be seen ahead of the bubble pushing fluid away from the tube axis. Velocity field data are available from the experimental study at a plane located 0.111*D* ahead of the bubble. The point of maximum radial velocity, as seen in Figure 6.4, is located halfway between the tube wall and the gas-liquid interface. For the axial velocities (shown in Figure 6.5), initially the fluid moves in an upward direction, but at a distance of about 0.66*D* from the tube axis, the flow changes direction from upward to downward. The transition from upward to downward flow is smooth. For the axial velocities, the agreement between numerical and experimental results is very good for all models. However, for the radial velocities all models seem to over predict the radial velocities near to the wall. The experimental data suggest that at about 0.8*D*, the radial velocity decays to zero but this is not in agreement with the numerical methods which show a much smoother and more physically intuitive behaviour. Given the observable scatter in the experimental data, this is most likely explained by measurement difficulties near the wall. The two-fluid model is closer to the experimental results than the VOF model. The combined model also seems to over-predict the peak radial velocity, but near the tube axis and the tube wall it predicted the velocities with reasonable accuracy.

An interesting feature of the above results in the apparent significant variation of the model results at nominally the same position in the flow. The data are extracted at a fixed location relative to the nose of the bubble, but as has already been noted there is some uncertainty in the exact location of this point. It is clear from Figure 6.3 that the velocity field is changing rapidly near this location. Therefore, in Figure 6.6, the data of Bugg and Saad (2002) for the radial velocity are compared with results from the combined model at the nominal location and at locations 0.5 mm above and below this location. It is evident that this very small change in location has a relatively large effect on the predicted values and that the observed disagreement between the predictions and the data can easily be explained in terms of the uncertainty of locating the exact same location relative to the bubble nose. Recall that 0.5 mm is just two numerical cell widths, which again highlights the need for very fine numerical meshes to properly resolve the flow-field.

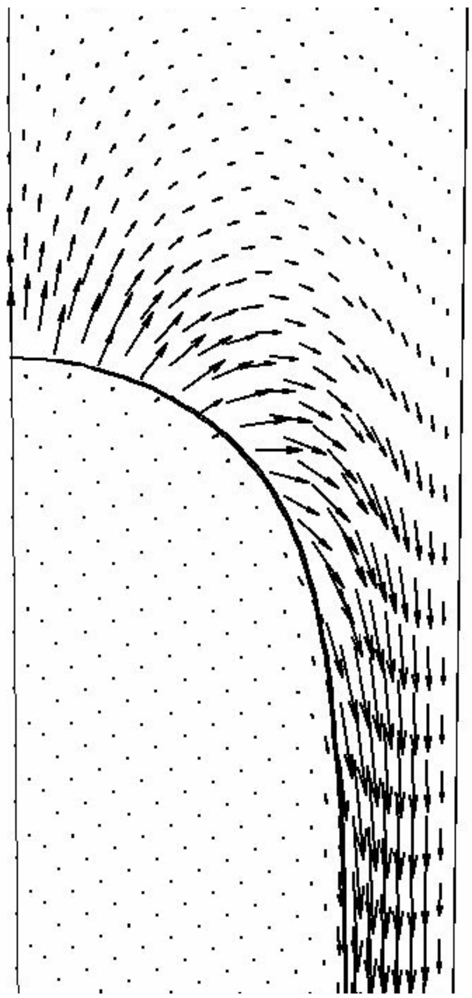

Figure 6.3. The velocity profile near the Taylor bubble nose. (Vectors are shown at only one fifth computational nodes for clarity.)

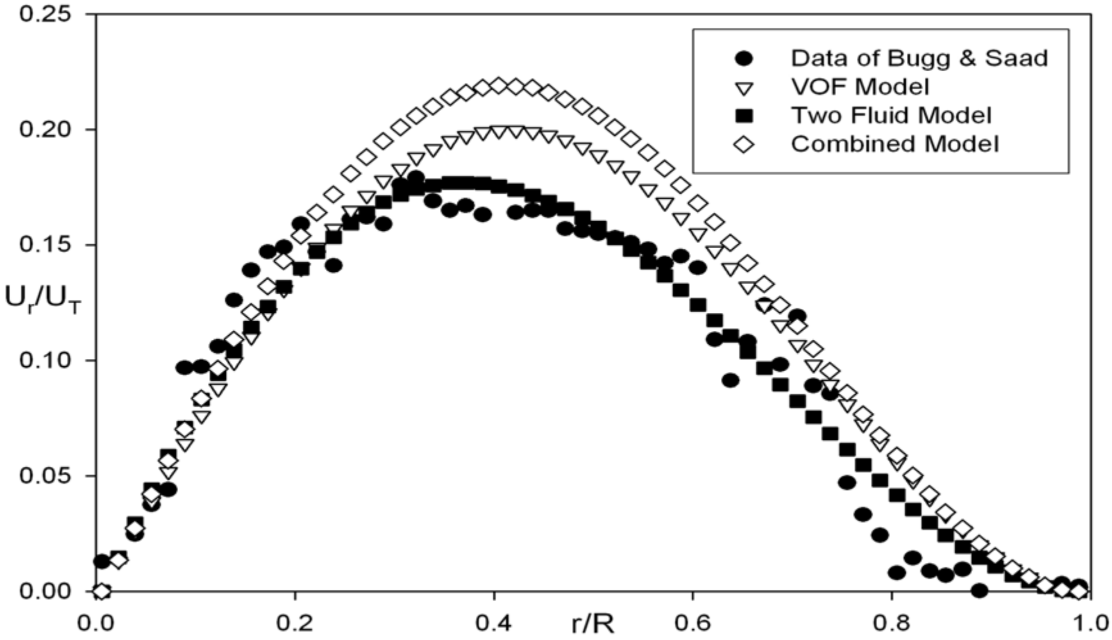

Figure 6.4. The radial velocity distribution across the tube 0.111*D* above the bubble nose and represented by cross-section A in Figure 6.1.

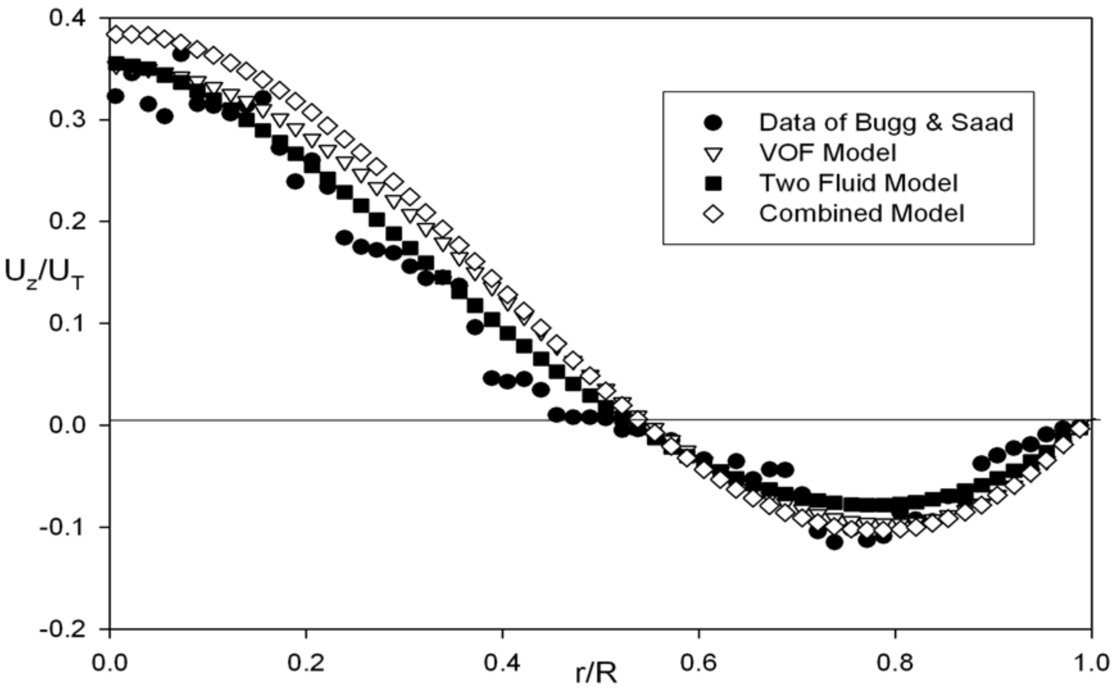

Figure 6.5. The axial velocity distribution across the tube 0.111*D* above the bubble and represented by cross-section A in Figure 6.1.

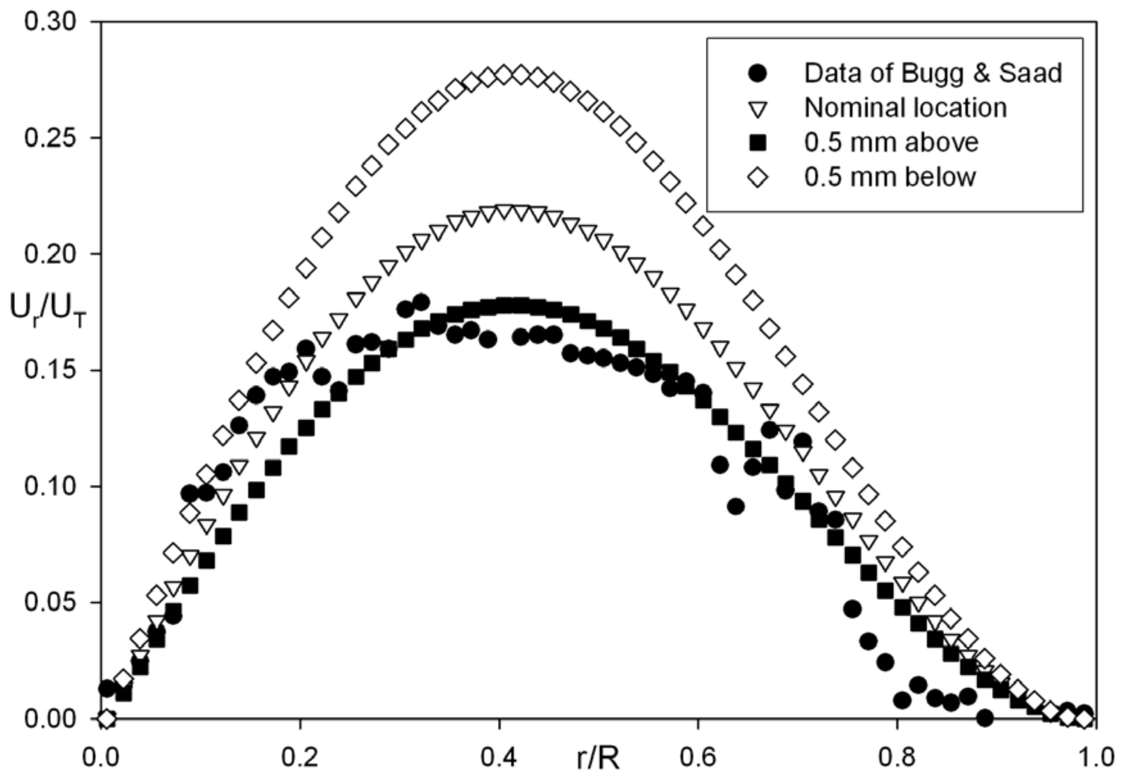

Figure 6.6. The effect of the sampling location on the radial velocity profile at a distance 0.111*D* above the bubble nose.

6.5.5 Flow profile in a developing film

In the developing film, near the bubble nose, the radial velocity is quite strong, particularly near the gas liquid interface, as the bubble pushes the liquid. The maximum radial velocity occurs near the liquid interface. At a point 0.504*D* below the bubble nose the radial velocities are reduced drastically as the fluid accelerates further and the developing film becomes thinner, as can be seen in Figure 6.7. On the other hand, the axial velocities become stronger and are high near the interface, as seen in Figure 6.8. The agreement between experimental and numerical results is good for both the radial and axial velocities.

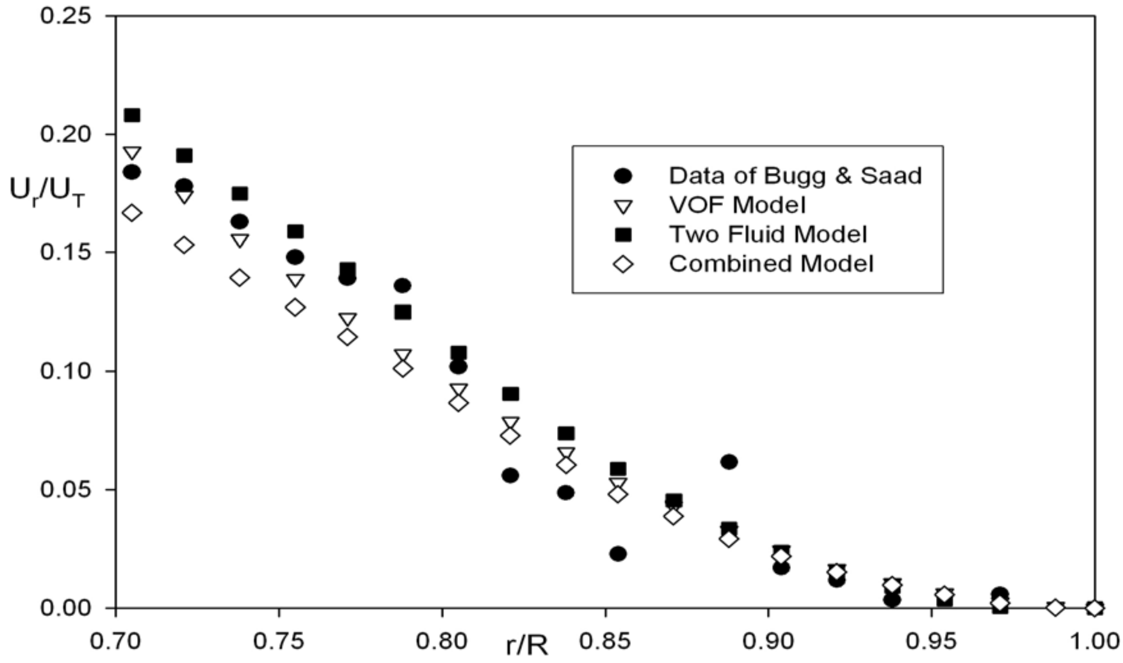

Figure 6.7. The radial velocity distribution in a developing film at a distance 0.504*D* below the bubble nose and represented by cross-section B in Figure 6.1.

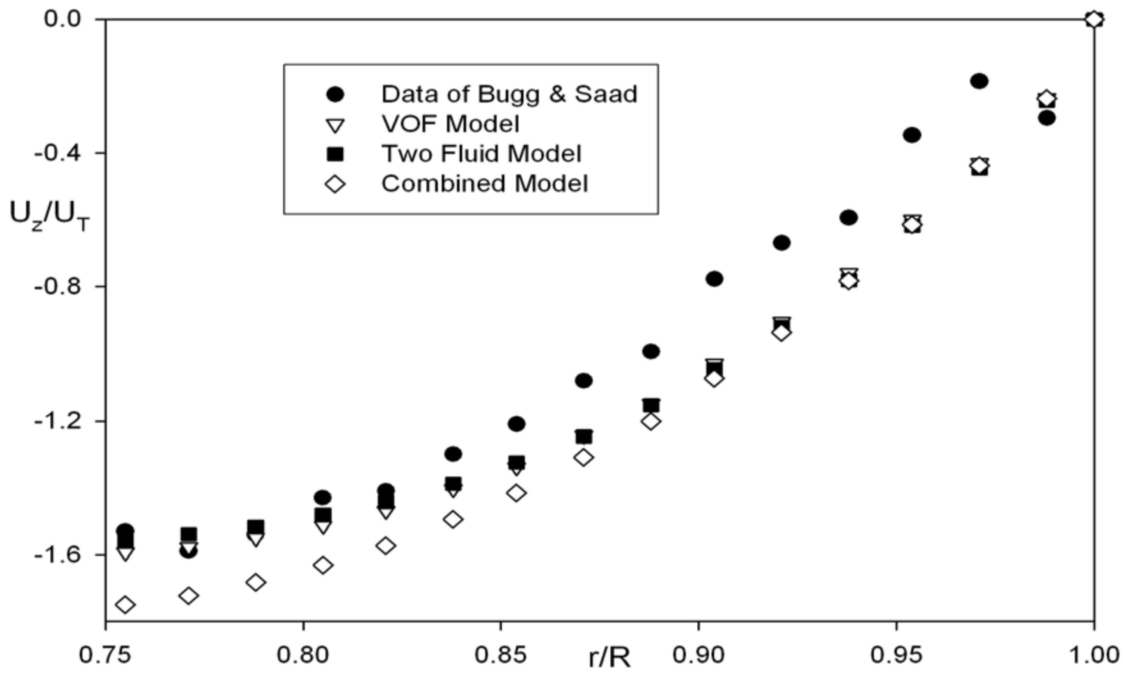

Figure 6.8. The axial velocity distribution in the developing film at a distance 0.504*D* below the bubble nose and represented by cross-section B in Figure 6.1.

6.5.6 Axial velocity in the fully developed film

The developing film accelerates and thins as it falls, until the shear stress at the wall is capable of supporting the weight of the film and a fully developed film is formed. The radial velocity in the film is then zero and the axial velocity profile no longer changes. Figure 6.9 shows the velocity profile across the fully developed film, from which it can be seen that the liquid near the gas-liquid interface moves faster than the liquid near the wall due to the negligible shear stress at the gas-liquid interface. The maximum axial velocity in the falling film is more than twice that of the bubble terminal velocity. Figure 6.8 shows excellent agreement between the results from all three numerical models and the experimental data, although the VOF results start to deviate close to the bubble interface because of the artificial mixing present in the wake region [see Figure 6.1(a)].

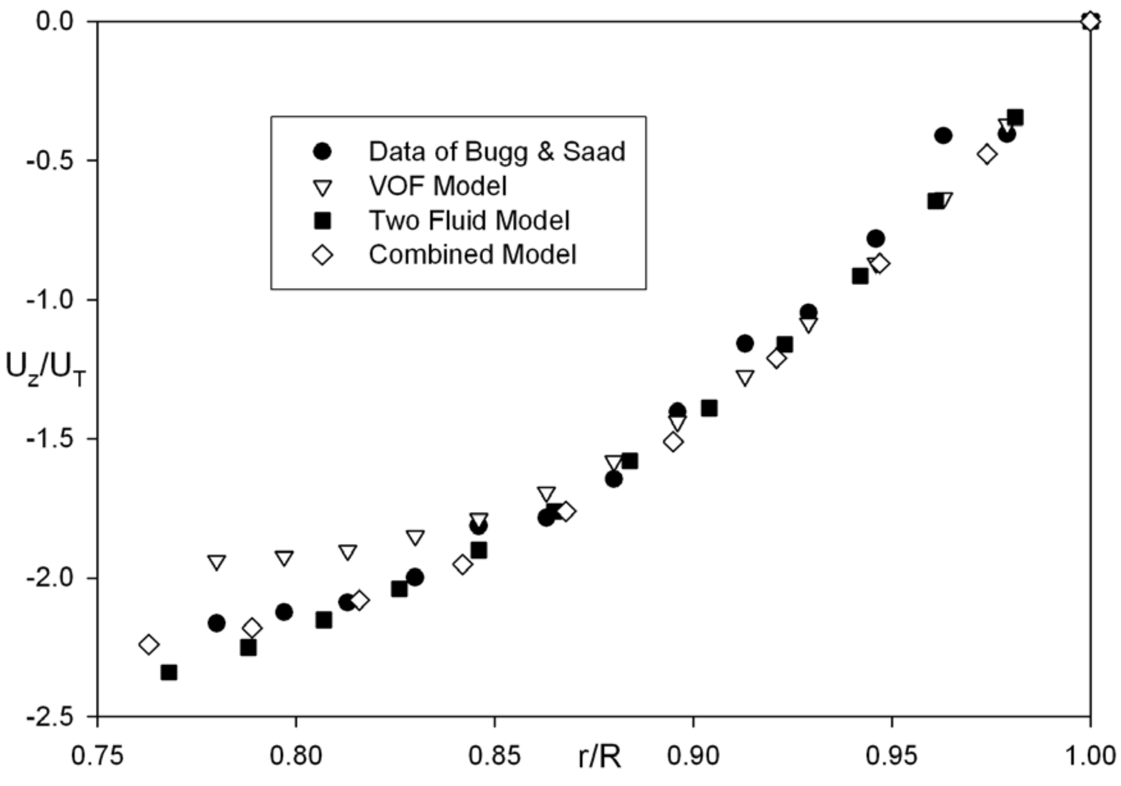

Figure 6.9. The axial velocity profiles in the fully developed falling film and represented by cross-section C in Figure 6.1.

6.5.7 Flow profile in the wake

Due to the interface mixing problem in the VOF model described earlier, only results from the two-fluid model and the combined model are presented for this region. The rapid change of flow direction in the wake region is shown in Figure 6.10. The axial velocities reduce dramatically compared with those in the falling film as the fluid changes direction and recirculation occurs in the wake. There is a strong radial velocity component in the wake region, which transfers fluid from the tube wall towards the axis. Radial velocities decay quickly to zero near the tube axis. The axial and radial velocities in the bubble wake are shown in Figures 6.11 and 6.12. These velocities were extracted at a point 0.5*D* below the bubble bottom. The agreement between the experimental and numerical results is again very good.

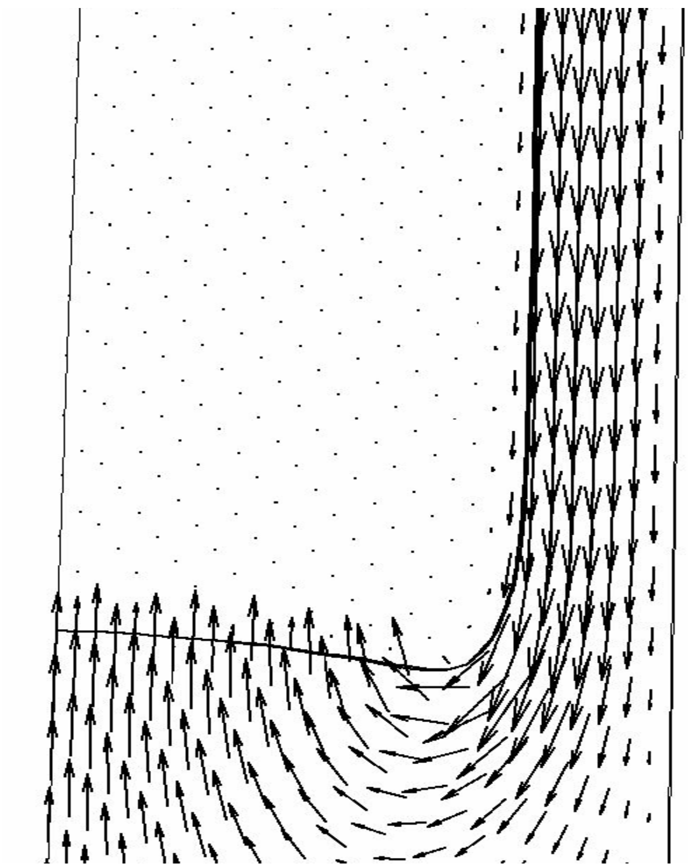

Figure 6.10. The velocity field in the wake region of the Taylor bubble. (Vectors are shown at only one fifth computational nodes for clarity).

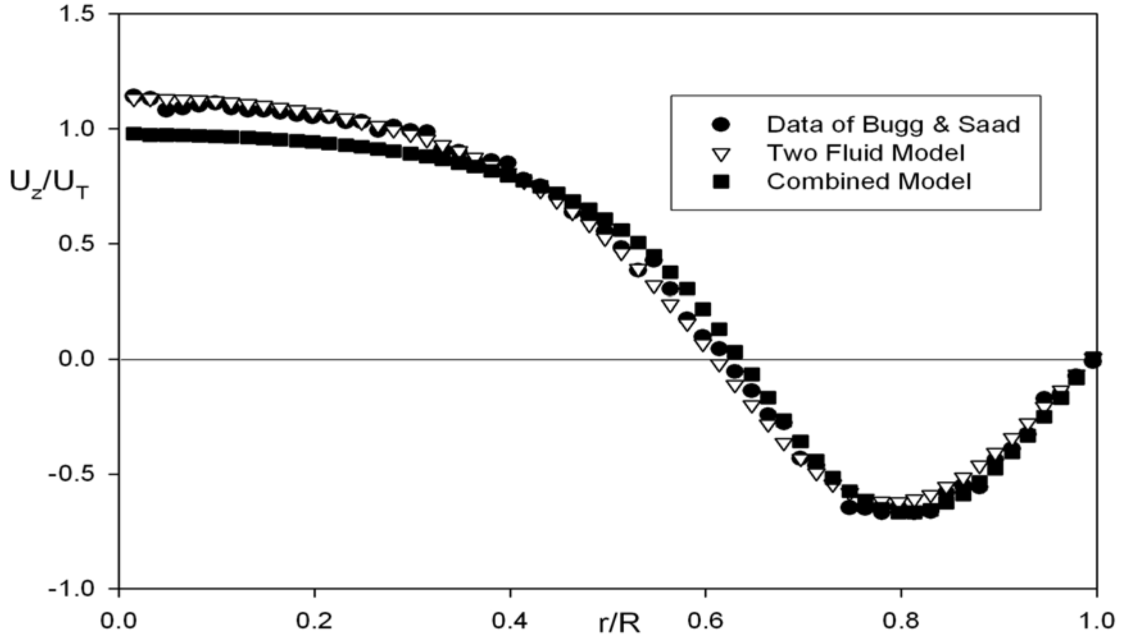

Figure 6.11. The axial velocity profile in the wake of the bubble. These velocities were extracted along plane D in Figure 6.1.

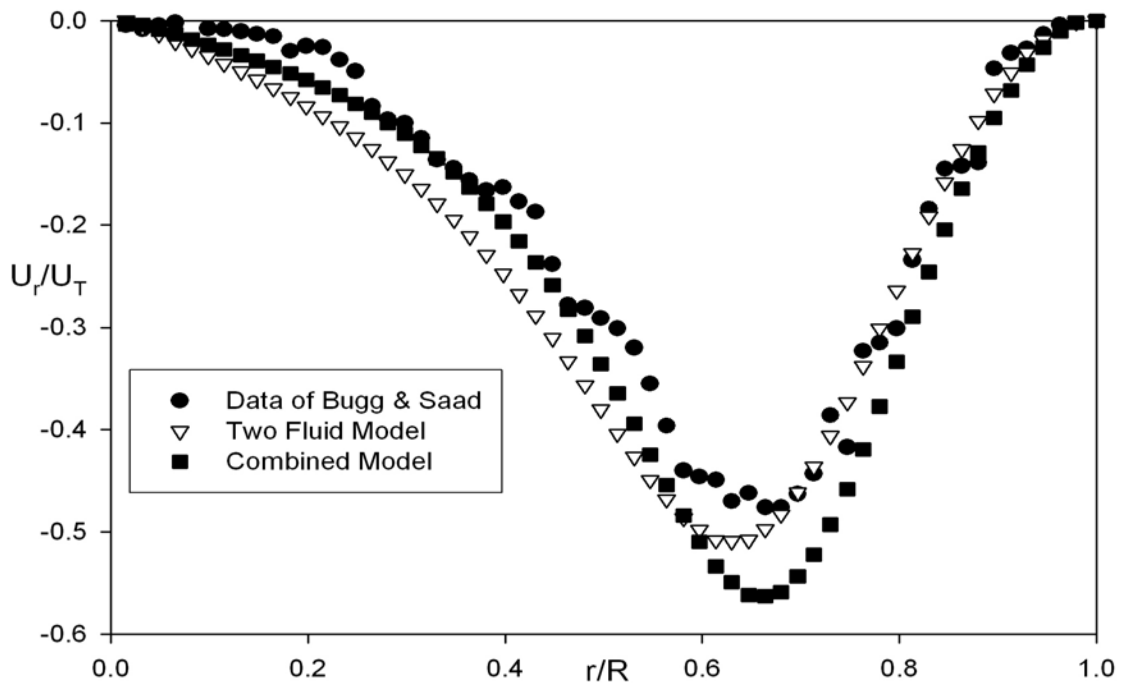

Figure 6.12. The radial velocity profile in the wake of the bubble. These velocities were extracted along plane D in Figure 6.1.

6.6 APPLICATION TO TUBULAR MEMBRANE SYSTEMS

Simulations were performed using the above model to investigate two specific issues of relevance to tubular membrane systems. Firstly, we investigated whether extraction of fluid at the membrane surface changes the flow behaviour in any way. Secondly, we investigated the wall shear stress distribution in order to determine the shape of the profile and the behaviour in the bubble wake.

6.6.1 Simulation Conditions

We used the same geometry and fluid properties as described above in these simulations, and therefore the *Eo* and *Mo* numbers are the same as those reported earlier. The only difference was that fluid was injected at the base of the tube and was allowed to exit at the top. Simulations were performed for inlet liquid velocities of 0.06 m/s and 0.1 m/s, corresponding to inlet Reynolds numbers of 114 and 190, respectively. In addition, extraction from the wall was varied between 0 - 20% for a pipe length of 16 pipe diameters. The pipe was oriented vertically so that the bubble rose due to buoyancy in the co-flowing liquid, exactly as in a real membrane system. Simulations were continued until a steady rise velocity was obtained.

6.6.2 Results

Axial shear stress profiles for the case of a liquid velocity of 0.06 m/s are shown in Figure 6.13. The shear stress is plotted against axial distance, with the profiles aligned so that the bubble is in the same physical location in each case. The figure shows the expected shear stress profile, with increased shear stress in the film region, a flat profile in the region of fully developed flow in the film and abrupt changes at the bubble nose and in the wake region. There is almost no effect of fluid extraction observable in the figure.

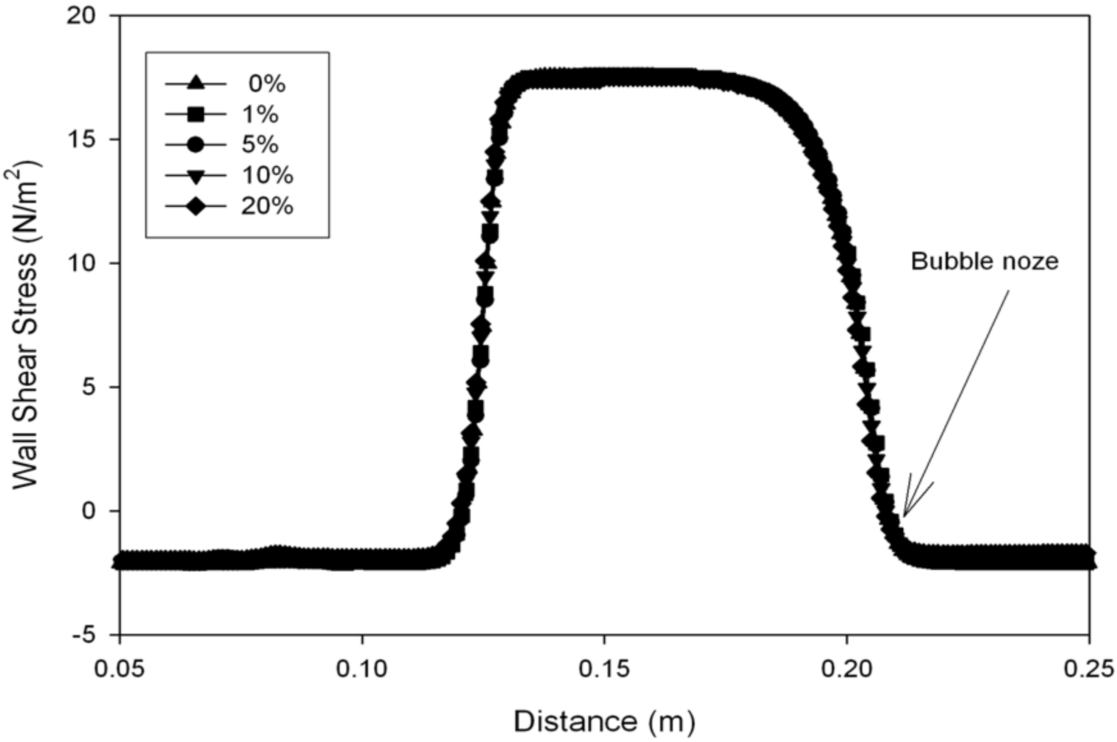

Figure 6.13. The wall shear stress distribution along the pipe for a liquid flow rate of 0.06 m/s showing the very minor effect of liquid extraction.

A detailed view of the wake region is shown in Figure 6.14. The figure shows that as the fluid is extracted there is a reduction in the magnitude of the shear stress due to the reduced flow, as expected. It also shows that there are small amplitude oscillations, which are resolved by the simulations. Examination of the velocity field shows that these are located in the region where the flow changes abruptly from vertically upwards in the pipe to descending in the film. Results for a simulation at a higher inlet liquid velocity of 0.1 m/s exhibited the same behaviour as at the lower liquid velocity and are therefore not shown here.

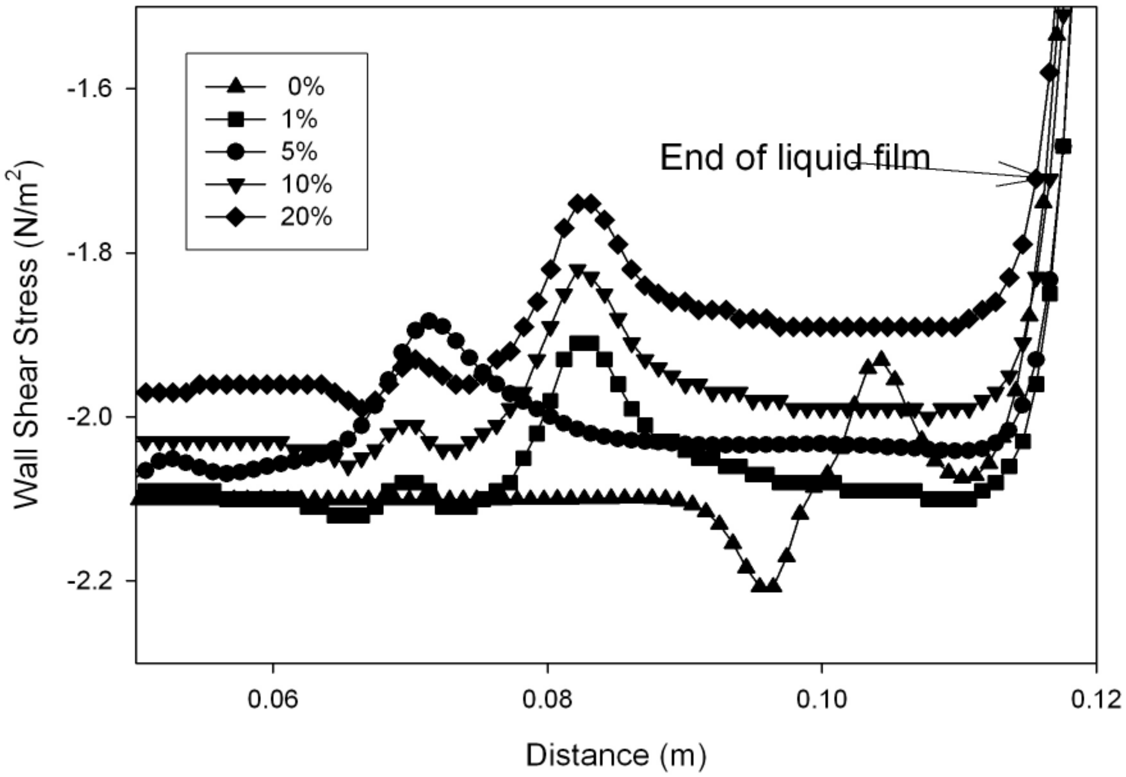

Figure 6.14. Details of the wall shear stress profile in the wake region for the liquid velocity of 0.06 m/s case and various extraction rates. The smooth nature of the stress profiles is evident.

6.6.3 Discussions

The above results show that there is almost no influence of extraction on wall shear stress profiles and that as far as flux enhancements effects caused by the rising bubble are concerned, allowing for fluid extraction is not warranted. This would apply even more so to cases where fouling has occurred, as the fluxes would be even lower.

A feature of the current results that is noteworthy is the very smooth variation of the shear stress profiles, even in the wake region. They suggest that a simple "top-hat" shaped shear stress function could be used in simplified membrane models to simulate the effect of the bubble. This is in stark contrast with the results presented by Taha and

Cui (2002b), who showed very high frequency oscillations with an amplitude of 20-50% of the peak shear stress. Their simulations were performed using similar (but not the same) numerical methods to us (see section 6.3). In addition, their flows were for higher Reynolds numbers, in the range of 1600-10,000, than those studied here (Reynolds numbers up to 200). A key difference in the simulation procedure was that they treated the simulations as being turbulent and used the RNG k-ε model to close the equations. This is a high Reynolds number turbulence model and is certainly not applicable at low Reynolds numbers. Their Reynolds number of 1600 case, which shows the very high amplitude, high frequency oscillations in the wake would be laminar and the higher Reynolds number flows would be transitional, without a fully developed log-law region near the wall, as required by high Reynolds number turbulence models. Therefore it seems most likely that their oscillations were numerical rather than physical in origin.

Note that the results presented here are restricted to laminar flow. The simulations presented are very costly because of the need to use fine meshes and small time steps to obtain accurate and stable solutions. Their extension to higher Reynolds numbers is not straightforward, as the Reynolds numbers are not high enough to assume fully turbulent flow with equilibrium log law layers at the wall. This conclusion is valid not only for the flow in the tube but is even more strongly the case in the film around the bubble.

6.7. CONCLUSION

Results for the simulation of laminar flow of a Taylor bubble in a tube with and without fluid extraction at the wall have been presented. A comprehensive validation exercise has been performed to validate a general purpose CFD code. These simulations are not limited to the determination of the steady-state bubble shape, as in most previous studies, but follow the transient evolution of the bubble. Three different models have been tested, namely a VOF model, a two fluid Eulerian model with a constant disperse phase bubble size and a combined model that uses a solution adapted disperse phase length-scale to obtain the best features of both models. The limitation of the validity of the VOF model in the wake region, due to excessive mixing, was an unexpected finding of this study, that necessitated the use of the two fluid model to overcome this numerical problem. In the two fluid model, the mixing can be avoided by defining the gas phase as a disperse phase with a large bubble size, so that any numerical mixing is undone by gravitational segregation.

In all regions around the Taylor bubble the predicted velocity profiles show good agreement with the experimental data. The bubble shape and terminal velocity are well predicted by the numerical models. Although the velocity profile in the wake region could not be obtained with the VOF model, this model produced good results in all other regions around the bubble. Using the combined model reduced the excessive thickness of the gas-liquid interface that was present in the two-fluid model that used a constant dispersed phase length-scale. The combined model produced a bubble with a sharp interface and gave the best results of the models investigated.

This exercise also highlighted the need for extremely fine computational meshes if this type of flow is to be properly resolved. There are very significant velocity gradients around the bubble nose and tail, with velocity values changing by 25% over distances of only 0.5 mm. This has implications not only for numerical modelling, where coarse grids are often used to cut the very high computational costs, but also for comparison with experimental data, where some uncertainty as to the exact location of the bubble interface is always present.

The presented results also show that there is no significant effect of the fluid extraction on the wall shear stress for conditions relevant to tubular membranes. Moreover, we show that there are no significant oscillations in the wall shear stress in the wake regions for the cases studied and that the shear stress change can be well represented by a “top-hat” profile. This conclusion is valid for a much higher range of extraction rates than used in commercial membrane systems and applies to systems with and without fouling.

Chapter 7

NUMERICAL SIMULATION OF THE EFFECT OF GAS SPARGING ON SUBMERGED FLAT SHEET MEMBRANES

7.1 INTRODUCTION

The experimental results of chapter 3 and 4 confirmed that gas-liquid two-phase flow is indeed very effective in reducing fouling for submerged flat sheet membranes. The reasons behind this effectiveness cannot yet be fully explained. In the literature there are many theories which have been proposed in order to explain why two-phase flow works (Cabassud et al., 2001; Cui et al., 2003; Pospisil et al., 2004). Therefore the aim of this chapter is to develop an understanding of the mechanisms involved in two-phase flow in order to investigate the validity of the existing theories. This aim is achieved by conducting numerical simulations of two-phase flow using two different numerical models, which have been validated in the previous chapter.

The investigation was divided into two parts. In the first part the influence of isolated bubbles rising in stagnant liquids was studied and in the second part the overall hydrodynamics in the column were studied when multiple bubbles were present. The VOF method was used to simulate isolated bubbles rising between narrow parallel plates and the two-fluid model was used to study the general behaviour of the two-phase flow dynamics when multiple bubbles are present. In both cases three-dimensional grids were used. The depth of the rectangular column used in both the experiments and simulations is very small (7 mm) and hence it might be tempting to use a two-dimensional grid, particularly for the Eulerian two-fluid simulations of bubbly flows, however, research by Pfleger and Becker (2001) showed that using a two-dimensional grid for a geometry of this nature compromises the accuracy of the solution. In their results they failed to obtain good agreement between the numerical and experimental results with a two-dimensional grid and better agreement was achieved with a three-dimensional grid. Also Wachem and

Schouten (2002) using a modified VOF model found that the computed rise velocities of bubbles in 2-D columns were much lower than those provided by the experiments of Grace (1973) in Wachem and Schouten (2002). In all the simulations presented here, the membrane was represented by an impermeable wall after having ascertained in chapter 6 that the flow through the membrane is not large enough to cause any significant changes in the macroscopic flow patterns inside the channel.

7.2 SIMULATIONS USING THE EULERIAN TWO-FLUID MODEL

The three-dimensional simulations of a single bubble rising in a stagnant liquid between parallel plates failed to produce a reasonable solution due to the multiple problems which are discussed later in this chapter. The intention of these simulations was to obtain information regarding the shear stress exerted on a membrane by a passing bubble, the liquid velocity profiles around a single bubble, the wake structure, and the variation in the pressure fields around the bubble. Instead of conducting single bubble simulations which are complex due to the fact that a gas-liquid interface needs to be resolved, an alternative approach is to use an Eulerian two-fluid model which does not explicitly calculate the gas-liquid interface. Two-fluid models are widely used to study gas-liquid two-phase flow structures in bubble columns (e.g. Delnoij et al., 1997; Buwa & Ranade, 2002). As pointed out in the review of bubble columns done by Jacobsen and co-workers (1997), many important hydrodynamic phenomena associated with the gas-liquid flow occurring in bubble columns, such as bubble formation, bubble coalescence, and bubble break-up are still not well understood despite the wide industrial occurrence of bubble columns. There is no general agreement about the final form of the governing equations and hence most numerical work on bubble columns is about development of proper numerical models. Also in bubble columns the main feature of interest is mass transfer. In this work, mass transfer was not considered; instead it was features such as gas and liquid velocity profiles, the shear stress on the membrane and calculation of the distribution of void fractions that were of interest. In this work, a generalized model available in a commercial CFD code was used. Unlike the three-dimensional single bubble simulations, this model does not require an extremely fine computational grid, as averaged equations are solved which do not resolve individual bubbles. This result in a huge saving in the amount of computer time and computer power needed.

7.2.1 The two-fluid model

In this model, the continuous (liquid) and the dispersed (gas bubbles) phases are considered in an Eulerian representation and the model is based upon mass and momentum balances for each phase, obtained over a volume within which the fluid can be treated as a continuum mixture. The basic description of this model, including the governing equations, have been presented in chapter 6, section 6.4.1. The additional information required for these simulations not included there, is discussed here. The two-fluid model treats each fluid as a continuum having its own velocity field and occupying the whole domain, with the presence of each fluid represented using a volume fraction. The model allows a slip velocity to exist between the liquid and the gas phases. In chapter 6, the model was applied to a problem involving an interface, however, this model is mostly used for cases where the bubble size is smaller than the grid size, as it is based on volume averaged equations. Unlike in Chapter 6, in which the model was applied to laminar conditions, here the liquid flow has been treated as turbulent. The standard two equation k-ε turbulence model has been used to account for turbulence in the liquid phase and the zero-equation dispersed phase model is used to account for turbulence in the gas-phase. The Sato particle-induced turbulence correction is used in order to model the extra turbulence created by the presence of the bubbles (Sato & Sekoguchi, 1975). The drag force has been modeled via the Grace correlation, which takes into account the fact that as the bubbles become larger, their shape changes, first to ellipsoidal and then to spherical cap, resulting in a volume fraction dependent drag coefficient (Sato & Sekoguchi, 1975). The turbulence dispersion force, which arises because of the liquid phase turbulence action on the bubbles, is modelled using the model of Lopez de Bertodano (1992).

7.2.2 Description of the Geometry

The geometry used in the experiments consists of a rectangular tank which is 540 mm high × 30 mm deep × 200 mm wide. The flat sheet membrane, which is about 2 mm thick, sits in the centre of the tank. The membrane is located 100 mm below the top of the tank. A gap of about 7 mm exists between the membrane and the side walls. The membrane occupies the whole width of the tank. The air diffuser is made up of a half inch diameter stainless steel tube with multiple nozzles. There are 10 nozzles on the diffuser varying from 0.5 to 2.0 mm in diameter. The diffuser is located 100 mm beneath the membrane and 50 mm above the bottom of the tank. The flow pattern on both sides of the membrane should be more or less the same, thus for the simulation purposes, only half of the tank was modeled by placing a symmetry plane along the width of the column. The geometry of the tank used in the simulations is shown in figure 7.1 (a) with the mesh shown in figure 7.1 (b). In another set of simulations, baffles were created in the gap between the membrane and the wall. The baffles were used in the experiments in order to improve the distribution of air across the membrane surface and hence to improve the uniformity of the wall shear stress. In the experiments, a fixed number of baffles were used, whereas in the CFD simulations different numbers of baffles were tested in order to understand the effect of the baffles on the overall wall shear stress and to establish an optimum number of baffles.   Figure 7.2 shows a typical geometry setup when baffles were used, and corresponds to a case with 13 baffles.

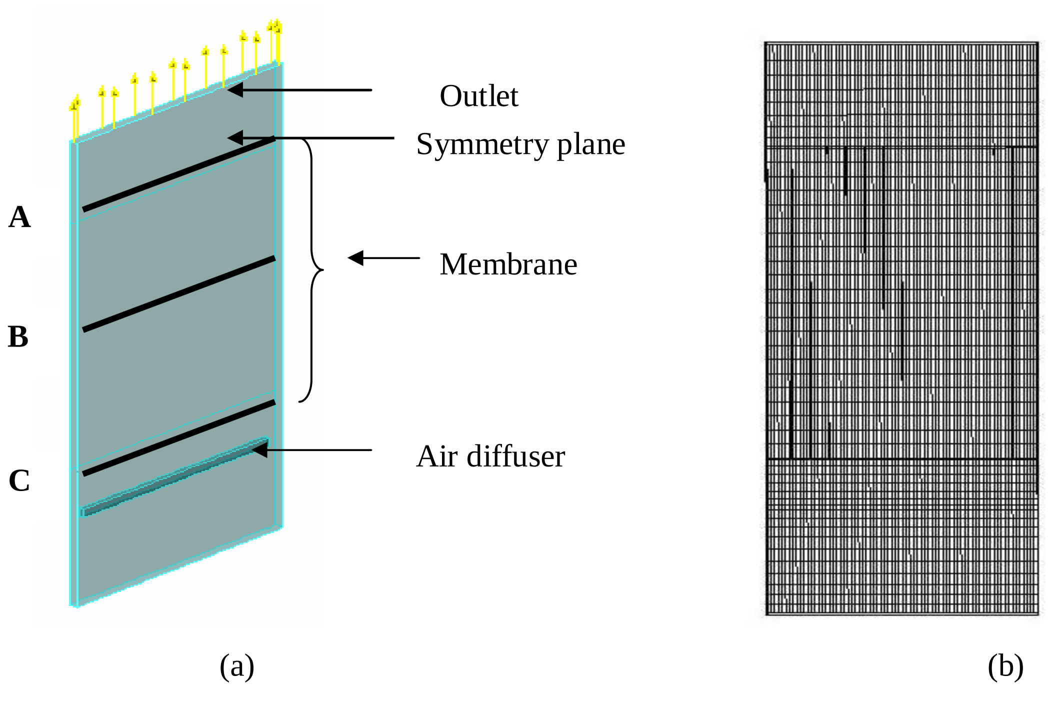

Figure 7.1. The geometry of the tank is shown in (a) and the computational mesh is shown in (b). Cross-section areas A, B and C (marked with a solid black line) represent graphical planes where data were extracted at 450 mm, 300 mm (halfway through the column) and 150 mm from the bottom respectively.

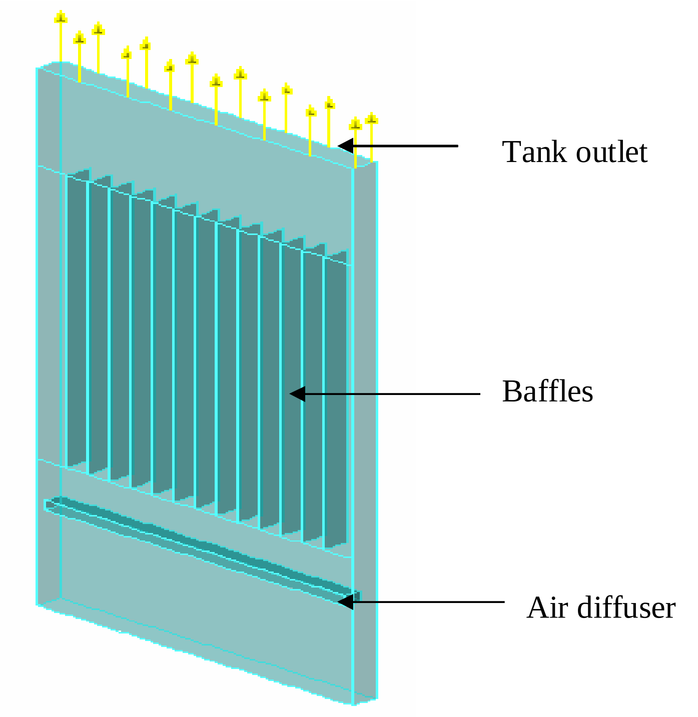

Figure 7.2. Schematic diagram of the tank showing baffles located between the membrane and the wall.

7.2.3 Simulations

The governing equations were solved using a commercial CFD code, CFX 5.6 from ANSYS. This code solves the equations on an unstructured grid using a finite volume method. However, for the Eulerian simulations described in this section, a three-dimensional structured grid generated using CFX Build was used. The grid was non-uniform and consisted of 42 cells (across the vessel height) $\times$ 43 cells (across the vessel width) $\times$ 8 cells (across the vessel depth). A fine enough grid was chosen to achieve grid independent results. An example of the grid used is shown in figure 7.1 (b). The grid size was biased, with cells expanding with height in the region above the membrane. This was done because this area is above the membrane and the flow pattern in that region is thus of little interest.

The flow was assumed to be transient. The fluids were water and air at 293 K. The fluids were assumed to be incompressible and isothermal and to have constant fluid properties. For all walls and the membrane, the boundary condition was set to free slip for air and no slip for water. The top wall of the column was specified as a degassing boundary condition to allow the air to escape. The air diffuser through which gas entered was treated as a volume source of air, having an air flow rate of between 2 and 8 l/min, depending on the experimental condition being modeled.

A constant time step of 5×10^{-2} s was used throughout the simulations. The maximum number of coefficient iteration loops per time step was set to five and this was sufficient to achieve convergence of the residuals during each time step. The high resolution differencing scheme was used with the first order backward Euler scheme being used for the transient terms. The simulations were run for a total real time of 140 seconds. This allowed sufficient time for air to rise to the top of the tank and for the flow to reach a fully developed state. Each simulations took about 48 hours on a 2.4 GHz Zeon Intel dual processor.

7.2.4 Shortcomings of the Euler-Euler two-fluid model

The major shortcoming of this model is that it represents a bubble population with a single bubble size. This differs significantly from the experimental conditions, where there is a bubble size distribution from very small to very large bubbles, all present at once. In order to understand the impact of bubble size, simulations were done with different bubble sizes. Experiments of Buwa and Ranade (2001a) have shown distinctly different dynamic characteristics for different bubble sizes. In our experiments there is also a significant amount of bubble coalescence, as shown in chapter 5. This effect is not taken into account by the two-fluid model used in this study. Nevertheless, the predictions obtained from the model could be generalized to indicate what happens in the experiments as variables are modified. For example, the variation of the overall shear stress with air flow rate predicted by the model gives an indication of what happens in the experiments as the air flow rate is increased.

7.3 RESULTS

Firstly, the effect of inlet air flow rate on gas and liquid flow profiles is presented, followed by the effect of bubble size. Then membrane wall shear stress distribution is discussed and lastly the effect of the baffles on the wall shear stress at the membrane surface is presented. The predicted influence of gas velocity, bubble size and baffles on flow profiles and wall shear stress are compared with experimental data in the discussion section.

7.3.1 The influence of gas inlet velocity

In this section the effect of the air injection rate on the gas and liquid velocity flow profiles in the tank is examined. The bubble diameter for these simulations was specified as 5 mm. The effect of bubble size is presented in the following section. Figure 7.3 shows the vector plots for superficial gas velocity profiles at different times for the flow rate of 2 l/min and figure 7.4 shows the vectors for the 8 l/min flow rate. As soon as the gas leaves the diffuser it moves towards the edges of the column as it rises. The gas seems to divide into two main streams that flow upwards near the edges of the column. In addition, these two main plumes of gas move up in a meandering manner. The degree of meandering is small for the low air flow rate of 2 l/min and is much higher at the higher flow rate of 8 l/min. Meandering of gas plumes has been reported by other researchers, such as Pfleger & Becker (2001), Vitankar et al. (2002), and Buwa & Ranade (2002) who found that the amplitude of the gas plume oscillation increased with an increase in the gas flow rate, with bubbles almost touching the sidewalls at very high gas flow rates. The meandering of the gas stream has also been observed both experimentally and numerically by several researchers (Delnioj et al., 1997; Jacobsen et al., 1997; Spicka et al., 2001; Deen et al., 2001) and was observed visually in this study. According to Delnioj et al. (1997), it is the vortices in the liquid stream that causes the gas to move in a meandering fashion. At low gas flow rates, Kuwagi et al. (2000), observed that the gas bubbles rise almost in a straight line in a stagnant liquid and start to move in a zigzag fashion only when the gas flow rate was increased.

The migration of bubbles towards the column walls as seen in these simulations was also observed by other researchers in two-dimensional (2-D) rectangular columns such as Tzeng et al. (1993). Tzeng et al. (1993) studied bubble migration rates in 2-D columns and concluded that they are proportional to the bubble size and inversely proportional to the bubble-to-wall distance. They attributed this migration to the uneven dissipation of turbulence generated by bubble wakes. Sekoguchi et al. (1974) studied isolated bubbles in a rectangular column and observed that small bubbles (less 5 mm diameter) moved to a region near the wall regardless of their inlet location and larger bubbles (greater than 5 mm) migrated towards the core of the duct.

Figure 7.5 and 7.6 represents liquid velocity profiles at different times during the simulation for the gas flow rate of 2 and 8 l/min, respectively. There is strong liquid upflow near the column edges, where most of the gas is flowing up and liquid flows downward along the centre of the column and along the edges. The meandering of the gas bubbles also causes the liquid to meander and hence at low gas velocity there is less meandering of the liquid as compared with high gas velocities.

The flow pattern described above differs slightly to what was observed experimentally at air flow rates of 4 l/min upwards. In the experiments, bubbles were observed moving away from the column edges towards the centre except for the lower flow rates, such as 2 l/min, where bubbles rose in an almost rectilinear path as shown in ‘Video 3’ in Appendix B. Migration of bubbles towards the column centre has also been observed on other bubble column studies (Jakobsen et al., 1997; Lapin & Lübert, 1994a). It is not clear what constituted this difference in the observed and simulated flow patterns but it may be linked to the fact that it was difficult to model the gas sparger exactly as it was in the experiments. Sekoguchi et al. (1974) observed that bubbles smaller than 5 mm migrated towards the column walls and those larger than 5 mm tended to migrate towards the column centre. This agrees with the trend that was observed in the simulations of this study for the bubble size of 5 mm. However, simulations with larger bubble sizes, 10 and 15 mm, also showed bubbles moving towards the column walls. This is contrary to both the observations of Sekoguchi et al. (1974) and to the experimental observations of this study. It is assumed that this discrepancy does not a have a significant bearing on the membrane cleaning mechanisms of two-phase flow which this study is trying to establish.

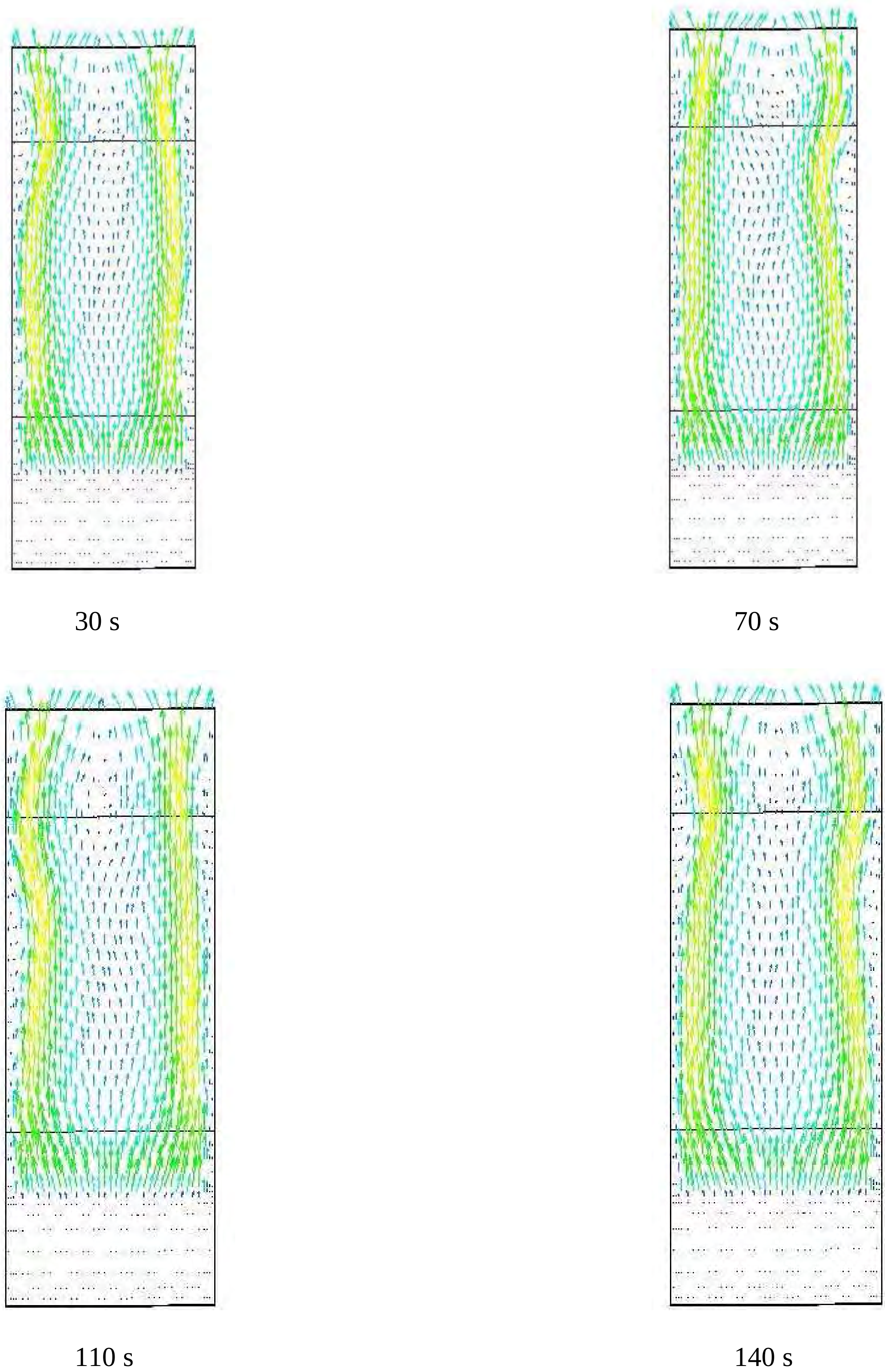

Figure 7.3. Air superficial velocity profiles at different times for an air flow rate of 2 l/min. The maximum air velocity is about 0.05 m/s.

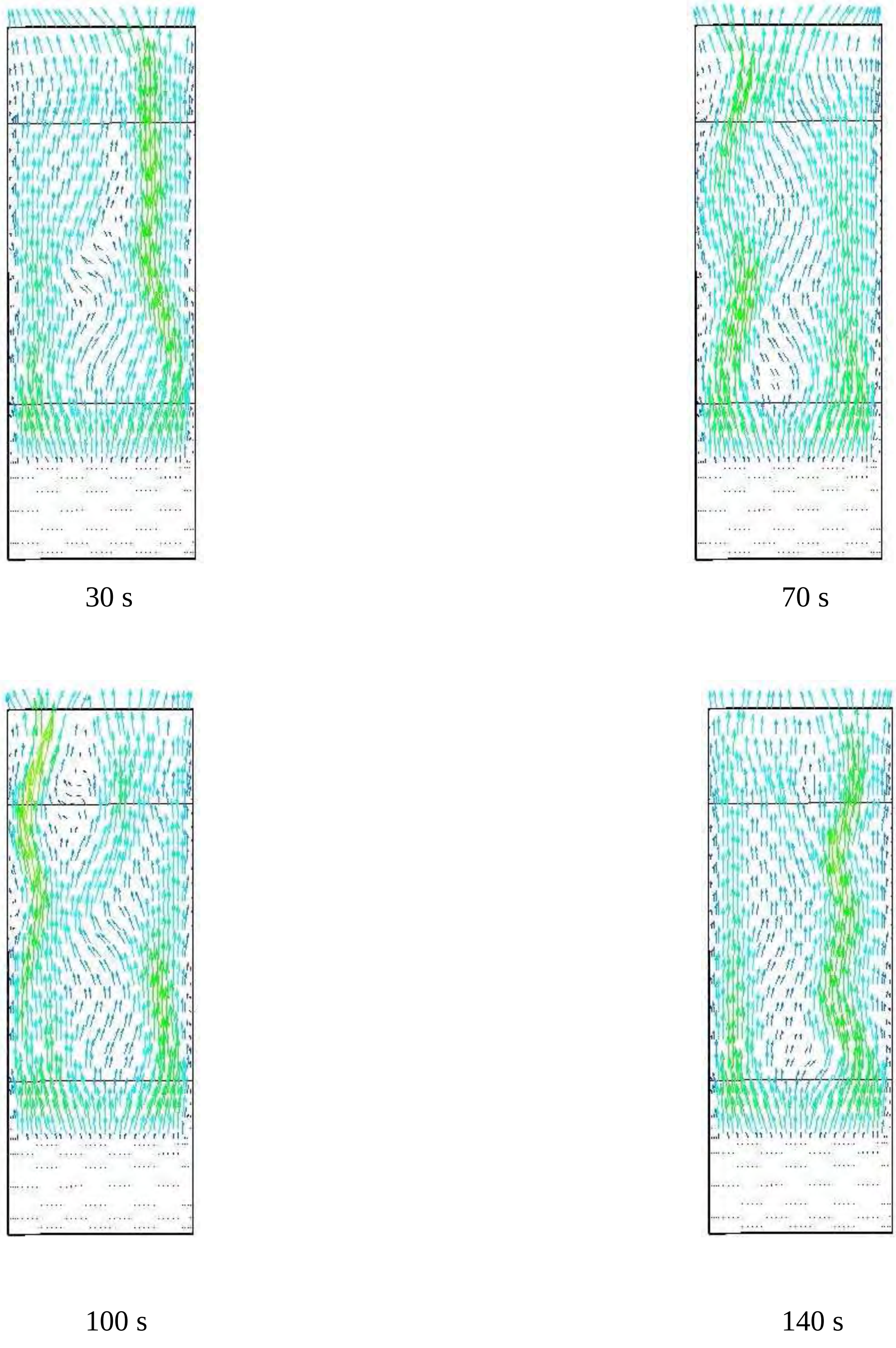

Figure 7.4. Air superficial velocity profiles at different times for an air flow rate of 8 l/min. The maximum air velocity is about 0.36 m/s.

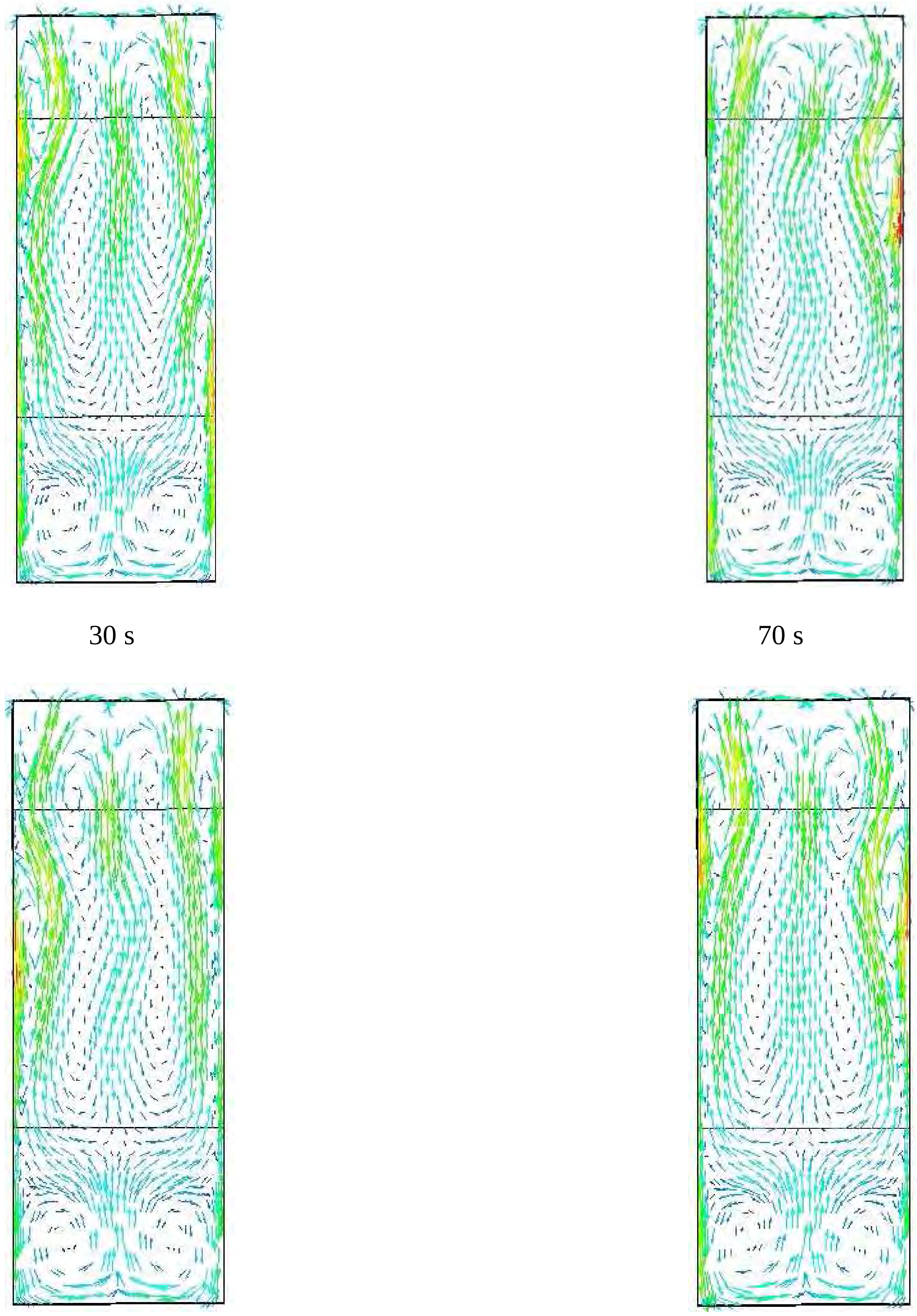

30 s 70 s

110 s 140 s

Figure 7.5. Water superficial velocity profiles at different times for an air flow rate of 2 l/min. The maximum water velocity is about 0.32 m/s.

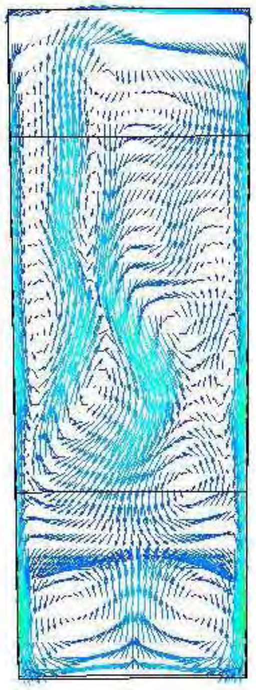

30 s

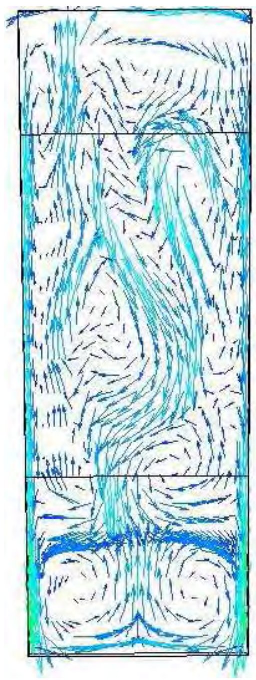

70 s

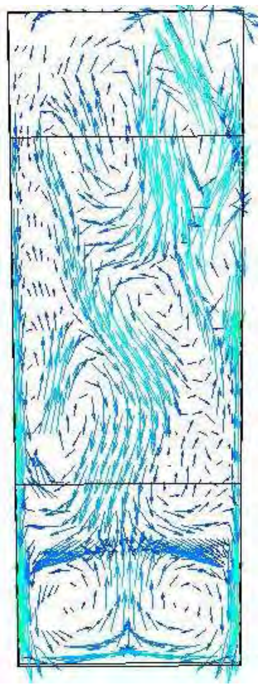

100 s

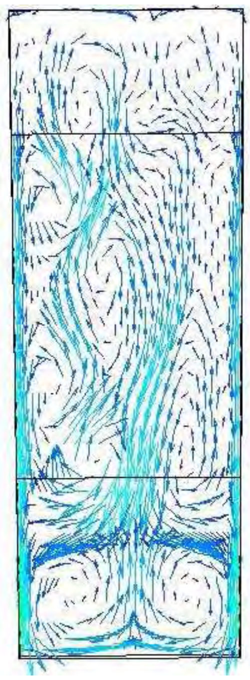

140 s

Figure 7.6. Water superficial velocity profiles at different times for an air flow rate of 8 l/min. The maximum water velocity is about 0.77 m/s.

The influence of air injection rate on vertical air and water velocities in the tank was examined. The air vertical velocity profile distributions halfway through the column are presented in figure 7.7, whilst those for the water are presented in figure 7.8. Both the air and the water vertical velocity distributions confirm the trends observed in the vector plots of figures 7.3 to 7.6. All the gas velocities are positive implying that all bubbles are flowing up and for water there are strong downward (negative) velocities at the centre of the column and near the column edges. The highest magnitude of the liquid downward velocity is almost the same as that of the upward velocity (around 0.24 m/s).

The vertical velocities are presented only for a cross-section halfway through the column but almost similar trends were observed near the top of the column and near the bottom of the column. What can be observed from these vertical velocity profiles presented here is that they do not show a strong dependence on the gas injection rate although slight differences exist. The air flow rates of 2 and 4 l/min seem to have higher magnitudes of maximum velocities than the air flow rates of 6 and 8 l/min but the plots for the air flow rates of 6 and 8 l/min have more up and down fluctuations which is indicative of the meandering behaviour of the gas stream at such higher air flow rates. This suggests that the meandering of the gas causes its upward / vertical velocity to be reduced slightly. In the two sections of the column where there is strong up flow of air, the air velocities are much greater (almost by 40%) than those of water thus indicating as expected that air bubbles are rising faster than water since air is blown into a stagnant liquid and rises due to buoyancy.

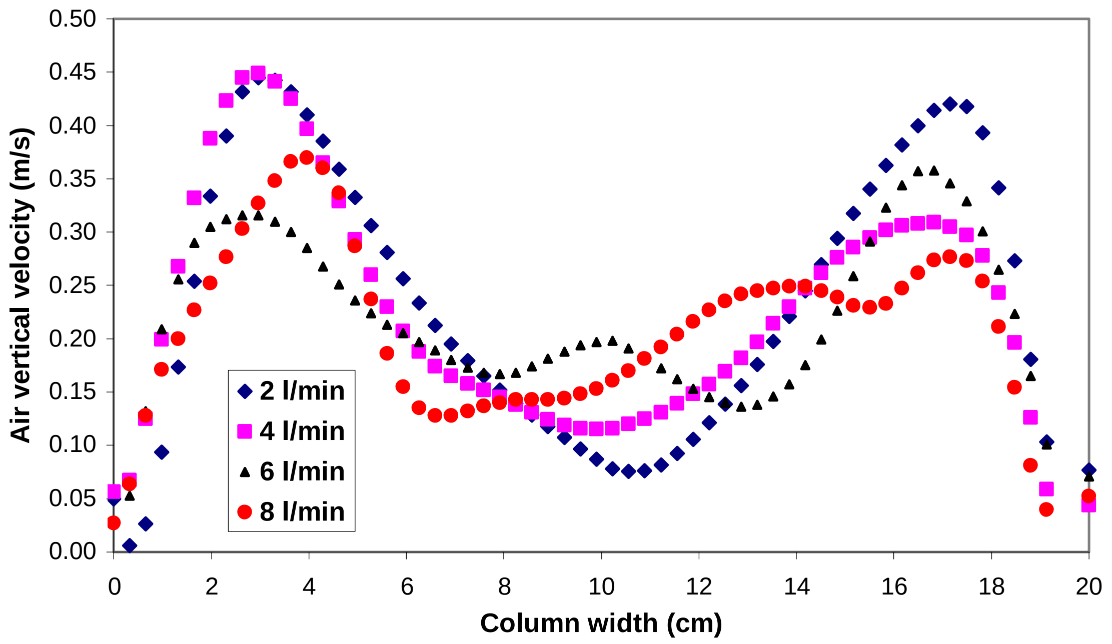

Figure 7.7. Air vertical velocity profile distribution halfway through the column 300 mm from the bottom.

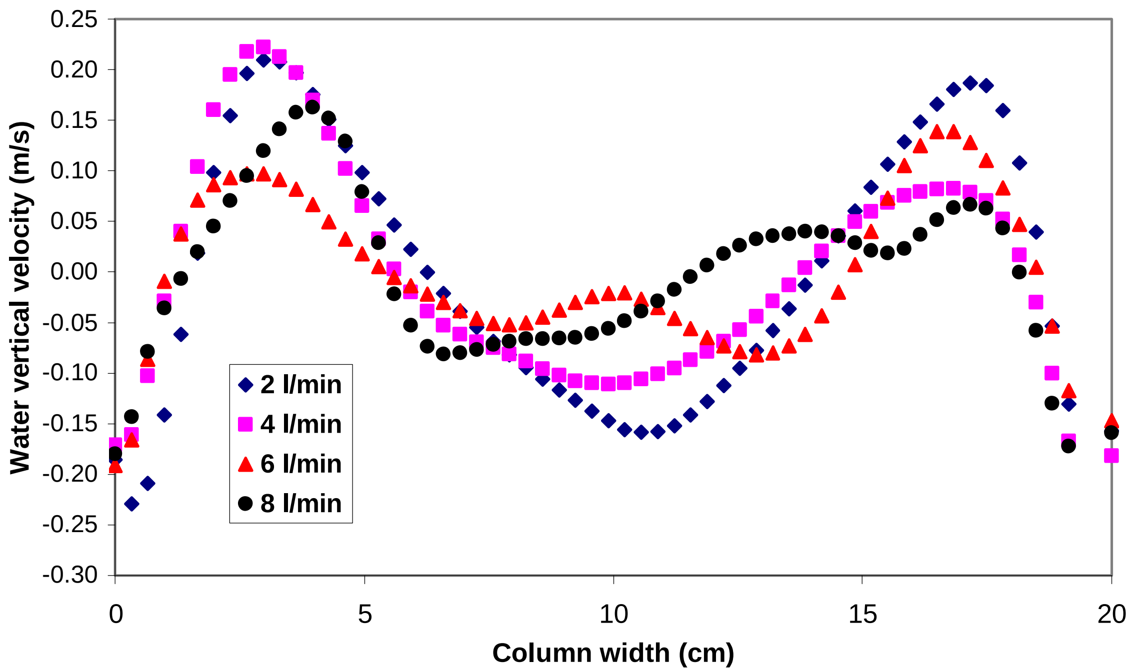

Figure 7.8. Water vertical velocity profile distribution halfway through the column 300 mm from the bottom.

The gas injection rate was found to have no pronounced effect on the transverse or horizontal velocity profiles. Air and water horizontal velocity distributions were extracted at the bottom of the column (30 mm above the air diffuser) and near the top of the column (50 mm below the air-water interface or degassing boundary). At both locations the horizontal velocity profiles for both air and water look almost similar but the actual velocities are slightly different with those of air being marginally higher. Only the plots for air are shown. Figure 7.9 shows air horizontal velocities across the column near the bottom of the column for gas injection rates of 2 to 8 l/min. From this figure it can be seen that there is strong horizontal movement of the gas away from the column centre and moving towards the column edges. This causes the gas to be divided into two main streams which rise close to the column edges. Near the top of the column (Figure 7.10) the horizontal movement of the gas is random and the maximum horizontal velocity is almost half of that in the lower part of the column. Due to meandering of the gas streams, it is expected that the horizontal velocities of air fluctuate from time to time, however the vertical component of the gas velocity is almost 85% higher than the horizontal component based on the maximum velocities observed. Thus the horizontal movement of the gas is less significant than the vertical movement.

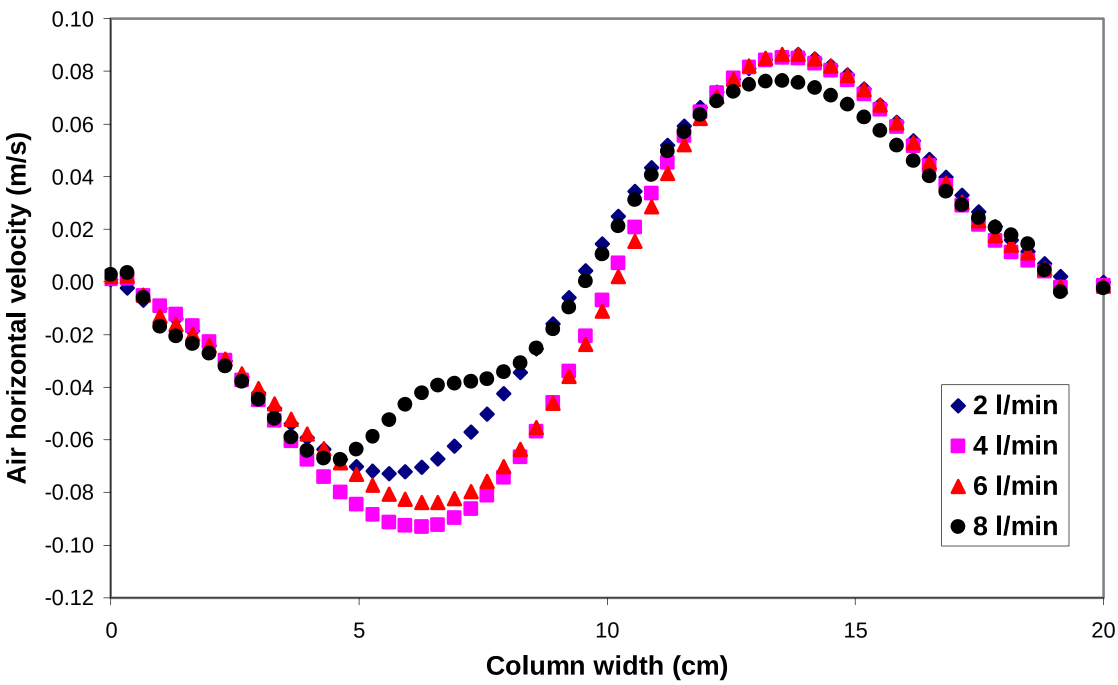

Figure 7.9. Air horizontal velocity profiles distribution near the bottom of the column 150 mm from the bottom.

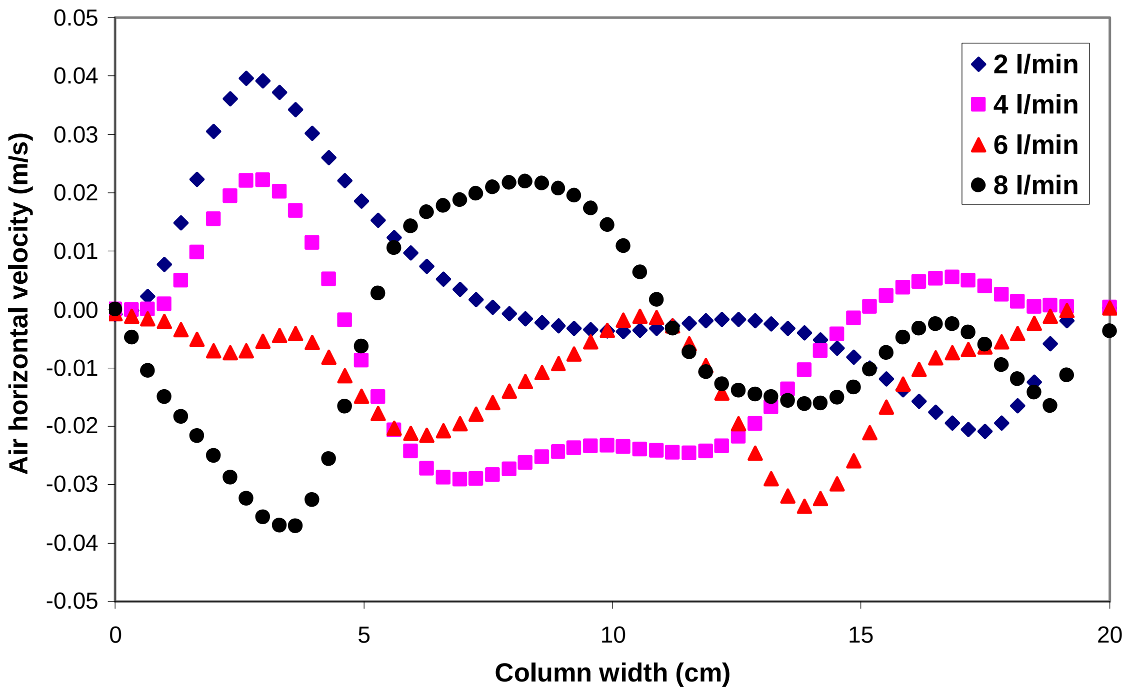

Figure 7.10. Air horizontal velocity profiles distribution near the top of the column 450 mm from the bottom.

Thus far, the gas injection rate has been shown to have no significant effect on the instantaneous vertical and horizontal velocities of both air and water in the column at various locations except that higher oscillations of the gas and the water streams were observed at higher air flow rates. This strongly suggests that bubble rise velocity depends mainly on the bubble size and not on the gas injection rate, however, in single bubble simulations Valencia et al. (2002) did find the bubble rise velocity to increase with the gas injection rate although their bubble size was not really constant.

The distribution of gas hold-up in the column could play a very important role with regards to the application of gas-liquid two-phase flow as a cleaning mechanism for submerged membrane systems. Gas hold-ups at various cross sections of the column were extracted and plotted against the air flow rate. A similar trend was observed at all cross sections. A typical plot of gas volume fraction versus air flow rate across the column is shown in figure 7.11. This plot represents gas volume fraction distributions halfway through the column. Figure 7.11 shows that gas hold-up in the column increases with the air injection rate as expected but most importantly, this figure shows that as gas injection rate increases, the distribution of gas hold-up becomes more uneven. The data in Figure 7.11 also agrees with the experimental data of Figure 5.7 in chapter 5.

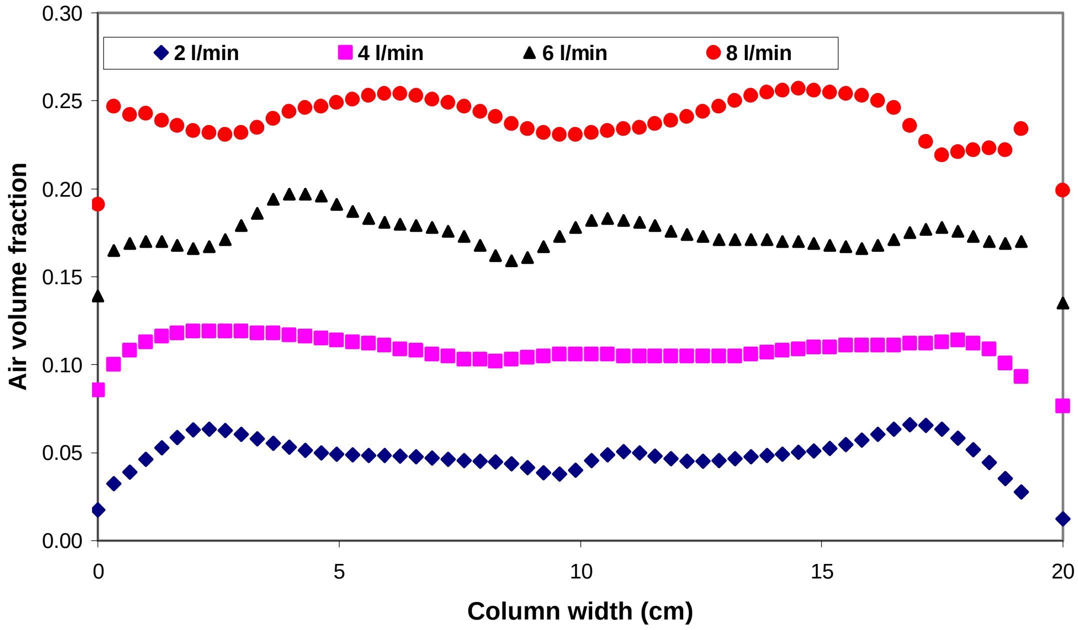

Figure 7.11. Distribution of air volume fraction halfway across the column (300 mm from the bottom) for various air flow rates.

7.3.2 Effect of bubble size on air and water velocity profiles

Buwa and Ranade (2001a) have reported experimental data on the dynamics of gas-liquid flows with different spargers, as well as with different gas injection rates. Their results indicated that the key dynamic characteristics depend on the bubble size and bubble size distribution. However, with the current two-fluid model we were unable to study the effects of bubble size distribution, only the effects of bubble size could be investigated. As pointed out in the introduction, one of the limitations of the standard Eulerian two-fluid model available is that the bubble size has to be specified and only one bubble size can be used per simulation. All the results presented in the previous section were those obtained with a bubble size of 5 mm. In the actual experiments, a bubble size distribution exists at all air flow rates. The analysis done in chapter 5 indicated that the bubble size does play a role in terms of the effectiveness of two-phase flow on membrane cleaning. In order to obtain some further understanding of the effect of bubble size on the efficiency of the two-phase flow, simulations were done with different bubble sizes and the results were compared. For these investigations the air flow rate was kept constant at 4 l/min. This air flow rate was chosen because, based on the previous results, at this air flow rate, the meandering of the gas starts to become pronounced, whereas at 2 l/min bubbles rise almost vertically.

Figure 7.12 presents air velocity profiles for bubbles of different sizes at the final time of the simulation, whilst figure 7.13 presents the corresponding water velocity profiles. The vector plots for both air and water show an increase in the degree of meandering as the bubble size is increased. This is more apparent in the water velocity vector plots. For the 2 mm bubbles (Figure 7.13 a), there is a slight sideways movement of the water stream but when the bubble size is 15 mm (Figure 7.13 d) the amplitude of the water stream meandering is increased quite significantly. Similar observations were made by Buwa & Ranade (2002), who noted that the plume oscillation period of around 10 s for larger bubbles (20 mm) was much greater than that of smaller bubbles (5mm). The improved liquid recirculation at larger bubble sizes may assist in minimising fouling on the membrane. The 15 mm bubbles used in the simulations are not as large as some of the bubbles that were measured experimentally, which were about 70 mm but the bubble size distributions reported in chapter 5 indicated that the percentage occurrence of such large bubbles is low and that the bubble size with the highest frequency was 4 to 6 mm. Thus the simulation results obtained using a 5 mm bubble can be used with high confidence in terms of understanding the overall behaviour of the experimental system. The effect of bubble size on membrane shear stress is discussed in the following section.

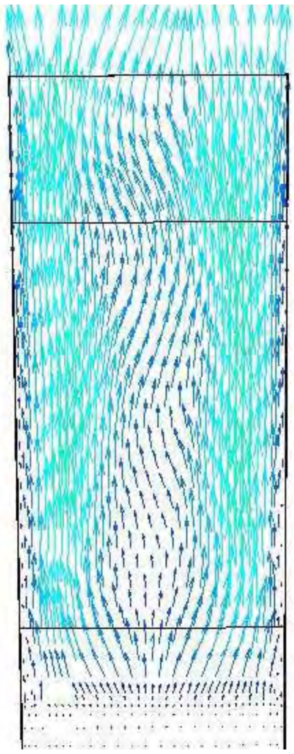

(a) 2 mm

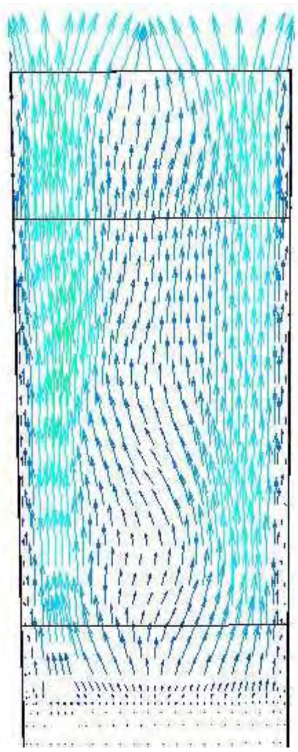

(b) 5 mm

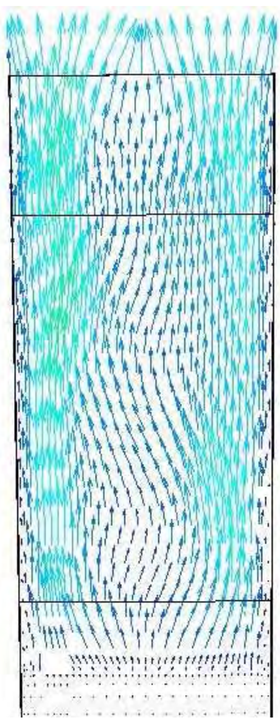

(c) 10 mm

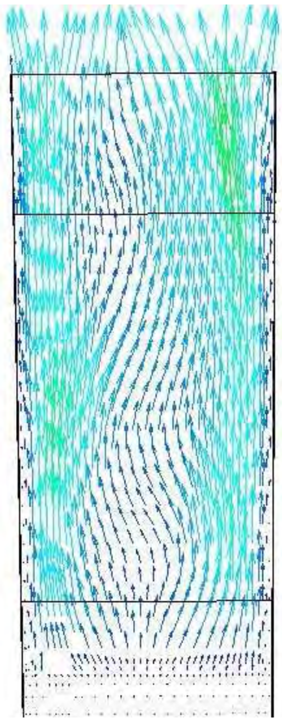

(d) 15 mm

Figure 7.12. Air superficial velocity profiles for bubbles of different sizes at the end of the simulation. The air velocity ranges from 0.097 to 0.1m/s.

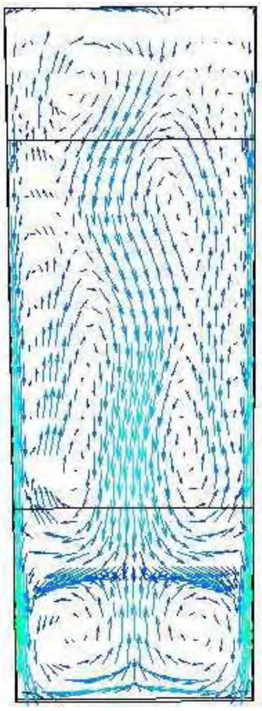

(a) 2 mm

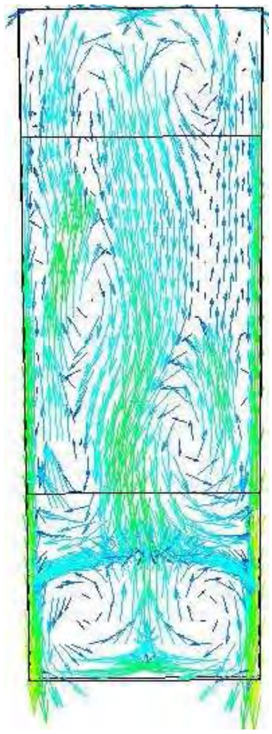

(b) 5 mm

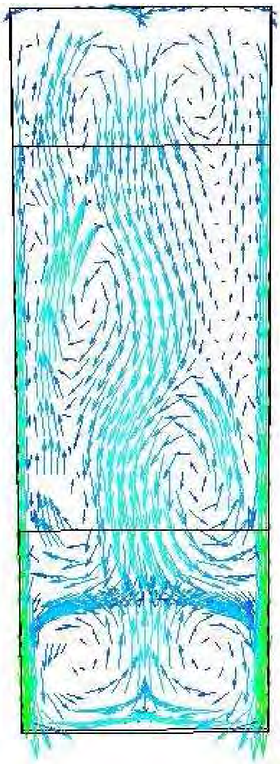

(c) 10 mm

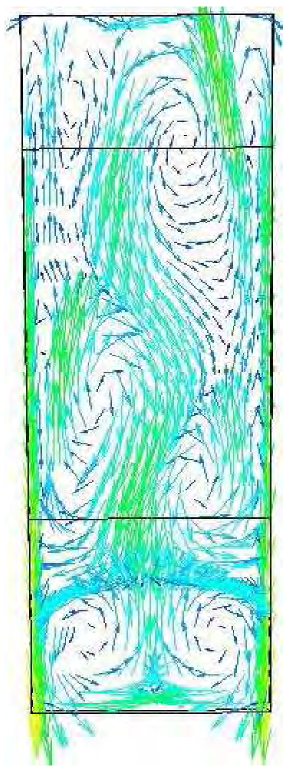

(d) 15 mm

Figure 7.13. Water superficial velocity profiles for bubbles of different sizes at the end of the simulation. The water velocity ranges from 0.36 to 0.58 m/s.

Having observed that the liquid recirculation improves with the bubble size, the dependence of the vertical liquid velocity on bubble size was explored. Vertical liquid velocities were plotted halfway through the column for all bubble sizes as shown in figure 7.14. The general profile of the velocities is similar to that presented previously (Figure 7.8) with water flowing down in the centre of the column and along the column edges and flowing up behind the two main gas streams. From figure 7.14 it can be seen that the 2 mm bubble clearly induces smaller vertical velocities than the other bubble sizes. The maximum downward and upward induced liquid velocities increase with the bubble size. Analyses of the vertical vector plots were done at different cross sections and all revealed almost the same profile as the one that has been presented. Thus it, can be concluded that an increase in bubble size leads to an increase in the water superficial velocities induced by the gas bubbles.

Figure 7.15 represents the gas hold-up profiles across the column, halfway up the column. These plots were also done at different cross sections along the column height and similar trends as those shown in figure 7.15 were observed. The gas hold-up is slightly lower at the centre and along the column edges as expected. The most important observation here is that the gas hold-up decreases with an increase bubble size. For the 2 mm bubbles, the highest gas hold-up is about 0.14 (14%) and yet for the 15 mm bubbles it is about 0.1(10). This is consistent with the fact that the smaller bubbles rise slower and thus accumulate in the tank, compared with the larger bubbles which rise faster and thus have a shorter residence time in the tank. From the membrane cleaning point of view, the question that needs to be asked is: which is more effective; small bubbles with longer residence time or larger bubbles with higher rise velocities and lower residence times? This will be addressed in the discussion section of this chapter.

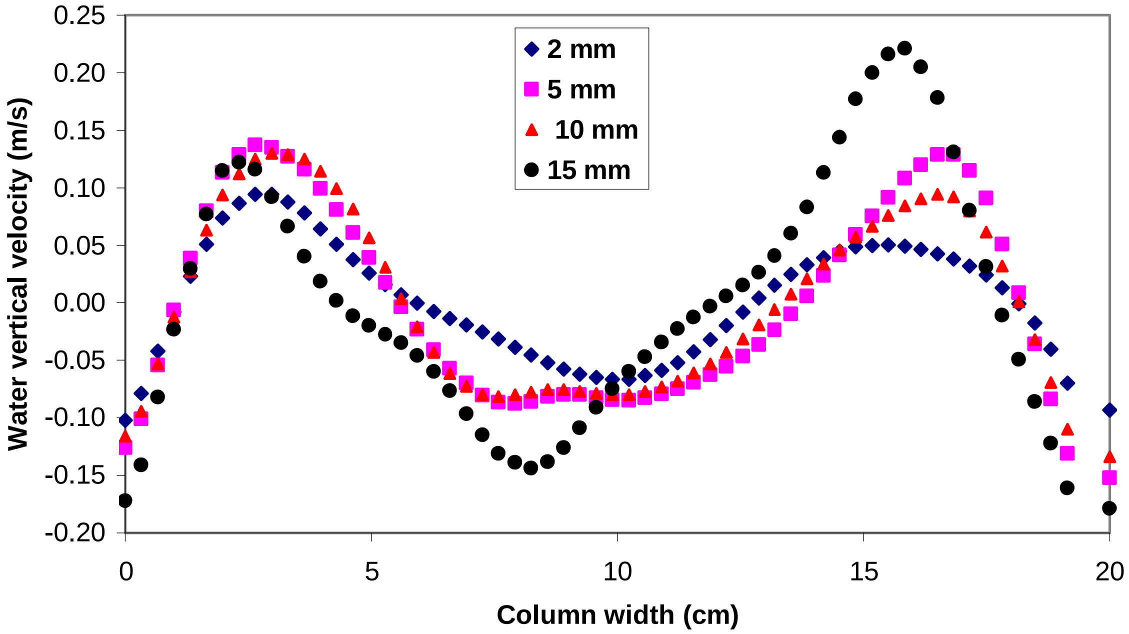

Figure 7.14. Water vertical velocity profile halfway through the column (300 mm from the bottom) for bubbles of different sizes.

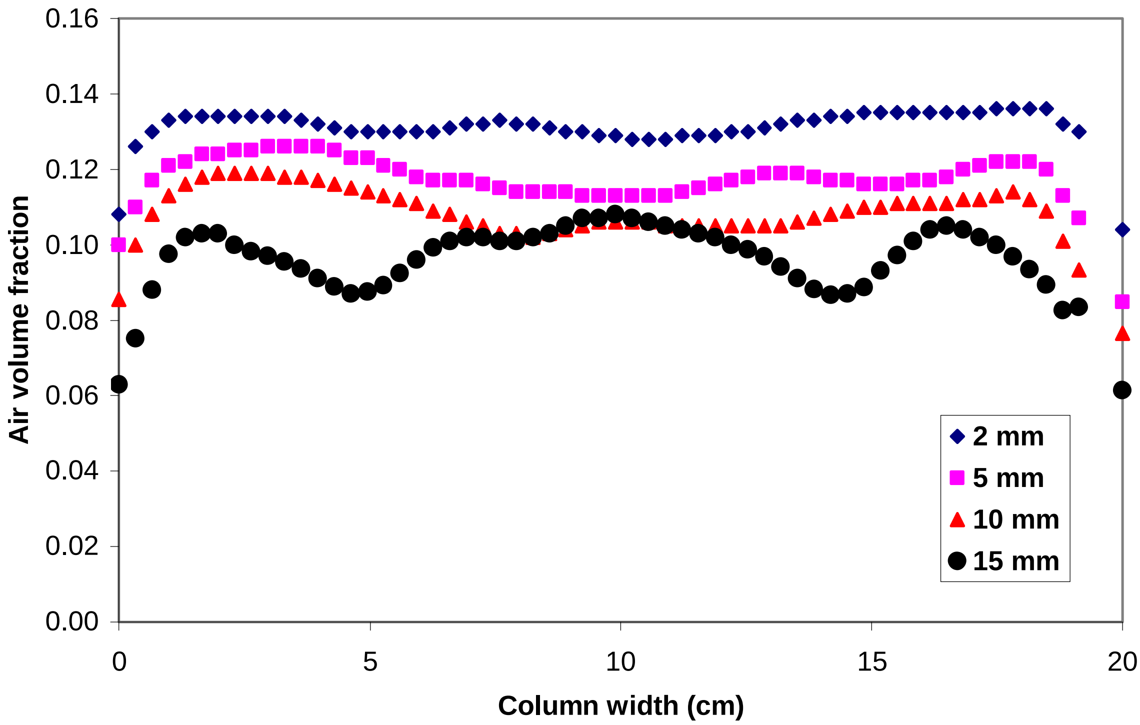

Figure 7.15. Distribution of air volume fraction halfway across the column (300 mm from the bottom) for bubbles of different sizes.

7.3.3 Analysis of shear stress distribution on the membrane surface

It is generally accepted in the literature that flux enhancement by two-phase flow is partly due to enhanced shear stress on the membrane (Cui & Wright, 1996; Mercier-Bonin et al., 2000b; Cabassud et al., 2001). Cabassud et al. (2001) have actually been able to develop a correlation between shear stress and flux enhancement by measuring shear stress using an electrochemical method. The main objective of this chapter is to analyse the shear stress distribution on the membrane surface and to determine how it varies with changes in the experimental conditions, such as an increase in air flow rate, an increase in bubble size and how it is affected by the use of baffles. Figure 7.16 shows the shear stress distribution on the membrane surface at the end of the simulations for different air flow rates. To make the comparison easy, the maximum shear stress shown on each plot has been limited to 0.5 Pa. All the pictures in this figure show that regions of high shear stress coincide with the regions where there is strong up-flow of air, such as near the column edges. In the centre of the column, where there is mostly water flowing down, the shear stress is relatively low despite the fact that maximum downward velocity of water is almost the same as that of the upward velocity. Therefore, the regions of high shear stress coincide with the presence of bubbles. This phenomenon has been observed experimentally in cross-flow tubular filtration (Mercier et al., 1995), where the shear stress was higher in the presence of bubbles than when liquid was flowing alone, even though the superficial liquid velocity was similar in both cases.

From figure 7.16 it can also be seen that the average area of high shear stress increases with the air flow rate. Thus, at higher liquid flow rates there are more areas of the membrane which are exposed to a high shear stress. Figure 7.17 shows the variation of the shear stress on the membrane surface at different times during the simulation for an air inlet flow rate of 8 l/min. This figure shows that the distribution of shear stress across the membrane varies with time and that it follows the path where there is strong air flow. Since the air moves in a zigzag manner, it implies that most parts of the membrane will from to time experience a high shear stress. Thus with less meandering of air, as in low air flow rates, the area of the membrane which does not experience high shear also increases. Therefore, it can be concluded that a better distribution of air across the membrane will lead to a better distribution of shear stress and thus enhance the efficiency of the gas-liquid two-phase flow cleaning process. This can be achieved by using baffles and is examined in the next section.

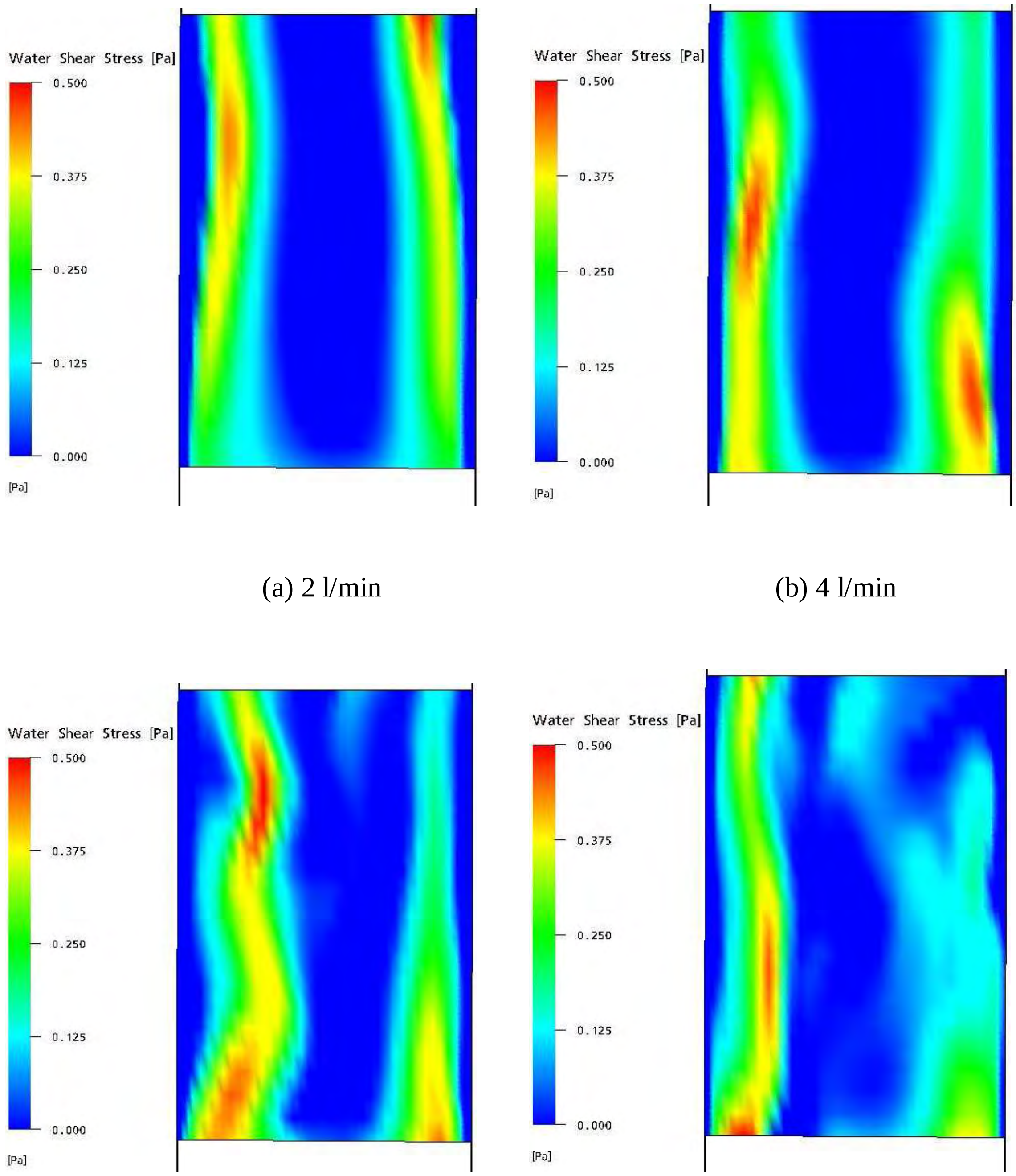

(a) 2 l/min

(b) 4 l/min

(c) 6 l/min

(d) 8 l/min

Figure 7.16. Shear stress distribution at the end of the simulation for different air flow rates.

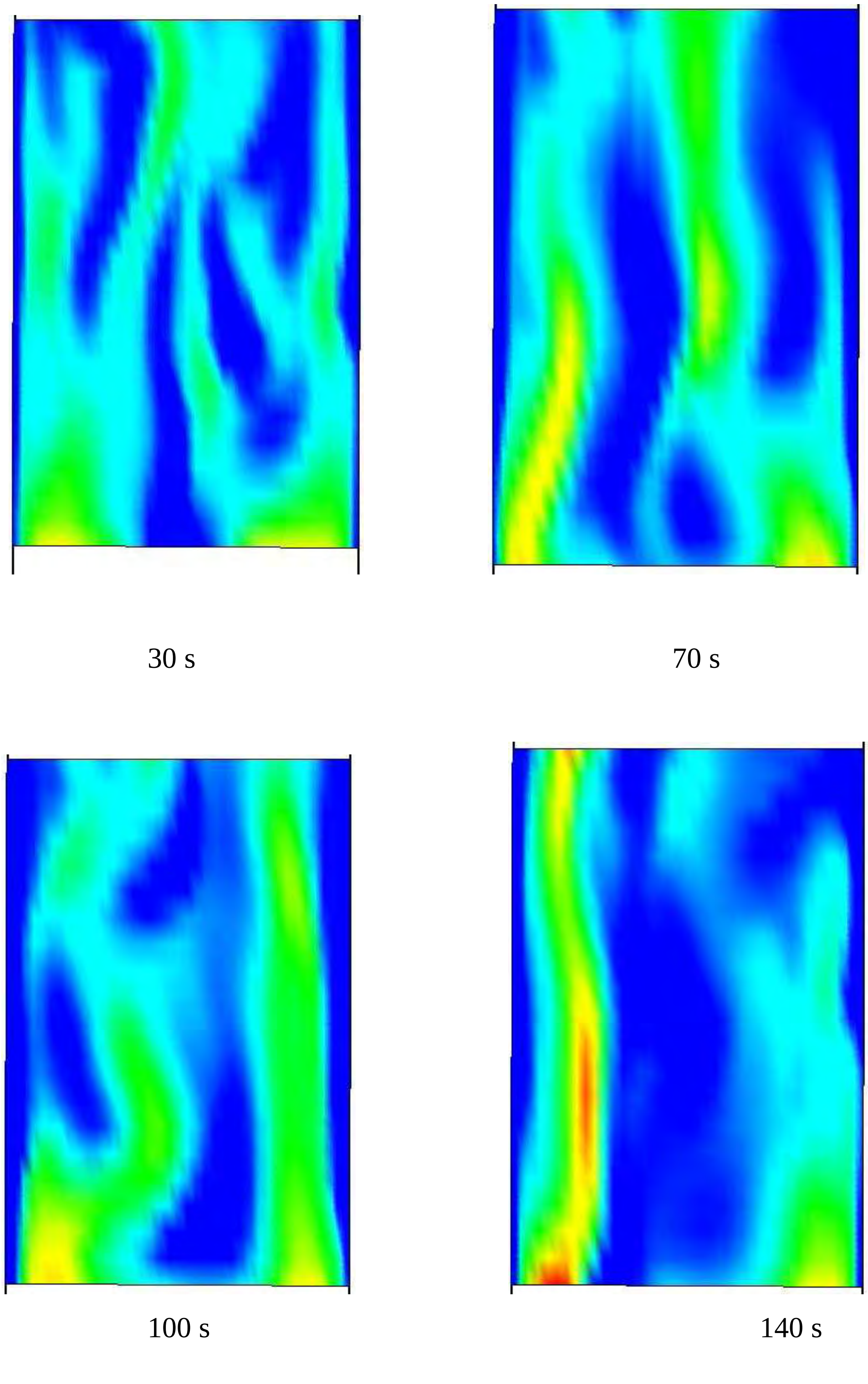

Figure 7.17. Shear stress distribution at different times during the simulation for an air flow rate of 8 l/min.

The effect of bubble size on the membrane shear stress has also been examined. Figure 7.18 shows the shear stress distribution on the membrane at the end of each simulation for different bubble sizes. To make comparison of the plots easy, the maximum shear stress shown in each picture is again limited to 0.5 Pa. From these pictures it can be observed that higher shear stresses cover a larger area for the larger bubble sizes of 10 and 15 mm. The maximum shear stress for the 2 mm bubbles, for example, is below the specified maximum of 0.5 Pa. The conclusion is therefore that the shear stress increases with the bubble size and that the distribution of shear stress across the membrane also improves with bubble size.

The average shear stresses and the maximum shear stresses on the membrane were calculated at ten seconds intervals from the start to the end of the simulation at different air injection rates and different bubble sizes. The average shear stresses were always found to be highest for the air flow rate of 8 l/min and lowest for 2 l/min at any time during the simulations even though the average shear stresses were fluctuating from time to time (figure 7.19). On the other hand, the maximum shear stress was found to be constant for most of the time during the simulation. The maximum value of the shear stress was found to increase with the air flow rate (figure 7.20). From 2 l/min to 8 l/min the maximum shear stress increased from 0.491 Pa to 0.711 Pa which represents an increase of about 31%. Therefore it can be concluded that the greater meandering of the gas stream seen at higher air flow rate is accompanied by an increase in the overall imposed shear stress on the membrane which would be good for the membrane cleaning process. However, a balance needs to be maintained between high shear rates from high air flow rates and energy consumption.

For different bubble sizes at constant air flow rate, the average shear stress did not seem to differ that much from one bubble size to another, as reflected in figure 7.21. This suggests that the average shear stress is affected more by the air injection rate than by the bubble size. However, the maximum shear stress did show an increase with the bubble size up to a bubble size of 10 mm (figure 7.22). When the bubble size was increased from 10 to 15 mm, the increase in maximum shear stress was minor.

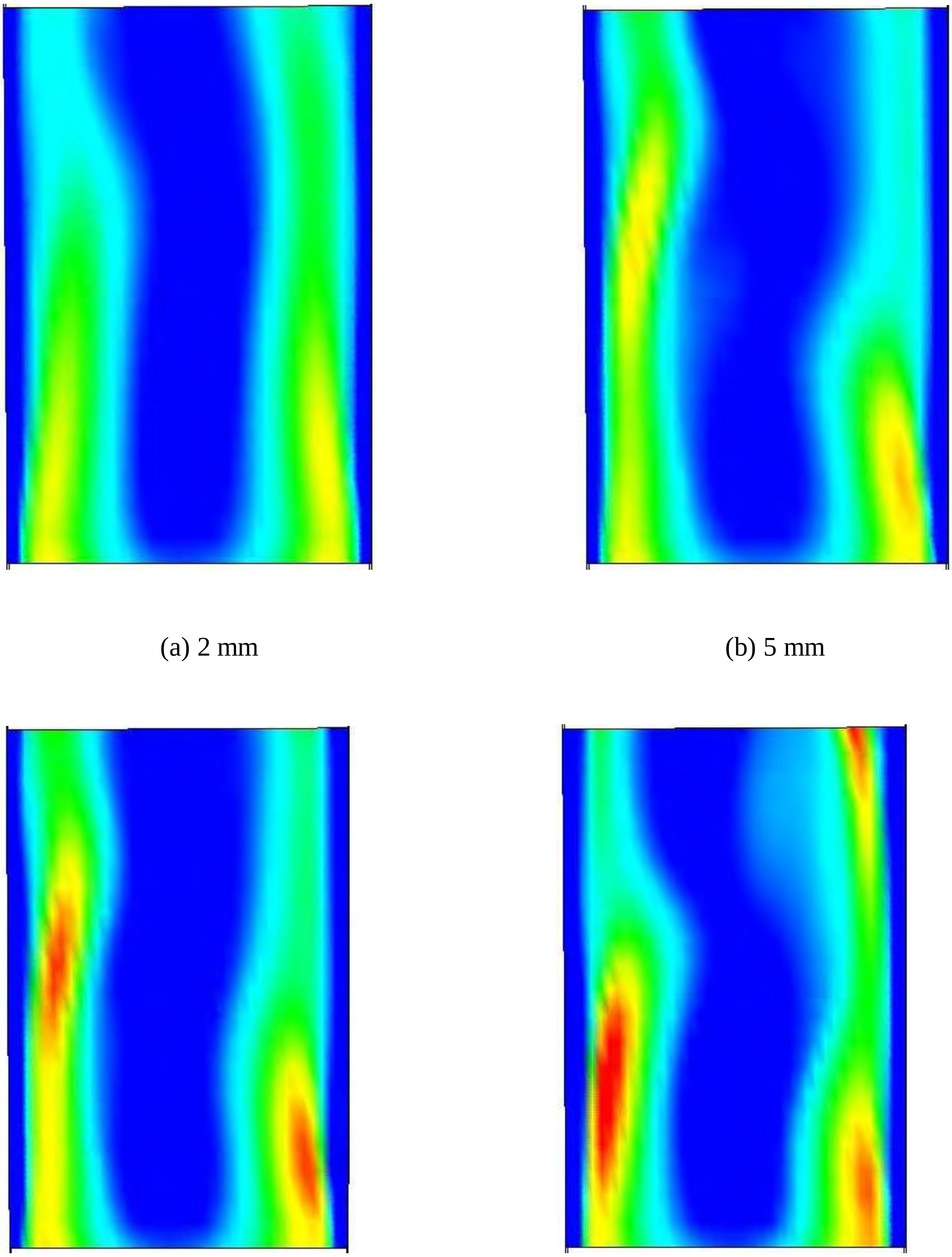

(a) 2 mm

(b) 5 mm

(c) 10 mm

(d) 15 mm

Figure 7.18. Shear stress distribution at the end of the simulation for different bubble sizes.

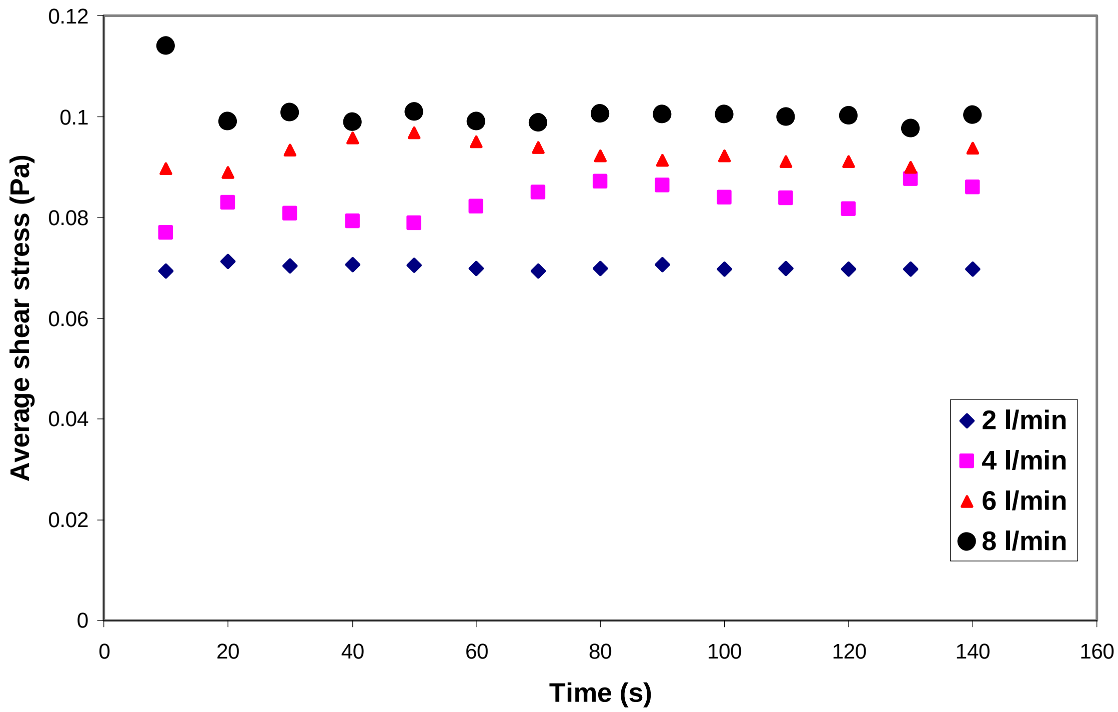

Figure 7.19. The evolution of average shear stress with time at various air flow rates.

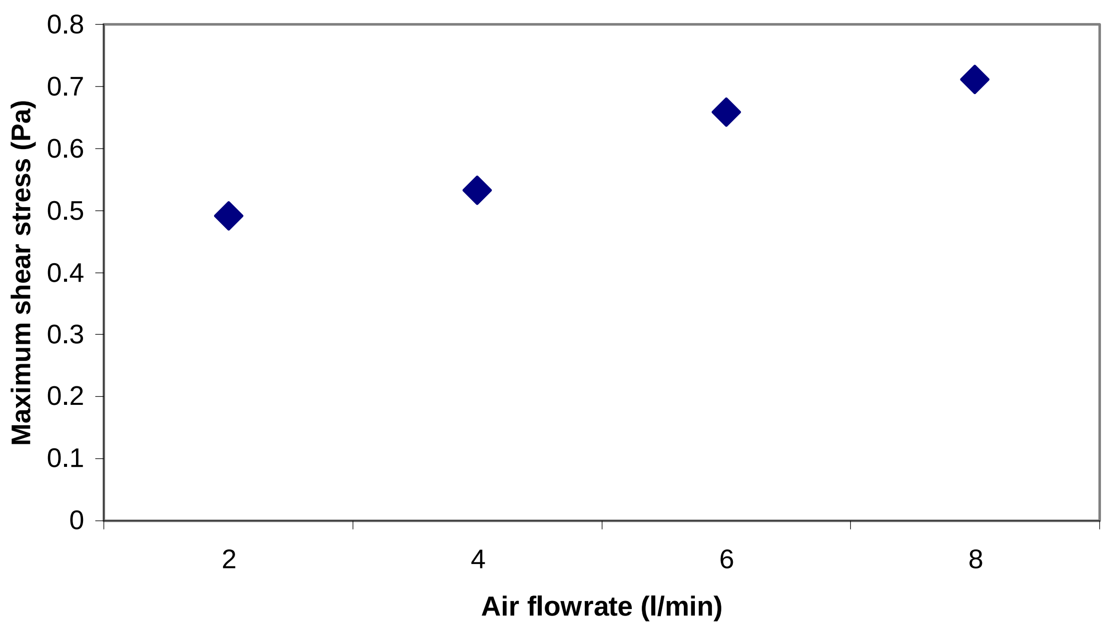

Figure 7.20. Maximum shear stress on the membrane versus air flow rate.

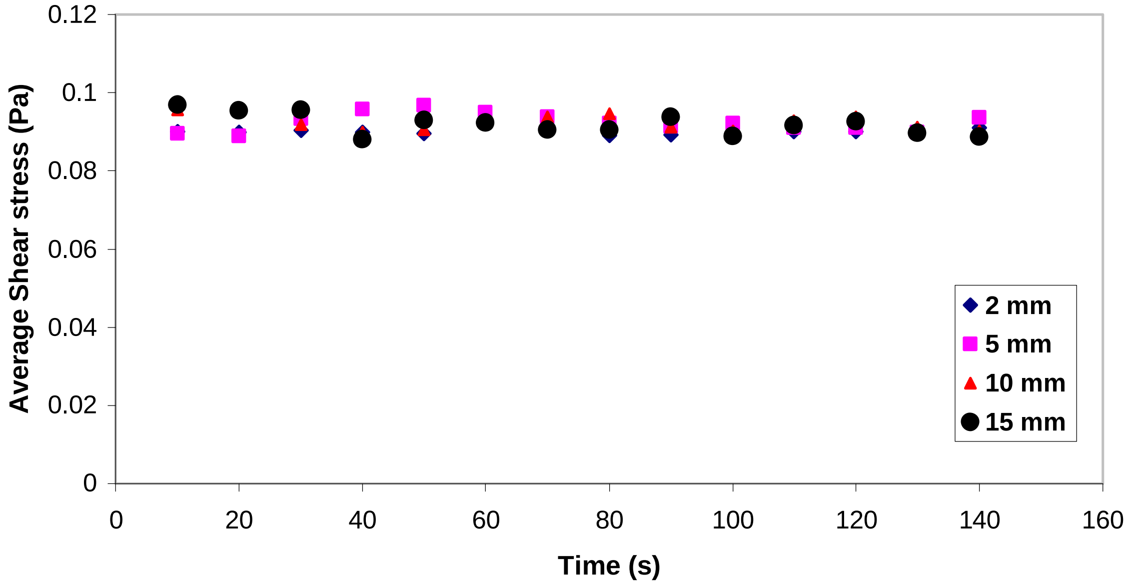

Figure 7.21. The evolution of average shear stress with time for various bubble sizes.

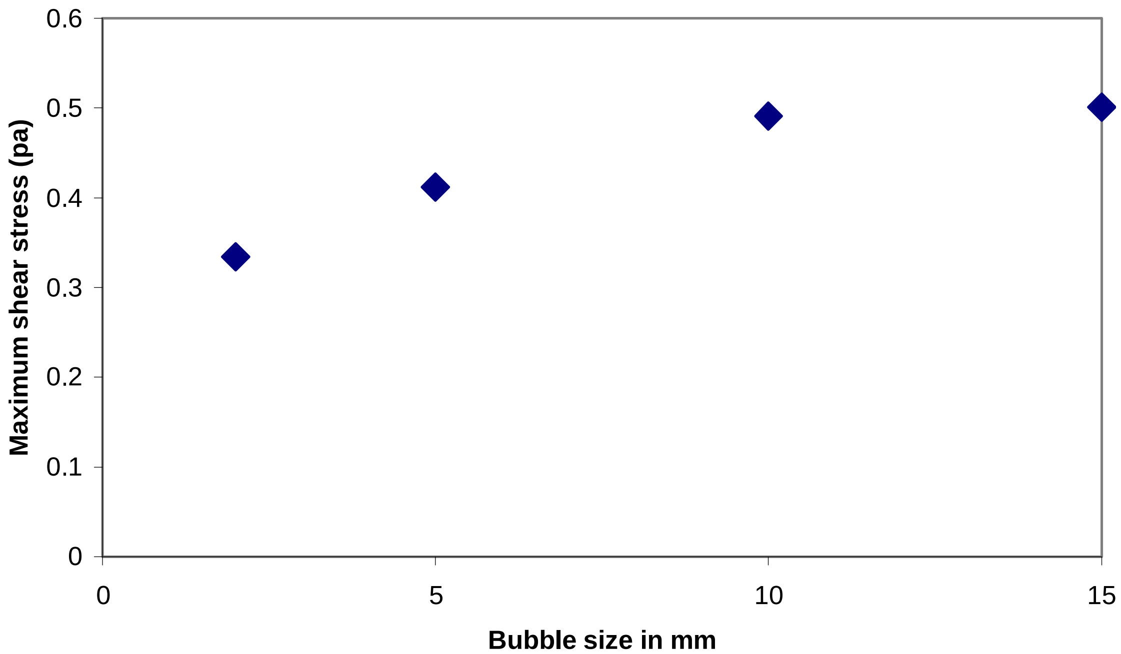

Figure 7.22. Maximum shear stress on the membrane versus bubble size.

7.3.4 Effect of baffles on the efficiency of two-phase flow flux enhancement

For submerged flat sheet membranes, there exists a small gap between the membrane plates. The size of this gap varies from one commercial system to another as explained in chapter 3, section 3.5.7. Since in this study only one flat sheet membrane was involved, the gap between the membrane and the wall was kept fixed at 7 mm, which is a typical gap used for the Kubota membrane bioreactor process (Churchouse & Wildgoose, 1998). Visual observations from the experiment show that the bulk of the air when flowing across the membrane migrates towards the centre of the column [see figure 3.8 (a) in chapter 3], despite the fact that the air inlet nozzles are distributed evenly across the bottom of the tank. Migration of bubbles towards the centre of the column has been observed and reported in bubble column studies. It was revealed in chapter 3 that this uneven distribution of air across the membrane causes some parts of the membrane to be cleaner than others and this situation was improved by the insertion of baffles between the membrane and the wall in order to attain a better distribution of air. The use of baffles in the experiments improved trans-membrane pressure reduction but the actual reason why baffles are more effective is not yet fully understood. Thus, simulations with baffles inserted in the geometry were conducted in order to obtain a better understanding of why baffles are effective.

In the experiments presented in chapter 3 only a fixed number of baffles (13 baffles) were used but in the simulations the number of baffles was varied in order to gain an insight into the effect of the number of baffles. Simulations were conducted with 3, 7 and 13 baffles (equally spaced across the membrane) and these results were compared with the cases without baffles, which have been presented in the previous sections of this chapter. For the simulations with baffles, only the bubble size of 5 mm was used and air flow rates of 2 to 8 l/min were investigated, however, the results presented here are only for the air flow rate of 8 l/min, as similar effects or trends were obtained with the other air flow rates. Figure 7.23 shows air superficial velocity vectors for simulations with different numbers of baffles. Clearly the case with no baffles shows meandering of air which becomes limited as baffles are inserted and the number of baffles is increased. The case with 3 baffles does show a slight meandering of the bubble plume but for 7 and 13 baffles the air is distributed uniformly across the membrane, so that each part of the membrane is exposed to almost the same amount of air flow which implies that overall shearing over the entire membrane surface is almost uniform.

Figure 7.24 shows shear stress plots on the membrane surface at the end of the simulations for cases with different baffles. For effective comparison of the plots, the maximum shear stress displayed in each plot has again been fixed at 0.5 Pa. It is evident that the size of the regions of high shear stress increases as the number of baffles is increased. The area of low shear stress is very large in the case with no baffles covering almost more than half of the membrane, whereas in all the cases with baffles the low shear stress area is very small. These pictures also show that the lower part of the membrane experiences much higher shear stresses than the top part of the membrane. This could be due to the fact that the starting point of the baffles coincides with the bottom of the membrane and therefore this is a point where the air stream divides into smaller streams as guided by the baffles. Thus this "collision of the air stream" with baffles leading to division of the air stream could be giving rise to higher turbulence resulting in high shear rates at the bottom of the membrane. The increase in turbulence in this region is evidenced by the increase in turbulence kinetic energy, as shown in figure 7.25. As the bubbles continue to rise, the flow becomes smoother which results in a slight reduction of the wall shear stress.

The values of the average and maximum shear stress on the membrane were extracted at ten seconds intervals during the simulation to monitor their progression. It was found that both the average and maximum shear stress values did not change significantly with time for the cases with baffles, unlike in the case without baffles, where the average shear stress varied substantially with time during the simulation. Figure 7.26 shows that the maximum shear stress increases with the number of baffles. From the case without baffles to the case with 13 baffles, the maximum shear stress increased by about 29%. The average shear stress over the entire membrane surface also increased with the number of baffles (figure 7.27). The average shear stress for the case without baffles was computed and is also shown in this figure.

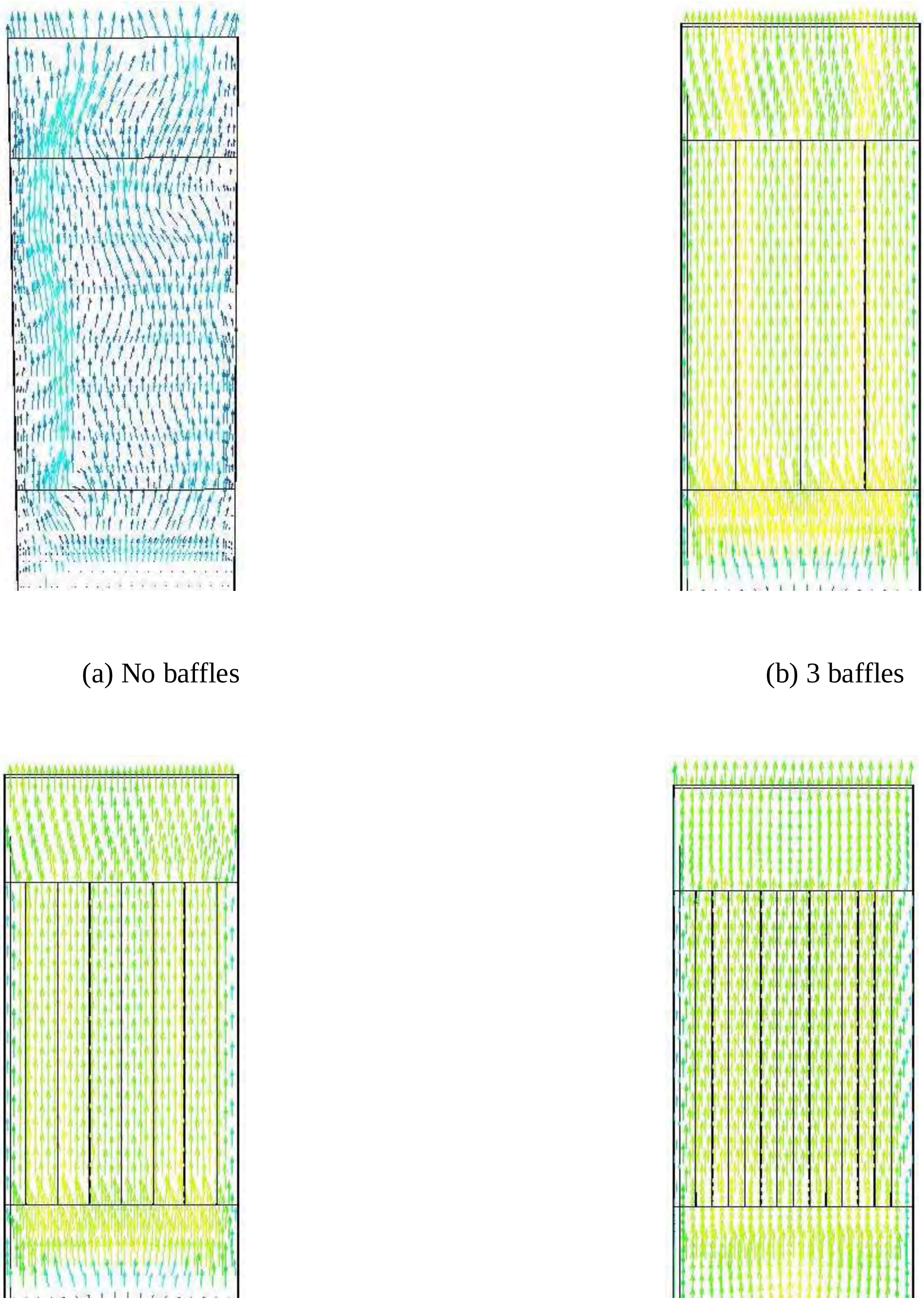

(a) No baffles

(b) 3 baffles

(c) 7 baffles

(d) 13 baffles

Figure 7.23. Air superficial velocity profiles for runs with different number of baffles at 8 l/min.

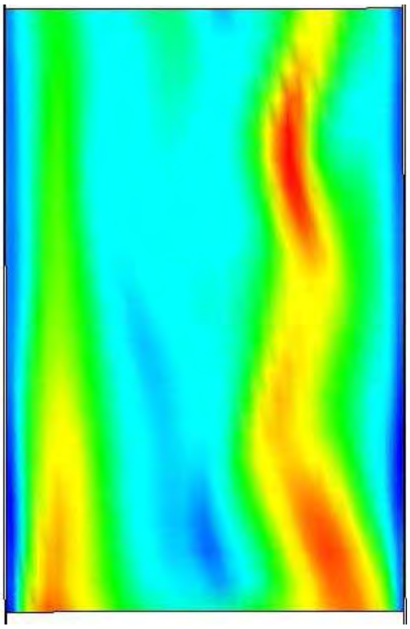

(a) No baffles

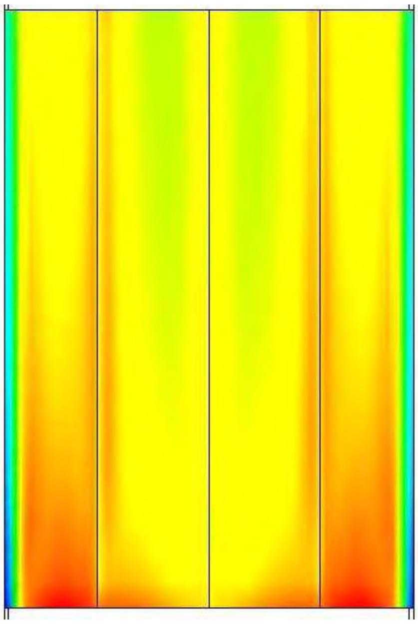

(b) 3 baffles

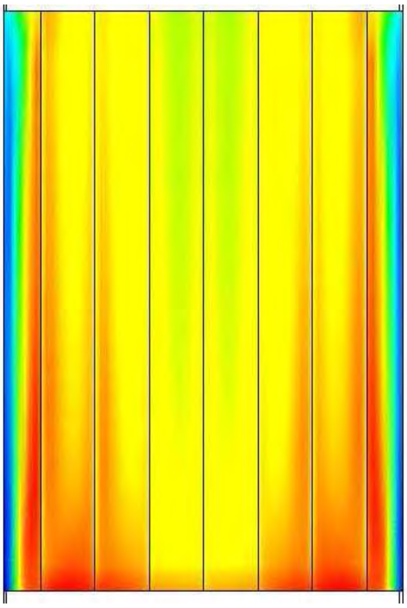

(c) 7 baffles

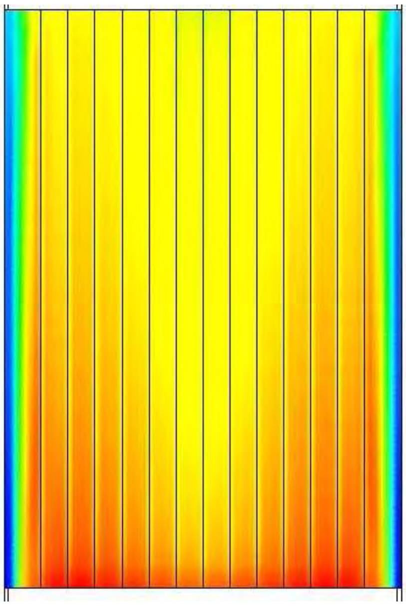

(d) 13 baffles

Figure 7.24. Shear stress distribution on the membrane for simulations with different numbers of baffles at an air flow rate of 8 l/min.

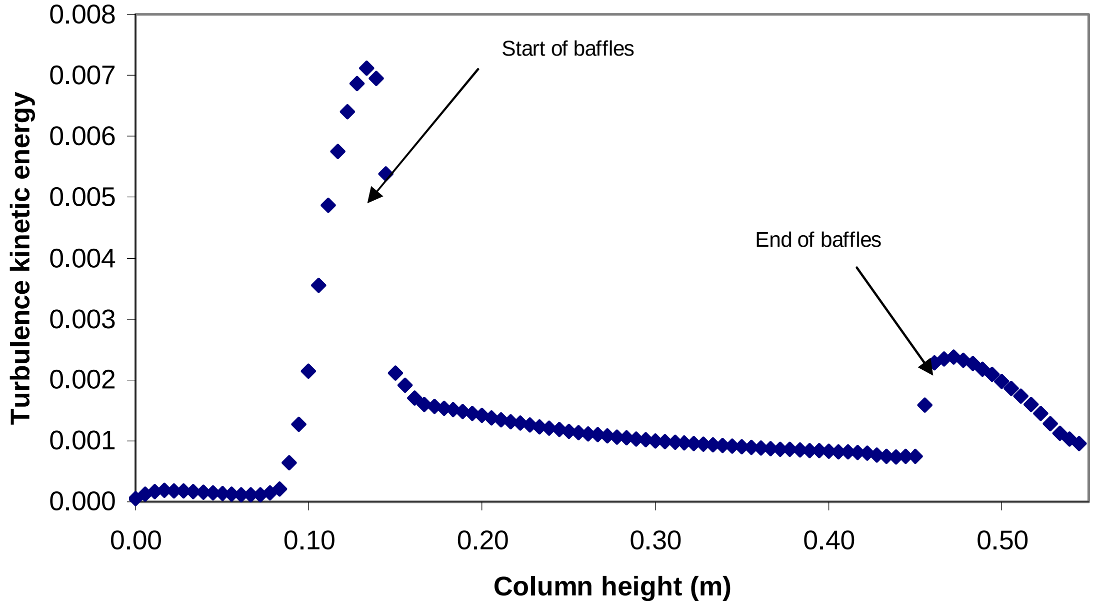

Figure 7.25. The distribution of turbulence kinetic energy along the column height.

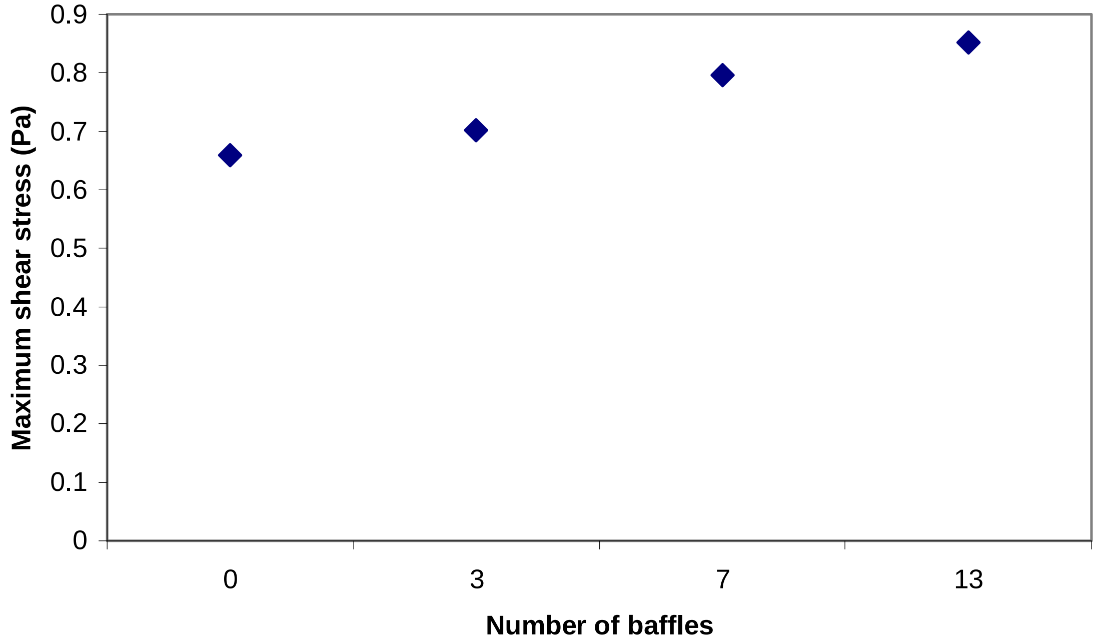

Figure 7.26. Maximum shear stress on the membrane versus number of baffles.

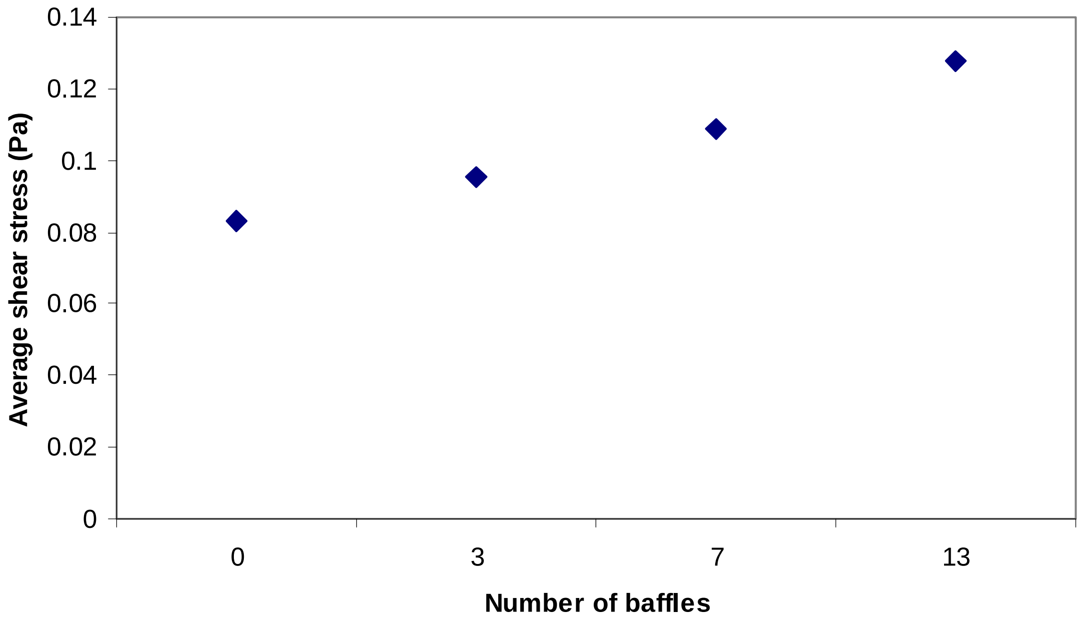

Figure 7.27. Average shear stress on the membrane versus number of baffles.

7.4 SINGLE BUBBLE SIMULATIONS

The results of the two-fluid model which have been presented thus far were able to yield information such as the distribution of shear stress on the membrane, gas hold-up in the tank, and air and liquid velocity profiles. However, with these Euler-Euler simulations it is not possible to track individual bubbles and to study parameters such as bubble shape development, effects of bubble properties on shear stress, pressure fields around the bubble and so forth. From a membrane point of view, these features could play a very prominent role in combating fouling and hence their understanding is crucial for the optimization of two-phase flow. It was therefore desirable to carry out simulations of a single bubble rising in a stagnant liquid between narrow walls in order to evaluate parameters which otherwise would be extremely difficult to elucidate experimentally. Even for model development work that is done in bubble columns, some researchers (Chen et al., 1999; Wachem & Schouten, 2002) have realized that it is important to first understand the physics involved in single bubble interactions with the continuous phase before realistic two-fluid models could be developed. The objectives of the single bubble simulations were as follows:

- Study the bubble shape development for bubbles of different sizes.
- Evaluate the effect of nozzle size and geometry on bubble parameters such shape development, the Eötvös number, the Morton number and the bubble terminal velocity.
- Assess shear stress distribution on the membrane along the falling film and the wake regions of the bubble.
- Study wake structures for bubbles of different sizes and different terminal velocities.
- Study the distribution of pressure fields around bubbles of different sizes.
- Study the effect of gap width between the membrane and the wall on liquid velocity profiles and shear stress distribution.

There are many studies reported in the literature of simulations of single bubbles rising in stagnant liquids (e.g., Chen et al., 1999; Krishna & Baten, 2001; Valencia et al., 2002) and the primary aim of most of these studies have been to test and validate newly developed numerical models. Consequently, the key components of two-phase flow that this study is mainly interested in, as identified in the objectives, were not given sufficient attention. There are only two studies that were found in literature which have reported single bubble simulations primarily with an aim of understanding flux enhancement in membrane processes by bubbling. One of these studies involves a Taylor bubble rising inside a tubular geometry which could represent a tubular membrane (Taha & Cui, 2002b) and the second study looks at a bubble rising across a flat sheet membrane in a rectangular geometry (Essemiani et al., 2001). Both these studies used two-dimensional grids, whereas in our case a three-dimensional grid was used. The study by Essemiani et al. (2001) used a very similar geometry to this study but their physical dimensions were much smaller. They only studied one bubble size, where they looked at shape development, bubble path and the pressure field around the bubble. They also specified as an initial condition a bubble with a perfectly spherical shape. As will be revealed in the following sections, their simulations were very different from ours and did not yield the type of information that this study was seeking to obtain.

Accurate simulation of fluid flow with a sharp front presents a problem of considerable difficulty which has challenged inventors and users of numerical methods since the beginning of large-scale computational work. When a large discontinuity is involved, for example, a discontinuity of 850 in density ratio as for the water-air system, numerical difficulties may arise in identifying an 'exact' interface and defining the fluid properties (Chen & Li, 1998). The interface tracking methods, for example, the volume-of-fluid (VOF) of Hirt and Nichols (1981), provide detailed information on the flow field around bubbles without using empirical closure laws, however, they require a lot CPU time so that only a few bubbles can be simulated (Tomiyama et al., 1997). If a numerical method is of low order, excessive numerical diffusion will quickly destroy the sharpness of the front; a higher order scheme will lead to numerical oscillations around the front that may couple into other parts of the solution in an undesirable way (Sussman et al., 1994). Due to such difficulties some of the objectives stated earlier were unmet.

7.4.1 The Numerical methods

Initially simulations were carried out using a standard Volume-of-Fluid method [Hirt & Nichols (1981)] as available in CFX 5.6. This method resulted in a bubble with a smooth interface at the top but excessive smearing of the gas occurred at the bubble wake due to a lack of slip velocity between the gas and the liquid phases. Simulations using the Euler two-fluid methods yielded opposite results with a bubble having a smooth interface at the bottom (bubble wake) but a smeared interface elsewhere around the bubble. A new method was developed which combined both the VOF and the two-fluid model together basically by applying the VOF model everywhere around the bubble and the two-fluid model in the wake region of the bubble. A detailed description of these numerical methods has been given in chapter 6.

7.4.2 The geometry description

The real tank geometry of the experiments consists of a rectangular tank which is 540 mm high × 30 mm deep × 200 mm wide with the flat membrane inserted in the centre. Since only a single bubble was being investigated, a much smaller geometry in the simulation was used in order to reduce mesh size and simulation time. However, the distance between the two walls through which the bubble rises was kept the same as that in the real experiments (7 mm). The height of the tank was chosen based on the time it takes for a typical bubble to reach its terminal velocity. According to Clift et al. (1978), a spherical bubble of 5 mm will take about 0.8 seconds to reach its terminal velocity in a stagnant liquid. Simulations were done with columns of different heights and it was realized that with a height of 100 mm it takes about 0.95 seconds for a bubble of 5 mm diameter to rise through the column, therefore this height was assumed to be long enough for bubbles to attain their terminal velocity before exiting the column.

Having decided on the depth and height of the column, the last parameter to be decided upon was the width of the column. Again simulations were done with columns of different widths ranging from 20 mm to 80 mm. Simulations were terminated when the bubble was halfway through the column and the vertical liquid velocities along the width of the column were extracted. As the bubble rises it pushes away the liquid ahead of it and pushes it sideways. This liquid then flows down around the bubble and re-circulates around the bubble wake. If the column is wide enough, only the liquid near the bubble will be influenced by the rising bubble. If the column is not wide enough, the bubble will not expand freely and this will affect the velocity profile around the bubble. As Wachem and Schouten (2002) observed, an increase in the column width resulted in an increase in the bubble terminal velocity. Thus the column should be wide enough such that the terminal velocity of the bubble is not affected by the width.

Figure 7.28 shows the vertical liquid velocity plots for four different widths of the column. From this figure, it can be seen that from the width of 60 mm onwards, the vertical velocity plots around the bubble have almost the same values, which indicates that above the width of 60 mm, the column width no longer has any impact on the velocity profiles and hence on the bubble shape development and path. Thus, for all simulations the column width was kept at 60 mm. Using a computational domain of 4 by 40 bubble diameters, Liovic et al. (2001) showed that at 4 bubble diameters, the container walls had little effect on the bubble rise velocity. In this study, 5 mm bubbles were used and clearly the width of 60 mm is much greater than 4 bubble diameters.

The final dimensions of the geometry used in all simulations were therefore as follows: the height was 100 mm, the width was 60 mm and the depth was 7 mm. Since this is a rectangular geometry, it was assumed that flow would be symmetrical in order to reduce computational time and therefore only a quarter of the tank was modelled. An example of the geometry used in the simulation is shown in figure 7.29. The air was injected at the bottom the tank through a nozzle. The duration and speed of the injection was based on the amount of air required to have the same volume as the required bubble. The initial nozzle was chosen to be circular with a diameter of 1.0 mm and it was desired to study nozzles of different sizes and geometries. Unlike in the two-fluid simulations presented earlier, an unstructured grid was utilized for the single bubble simulations.

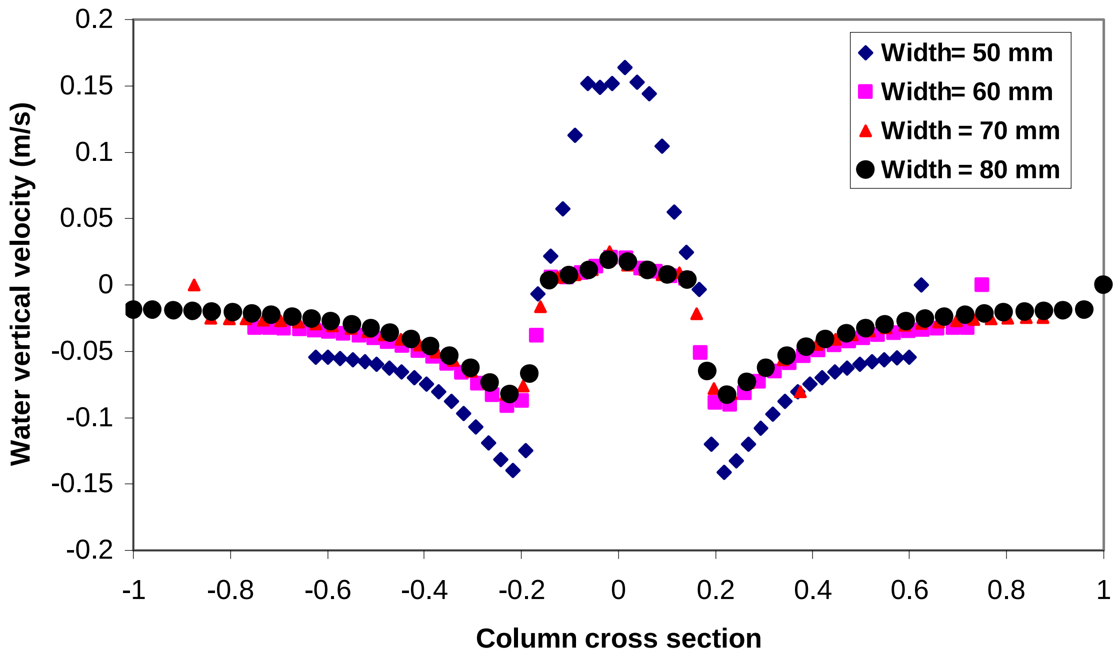

Figure 7.28. Water vertical velocity profiles halfway through the column at different column widths.

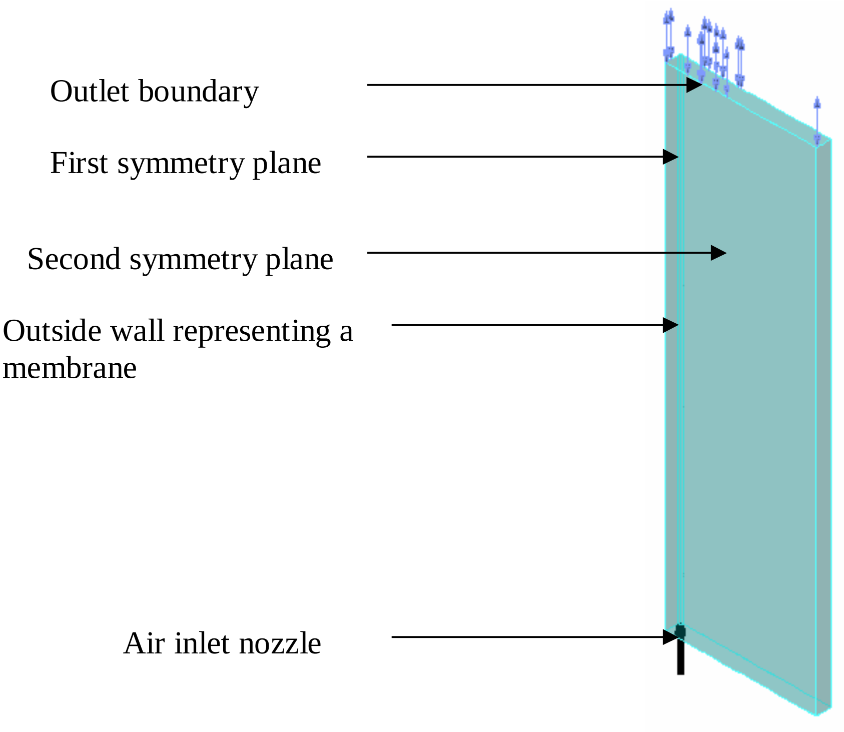

Figure 7.29. Schematic diagram of the geometry used in the single bubble simulations.

In the central part of the column, where the bubble rises, the mesh was made finer, with a mesh length of 0.5 mm being the smallest that was used. Outside this region, the mesh spacing was relaxed with a mesh length of about 2.0 mm. An example of the grid used is shown in figure 7.30. In this figure, only the mesh for half of the tank is depicted. Figure 7.30 (b) shows in much better detail the contrast between the fine and the coarse mesh. To obtain a much better resolution of the flow near the walls, an inflated mesh was created on the wall boundaries with eight layers of inflation. An example of the mesh with inflation near the walls is shown in figure 7.31.

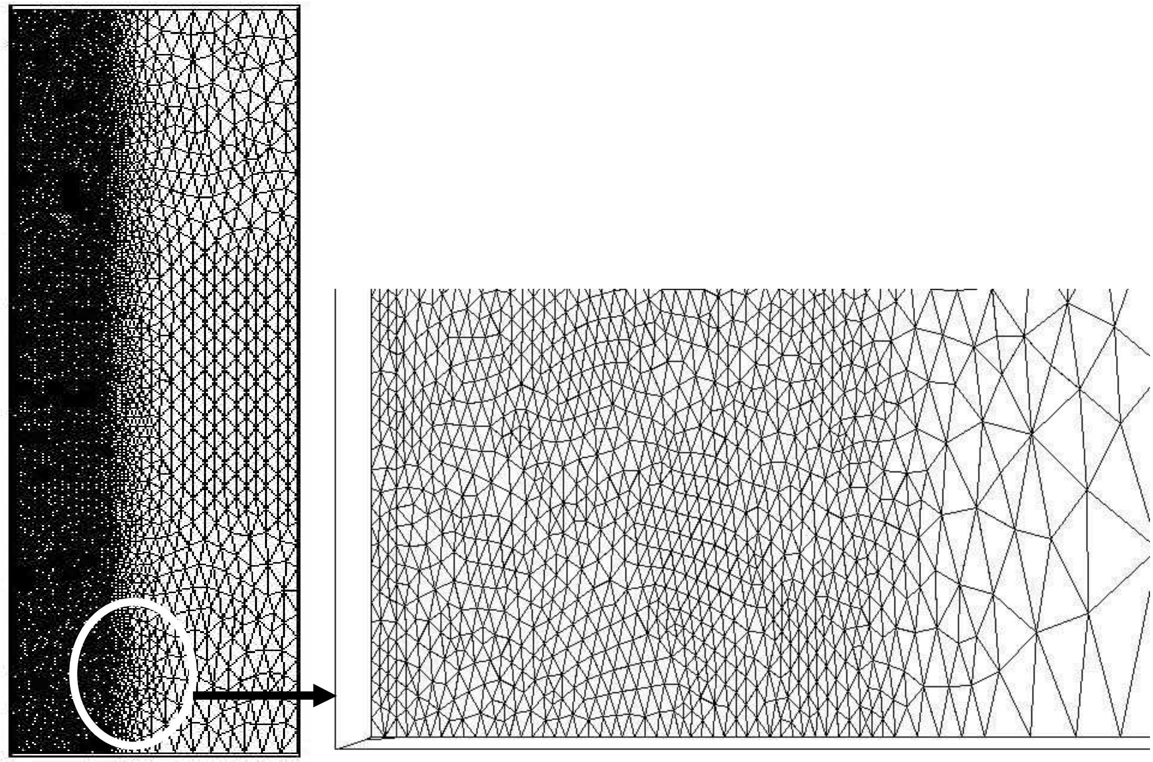

(a) **(b)**

Figure 7.30. A typical grid used in the single bubble simulations.

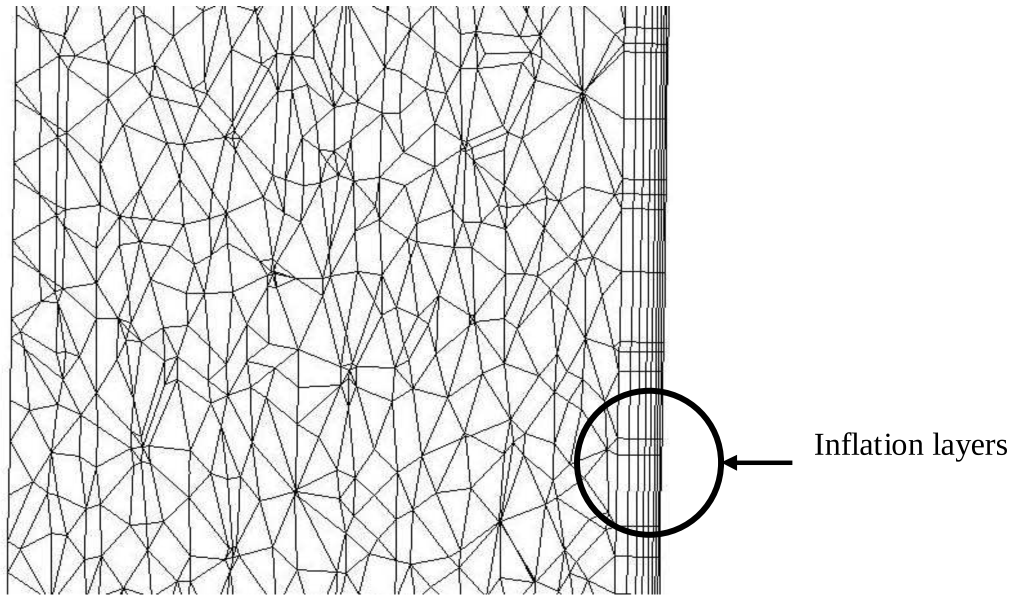

Figure 7.31. An example of a grid with wall inflation layers.

7.4.3 Details of the simulation procedure

Simulations were performed using the commercially available CFD software package CFX 5.6 from ANSYS using the numerical methods validated in chapter six. In the initial simulations air was injected continuously through the nozzle with the hope that bubbles would form automatically. However as figure 7.32 shows, this did not happen, but rather a continuous column of air formed. It was then resorted to forming bubbles manually by injecting only a small amount of air over a short period of time. The flow in the solution domain was defined as laminar. For all walls, the boundary conditions were set to free slip for air and no slip for water for the two-fluid and combined model, and the no slip for the VOF model. The top boundary was defined as a pressure boundary with static pressure equal to zero in the VOF model and was described as a degassing boundary in the two-fluid model and the combined model. The air nozzle was defined as an inlet boundary with the air flow normal to the boundary at a particular velocity which was set at 16 m/s for the results to be discussed in the following section.

A constant time step of 1×10^{-3} s was used for most simulations and a typical simulation lasted for at least two weeks on a 2.4 GHz Zeon Intel dual processor. A time step of 1×10^{-4} s was also used but it did not result in an improved solution even though it took much longer. It was therefore decided that it was impractical to continue with the smaller time steps. The maximum number of coefficient iteration loops per time step was set to ten and this was barely sufficient to achieve convergence of the residuals. In most runs, convergence was good earlier on in the run but later on most runs diverged. The high resolution differencing scheme was used with second order backward Euler being used as the transient scheme. However, due to the poor results obtained by this combination, the lower resolution differencing scheme, upwind, and the first order backward Euler transient scheme were also investigated. The simulations were scheduled to run for a total real time of one second but only a few simulations were ever allowed to run to the end.

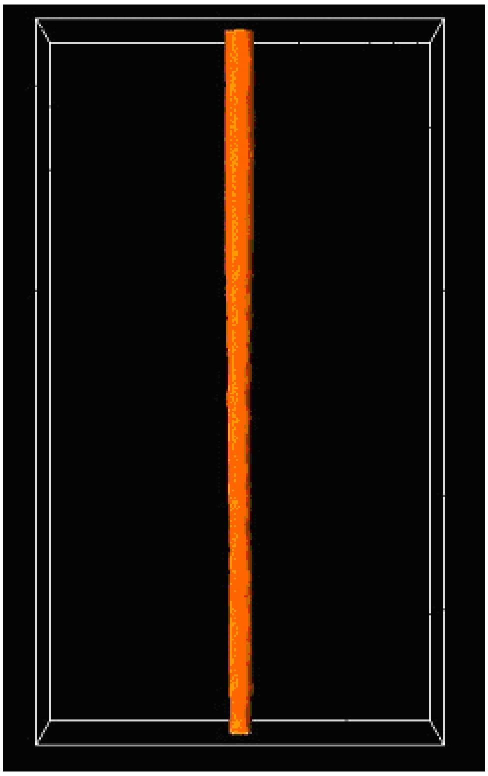

Figure 7.32. Flow pattern observed with continuous injection of air.

7.4.4 Bubble characterization

Bubbles can be characterized by their Eötvös number (*Eo*), Morton number (*Mo*) and Froude number (*Fr*). The equations describing these dimensionless groups have been given in chapter six. For all the simulations presented here, the *Eo* number was 3 and the *Mo* number was 1.4×10^{-8}. The *Fr* number can only be found once the bubble has reached its terminal velocity.

7.5 RESULTS OF THE SINGLE BUBBLE SIMULATIONS

7.5.1 VOF simulations

Numerous simulations were performed with the VOF model using different grid sizes (0.5 mm mesh length being the smallest that was used), different advection schemes (high resolution and upwind), different transient schemes (first and second order backward Euler) and different time-steps (1×10^{-4} s being the smallest time step that was used). These simulations took a considerable amount of time (minimum two weeks per simulation on an SGI Irix 2000 supercomputer with 16 processors). A satisfactory solution was never achieved with any combination.

The major problem encountered in the VOF simulations was the disintegration of the bubble. There was excessive smearing of the bubble interface particularly at the bubble wake and also the bubble became wet (meaning water was mixed into the air) as it rose. This caused most of the simulations to diverge. Figure 7.33 shows the evolution of the bubble at different times during the simulation. These pictures were obtained by plotting a volume fraction of air fringe plot on a plane located in the centre of the column. During the injection process the bubble develops well, the interface is sharp and the bubble is dry. But as soon as the injection is over and the bubble starts to rise, smearing of the interface begins and the bubble also starts to become wet. At 0.05 s the bubble shape is almost spherical, then at 0.3 s the bubble shape has changed to ellipsoidal and finally at 0.45 s the bubble has a spherical-cap shape. For bubbles of almost the same size, similar changes in shape development have also been observed by other researchers (Essemiani et al., 2001; Krishna & Baten, 2001). These pictures were obtained with a high resolution advection scheme and second order backwards Euler transient scheme. The bubble rises in an almost rectilinear path and exhibits an oscillatory motion. The bubble oscillatory motion is caused by vortices which are shed in an alternating mode at the left and right rear part of the bubble. Krishna & Baten (2001) also made similar observations for bubbles of almost similar size. In their case, the bubble *Eo* number was 2 and *Mo* number was 2.5×10^{-11}. The model also predicts two small bubbles being shed off from the side of the bubble; however, this does not agree with the results of Krishna & Baten (2001) and therefore could be due to a numerical error.

According to Chen and Li (1998) “when a single bubble rises due to buoyancy force, the pressure gradient at the lower surface of the bubble is higher than at the top surface of the bubble and the vortex sheet developing at the surface has a sense of rotation, which induces a tongue-like liquid jet that pushes into the bubble from below, which causes deformations of the bubble, giving the bubble a concave shape”. This is clearly shown in figure 7.34. From this figure two water recirculation regions can be seen in the bubble wake, and the length scale of the bubble wake is much larger than the bubble size. For bubbles with $Eo = 21$ and $Mo = 2.5 \times 10^{-11}$, the computed wake by Delnoij et al. (1997)

was seen to extend downstream of the bubble over a distance of four to five bubble diameters. Shear stress analysis on the wall actually revealed that the region of maximum shear stress on the wall coincide with the region of maximum liquid velocity behind the bubble (as shown in figure 7.34).

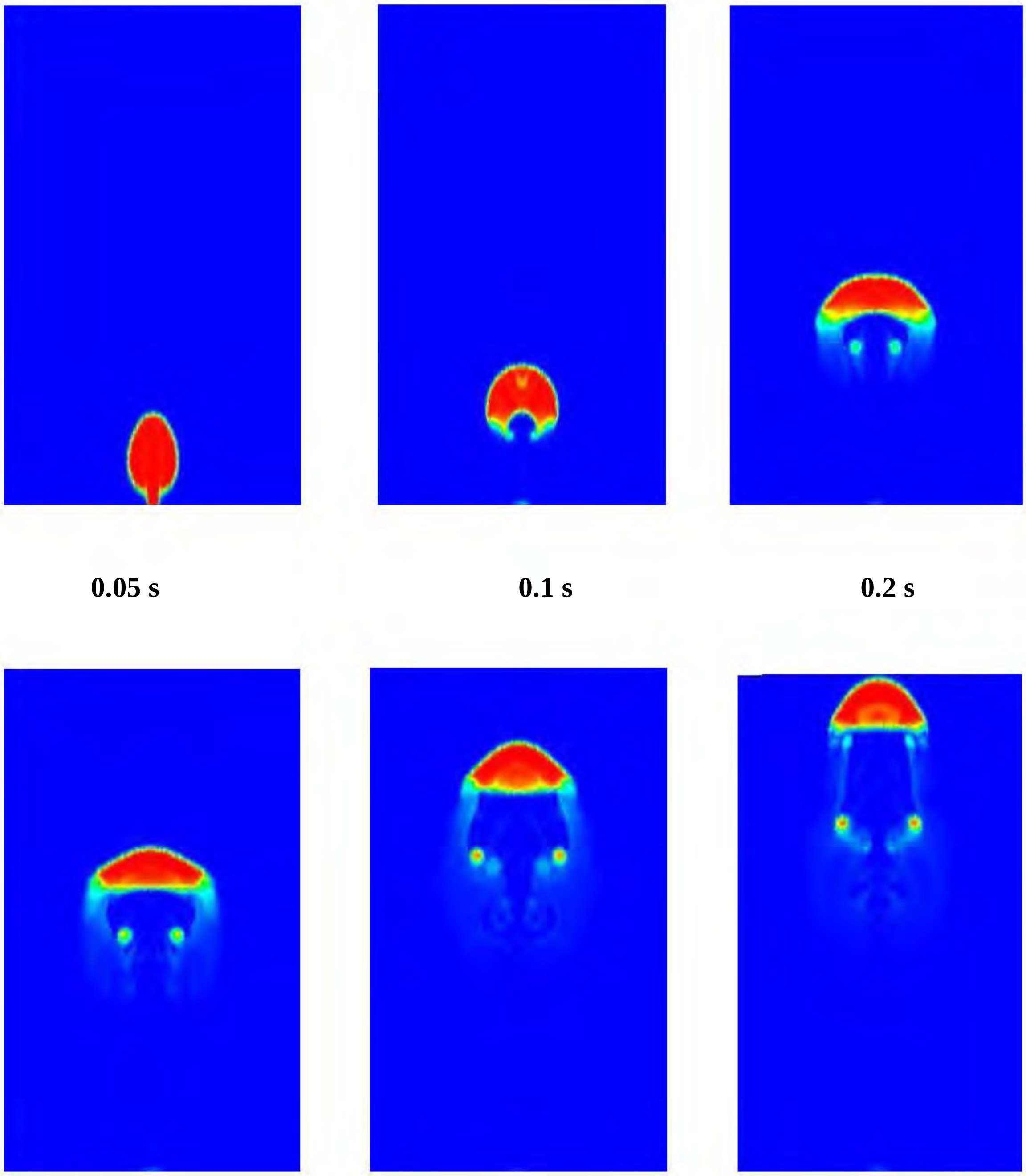

0.05 s **0.1 s** **0.2 s**

0.3 s **0.4 s** **0.45 s**

Figure 7.33. The evolution of the bubble shape with time obtained with a standard VOF model.

Another property which has been linked to the two-phase flow enhancement of flux is the thin liquid falling film between the bubble and the wall (Taha & Cui, 2002a). Figure 7.35 shows a bubble rising between two narrow walls as viewed from the other side of the tank. From this view, the bubble looks almost like a Taylor bubble. Figure 7.36 shows the liquid velocity vectors in the region between the bubble and the wall. From this figure, it can be seen that there is very little liquid moving through this region. The bulk of the fluid flows on the side of the bubble where there is no restriction as shown in figure 7.34. The presence of small amount of fluid in the falling region could also be due to the insufficient resolution of the flow in this region due to mesh limitations. This could be overcome by using more inflation layers, but this increases computational time significantly. From the bubble nose to the distance of about two-thirds down the bubble length, most of the liquid is being pushed up as shown by the liquid vectors. Below this region there is a stagnation point which is followed by the liquid flowing down. Thus, in contrast to what was observed in chapter six, the falling film in this case is very small and therefore it probably does not contribute much to the flux enhancement process. It was also partly due to these CFD observations that a decision was taken to insert baffles between membrane and the walls in the experiments in order to confine the bubble in all directions hence forcing more liquid to go into the falling film region and thus enhancing the shear stress in this region. It was shown in chapter six that the shear stress in this region is significantly higher than shear stress in the wake region.

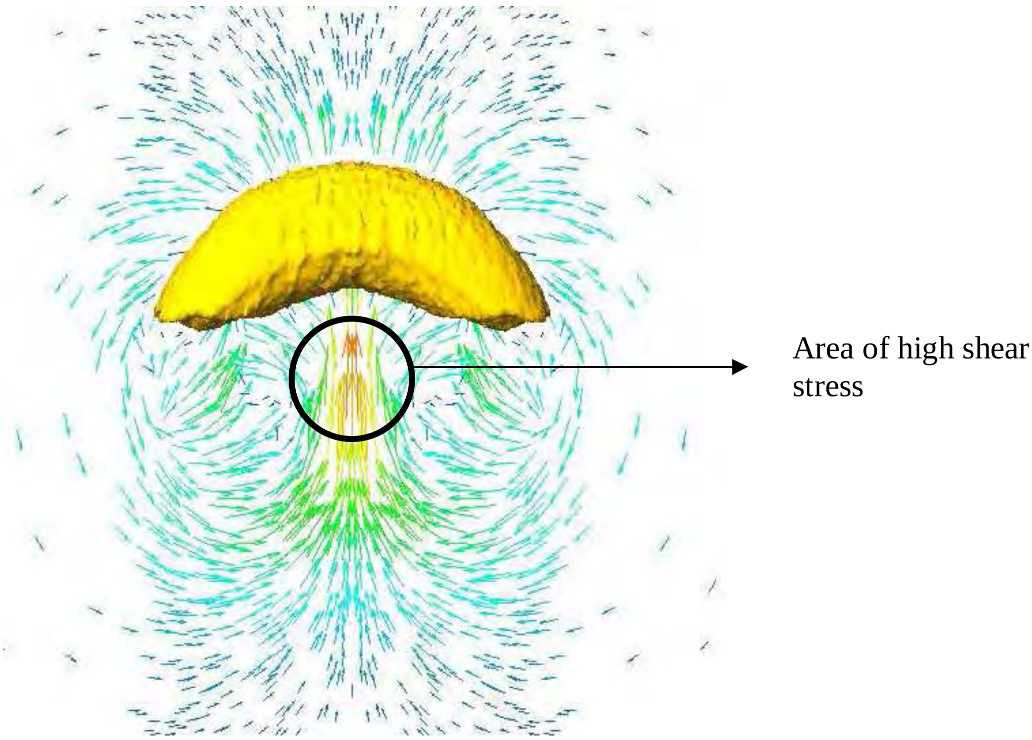

Figure 7.34. Liquid velocity fields around a rising bubble.

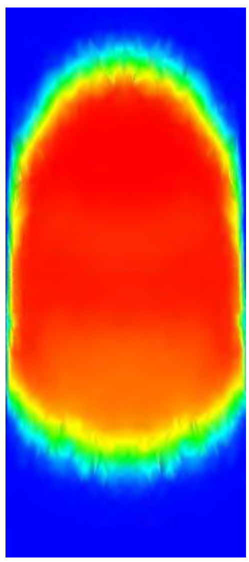

Figure 7.35. A single bubble rising between narrow parallel plates showing that the bubble has a Taylor bubble shape when viewed from this angle.

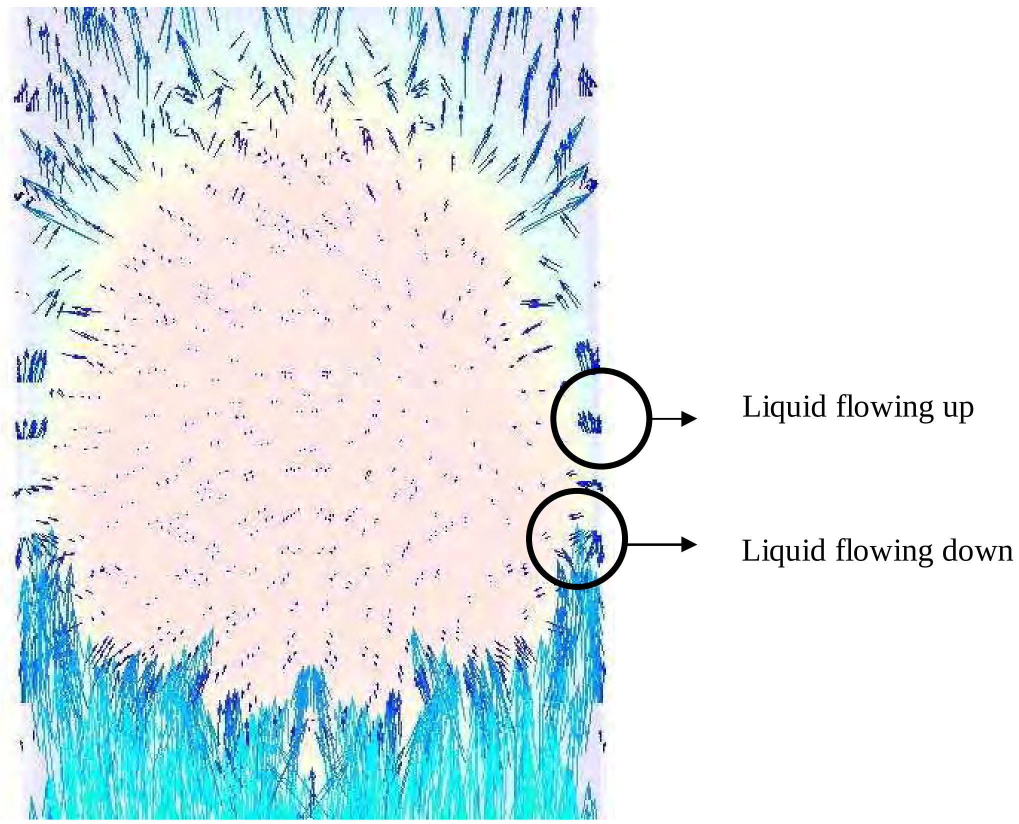

Figure 7.36. Liquid flow patterns in the region between the bubble and the wall/ membrane.

The results which have been presented thus far were obtained with a high resolution advection scheme and the second order backwards Euler transient scheme. This combination produced results which were much better than any other combination that was investigated. For example, with the low resolution upwind advection scheme, and first order backward Euler transient scheme, mass conservation of air was very poor. The bubble was seen to shrink with time and eventually split into two bubbles (figure 7.37). The bubble also became wet. However, the smearing of the interface was much less in the wake region as compared with the bubble in the previous section. Although the breaking up of the bubble into two has been observed experimentally, it usually occurs for much larger bubbles than the one in our simulation and usually for more viscous fluids (Chen et al., 1999). Thus, the predicted breaking up of the bubble is purely a result of numerical deficiency of the upwind advection scheme.

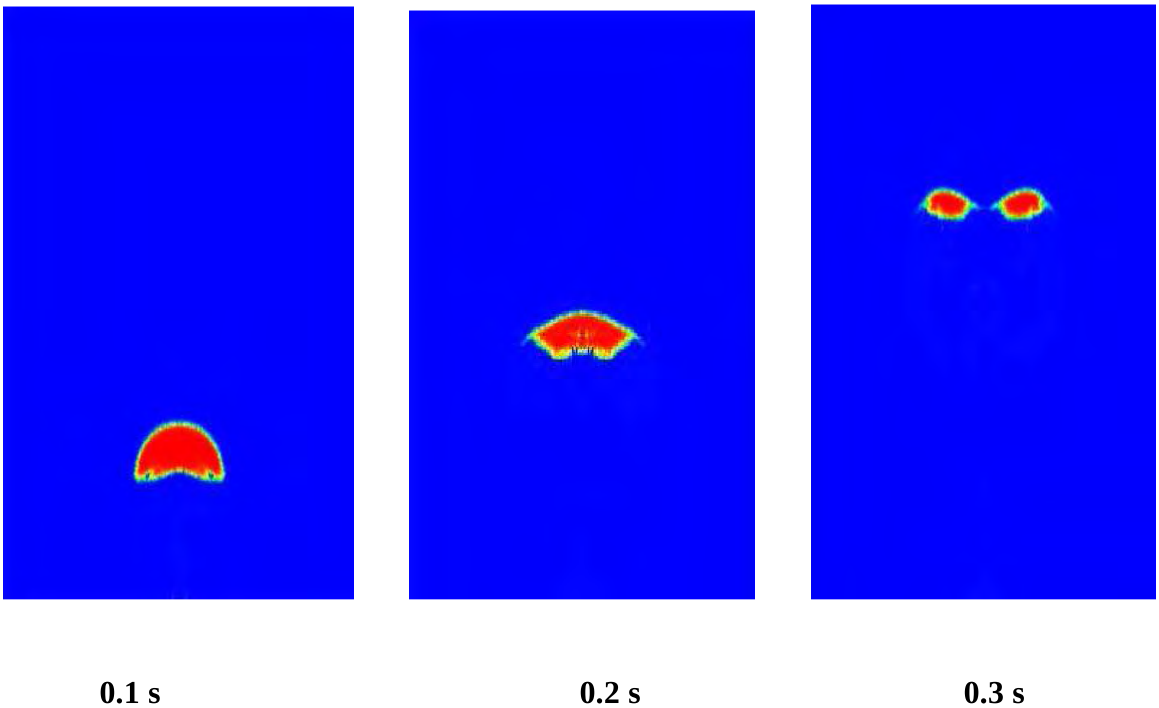

Figure 7.37. Bubble shape development obtained with a low order upwind advection scheme.

7.5.2 Simulations with a two-fluid model using gas phase length-scale of 5 mm

Due to the problems encountered with the VOF model, VOF simulations were abandoned and the two-fluid model was used instead. The two-fluid model used in chapter six for two-dimensional simulations of Taylor bubble was implemented here for the three-dimensional simulations of single bubbles rising in stagnant liquids. Figure 7.38 shows a typical bubble that was obtained using the two-fluid model. The problem of interface smearing still persisted, though this time it was more severe in the top part of the bubble than the bottom part. This picture also shows that the bubble is starting to split from the top downwards which is not a physical phenomenon. Further simulations with the two-fluid model were thus discontinued.

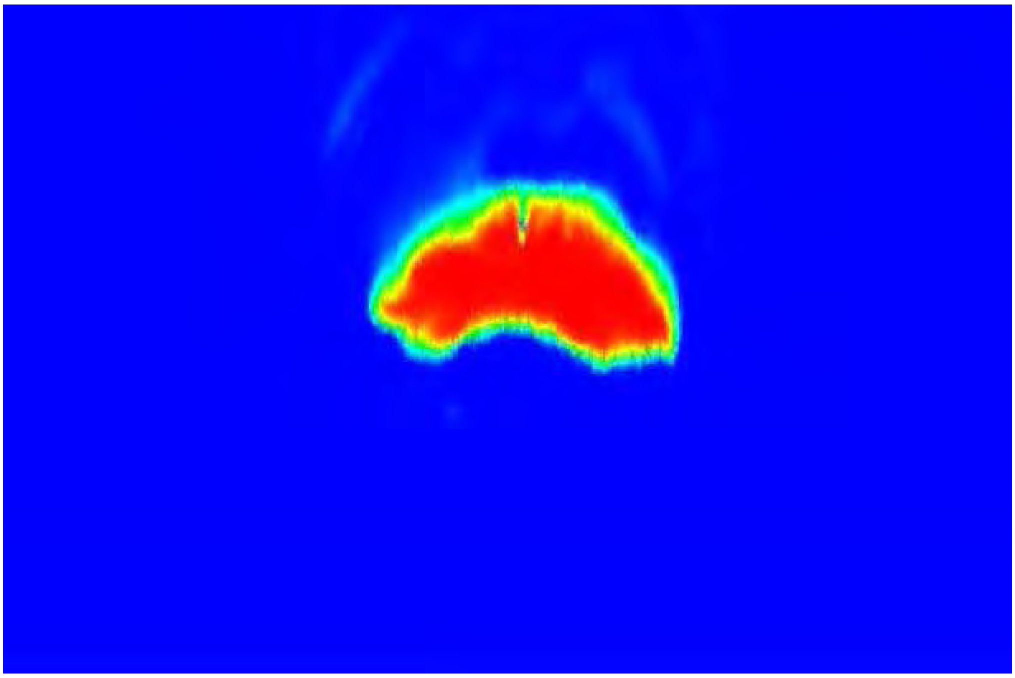

Figure 7.38. Shape of the bubble obtained with a standard two-fluid model.

7.5.3 Simulations with the combined two-fluid / VOF model

The combined two-fluid / VOF model was successfully used in chapter six in the simulations of a Taylor bubble rising in a stagnant liquid where a very sharp interface was achieved all around the bubble. Sample results of the bubble shape development obtained by this model are shown in figure 7.39. As with the VOF model, the bubble started well but then disintegrated with time. The major problem was the bubble getting wet (as shown by the bubble results at 0.13 s) and the shape of the bubble did not appear physical. Another problem with these simulations was that most of them diverged. Increasing the number of coefficient iteration loops per time step improved convergence to a certain extent, however this required a much longer computational time.

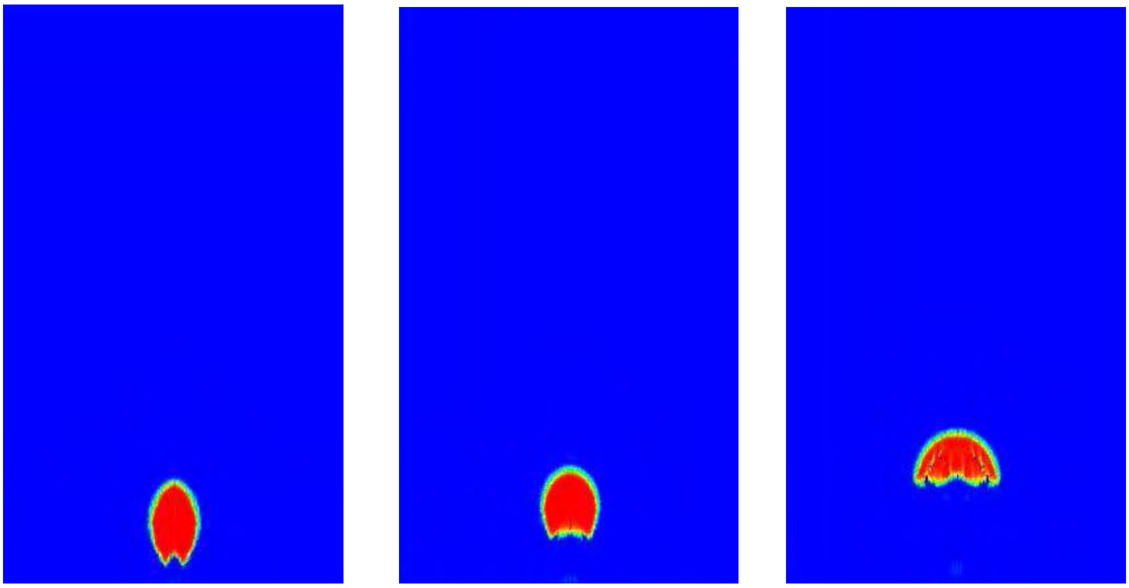

Figure 7.39. Bubble shape development obtained with the combined VOF/two-fluid model.

7.6 DISCUSSIONS

7.6.1 The Eulerian two-fluid simulations

The Eulerian two-fluid simulations were carried out mainly to investigate the hydrodynamic features of two-phase flow that are responsible for flux enhancement in the submerged flat-sheet membrane system. Increasing the gas injection rate resulted in greater meandering of the gas and liquid streams in the tank. The amplitude of meandering was also higher with the higher gas flow rate. This implies that with more air, there is greater mixing occurring in the tank. Greater mixing of the liquid will minimize the extent to which particles will settle on the membrane, thus, fouling will be reduced and flux will be enhanced. With the lower air flow rate the meandering is small and restricted only to certain parts of the membrane, whereas at higher air flow rates the meandering is large and spreads over large parts of the membrane. This could therefore explain why, with the lower gas flow rates, the flux enhancement is lower compared with higher gas flows.

Upon examination of the liquid induced superficial velocities, the magnitude of the maximum induced velocity did not show any dependence on the gas flow rate. However, the vertical velocity plots across the column did show a higher degree of fluctuation as the air flow rate was increased. The liquid vertical velocities appeared to be changing direction more frequently at higher air flow rates than at lower ones. The larger fluctuations of the liquid stream at higher air flow rates could be a contributing factor when it comes to fouling reduction rather than the magnitude of the induced velocities. The maximum induced superficial liquid velocity was about 0.24 m/s and was almost similar for all air flow rates. Churchouse and Wildgoose (1998) reported induced velocities of up to 0.5 m/s in the Kubota membrane bioreactor process, however, they used injection rates which were much larger than the ones used in our experiments and simulations.

The simulations also revealed that gas hold-up increased with the air flow rate. Thus there are more bubbles present across the membrane at larger air flow rates. The question that was raised in chapter five was whether it is the number or the size of the bubbles that has more effect. This question could not be fully answered because the pictures analysed in chapter five contained bubbles of different sizes. In the simulations, all the bubbles are of the same size and hence this suggests that the total number of bubbles that are present also contribute towards fouling retardation since with higher air flow rates there are more bubbles as the volume fraction distribution indicates. Therefore the air flow rate of 8 l/min, which was found to be the most effective in chapter three, could be the most effective because it creates the most number of bubbles and has the highest gas hold-up in the system.

The effect of increasing the bubble size also resulted in an increase in the degree of meandering of the gas and liquid streams just as increasing the air flow rate did. Moreover, increasing the bubble size also had an effect on the maximum induced liquid velocity, with the largest bubble size of 15 mm inducing the largest superficial liquid velocity. This could partly be due to the fact that larger bubbles rise faster. In tubular systems, the shear stress on the membrane has been found to be directly proportional to the liquid velocity across the membrane (Cabassud et al., 2001) and thus larger bubbles may be more effective in reducing fouling due to increased induced liquid velocities. In the picture analysis of chapter five, it was observed that the frequency of larger bubbles is much higher at higher air flow rates, thus this partly explains why the higher air flow rates were found to be more effective in the experiments. On the contrary, gas hold-up was found to decrease with an increase in the bubble size. This could be explained by the fact that larger bubbles are rising faster and thus spend less time in the column. It is thus difficult to judge which has a greater influence between larger bubbles rising faster and spending less time in the tank and smaller bubbles with longer residence times. The effect of bubble size could not be elucidated experimentally since in the experiments bubbles of different sizes were present at all air flow rates. Though increasing the air flow rate increased the number of large bubbles substantially, the number of small bubbles also increased. Thus at this stage, any improvement in the cleaning process cannot be directly linked to the existence of a particular bubble size.

Wall shear stress is probably the major factor responsible for reduction of fouling in membrane systems. All fouling minimization strategies have focused on improving the shear stress on the membrane by creating turbulence (Finnigan & Howell, 1990; Millward et al., 1995; Moulin et al., 1996). Analysis of the shear stress distribution on the membrane showed that the areas of higher shear stress on the membrane coincide with regions where the bulk of the air passes through. The size of the regions of high shear stress increased as the air flow rate increased. Also the locations of these regions varied with time during the simulation depending on the path of air flow, thus covering a large fraction of the membrane area over time, particularly at higher gas flow rates. The average shear stress on the membrane was always higher at the air flow rate of 8 l/min than the other smaller air flow rates at any time during the simulation. However the average shear stress for different bubble sizes did not show any dependence on the bubble size. On the other hand, the maximum shear stress increased with both the air flow rate and the bubble size. This analysis of the shear stress is helpful in understanding the trends observed experimentally where the degree of fouling reduction increased as the air flow rate was increased. Increase of maximum shear stress with the bubble size, seems to indicate that larger bubbles may be more effective than smaller bubbles in terms of combating fouling.

Baffles were used in the experiments in order to improve the distribution of flow across the membrane. The simulations were thus carried out to help understand how the presence of baffles affects the flow distribution and the shear stress across the membrane. In the experiments, only a fixed number of baffles were used but in the simulations the number of baffles was varied to gauge whether the actual number of baffles had any effect. It was observed that the presence of baffles completely stopped the meandering of the gas and liquid stream resulting in the bubbles rising in the straight path. There is no migration of bubbles towards the edges of the column. Analysis of the shear stress on the membrane surface revealed that most of the membrane experienced larger shear stresses when baffles are present as compared with the cases without baffles. Both the average and the maximum shear stress also increased with the number of baffles. In the experiments, fouling reduction increased when baffles were present at all flow rates. This increase in fouling reduction can therefore be linked with an increase in overall shear stress on the membrane. The increase of shear stress with the number of baffles shows that as the bubbles become more confined they exert a higher shear stress on the membrane. However, the number of baffles can only be increased to a certain extent, otherwise the column will become too congested and this may affect biological activity in a membrane bioreactor and increase the pressure drop to unacceptable levels.

7.6.2 Single bubble simulations

Numerous problems were encountered with the single bubble simulations as has been outlined in section 7.5.1. Single bubble simulations were therefore discontinued before any of the desired objectives were achieved. From the results obtained from the single bubble simulations of this chapter and that of chapter six, it is clear that in order for these simulations to work, an extremely fine grid is required. The geometry in chapter six was smaller and the simulations were two-dimensional and axis-symmetric which enabled the utilization of a very fine grid without resulting in excessively long computational times. The grid spacing used for the simulations in chapter six was 0.25 mm but in the simulations of this chapter such a grid could not be utilised because of the computational time that would be required to solve the problem. It was realized that on top of an extremely fine mesh, another requirement for these simulations to work is very small time steps. In the single bubble simulations the smallest time step that was used was 1×10^{-4} s and this simulation took about a month for a bubble to rise just halfway up the column. Accompanying small time steps, the number of coefficient iteration loops per time step needed to be increased to a high number to achieve good convergence of residuals per time step.

7.7 CONCLUSIONS

The results of the simulations have been very helpful in explaining the trends which were observed in the experiments. Fouling reduction in the experiments obtained by increasing the air flow rate and by using baffles has successfully been linked to the increase in the overall shear stress on the membrane. Other hydrodynamic features responsible for effectiveness of two-phase flow in membrane cleaning for submerged membranes are the meandering of the bubble plume for cases without baffles which increases with the gas flow rate and the liquid induced velocities which increase with the bubble size.

Chapter 8

CONCLUSIONS AND RECOMMENDATIONS

8.1 OVERALL CONCLUSIONS

The aim of this thesis was to investigate and optimise the use of gas-liquid two-phase flow as a fouling minimisation strategy for submerged flat sheet membranes. Submerged flat sheet membranes are predominantly used in membrane bioreactors (MBR) for wastewater treatment, however, this study focused only on the hydrodynamic aspects of the MBR system and therefore the biological aspect was not considered. Consequently a model suspension of commercial baker's yeast was deemed suitable to use for experimentation, and furthermore, results obtained from the yeast suspension were later verified by using waste activated sludge as a feed. The correlation between the yeast and the activated sludge suspension results was very good and indicated that the less complex and easy to prepare yeast suspension can be used with confidence in studying at least the effects of hydrodynamic parameters in a real MBR system. This research project involved conducting experimental and CFD simulations of the various hydrodynamic conditions. Hydrodynamic factors that were investigated were: air flow rate, nozzle size, nozzle geometry, concentration of the feed, intermittent filtration, intermittent bubbling, effect of the channel gap width, effect of using membrane baffles, effect of bubble size and bubble size distribution, and effect of bubble rise velocity. The numerical methods for modelling two-phase flow as available in the commercial CFD code, CFX 5.6 from Ansys, were first successfully validated against published experimental data before being used to study the characteristics of two-phase as encountered in this study. Since the system studied was not a true MBR, some of the results are not directly applicable to MBRs and the extent to which each finding is applicable to a real MBR will be described in the following sections.

8.1.1 The effect of air flow rate

By looking at various factors such as trans-membrane pressure (TMP) versus time, rate of change of TMP (dTMP/dt), specific cake resistance versus time, the effect of air flow rate on fouling reduction was investigated. The benefit obtained by injecting the gas was found to increase with the gas flow rate for all nozzle sizes considered except in the cases where baffles were employed where the maximum benefit was obtained at the lowest air flow rate. For the activated sludge suspension an optimum bubbling rate of about 12 l/min (120 l/min per m^2 of membrane area) was observed. Although this air flow rate may seem high compared to the one which commercial plants are moving towards (which is 10 l/min per m^2 of membrane area), it has to be remembered that in this study only one membrane (0.1 m^2) was used and the same air flow rate could be delivered to a cassette of 16 membranes (1.6 m^2) with probably the same hydrodynamic effects being achieved. In the latter case the optimum flow rate would be around 7 l/min per m^2 of membrane area. This applies to the standard Kubota module setup which was used in this study. Therefore whilst the actual optimum air flow rate may be different for a real submerged MBR, the results of this study strongly suggest that optimal bubbling rates do exist for submerged flat sheet MBRs.

By using particle imaging software, AnalySIS®, the greater reduction of fouling with increasing air flow rate was linked to the increase in the average bubble size, increase of bubble rise velocity, increase in the gas hold-up and an increase in the percentage flow that ends up as large bubble flow, that is, flow consisting of bubbles larger than 10 mm in diameter. CFD simulations revealed that increasing the air flow rate increases the average shear stress on the membrane. The simulations further revealed that the liquid recirculation and degree of meandering of the gas stream increases with the air flow rate. Therefore these observations strongly suggest that the enhancement effect obtained by bubbling is both due to enhanced shear stress on the membrane and increased liquid recirculation. The two factors complement each other and we were unable to distinguish which one plays a larger role.

The bubble size distribution analysis results indicated that the size of the bubble plays an important role in the two-phase flow cleaning mechanism. As the air flow rate was increased, the bubble size distribution analyses showed an increase in the number of medium (2 – 10 mm) and large bubbles (greater than 10 mm) whilst the percentage flow ending up as large flow increased with air flow rate. The channel gap between the membrane and the wall was 7 mm, therefore bubbles larger than about 7 mm in diameter became slugs. Slug flow has been identified in many other studies as the most effective type of two-phase flow for fouling retardation. Reasons for this were discussed in chapter 2. Thus with increasing air flow rate, the percentage of slug flow is increased which improves the cleaning effect on the membrane. It was not experimentally possible to study bubbles of different sizes as the process of bubble generation could not be manipulated, however, this was possible numerically via CFD simulations. The simulations revealed that when the bubble diameter was increased from 2 mm to 5 mm and then to 10 mm, significant increase in the average shear stress on the membrane occurred with each increase, the bubble rose faster and the intensity of liquid recirculation and bubble plume meandering increased. However, when the bubble size was increased from 10 mm to 15 mm, the increase in average shear stress and liquid recirculation was minor. Since for bubble diameters of 7 mm and larger, the flow becomes slug flow, these results suggested that once slug flow is attained, increasing the bubble size (by increasing the air flow rate experimentally) becomes less significant. This can also explain why an optimum bubbling rate was observed in chapter 4. Once slug flow is achieved further improvement in the cleaning effects of the two-phase flow can be achieved by controlling the frequency of the slug generation and this can be achieved by installing a device such as a solenoid valve on the air injection line. This work could be included in future studies. The effect of bubble size and bubble size distribution as observed in this study should be directly applicable to real submerged MBR system which utilises a gap width similar to the one used in this study.

8.1.2 The effect of membrane baffles

Early visual observations in this study showed that the majority of the gas bubbles, after being released from the nozzles, migrate towards the centre of the vessel and stay in that vicinity as they rise and this was also supported by literature from bubble column studies. This uneven distribution of air bubbles across the membrane surface led to spatial variation of fouling deposits on the membrane which was confirmed by conducting an analysis of carbohydrates deposited on selected locations on the membrane. CFD simulations also revealed that for isolated bubbles rising between narrow parallel plates, the bulk of the liquid flows around the bubble on the unconstrained sides and very little liquid passes between the bubble and the membrane. This could mean less scouring of the membrane by the bubble. To improve the distribution of bubbles across the surface of the membrane and improve the scouring effects of bubbles, baffles were fabricated and inserted between the membrane and the wall. This forced bubbles to move up in a straight line. The only negative impact of this was that the scouring effect induced by bubble plume meandering was eliminated. With the baffles being only 10 mm apart, bubbles larger than 10 mm were constrained and instead of becoming oblate spheroids, ellipsoidal or hemispherical cap bubbles, they became Taylor bubbles which are known to be the most effective for fouling reduction in tubular and hollow fibre modules. The use of baffles ensured that bubbles were constrained on all sides rather than on just two sides as is the case with no baffles. With constrained bubbles more liquid was forced to pass between the membrane and the bubble in a form of a thin falling film. The shear stress in the thin falling film is known to be very high. In the validation of numerical methods study that was carried out using Taylor bubbles (chapter 6), we found shear stresses in the falling film to be up to six times higher than shear stresses in the liquid slugs. Fouling reduction was always found to be higher in runs with baffles than those without baffles at all air flow rates considered. Simulations revealed that average shear stress on the membrane was at least 3 times higher for runs with baffles than those without. Thus with baffles, most of the membrane was exposed to bubble flow and shear stress on the membrane was also increased. Since baffles ensured that slug flow conditions are achieved, this can give some indication as to why the enhancement effects decreased with an increase in the air flow rate in the presence of baffles. In the slug flow, increasing air flow rate reduces the length of the liquid slug, thus reducing the effectiveness of the bubble wake. Further increase in the air flow rate can eventually lead to bubble overlap, eliminating the bubble wake completely and thus having a negative impact on the cleaning effect of the two-phase flow since the turbulence in the bubble wake is thought to have a significant contribution to the effectives of slug-flow in fouling reduction. The effects of baffles as observed in this study should be equally the same in real MBR systems with identical setup. Thus real MBRs should obtain the same benefits if baffles are used.

8.1.3 The effect of nozzle size and geometry

Reduction of fouling was found to increase with the nozzle size whilst with regards to the nozzle geometry, the circular nozzles performed better than the square nozzles of the same surface area when the air flow rate was kept constant. The superiority of the circular nozzles together with the increasing effectiveness of two-phase flow as the nozzle size increased was linked in chapter 5 with a shift in bubble size distribution. It was found that the number of larger bubbles in the bubble size distribution profile and the percentage of flow that ends up as large bubbles (greater than 10 mm) increased with the nozzle size. Bubble rise velocities were also found to increase slightly with the nozzle size. Through CFD simulations in chapter 7 it was established that larger bubbles rise faster and generate higher shear stresses on the membrane. Therefore these results suggest that it is not just the volume of air that is pumped into the system that matters but also it is the size of bubbles in the bubble population that is important. Larger bubbles seem to be more effective for submerged flat sheet membranes whilst the opposite seems to hold for submerged hollow fibre membranes where the flow is less likely to be slug flow (Wicaksana et al., 2006). Whilst the most effective nozzle size and geometry as observed in this study may not necessarily be the most effective in a real MBR, the results indicate that the selection of nozzle size and geometry have to be taken into serious consideration when designing a MBR. These factors should not be chosen arbitrarily.

8.1.4 Intermittent filtration versus intermittent bubbling

For almost all MBRs, aeration required for cleaning the membrane and for biological activity, consumes about 80% of the total energy required. Operating strategies such as intermittent filtration and intermittent bubbling can reduce the total amount of energy required. In this study, intermittent bubbling was found to be less effective than continuous bubbling. However, it is possible that better results can be obtained by conducting more investigations at different intermittent bubbling frequencies. Currently, there are no commercial submerged flat sheet MBRs that use intermittent bubbling, although the practice is used for some submerged hollow fibres. On the other hand intermittent filtration was found to be very effective. Final TMPs with intermittent filtration were at least 70% lower than those for continuous filtration. These results should be directly applicable to real MBR systems.

8.1.5 Critical fluxes

Experiments conducted using various methods to determine critical fluxes seem to indicate that critical fluxes do exist for the type of submerged membrane systems investigated here with the yeast suspension as feed. Identified critical fluxes were found to increase with the air flow rate and decrease with concentration. The use of baffles also improved the critical flux under given conditions. Operating below the nominal critical flux should allow operation for a long period of time before any chemical clean should be necessary. The values of critical flux observed in this study would be different from those which can be found in a real MBR, and it has been suggested that for the MBRs the presence of EPS causes slow fouling at any flux. Thus MBRs operate at 'nominally subcritical' fluxes. The appropriate conditions could be determined using methods used in this study.

8.2 RECOMMENDATIONS

From the outcomes of the present study, a number of recommendations for future work are proposed.

8.2.1 Optimisation of the two-phase flow cleaning method

The results of this study showed an increasing cleaning effect of the two-phase flow with an increase in the nozzle size, however, only a limited number of different nozzle sizes were studied here. More work should be completed in order to establish the optimum nozzle size for submerged flat sheet MBR systems.

From investigations conducted on the effect of nozzle geometry, results suggested that the geometry of the nozzle does have an impact on the bubble size distribution. More work needs to be done on nozzles of different geometries and sizes in order to determine the optimum nozzle design for submerged flat sheet membranes.

Although an optimum air flow rate was established, this was done using one membrane only. Scaling up of the system to a pilot / full scale plant may affect the hydrodynamic conditions, thus optimisation of the two-phase flow cleaning method needs to be undertaken on a pilot plant scale with multiple membranes using the results from this laboratory scale study as a guideline.

Future work also needs to be conducted in order to optimise the frequencies for intermittent bubbling and intermittent filtration. The frequencies used in this study were chosen arbitrarily and were not optimised as investigations into the effect of intermittent bubbling and intermittent filtration were not a major focal points of the thesis.

8.2.2 Improving the design of baffles

The design of baffles needs to be optimised in terms of the type of the most appropriate baffle structure / geometry as well as dimensions.

The effects baffles will have on the biological activity in a real MBR needs to be carefully studied. Similarly the potential effects of biofilms on the baffles need to be assessed.

REFERENCES

Baker, R. J., Fane, A. G., Fell, C. J. D. & Yoo, B. H. (1985); Factors affecting flux in crossflow; Desalination, **53**, pp81.

Bauser, H., Chemiel, H., Stroh, N. & Waltiza, E. (1982); Interfacial effects with microfiltration membranes; J. Memb. Sci., **11**, pp321.

Beek, W. J. & Muttzall, K. M. K. (1975); Transport phenomena; Wiley, London.

Bellara, S. R., Cui, Z. F. & Pepper, D. S. (1996); Gas sparging to enhance permeate flux in ultrafiltration using hollow fibre membranes; J. Memb. Sci., **121**, pp175.

Bellara, S. R., Cui, Z. F. & Pepper, D. S. (1997); Fractionation of BSA and lysozyme using gas sparged ultrafiltration in hollow fibre membrane modules; Biotech Prog., **13**, pp869.

Ben Aim, R. (2002); Personal communication.

Benefiled, L. D. & Randall, C. W. (1980); Biological process design for wastewater treatment; Prentice-Hall, New Jersey.

Bertram, C. D., Raymond, C. J. & Pedley, T. J. (1991); Application of nonlinear dynamics concepts to the analysis of self-excited oscillations of a collapsible tube conveying a fluid; J. Fluids and Structures, **5**, pp391.

Bouhabila, E. H., Ben Aim, R. & Buisson, H. (1998); Microfiltration of activated sludge using submerged membrane with air bubbling (application to wastewater treatment); Desalination, **118**, pp315.

Bouhabila, E. H., Ben Aim, R. & Buisson, H. (2001); Fouling characterization in membrane bioreactors; Separation and Purification Technol., 22, pp123.

Brackbill, J.U., Kothe, D.B. & Zemach, C. (1992); A continuum method for modeling surface tension; J. Comp. Physics, **100**, 335.

Brans, E. H. P. (1997); The scarcity of water: emerging legal and policy responses; London, Boston: Kluwer Law International.

Brewster, M. E., Chung, K. Y. & Belfort, G. (1993); Dean vortices with wall flux in a curved channel membrane system 1. A new approach to membrane module design; J. Memb. Sci., **81**, pp127.

Brockmann, M. & Seyfired, E., F. (1996); Sludge activity and cross-flow microfilatration – a non-beneficial relationship; Wat. Sci. Tech., **34**, pp205.

Bugg, J. D., Mack, K. & Rezkallah, K. S. (1998); A numerical model of Taylor bubbles rising through stagnant liquids in vertical pipes; Int. J. Multiphase Flow, **24**, 271.

Bugg, J. D. & Saad, G. A. (2002); The velocity field around a Taylor bubble rising in a stagnant viscous fluid: numerical and experimental results; Int. J. Multiphase Flow, **28**, 791.

Buwa, V. V. & Ranade, V. V. (2001a); Dynamics of gas-liquid flow in 2-D bubble columns: Influence of sparger design, column geometry and physical properties; Proc. Intl. Conference on Multiphase flows, 2001, New Orleans, USA.

Buwa, V. V. & Ranade, V. V. (2002); Dynamics of gas-liquid flow in a rectangular bubble column: experiments and single/multi-group CFD simulations; Chem. Eng. Sci., **57**, pp4715.

Cabassud, C. & Ducom, G. (2001); Air sparging in flat sheet nanofiltration membranes: effect on cake deposit and on concentration polarization, 6th World Congress of Chemical Engineering, Melbourne, Australia, 23-27 September.

Cabassud, C., Laborie, S., Durand-Bourlier, L. & Laine, J. M. (2001); Air sparging in ultrafiltration hollow fibres: relationship between flux enhancement, cake characteristics and hydrodynamic parameters; J. Memb. Sci., **181**, pp57.

Cabassud, C., Laborie, S. & Laine, J. M. (1997); How slug flow can improve ultrafiltration flux in organic hollow fibres; J. Memb. Sci., **128**, pp93.

Cao, Z. (1998); Feed channel spacer characterisation and their optimisation; PhD Thesis, University of New South Wales, Sydney, Australia.

Chang, I. S., Le-Clech, P., Jefferson, B. & Judd, S. (2002); Membrane fouling in membrane bioreactors for wastewater treatment; J. Environ. Eng., **128**, pp1018.

Chang, S. (2001); Optimization of submerged hollow fibre membrane modules; PhD Thesis, Universisty of New South Wales, Sydney, Australia.

Chang, S. & Fane, A. G. (2000); Filtration of biomass with axial inter-fibre upward slug flow: performance and mechanisms; J. Memb. Sci., **180**, pp57.

Chang, S. & Fane, A. G. (2001); The effect of fibre diameter on filtration and flux distribution – relevance to submerged hollow fibre modules; J. Memb. Sci., **184**, pp221.

Chen, L., Garimella, S. V., Reizes, J. A. & Leonardi, E. (1999); The development of a bubble rising in a viscous liquid; J. Fluid Mech., **387**, pp61.

Chen, L. & Li, Y. (1998); A numerical method for two-phase flows with an interface; Envinm. Modeling And Software, **13**, pp247

Chiemchaisri, C., Wong, Y. K., Urase, T. & Yamamoto, K. (1992); Organic stabilization and nitrogen removal in a membrane separation bioreactor for domestic wastewater treatment; Wat. Sci. Tech., **25**, pp231.

Cho, B. D. (2002); Treatment of high strength wastewater using membrane bioreactors; PhD Thesis, University of New South Wales, Sydney, Australia.

Cho, B. D. & Fane, A. G. (2002); Fouling transients in nominally subcritical flux operation of a membrane bioreactor; J.Memb.Sci., **209**, pp391.

Chua, H. C., Arnot, T. C. & Howell, J. A. (2002); Controlling fouling in membrane bioreactors operated with a variable throughput; Desalination, **149**, pp225.

Churchouse, S. (1998); Kubota maintains popular trend; Water and Environment, November 1998, pp27.

Churchouse, S. & Wildgoose, D. (1998); Membrane bioreactor progress from the laboratory scale to full-scale use; Memb. Technol., **111**, pp4.

Churchouse, S. & Wildgoose, D. (1999); Membrane bioreactors hit the big time – from lad scale to full-scale application; MBR2 – Proc. 2nd Intl. Mtg. membrane bioreactor for wastewater treatment, Cranfield University, UK, pp14.

Clarke, A. & Issa, R.I. (1997); A numerical model of slug flow in vertical tubes; Computers & Fluids, **26**, 395.

Clift, R., Grace, J. R. & Weber, M. E. (1978); Bubbles, drops and particles; Academic Press, New York.

Colman, D. A. &, Mitchell, W. S. (1990); Enhanced mass transfer for membrane processes; IChemE. Symposium Series No. **118**, pp119.

Cote, P. & Thompson, D. (1999); Wastewater treatment using membranes: the North American experience; Proceedings Membrane Technology in Environmental Management (Tokyo), pp46.

Cui, Z. F., Bellara, S. R. & Homewood, P. (1997); Airlift crossflow membrana filtration – a feasibilty study with dextran ultrafiltration; J. Memb. Sci., **128**, pp83.

Cui, Z.F., Chang, S. & Fane, A.G. (2003); The use of gas bubbling to enhance membrane processes – A review; J. Memb. Sci., **221**, pp1.

Cui, Z. F. & Taha, T. (2003); Enhancement of ultrafiltration using gas sparging: a comparison of different membrane modules; J. Chem. Technol. Biotechnol., **78**, pp249.

Cui, Z. F. & Wright, K. I. T. (1994); Gas-liquid two-phase cross-flow ultrafiltration of BSA and dextran solutions; J. Memb. Sci., **90**, pp183.

Cui, Z. F. & Wright, K. I. T. (1996); Flux enhancement with gas sparging in downwards crossflow ultrafiltration: performance and mechanism; J. Memb. Sci., **117**, pp109.

Davidson, J. F. & Schuller, B. O. (1960); Bubble formation at an orifice in an inviscous liquid; Trans. Inst. Of Chem. Engnrs., **38**, pp342.

Davis, R. H. & Grant, D. C. (1992a); Theory of dead end microfiltration in W. S. and K. K. Sirkar, Membrane handbook, Van Norstand Reinhold, New York, pp461.

Deen, N. G., Solberg, T. & Hjertager, B. H. (2001); Large eddy simulation of the Gas-Liquid flow in a square cross-sectioned bubble column; Chem. Eng. Sci., **56**, pp6341.

Defrance, L. & Jaffrin, M. Y. (1999); Reversibility of fouling formed in activated sludge filtration; J. Memb. Sci., **157**, pp73.

Delnoij, E., Kuipers, J. A. M. & Swaaij, W. P. M. (1997); Computational fluid dynamics applied to gas-liquid contactors; Chem. Eng. Sci., **52**, pp3623.

Dubios, M., Gilles, K.A., Hamilton, J. K., Rebers, P. A. & Smith, F. (1956); Colorimetric method for determination of sugars and related substances; Anal. Chem., **28**, pp350.

Ducom, G. & Cabassud, C. (2003); Possible effects of air sparging for nanofiltration of salted solutions; Desalination, **156**, pp267.

Ducom, G., Matamoros, H. & Cabassud, C. (2002a); Air sparging for flux enhancement in nanofiltration membranas: Application to O/W stabilised and non-stabiblised emulsions; J. Memb. Sci., **204**, pp221.

Ducom, G., Puech, F. P. & Cabassud, C. (2002b); Air sparging with flat sheet nanofiltration: a link between wall shear stresses and flux enhancement; Desalination, **145**, pp97.

Essemiani, K., Ducom, G., Cabassud, C. & Line, A. (2001); Spherical cap bubbles in a flat sheet nanofiltration module: experiments and numerical simulation; Chem. Eng. Sci., **56**, pp6321.

Fabre, J. & Liné, A. (1992); Modeling of two-phase slug flow; Ann. Rev. Fluid Mech., **24**, pp21.

Fane, A. G. (1986); Ultrafiltration: factors affecting flux and rejection; Prog. Filtr. Sep., **4**, pp101.

Fane, A. G. (2000); Membrane lectures; School of Chemical Engineering and Industrial Chemistry, the University of New South Wales.

Fane, A. G., Fell, C. J. D. & Nor, M. T. (1978); Wastewater treatment using a combined activated sludge and ultratfiltration system; Proc. Asian Pacific Confederation of Chem. Eng., Jakarta, November 1978, pp117.

Field, R. W., Wu, D., Howell, J. A. & Gupta, B. B. (1995); Critical flux concept for microfiltration fouling; J. Memb. Sci., **100**, pp259.

Finnigan, S. M. & Howell, J. A. (1989); The effect of pulsatile flow on ultrafiltration fluxes in a baffled tubular membrane system; Chem. Eng. Res. Design, **67**, pp278.

Finnigan, S. M. & Howell, J. A. (1990); The effect of pulsed flow on ultrafiltration fluxes in a baffled tubular membrane system; Desalination, **79**, pp181.

Fisher, E. & Raasch, J. (1985); Cross-flow filtration; Ger. Chem. Eng., **8**, pp211.

Ghosh, R. & Cui, Z. F., (1999); Mass transfer in gas sparged ultrafiltration: upward slug flow in tubular membranes; J. Memb. Sci., **162**, pp91.

Gleick, P. H. (2004); The world's water 2004 – 2005: the biennial report on freshwater resources; Washington, D. C., Island Press.

Guibert, D., Ben Aim, R. & Cote, P. (2002); Aeration performance of immersed hollow-fibre membranes in a bentonite suspension; Desalination, **148**, pp395.

Gupta, B. B., Blanpain, P. & Jaffrin, M. Y. (1992); Permeate flux enhancement by pressure and flow pulsations in microfiltration with mineral membranes; J. Memb. Sci., **70**, pp257.

Hamann, M. L., Li, J., Jacobs, E. P., Bradshaw, S. M., Sanderson, R. D. & Pillay, V. L. (2003); Investigation of system hydrodynamics for improved air-scouring of immersed woven membranes using ultrasonics; Proc. Of 5th Intnl. Conf. On Memb. Technol. (IMSTEC), CD ROM, November 2003, Sydney, Australia.

Hasar, H., Kinaci, C., Unlu, A. & Ipek, U. (2001); Role of intermittent aeration in domestic wastewater treatment by submerged membrane activated sludge system; Desalination, **142**, pp287.

Harvie, D.J.E. & Fletcher, D.F. (2000); A new volume of fluid advection algorithm: The stream scheme; J. Comp. Phys., **162**, pp1.

Hewitt, G. F. (1990); Multiphase fluid flow and pressure drop: Introduction and Fundamentals, G. F. Hewitt (Ed), Hemisphere Handbook of Heat Exchanger Design, Hemisphere Publishing Corp., New York.

Hirt, C.W. & Nichols, B.D. (1981); Volume of fluid (VOF) method for the dynamics of free boundaries; J. Comp. Physics, **39**, pp201.

Hong, S. P., Bae, T. H., Tak, T. M., Hong, S. & Randall, A. (2002); Fouling control in activated sludge submerged hollow fibre membrane bioreactors; Desalination, **143**, pp219.

Howell, J. A. (1995); Sub-critical flux operation of microfiltration; J. Memb. Sci., **107**, pp165.

Howell, J. A., Chua, H. C. & Arnot, T. C. (2004); In situ manipulation of critical flux in a submerged membrane bioreactor using variable aeration rates, and effect of membrane history; J. Memb. Sci., **242**, pp13.

Howell, J.A., Field, R.W., Mackley M.R. & Wang, Y. (1992); The simulation of particle advection in a porous baffled channel subject to pulsatile flow; Preprints IChemE Research Event, Rugby, pp386.

Howell, J. A., Field, R. W. & Wu, D. (1993); Yeast cell microfiltration: flux enhancement in baffles and pulsatile flow systems; J. Memb. Sci., **80**, pp59.

Illias, S. & Govind, R. (1990); Potential applications of pulsed flow for minimizing concentration polarization in ultrafiltration; Sep. Sci. Technol., **25**, pp13.

Imasaka, T., Kanekuni, N., So, H. & Yoshino, S. (1989); Cross-flow filtration of methane fermentation broth by ceramic membranes; J. Fermentation and Bioeng., **68**, pp200.

Issa, R. I. & Ubbink, O. (1999); Numerical prediction of Taylor bubble dynamics using a new interface capturing technique; in Proc. Of 3rd ASME/JSME Joint Fluids Eng. Conf., San Francisco, CA, pp18.

Jaffrin, M. Y. (1989); Innovative process for membrane plasma separation; J. Memb. Sci., **44**, pp115.

Jaffrin, M. Y., Ben Amar, R. & Gupta, B. B. (1989); Membrane fouling control in cross flow filtration of wine with mineral membranes; Proc. Intnl. Tech. Conf. On Memb. Sep. Processes , Brighton, UK.

Jaffrin, M. Y., Ding, L. H. & Laurent, J. M. (1992); Kinetics of concentration-polarisation formation in cross-flow filtration of plasma from blood: experimental results; J. Memb. Sci., **72**, pp267.

Jakobsen, H. A., Sannaes, B. H., Grevskott, S. & Svendsen, H. F. (1997); Modelling of vertical bubble-driven flow; Ind. Eng. Chem. Res., **36**, pp4052.

Jefferson, B. & Judd, S. (2003); Industrial water recycling with membranes: drivers, problems and economics; Proc. Of 5th Intnl. Conf. On Memb. Technol. (IMSTEC), CD ROM, November 2003, Sydney, Australia.

Jeffree, M. A., Peacock, J., Sobey, I. J. & Belhouse, B. J. (1981); Gel layer-limited haemofiltration rates can be increased by vortex mixing; Clin. Exp. Dias. Apheresis, **5**, pp373.

Judd, S. J., Le-Clench, P., Taha, T. & Cui, Z. F. (2001); Theoretical and experimental representation of a submerged bio-reactor system; Membrane Technology, **135**, pp4.

Kawaji, M., DeJesus, J.M. & Tudose, G. (1997); Investigation of flow structures in vertical slug flow; Nuclear Eng. Des., **175**, pp37.

Kennedy, T. J., Merson, R. L. & McCoy, B. J. (1974); Improving permeation flux by pulsed reverse osmosis; Chem. Eng. Sci., **29**, pp1927.

Kenning, D. B. R. & Kao, Y. S. (1972); Convective heat transfer to water containing bubbles: Enhancement not dependent on thermocapillarity; Intnl. J. Heat Transfer, **15**, pp1709.

Krishna, R. & van Baten, J. M. (2001); Simulating the rise characteristics of gas bubbles in liquids using CFD; Chem. Eng. Technol., **24**, pp427.

Kroner, K. H. & Nissinen, V. (1988); Dynamic filtration of microbial suspension using an axially rotating filter; J. Memb. Sci., **36**, pp85.

Kroner, K. H., Nissinen, V. & Ziegler, H. (1987); Improved dynamic filtration of microbial suspensions; Biotechniques, **5**, pp921.

Krstic, D. M., Tekic, M., N., Caric, M. D. & Milanovic, S. D. (2002); The effect of turbulence promoter on cross-flow microfiltration of skim milk; J. Memb. Sci., **208**, pp303.

Kumar, S. & Fan, L. S. (1994); Heat-transfer characteristics in viscous gas-liquid and gas-liquid-solid system, AIChE J., **40**, pp745.

Kuwagi, K., Kusu, S. & Ozoe, H. (2000); Transient three-dimensional numerical analyses of shallow bubble column; Chem. Eng. Sci, **78**, pp5.

Laborie, S. & Cabassud, C. (2005); Modelling and measurement of shear stress for a slug flow inside a capillary; AIChE Journal, **51**, pp1104.

Laborie, S., Cabassud, C., Durand-Bourlier, L. & Laine, J. M. (1997); Flux enhancement by a continuous tangential gas flow in ultrafiltration hollow fibres for drinking water production: effects of slug flow on cake structure; Filtration & Separation, **34**, pp887.

Laborie, S., Cabassud, C., Durand-Bourlier, L. & Laine, J. M. (1998); Fouling control by air sparging inside hollow fibre membranes – effects on energy consumption; Desalination, **118**, pp189.

Laborie, S., Cabassud, C., Durand-Bourlier, L. & Laine, J. M. (1999); Characterisation of gas-liquid two-phase flow inside capillaries; Chem. Eng. Sci., **54**, pp5723.

Lapin, A. & Lubbert, A. (1994a); Numerical simulation of the dynamics of two phase gas-liquid flows in bubble columns; Chem. Eng. Sci., **49**, pp3661.

Le-Clech, P., Jefferson, B. & Judd, S. J. (2003a); Impact of aeration, solids concentration and membrane characteristics on the hydraulic performance of a membrane bioreactor; J. Memb. Sci., **218**, pp117.

Le-Clech, P., Alvarez-Vazquez, H., Jefferson, B. & Judd, S. (2003b); Fluid hydrodynamics in submerged and sidestream membrane bioreactors; Wat. Sci. Technol., **48**, pp113.

Lee, C. K., Chang, W. G. & Ju, Y. H. (1993); Air slugs entrapped cross-flow filtration of bacterial suspensions; Biotech. and Bioeng., **41**, pp525.

Lee, W., Kang, S. & Shin, H. (2003); Sludge characteristics and their contribution to microfiltration in submerged membrane bioreactors; J. Memb. Sci., **216**, pp217.

Li, Q. Y., Cui, Z. F. & Pepper, D. S. (1997a); Effect of bubble size and frequency on the permeate flux of gas sparged ultrafiltration with tubular membranes; Chem. Eng. J., **67**, pp71.

Li, Q. Y., Cui, Z. F. & Pepper, D. S. (1997b); Fractionation of HSA and IgG by gas sparged ultrafiltration; J. Memb. Sci., **136**, pp181.

Li, Q. Y., Ghosh, R.,Cui, Z. F. & Pepper, D. S. (1998); Enhancement of ultrafiltration by gas sparging with flat sheet membrane modules; Separation and Purification Technol., **14**, pp79.

Liovic, P., Liow, J. L. & Rudman, M. (2001); A volume of fluid (VOF) method for the simulation of metallurgical flows; ISIJ International, **41**, pp225.

Longuet-Higgins, M. S., Kerman, B. R. & Lunde, K. (1991); The release of air bubbles from an underwater nozzle; J. Fluid Mech., **230**, pp365.

Lopez de Bertodano, M. A. (1992); Turbulent bubbly two-phase flow in a triangular duct; PhD Thesis (Nuclear Engineering), Rensselaer Polytechnic Institute, New York.

Lopez de Bertodano, M. A., Lee, S. J., Lahey Jr, R. T. & Drew, D. A. (1990); The prediction of two-phase turbulence and phase distribution phenomena using a Reynolds stress model; Transactions of ASME, **12**, pp107.

Lubbecke, S., Vogenpohl, A. & Dewjanin, W. (1995); Wastewater treatment in a biological high performance system with high biomass concentrations; Wat. Res., **29**, pp793.

Mackley, M. R. & Sherman, N. E. (1992); Cake filtration mechanism in steady and unsteady flows; Proc. Engn. Memb. Process, Bavaria, Germany.

Mao, Z.-S. & Dukler, A.E. (1991); The motion of Taylor bubbles in vertical tubes II. Experimental data and simulations for laminar and turbulent flow; Chem. Eng. Sci., **46**, pp2055.

Mavrov, V., Nikolov, N. D., Islam, M. A. & Nikolova, J. D. (1992); An investigation on the configuration of inserts in tubular ultrafiltration module to control concentration polarization; J. Memb. Sci., **75**, pp197.

Mercier, M., Fonade, C. & Lafforgue-Delorme, C. (1995); Influence of the flow regime on the efficiency of a gas-liquid two-phase medium filtration; Biotech Techniques, **9**, pp853.

Mercier, M., Fonade, C. & Lafforgue-Delorme, C. (1997); How slug flow can enhance the ultrafiltration flux in mineral tubular membranes; J. Memb. Sci., **128**, pp103.

Mercier, M., Maranges, C., Fonade, C. & Lafforgue-Delorme, C. (1998); Yeast suspensión filtration: Flux enhancement using an upward gas/liquid slug flor – an application to continuous alcoholic fermentation with cell recycle; Biotech. and Bioeng., **58**, pp47.

Mercier-Bonin, M., Fonade, C. & Gesan-Guiziou, G. (2004); Application of gas/liquid two-phase flows during crossflow microfiltration of skimmed milk under constant flux conditions; Chem. Eng. Sci., **59**, pp2333.

Mercier-Bonin, M., Gesan-Guiziou, G. & Fonade, C. (2003); Application of gas/liquid two-phase flows during crossflow microfiltration of skimmed milk under constant trans-membrane pressure conditions; J. Memb. Sci., **218**, pp93.

Mercier-Bonin, M., Lagane, C. & Fonade, C. (2000a); Influence of a gas/liquid two-phase flow on the ultrafiltration and microfilatration performances: case of a ceramic flat sheet membrane; J. Memb. Sci., **180**, pp93.

Mercier-Bonin, M., Maranges, C., Lafforgue, C., Fonade, C. & Line, A. (2000b); Hydrodynamics of slug flow applied to cross-flow filtration in narrow tubes; AIChE. J., **46**, pp476.

Mikulasek., P., Pospisil, P., Dolecek, P. & Cakl, J. (2002); Gas-liquid two-phase flow in microfiltration: relationship between flux enhancement and hydrodynamic parameters; Desalination, **146**, pp103.

Millward, H. R., Bellhouse, G. & Walker, G. (1995); Screw-thread flow promoters: an experimental study of ultrafiltration and microfiltration performance; J. Memb. Sci., **106**, pp269.

Morgan, R., Minnie, I. & Langford, M. (2003); Submerged membrane technology design and operation: Magnetic Island water recycling facility; Proc. Of 5th Intnl. Conf. On Memb. Technol. (IMSTEC), CD ROM, November 2003, Sydney, Australia.

Moulin, P., Rouch, J. C., Serra, C., Clifton, M. J. & Aptel, P. (1996); Mass transfer improvement by secondary flows: Dean vortices in coiled tubular membranes; J. Memb. Sci., **114**, pp235.

Mulder, M. (1996); Basic principles of membrane science and technology; 2nd Edition; Dordredit; Boston: Kluwer Academic.

Muller, J. & Kroner, K. H. (1992); Rotational shear-filtration of biosuspensions-influence tayer vortices on filtration performance; Proc. Engn. Memb. Process, Bavaria, Germany.

Nagaoka, H., Yamanishi, S. & Miya, A. (1998); Modeling of biofouling by extracellular polymers in a membrane separation activated sludge system; Wat. Sci. Technol., **38**, pp497.

Neal, P. R., Li, H., Fane, A. G. & Wiley, D. E. (2003); The effect of filament orientation on critical flux and particle deposition in spacer-filled channels, J. Memb. Sci., **214**, pp165.

Ndinisa, N. V., Wiley, D. E. & Fletcher, D. F. (2005); Computational fluid dynamics simulations of Taylor bubbles in tubular membranes – Model validation and application to laminar flow systems; Chem. Eng. Res. & Design, **83**, pp40.

Ognier, S., Wisniewski, C. & Grasmick, A. (2002); Characterisation and modelling of fouling in membrane bioreactors; Desalination, **146**, pp141.

Parameshwaran, K., Fane, A. G, Cho, B. D. & Kim, K.J. (2001); Analysis of microfiltration performance with constant flux processing of secondary effluent; Water Research, **83**, pp4349.

Parameshwaran, K., Visvanathan, C. & Ben Aim, R. (1999); Membrane as solid/liquid separator and air diffuser in a bioreactor; J. Environ. Eng., **125**, pp825.

Peri, C. & Dunkley, W. L. (1971); Reverse osmosis of cottage cheese whey, influence of flow conditions; J. Food Sci., **36**, pp395.

Perry, R. H. & Green, D. W. (1999); Chemical engineers' handbook; Seventh Edition, McGraw-Hill Companies.

Peters, T. A., Gunther, R. & Vossenkaul, K. (2000); Membrane bioreactors in wastewater treatment; Filtr. Sep., **2000**, pp18.

Pfleger, D. & Becker, S. (2001); Modelling and simulation of the dynamic flow behaviour in a bubble column; Chem. Eng. Sci., **56**, pp1737.

Pospisil, P., Wakeman, R. J., Hodgson, I. O. A. & Mikulasek, P. (2004); Shear stress-based modelling of steady-state permeate flux in microfultration enhanced by two-phase flows; Chem. Eng. J., **97**, pp257.

Ralph, M. E. (1986); Oscillating flows in wavy-walled tubes; J. Fluid Mech., **168**, pp515.

Ranade, V. V. (1997); Modelling of turbulence flow in a bubble column reactor; Chem. Eng. Res. Des., **75**, pp14.

Ranade, V. V. & Tayalia, Y. (2001); Modelling of fluid dynamics and mixing in shallow bubble columns reactors: Influence of sparger design; Chem. Eng. Sci., **56**, pp1667.

Riesmeier, B., Kroner, R. H. & Kula, M. R. (1987); Studies on secondary layer formation and its characterisation during cross-flow filtration of microbial cells; J. Memb. Sci., **34**, pp245.

Rittmann, B. E. (1987); Aerobic biological treatment; Environ. Sci. Technol., **21**, pp128.

Rodgers, V. G. J. & Sparks, R. E. (1991); Reduction of membrane fouling in the ultrafiltration of binary protein mixtures; AIChE J., **37**, pp1517.

Roest, H. F. (2002); Membrane bioreactors for municipal wastewater treatment; IWA Publishing, London.

Rosenberger, S., Kraume, M. & Szewyk, U. (1999); Sludge free management of membrane bioreactors; MBR2 –Proc. 2nd Intl. Mtg. on Membrane Bioreactors for Wastewater Treatment; Cranfield University, Cranfield, UK, pp10.

Rosenberger, S. & Kraume, M. (2002); Filterability of activated sludge in membrane bioreactors; Desalination, **151**, pp195.

Sato, Y. & Sekoguchi, K. (1975); Liquid velocity distribution in two-phase bubbly flow; Intl. J. Multiphase Flow, **2**, pp79.

Sekoguchi, K., Sato, Y. & Honda, T. (1974); An experimental investigation on bubble flow (first report); Trans. Japan Soc. Mech. Engrs., **40**, pp1395.

Shimizu, Y., Uryu, K., Okuno, Y. I. & Watanabe, A. (1996); Cross-flow microfiltration of activated sludge using submerged membrane with air bubbling; J. Fermentation Bioeng., **81**, pp55.

Shyu, J. C., Ding, P. P., Cheng, W. F. & Chen, P. H. (2002); Air bubble generation through a submerged micro-hole; Trans. IChemE, **80**, pp355.

Smith, S. R. & Cui, Z. F. (2004a); Gas-slug enhanced hollow fibre ultrafiltration – an experimental study; J. Memb. Sci., **242**, pp117.

Smith, S. R. & Cui, Z. F. (2004b); Analysis of developing laminar pipe flow – an application to gas slug enhanced hollow fibre ultrafiltration; Chem. Eng. Sci., **59**, pp5975.

Smith, C. W., Gregorio, D. & Talcott, R. M. (1969); The use of ultrafiltration membranes for activated sludge separation; Proceedings of the 24th Purdue Industrial Waste Conference, pp1300.

Smith, S., Taha, T. & Cui, Z. F. (2002); Enhancing hollow fibre ultrafiltration using slug-flow — a hydrodynamic study; Desalination, **146**, pp69.

Sokolichin, A. & Eigenberger, G. (1994); Gas-liquid flow in bubble columns and loop reactors: Part 1, detailed modeling and numerical simulations; Chem. Eng. Sci., **49**, pp5735.

Spicka, P., Dias, M. M. & Lopes, J. C. B. (2001); Gas-liquid flow in a 2D column: Comparison between experimental data and CFD modeling; Chem. Eng. Sci, **56**, pp6367.

Stephenson, T., Judd, S., Jefferson, B. & Brindle, K. (2000); Membrane bioreactors for wastewater treatment; IWA Publishing, London.

Sur, H. W. & Cui, Z. F. (2001); Experimental study on the enhancement of yeast microfiltration with gas sparging; J. Chem. Tech. and Biotech., **76**, pp477.

Sur, H. W. & Cui, Z. F. (2005); Enhancement of microfiltration of yeast suspensions using gas sparging – effect of feed conditions; Sep. Purification Tech., **41**, pp313.

Sur, H. W., Li, Q. & Cui, Z. F. (1998); Gas sparging to enhance crossflow ultrafiltration in tubular flow; IChemE Research Event 1998, Newcastle, UK.

Sussman, M., Smereka, P. & Osher, S. (1994); A level set approach for computing solutions to incompressible two-phase flow; J. Comp. Phys., **114**, pp146.

Taha, T. & Cui, Z. F. (2002a); Hydrodynamic analysis of upward slug flow in tubular membranes; Desalination, **145**, pp179.

Taha, T. & Cui, Z. F. (2002b); CFD modelling of gas-sparged ultrafiltration in tubular membranes; J. Memb. Sci., **210**, pp13.

Taitel, Y., Bonea, D. & Dulker, A. E. (1980); Modeling flow pattern transitions for steady upward gas-liquid flow in vertical tubes, AIChE J., **26**, pp345.

Taitel, Y., Shoham, O. & Brill, J.P. (1989); Simplified transient solutions and simulations of two-phase flow in pipelines; Chem. Eng. Sci., **44**, pp1353.

Tardieu, E., Grasmick, A., Geaugey, V. & Manem, J. (1998); Hydrodynamic control of bipartcile deposition in a MBR applied to wastwater treatment; J. Memb. Sci., **147**, pp1.

Torvik, R. & Svendsen, H. F. (1990); Modelling of slurry reactors: A fundamental approach; Chem. Eng. Sci., **45**, pp2325.

Tomiyama, A., Zun, I., Higaki, H., Makino, Y. & Sakaguchi, T. (1997); A three-dimensional particle tracking method for bubbly flow simulation; Nuclear Eng. And Des., **175**, pp77.

Tomiyama, A., Zun, I., Sou, A. & Sakaguch, T. (1993); Numerical analysis of bubble motion with the VOF method; Nuclear Eng. Design., **141,** pp69.

Tzeng, J. W., Chen, R. C. & Fan, L. S. (1993); Visualisation of flow characterisation in a 2-D bubble column and three-phase fluidized bed; AIChE. J., **39**, pp733.

Ueda, T., Hata, K. & Kikuoka, Y. (1996); Treatment of domestic sewage from rural settlements by a membrane bioreactor; Wat. Sci. Technol., **34**, pp189.

Valencia, A., Cordova, M. & Ortega, J. (2002); Numerical simulation of gas bubbles formation at a submerged orifice in a liquid; Intl. Comm. Heat and Mass Transfer, **29**, pp821.

Vera, L., Villarroel, R., Delgado, S. & Elmaleh, S. (2000); Enhancing microfiltration through an inorganic tubular membrane by gas sparging; J. Memb. Sci., **165**, pp47.

Vigneswara, S. & Visvanathan, C. (1995); Water treatment processes: simple options; Boca Raton: CRC Press.

Visvanathan, C., Ben Aim, R. & Parameshwaran, K. (2000); Membrane separation bioreactors for wastewater treatment; Crit. Rev. in Envronm. Sci. Technol., **30**, pp1.

Vitankar, V. S., Dhotre, M. T. & Joshi, J. B. (2002); A low Reynolds number k-ε model for the prediction of flow pattern and pressure drop in bubble columns reactors; Chem. Eng. Sci., **57**, pp3235.

Wachem, B. G. M. & Schouten, J. C. (2002); Experimental Validation of 3-D Lagrangian VOF Model: Bubble Shape and Rise Velocity; AIChE. J., **48**, pp2744.

Walter, J. K. & Davidson, J. F. (1963); The initial motion of a gas bubble formed in an inviscid liquid, Part 2: The three-dimensional bubble and the toroidal bubble; J. Of Fluid Mechanics, **17**, pp321.

Wang, Y., Howell, J.A., Field, R.W. & Wu, D. (1994); Simulation of cross-flow filtration for baffled tubular channels and pulsatile flow; J. Membr. Sci**., 95**, 243.

Wenten, I. G., Koenhen, D. M., Roesink, H. D. W., Rasmussen, A. & Jonsson, G. (1994); The backshock process – a novel backflush technique in microfiltration; Proc. Eng. Memb. Process II, Environmental Applications, Tuscany, Italy.

White, E.R. & Beardmore, R.H. (1962); The velocity of rise of single cylindrical air bubbles through liquids in vertical tubes; Chem. Eng. Sci., **17**, pp351.

Wicaksana, F., Fane, A. G. & Chen, V. (2006); Fibre movement induced by bubbling using submerged hollow fibres; J.Memb.Sci., **271**, pp186.

Winzeler, H. B. & Belfort, G. (1993); Enhanced performance for pressure-driven membrane process: the argument for fluid instability; J. Memb. Sci., **80**, pp35.

Wu, M. & Gharib, M. (2002); Experimental studies on the shape and path of small air bubbles rising in clean water; Phys. Of Fluids, **14**, pp49.

Yamamoto, K., Hiaga, H., Mahmood, T. & Matsuo, T. (1989); Direct solid-liquid separation using hollow fibre membrane in an activated sludge aeration tank; Wat. Sci. Tech., **21**, Brighton, pp43.

Yang, Z. L., Dinh, T. N., Nourgaliev, R. R. & Sehgal, B. R. (2001); Numerical investigation of bubble growth and detachment by the lattice-Boltzmann method; Intnl. J. Of Heat And Mass Transfer, **44**, pp195.

Yeom, I. T., Nah, Y. M. & Ahn, K. H. (1999); Treatment of household wastewater using an intermittently aerated membrane bioreactor; Desalination, **124**, pp193.

Zun, I., Kljenak, I. & Moze, S. (1993); Space-time evolution of the nonhomogeneous bubble distribution in upward flow; Intnl. J. Of Multiphase Flow, **19**, pp151.

Appendix A

CONSTANT TEMPERATURE ANEMOMETRY (CTA) MEASUREMENTS

In this experiment an attempt was made to utilise a hot wire anemometry probe to measure local liquid velocities across the membrane surface. However, because it was difficult to calibrate the sensor voltage output with liquid velocity for the flow channel involved, results were only analysed in terms of the hot-wire output voltage. The anemometer used was made of a fine 25.4 μm platinum wire. The sensor was heated electrically and when exposed to a flowing fluid the sensor was cooled by convection which was a measure of the fluid velocity. The sensor was connected to 0.4 mm copper wires that supported the sensor and connected it to a TSI 1750 CTA module. The sensor was insulated by a conformal coating. Further details about the sensor operation and development can be obtained elsewhere (Cao, 1998).

Figure A.1 shows the average voltage output from the sensor when the sensor was placed either in the centre of the membrane or in the lower right hand corner. There is a slight difference in voltage output from the two positions with the centre location having a slightly higher voltage output which implies slightly higher liquid velocities near the centre. In both locations the strength of the output increases with gas flow rate but seems to be approaching a maximum value. There is a strong up-flow of liquid near the centre of the membrane since this is the path of most bubbles and near the corners, the liquid is flowing down. This phenomenon was also observed in the CFD simulations which were discussed in chapter 7. Figure A.2 shows the results when the gap between the membrane and the wall was varied with the sensor located in line with the centre of the membrane but attached to the wall for three different gaps. From this figure it is seen that there is no difference in the sensor voltage output from the three gaps. These results are problematic to interpret. While the differences in anemometer response in figure A.1 may be due to differences in liquid phase recirculation in the two locations, the lack of effect of gap width on liquid velocity is contradictory.

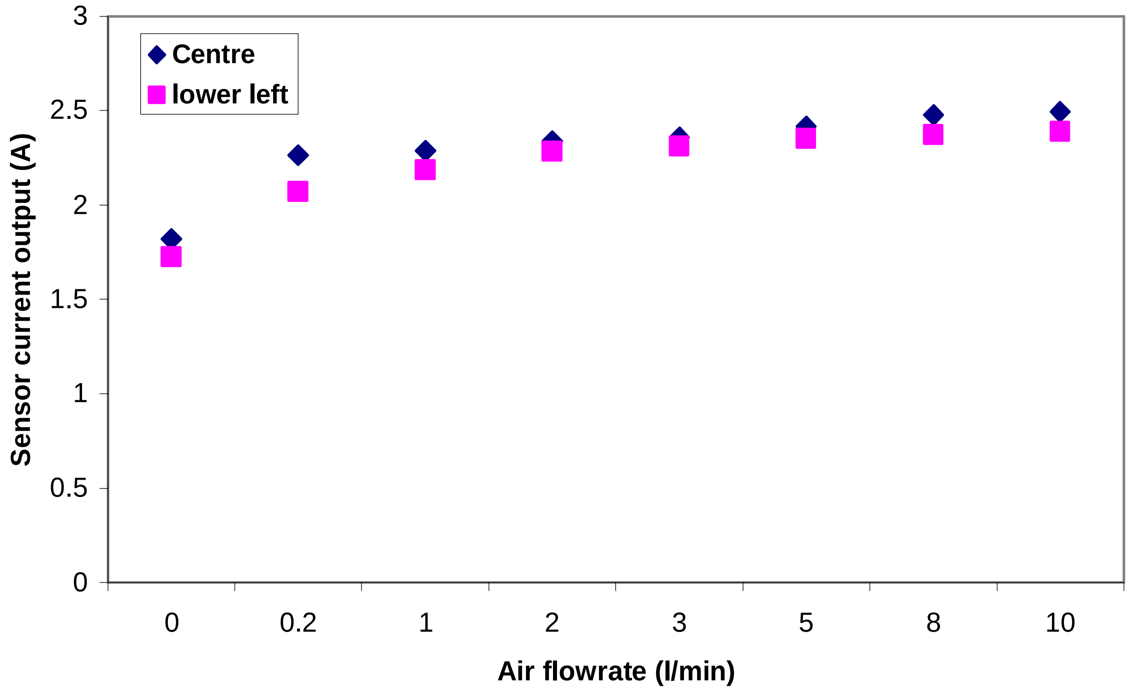

Figure A.1. CTA measurement at different positions on the membrane.

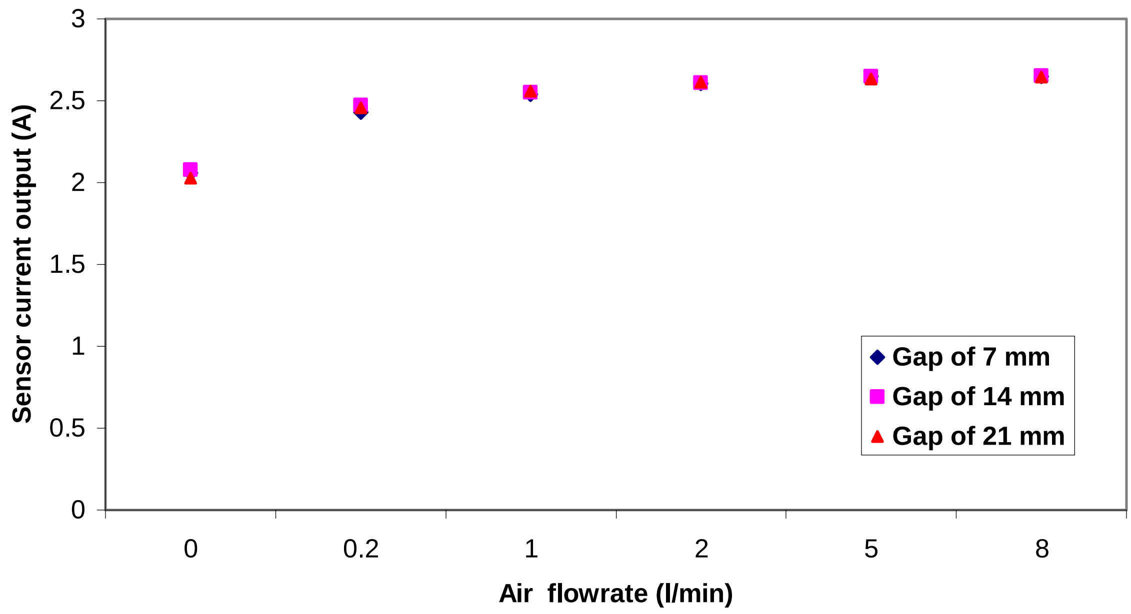

Figure A.2. CTA measurements at different gaps between the membrane and the wall.

Appendix B

SHORT VIDEOS OF TWO-PHASE FLOW

See the attached Compact Disc for the videos. There are three videos in the CD and they are entitled Video 1, Video 2, and Video 3.

Video 1

This video shows the nature of the two-phase flow profile across a submerged flat sheet membrane in the absence of baffles. The air flow rate in this video was 8 l/min.

Video 2

This video shows the two-phase flow profile when the baffles are inserted. The air flow rate is the same as in Video 1 of 8 l/min.

Video 3

In contrast to Video 1, this video shows the two-phase flow profile in the absence of baffles but at low gas flow rates. The air flow rate in this video is 2 l/min.